UNIVERSITY OF CINCINNATI

Date: 1/31/2008

I, Stuart A Willison,

hereby submit this work as part of the requirements for the degree of:

Doctorate of Philosophy (Ph.D.)

in:

Chemistry

It is entitled:

Synthesis and Investigation of Pyrazole-Containing Platinum Complexes for the Design of Macrocyclic Molecules and Potential Two-electron Reagents

This work and its defense approved by:

Chair: Dr. William Connick

Dr. Michael Baldwin

Dr. Anna Gudmundsdottir

Synthesis and Investigation of Pyrazole-Containing Platinum Complexes for the Design of Macrocyclic Molecules and Potential Two-electron Reagents

A dissertation submitted to the

Division of Research and Advanced Studies
of the University of Cincinnati

in partial fulfillment of the
requirements for the degree of

DOCTORATE OF PHILOSOPHY (Ph.D.)

In the Department of Chemistry
of the College of Arts and Sciences

2008

by

Stuart A. Willison

B.S., University of Cincinnati, 2002

Committee Chair: Dr. William B. Connick

Abstract

A detailed study involving platinum(II) compounds with *bis*-2,6-pyrazolyl-phenyl type ligands have been undertaken in an effort to design a new architecture for building macrocyclic molecules with potentially coordinating tridentate ligands. Initial reports focused on platinum complexes with 2,6-*bis*-pyrazolyl-pyridine ligands. One complex, Pt(bpp)Ph^+, exhibited an intense pink emission of the solid at 77 K, which is one of the first examples of a luminescent platinum compound with a *bis*-pyrazolyl-pyridine ligand. Herein we report the investigation of steric influence to promote C-H activation on the formation of monomeric and macrocyclic platinum(II) complexes, using methyl substituents on a series of anionic *bis*-pyrazolyl-phenyl ligands. Further studies of concentrated reaction mixtures at long reaction times result in exclusively trimeric products, whereas more dilute mixtures and shorter reaction times give only monomer products. Thus, careful control of the reaction conditions allows for selective activation of C-H bonds on the ligand giving isolated products of expected monomers and trimers, as well as surprising new dimeric products. In the course of our investigations of the monomeric platinum(II) products, we have discovered that four complexes react with dithiocarbamate accelerators most commonly used in latex processing, giving a colored response. Thus, the platinum complexes can be used as colorimetric indicators to detect allergenic dithiocarbamate compounds in latex products. In addition, we describe the synthesis and preliminary characterization of a potential two-electron reagent using a monomeric complex, Pt(**4**)Cl, and pip_2NNN, where **4** is 1,3-*bis*(3,5-dimethylpyrazolyl)benzene and (pip_2NNN) is 2,6-*bis*(piperidylmethyl)pyridine, to give Pt(**4**)($pip_2NNN)^+$.

Acknowledgements

I have experienced nearly as many things as one could possibly experience on this campus at the University of Cincinnati, merely because I have been a student since 1999, as an undergraduate and intercollegiate athlete and now a graduate student. I was naïve in many ways when I first arrived, but I've learned so much since then. We can always learn more, expect more and constantly find something we never expected. I have learned several lessons since my first year here; as expected some good and some bad. When I first began school, I was uncertain what I wanted to achieve, what I wanted to do, and what would interest me with great passion. This took a while to figure out, but like everything, whether you want it to or not, things always have a way of working themselves out. I am proud of what I have become because I sometimes questioned if it were possible. This is true in many cases, when I didn't think I could have set the record as the University of Cincinnati's fastest breaststroker, and certainly now when I have completed my doctoral degree in chemistry. No one person can ever succeed without the encouragement and help from others and for that I am sincerely grateful. First and foremost, I'd like to thank Dr. Bill Connick. His passion for the field and teaching others is the greatest I've ever witnessed from one man. His plethora of knowledge has not only increased my knowledge base, but more importantly, it will always leave me wanting to learn more and be as creative as he is. Furthermore, not only was he willing to listen about the science aspects of my life, but also the personal aspects and when I was struggling, he would go out of his way to help me in any way possible, no matter how time consuming. His encouragement, concern and advice are attributes that I will always cherish and be thankful for. I would like to thank Drs. Baldwin and Gudmundsdottir for their expertise and guidance through this process as well.

I would also like to thank several Connick group members as well. The everyday interaction with past and present labmates has made this process all worthwhile. To former members: Hershel, who was always willing to help, no matter how busy he was, and being a friend. Tyler, a friend who constantly pushed me mentally, yet made it fun to enter the lab with his singing antics during songs. P.J., who was always willing to listen and constantly made me laugh! To present members: Dev, oh so much to say yet so little room, thanks for filling the shoes of the former members, by making me laugh and willingness to take the time for anything that I needed, the dev-a-stator. Thanks to Levi, Jenny, Seher, Amber, Stephen and Ronnie for being great labmates as well. I wouldn't have changed anything about my experience working with all of you! I would also like to thank others within the department: Daisy, who has become a close and wonderful friend. Thank you for making me laugh, for listening to me when I struggled and for your sarcastic, dry humor. Doug, a great friend, lifting partner and drinking buddy. I owe you for my birthday! Kirk, my new lifting partner, thanks for being a good friend. Thanks to Lisa and Chris as well! Lastly from this great department, I would like to thank Kady, for being patient, kind, for making me laugh and think, keeping me on my toes, and constantly reminding me of how thankful I am with her presence. I remember when I first met her, she was visiting UC on her recruiting trip. She claims she looked at me and I was staring at her, not true. I remember she was the one looking at me, admiring my eyes (as Daisy did in her near death experience) when we were playing the wonderful game of flip cup. I'll admit I was somewhat in awe, but she seemed like the girl that I would become very good friends with at the very least, and I'm glad it has turned into a great relationship. I admire and am thankful for everyone in this department, especially these people.

For all of my swimming friends, Karl, without his friendship and encouragement, I probably would not have come to this University to swim and meet all of these wonderful people: Joe, Kevin, Ryan, Marcel, Enrique, Carlo, Aaron (Chavez), Michael, Jaimi, Quinn, Kim, Shauna, Louise, Lulu, Steve, Krista, David, Honza, Maria, Aaron (Rocky), Randi, and my coach, Monty Hopkins, who without his help, encouragement, and advice, and his willingness to just give me a chance, I would not have been able to accomplish so much and be so successful.

Lastly I would like to thank my family for all of their love and support. They didn't understand a word of my dissertation or any of the chemistry I was doing, but are still very proud of everything I have accomplished.

Tables of Contents

List of Tables

List of Schemes

List of Figures

List of Abbreviations and Symbols

Å	angstrom
α	alpha
bdmpp	2,6-bis(3,5-dimethyl-*N*-pyrazolyl)pyridine
bpp	*bis*-pyrazolylpyridine
$bpzph^-$	1,3-*bis*(pyrazolyl)benzene
$CHCl_3$	chloroform
CH_2Cl_2	methylene chloride
CH_3CN	acetonitrile
CH_3OH	methanol
C	Celsius
COSY	correlation spectroscopy
cm	centimeter
cm^{-1}	wavenumber
DMF	dimethylformamide
DMSO	dimethylsulfoxide
DPG	Diphenylguanidine
ε	extinction coefficient (M^{-1} cm^{-1})
ESI	electrospray ionization
Et_2O	diethyl ether
EtOH	ethanol
FW	formula weight

fwhm	full width at half maximum
γ	gamma
g	gram
h	hour
HOMO	highest occupied molecular orbital
Hz	Hertz (s^{-1})
IPA	isopropyl alcohol
K	Kelvin
kcal	kilocalorie
kJ	kilojoule
λ	wavelength
LF	ligand field
LUMO	lowest unoccupied molecular orbital
M	molarity
MBT	Mercaptobenzothiazole
MBS	2-Morpholinothiobenzothiazole
mV	millivolts
m/z	mass/charge
mer	meridional
Me	methyl
ml	milliliter
MLCT	metal-to-ligand charge transfer
mol	mole

MS	mass spectrometry
nm	nanometer
ns	nanosecond
NOESY	nuclear overhauser spectroscopy
NMR	nuclear magnetic resonance
NPA	*N*-(2'-pyridyl)-7-azaindole
PF_6	hexafluorophosphate
Ph	phenyl
Phbpy	phenylbipyridine
pip_2NCN	2,6-*bis*(piperidylmethyl)phenyl
ppm	parts per million
Pt	platinum
Ru	ruthenium
τ	lifetime
$TBAPF_6$	tetrabutylammonium hexafluorophosphate
TMS	tetramethylsilane
TOF	time-of-flight
tpy	2,2′:6′,2″-terpyridine
V	volt
ZDEC	Zinc diethyldithiocarbamate

Chapter 1

Synthesis and Investigation of Pyrazole-Containing Platinum Complexes for the Design of Macrocyclic Molecules and Potential Two-electron Reagents

There is enormous interest in the assembly of molecular polygons because of their inherent properties, such as defined cavity size, shape, and binding specificity, which are potentially useful for chemical storage (*e.g.*, hydrogen), chemical sensing, catalysis and chemical separations.[1] Complexes of late transition metals, such as Pt, Pd, Os, Ir, Ru, Au and Rh, have been investigated as building blocks for molecular polygons known as metallocycles.[2-9] The resulting metallocycles are capable of making channels or cavities capable of performing the above applications. Typically, rigid-ligand linkers of various sizes are employed to drive directional self assembly processes. Coordination geometry, as well as ligand size and structure, plays an important role in determining the shapes and sizes of the resulting polygons. Predictable geometries allow for one-pot synthetic reactions that produce metal-containing macrocyles in high yields.

The development of macrocycles based on platinum(II)-containing subunits is a particularly attractive avenue of investigation because platinum(II) complexes have predictable square-planar geometries and good kinetic stability. Two examples of platinum metallocycles from Professor Peter Stang's laboratory at the University of Utah are shown in Figure 1.1.[10] In addition to synthetic advantages, platinum(II) complexes give rise to intense luminescence.[11] For example, Hupp et al. has shown that changes in luminescence intensities of a macrocycle based on cavity size allows for applications in molecular sensing.[12]

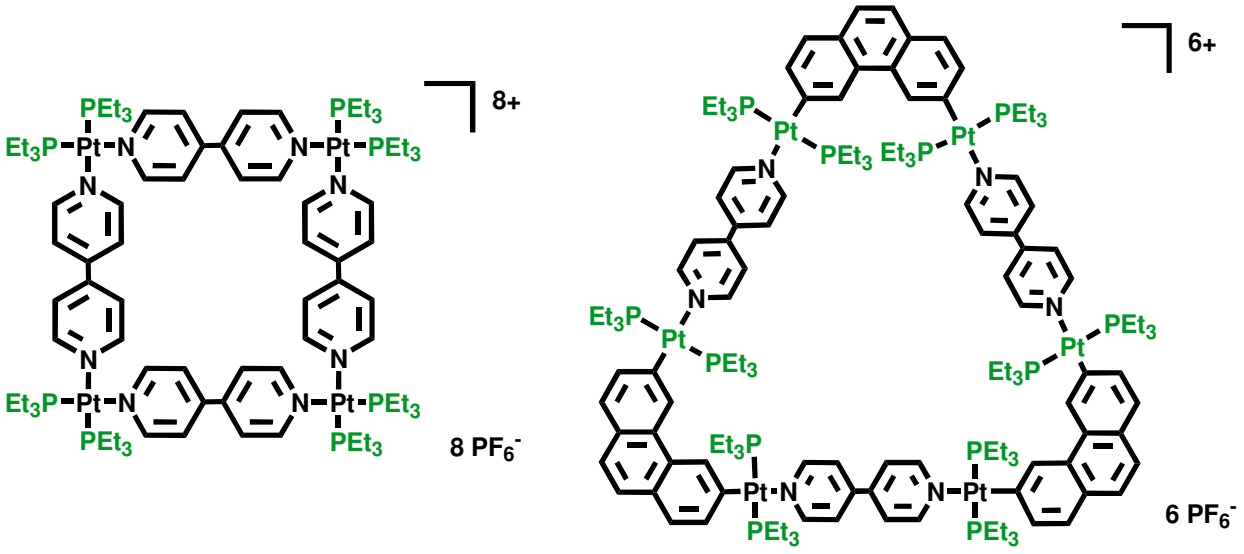

Figure 1.1. Platinum-containing macrocycles varying in shape and size.

Metallocycles based on square planar platinum(II) most often consist of subunits bridged by N-donor ligands. Commonly employed N-donor ligands contain five and six-membered rings such as pyridine, pyrazole, pyrazine, pyrimidine and imidazole. The general strategy for designing polygons uses rigid, organic linkers with well-defined bonding directionality. N-type ligands offer kinetic lability, with relatively strong bond formation between donor and acceptor, resulting in thermodynamic products. Classic architecture of macrocycles use bidentate building blocks in two different coordination geometries. The bridging ligands (L_B) can align in *cis*-configuration with respect to the metal center, or in a *trans*-configuration (Figure 1.2). For when the ligands are situated in a *cis*-configuration, the metal complexes act as a corner component of a polygon, but in a *trans*-configuration, the resulting metal complexes act as edge components. As shown in Figure 1.1, the organic linkers (*e.g.* 4, 4'-bipyridine) play an important role in the structural conformations of polygons. Furthermore, metal centers (*e.g.* Pt) with predictable geometries are as essential as rigid ligand systems in the role of structural determination.

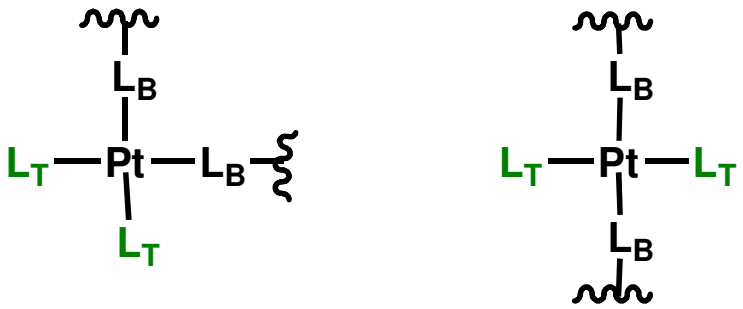

Figure 1.2. *Cis*- and *trans*-configurations of platinum complexes. (L_T = terminal ligands, L_B = bridging ligand).

To date, nearly 100 platinum polygons have been reported using this strategy.[13,14] Shapes can range from the smallest macrocycle, triangle, to higher order dendrimeric-like structures with varying cavity sizes, allowing for substrate specificity. The resulting polygons can also stack forming channels. N donor ligands not only help with directionality, but give kinetically stable complexes, most likely ionic in nature, allowing for differentiation between anionic substrates for applications in molecular sensing and storage.[3,15,16]

One characteristic property of the platinum(II)-based polygons is their relatively shallow cavities, resulting from their annulus-like structures. In addition, the molecular cavities have significant conformational flexibility due to rotation about the Pt-N bonds.[17] This architecture restricts the surface area available for interaction between guest-host molecules. Therefore, there is interest in designing polygons with increased depth and rigidity to allow for better control over guest recognition properties. Moreover, deeper cavities may allow for interaction of the metal centers with the substrate, possibly resulting in chemical activation. Typical synthetic methodology incorporates the use of Pt-N bonds between metal and bridging ligands. Elaboration of the kinetic lability between metal-ligand bonds with Pt-C bonded systems would

result in more robust structures. Furthermore, there is an interest to design chiral metallocycles for enantioselective processes, yet challenging due to use of achiral ligands.

In the course of our investigations of platinum(II) complexes with tridentate ligands,[18-24] we became interested in the notion of utilizing traditional tridentate ligands to synthesize more rigid metallocycles. These initial studies were stimulated by the discovery of platinum two-electron transfer reagents which undergo nearly reversible cooperative outer-sphere two-electron transfer.[22] These complexes consist of two potentially meridionaly coordinating ligands bonded to a platinum center. In d^8-electron platinum(II) case, one ligand is tridentate whereas the other is monodentate. In d^6-electron platinum(IV) case, both ligands are believed to be tridentate. Thus, the cyclic voltammogram of $Pt(pip_2NCN)(tpy)^+$ (Figure 1.3) in 0.1 M electrolyte in solvent at 0.01 V/s shows a nearly a two-electron wave at 0.40 V vs. Ag/AgCl. The separation between the anodic and cathodic peaks (ΔE_p) is 43 mV, which is well below the one-electron limit (59 mV) and near the two-electron limit (30 mV) for a Nernstian process.[22,25,26]

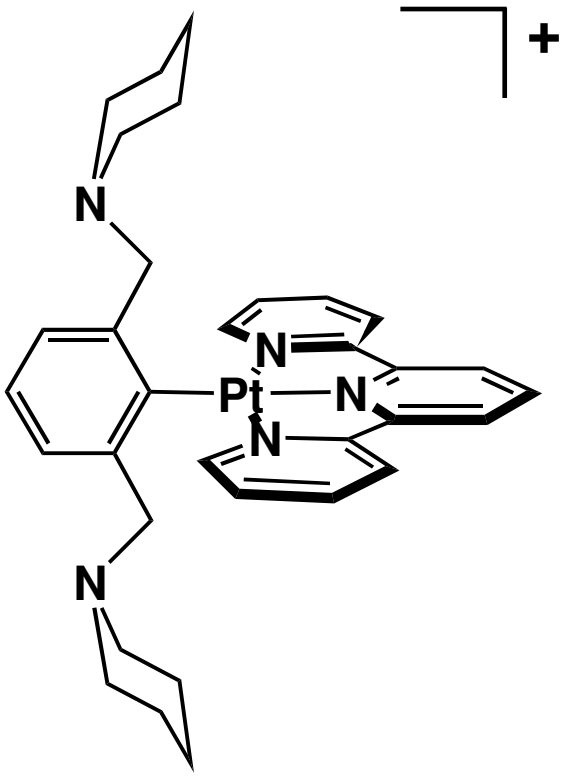

Figure 1.3. Line drawing of $Pt(pip_2NCN)(tpy)^+$ complex.

At first glance, typical tridentate chelating ligands, such as terpyridine (tpy) and 2,6-*bis*(piperidylmethyl)phenyl anion (pip_2NCN^-) (Figure 1.3), would seem unlikely components of a platinum(II) metallocycle. Tridentate coordination leaves only one site available for coordination, and therefore these ligands would appear to be better suited to formation of rod-like molecules.[20] However, there exists literature precedence for bidentate coordination of terpyridine to platinum(II).[27] This coordination geometry allows for the possibility that the remaining dangling pyridyl group can act as a nucleophile and bind to another metal center. Bidentate coordination has been encountered in cases where there are only two sites available for ligand coordination.[28-30] On the other hand, Minghetti, Doppiu and Stoccoro have discovered that reaction of tpy with electron-rich $Pt(CH_3)_2(DMSO)_2$ results in $Pt(\mu\text{-tpy-2H})(CH_3)_2(DMSO)_2$, where the doubly deprotated tpy ligand, $(tpy\text{-}2H)^{2-}$, acts as an NC^CN bridging ligand (Figure

1.4(a).[27] This type of bridging geometry is expected to result in dimers and possibly more elaborate architectures, including new metallocycles. However, platinum(II) metallocycles with bridging tpy units have not yet been isolated. Deprotonation of 6-phenyl-2,2'-pyridine (phbpyH) also can produce bridged platinum(II) structures. In that case, the ligand bonds one Pt center in a tridentate fashion and the other in a bidentate geometry, as shown in Figure 1.4(b).[31,32] 1,3-dipyridylbenzene, also is known to form a variety of bridged structures with Pd but not Pt,[33] however, platinum(II) bridged structures have been reported with 1,3-diphenylpyridine.[34,35]

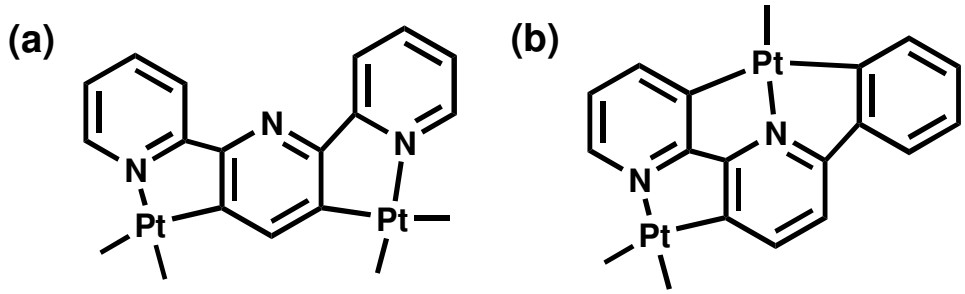

Figure 1.4. Atypical bridging ligand coordination modes for platinum(II) dimers with (a) doubly deprotonated tpy[27] and (b) doubly deprotonated phenylbipyridine ligands.[31,32]

Formation of bridged structures and metallocycles with conventional tridentate ligands requires selective C-H activation of an aromatic ring to give one or more Pt-C bonds. This approach is attractive since the kinetic stability of Pt-C bonds, as compared to Pt-N bonds, can be expected to result in especially stable polygons. In addition, the chelating coordination geometry favored by tridentate ligands is anticipated to produce more rigid metallocycles. Recently Zhao and co-workers reported formation of a platinum(II) molecular square using a deprotonated *N*-(2'-pyridyl)-7-azaindole ligand (NPA).[36] The ligand forms monomeric complexes by binding the metal through the pyridyl and 7-azaindole N atoms (Figure 1.5 (a)). Alternatively, the

deprotonated ligand can bond to one platinum center through the the pyridyl N atom and the 2-azaindole C atom, leaving the 7-azaindole N available to bridge to another platinum center (Figure 1.5 (b). Despite this success, precise control of cyclometallation reactions remains a challenging problem and products are often unpredictable. In addition, there remain open questions about the mechanism of how C-H reactions proceed, and there is a continuing need to develop new C-H activation reactions.[37]

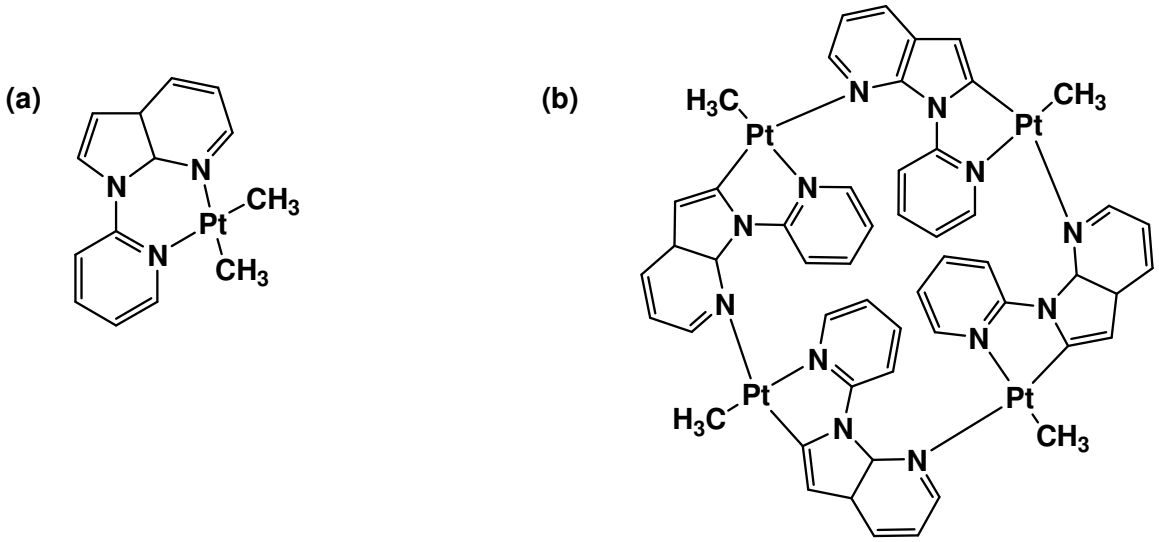

Figure 1.5. Zhao's (a) monomeric platinum complex and (b) tetrameric platinum polygon.

Our working hypothesis in this study is that destabilization of the tridentate chelation geometry will tend to favor formation of the bidentate-bridging ligand geometry. In the case of $Pt(tpy)Cl^+$, the trans N-Pt-N bond angle is somewhat less than the idealized angle for square planar complexes (180°), ranging from 161.2° to 163.5°.[38] Nevertheless, terpyridyl ligands adopt a tridentate geometry for the vast majority of their known platinum(II) complexes. $Bpzph^-$ and bpp (Figure 1.6) are close analogs of tpy in which the smaller five-membered pyrazole rings replace the peripheral pyridyl groups. It may be anticipated that the relative geometric constraints of the five-membered pyrazolyl rings, as compared to six-membered pyridyl rings,

will tend to destabilize tridentate coordination. The focus of this dissertation is on the synthesis and characterization of platinum complexes with the pyrazole-containing ligands shown in Figure 1.6, as well as related derivatives. The research has provided insight into the electron-donor properties of these ligands and the luminescence properties of their resulting platinum(II) complexes.[39] This work also has led to the discovery of a new class of molecular polygons, resulting from a surprising C-H activation reaction. Thus, in addition to monomers, several dimers and trimers have been synthesized and characterized. Characterization of the monomers has led to a new avenue of research dealing with the reactions of these compounds on processed latex surfaces. Preliminary results suggest that the complexes may serve as colorimetric indicators for the presence of allergenic dithiocarbamate compounds in latex products. In addition, we report progress toward synthesizing outer-sphere two-electron reagents that incorporate deprotonated 1,3-*bis*(*N*-pyrazolyl)benzene ligands. A short summary of each chapter is provided below.

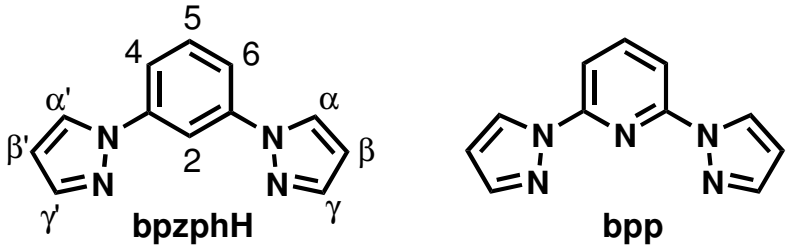

Figure 1.6. Potentially coordinating tridentate ligand derivatives of terpyridine.

Chapter 2 describes the synthesis and characterization of four platinum complexes with the *mer*-coordinating tridentate ligands, 2,6-bis(*N*-pyrazolyl)-pyridine (bpp) and 2,6-bis(3,5-dimethyl-*N*-pyrazolyl)pyridine (bdmpp). Each of the four complexes exhibits weak or no emission at room temperature. Even at low temperature, the emissions from three complexes are decidedly weak. However when cooled to 77 K, [Pt(bpp)(Ph)](PF_6) exhibits a remarkably

intense pink emission. Interestingly, variable temperature X-ray crystallography down to 85 K reveals no evidence of a significant structural rearrangement or phase change that might account for the intense emission at low temperature. Overall, the accumulated spectroscopic and electrochemical data for the four complexes are consistent with weaker σ-donor and π-acceptor properties of bpp, as compared to tpy.

Chapter 3 describes the synthesis and structures of monomeric and trimeric platinum compounds with a deprotonated 1,3-*bis*(pyrazolyl)benzene ligand (bpzph$^-$). By carefully controlling the reaction conditions exclusively Pt(bpzph)Cl or [Pt(μ-bpzph)Cl]$_3$ is isolated. In the case of the C_3-symmetric molecular triangle, each bpzph$^-$ ligand is bidentate with the metal bonded to one pyrazolyl group and to the phenyl group at the 6-position; the remaining pyrazolyl group bridges to an adjacent Pt center. The crystal structure confirms that each trimer is chiral with an unusually deep (~8 Å) intramolecular cavity. NMR studies establish that the trimer exhibits excellent thermal and kinetic stability. Substitution of the chloride ligands for bromide is shown to be a promising strategy for elaborating the macrocycle.

Chapter 4 describes an expanded investigation of the reaction of platinum(II) starting materials with various substituted 1,3-*bis*(pyrazolyl)benzene derivatives. This study reveals a surprisingly rich array of products, including monomers, dimers and trimers (molecular triangles.) Sterics are shown to play an important role in the structures of the resulting products. For example, reaction of $K_2[PtCl_4]$ with 1,3-*bis*(4-methylpyrazolyl)benzene affords exclusively trimer. However, substitution of methyl groups at the γ and γ' positions of the pyrazoyl groups results in exclusively monomer formation. Presumably the steric demands of the methyl groups destabilize the trimer product.

Chapter 5 describes the reactions of platinum monomer complexes from Chapter 4 on latex surfaces. The complexes dissolve in organic solvents (*e.g.*, CH_3OH, EtOH, CH_3CN, acetone, CH_2Cl_2) to give colorless solutions that remain colorless when applied to commercially processed latex (*e.g.*, conventional latex laboratory gloves.) However, upon evaporation of the solution, four complexes produced a stain on the latex surface, ranging from red to purple in color. The compounds did not give a similar response when applied to raw latex (*i.e.*, unprocessed) or several common latex additives (*e.g.*, sulfur, ZnO). However, solutions of the compounds produced similar colors when evaporated on dithiocarbamate accelerators (*e.g.*, sodium diethyldithiocarbamate) used in latex manufacturing. These results suggest that these platinum compounds can be used as colorimetric indicators for residual dithiocarbamate species in latex.

Chapter 6 describes efforts to synthesize a two-electron platinum reagent similar to $Pt(pip_2NCN)(tpy)^+$ (Figure 1.3), except with a *bis*(pyrazolylphenyl anionic ligand in place of pip_2NCN^- and a 2,6-*bis*(piperidylmethyl)pyridine ligand in place of tpy. New reagents of this type are expected to significantly expand our repertoire of two-electron complexes and provide new opportunities for tailoring their properties. The resulting complex was characterized by NMR and mass techniques. Electrochemical data confirm that the product undergoes quasi-reversible electron-transfer.

References.

(1) a) Lehn, J. M., *Supramolecular Chemistry-Concepts and Perspectives*; VCH: New York, **1995**; b) P. J. Stang, B. Olenyuk, *Acc. Chem. Res.* **1997**, *30*, 502; c) S. Leininger, B. Olenyuk, P. J. Stang, *Chem. Rev.* **2000**, *100*, 853; d) Steed, J. W., *Supramolecular Chemistry*; VCH: Toronto, **2000**; e) R. S. Seidel, P. J. Stang, *Acc. Chem. Res.* **2002**, *35*, 972.

(2) Vicente, J.; Chicote, M. T.; Alvarez-Falco´n, M. M.; Jones, P. G. *Chem. Commun.* **2004**, 2658-2659.

(3) Qin, Z.; Jennings, M. C.; Puddephatt, R. J. *Chem. Commun.* **2001**, *2001*, 2676-2677.

(4) Chatterjee, B.; Noveron, J. C.; Resendiz, M. J. E.; Liu, J.; Yamamoto, T.; Parker, D.; Cinke, M.; Nguyen, C. V.; Arif, A. M.; Stang, P. J. *J. Am. Chem. Soc.* **2004**, *126*, 10645.

(5) King, R. B. *J. Cluster Science* **1995**, *6*, 5-20.

(6) Lehaire, M.-L.; Scopelliti, R.; Herdeis, L.; Polborn, K.; Mayer, P.; Severin, K. *Inorg. Chem.* **2004**, *43*, 1609-1617.

(7) Hiraoka, S.; Harano, K.; Shiro, M.; Ozawa, Y.; Yashuda, N.; Toriumi, K.; Shionoya, M. *Angew. Chem. Int. Ed.* **2006**, *45*, 6488-6491.

(8) Yang, G.; Raptis, R. G. *Inorg. Chem.* **2003**.

(9) Sun, S. S.; Lees, A. J. *Inorg. Chem.* **1999**, 4181-4182.

(10) Addicott, C.; Das, N.; Stang, P. J. *Inorg. Chem.* **2004**, *43*, 5335-5338.

(11) Fleeman, W. L.; Connick, W. B. *Comments Inorg. Chem.* **2002**, *23*, 205-230.

(12) a) Slone, R. V.; Hupp, J. T.; Stern, C. L.; Albrecht-Schmidt, T. E. *Inorg. Chem.* **1996**, 4096; b) Slone, R. V.; Hupp, J. T. *Inorg. Chem.* **1997**, 5422; c) Slone, R. V.; Benkstein, K. D.; Belanger, S.; Hupp, J. T.; Guzei, I. A.; Rheingold, A. L. *Coord. Chem. Rev.* **1998**, 221; d) Belanger, S.; Hupp, J. T.; Stern, C. L.; Slone, R. V.; Watson, D. F.; Carell, T. G. *J. Am. Chem. Soc.* **1999**, 557.

(13) a) P. J. Stang, B. Olenyuk, *Acc. Chem. Res.* **1997**, *30*, 502; b) S. Leininger, B. Olenyuk, P. J. Stang, *Chem. Rev.* **2000**, *100*, 853; c) R. S. Seidel, P. J. Stang, *Acc. Chem. Res.* **2002**, *35*, 972.

(14) For examples, see: a) R. D. Schnebeck, E. Freisinger, F. Glahe, B. Lippert, *J. Am. Chem. Soc.* **2000**, *122*, 1381; b) M. Schweiger, S. R. Seidel, A. M. Arif, P. J. Stang, *Angew. Chem. Int. Ed.* **2001**, *40*, 3467; c) A. Sautter, D. G. Schmid, G. Jung, F. Wurthner, *J. Am. Chem. Soc.* **2001**, *123*, 5424; d) Z. Qin, M. C. Jennings, R. J. Puddephatt, *Chem. Commun.* **2001**, *2001*, 2676; e) M. Ferrer, M. Mounir, O. Rossell, E. Ruiz, M. A. Maestro, *Inorg. Chem.* **2003**, *42*, 5890; f) Y. K. Kryschenko, S. R. Seidel, M. Arif, P. J. Stang, *J. Am. Chem. Soc.* **2003**, *125*, 5193; g) Z. Qin, M. C. Jennings, R. J. Puddephatt, *Inorg. Chem.* **2003**, *42*, 1956; h) C. Addicott, N. Das, P. J. Stang, *Inorg. Chem.* **2004**, *43*, 5335; i) B. Chatterjee, J. C. Noveron, M. J. E. Resendiz, J. Liu, T. Yamamoto, D. Parker, M. Cinke, C. V. Nguyen, A. M. Arif, P. J. Stang, *J. Am. Chem. Soc.* **2004**, *126*, 10645; j) K.-W. Chi, C. Addicott, A. M. Arif, P. J. Stang, *J. Am. Chem. Soc.* **2004**, *126*, 16569; k) J. Fornies, J. Gomez, E. Lalinde, M. T. Moreno, *Chem. Eur. J.* **2004**, *10*, 888; l) G. R. Owen, F. Hampel, J. A. Gladysz, *Organometallics* **2004**, *23*, 5893; m) L. Zhang, Y. H. Niu, A. K.-Y. Jen, W. Lin, *Chem. Commun.* **2005**,1002; n) H. B. Yang, N. Das, F. Huang, A. M. Hawkridge, D. C. Muddiman, P. J. Stang, *J. Am. Chem. Soc.* **2006**, *128*, 10014.

(15) Schnebeck, R. D.; Freisinger, E.; Lippert, B. *Chem. Commun.* **1999**, 675-676.

(16) Schnebeck, R. D.; Freisinger, E.; Glahe, F.; Lippert, B. *J. Am. Chem. Soc.* **2000**, *122*, 1381-1390.

(17) Fuss, M.; Siehl, H.-U.; Olenyuk, B.; Stang, P. J. *Organometallics* **1999**, *18*, 758-769.

(18) Tastan, S.; Krause, J. A.; Connick, W. B. *Inorg. Chim. Acta* **2006**, *359*, 1889-1898.

(19) Willison, S. A.; Jude, H.; Antonelli, R. M.; Rennekamp, J. M.; Eckert, N. A.; Krause Bauer, J. A.; Connick, W. B. *Inorg. Chem.* **2004**, *43*, 2548-2555.

(20) Jude, H.; Krause Bauer, J. A.; Connick, W. B. *Inorg. Chem.* **2005**, *44*, 1211-1220.

(21) Jude, H.; Krause Bauer, J. A.; Connick, W. B. *Inorg. Chem.* **2004**, *43*, 725-733.

(22) Jude, H.; Krause Bauer, J. A.; Connick, W. B. *J. Am. Chem. Soc.* **2003**, *125*, 3446-3447.

(23) Jude, H.; Krause Bauer, J. A.; Connick, W. B. *Inorg. Chem.* **2002**, *41*, 2275.

(24) Grove, L. J.; Rennekamp, J. M.; Jude, H.; Connick, W. B. *J. Am. Chem. Soc.* **2004**, *126*, 1594-1595.

(25) Thompson, B. J., Ed. *In Energy, Simulation-Training, Ocean Engineering and Instrumentation: Research Papers of the Link Foundation Fellows.*; University of Rochester Press: Rochester, N.Y., **2003**; Vol. 3, pp 37-52.

(26) Jude, H. In *www. ohiolink.edu/etd/view.cgi?acc%5Fnum=ucin1077152*; University of Cincinnati: Cincinnati, OH, 2004, p 384.

(27) a) Doppiu, A., Minghetti, G., Cinellu, M.A., Stoccoro, S., Zucca, A., Manassero, M., *Organometallics*, **2001**, 1148, 6; b) Stoccoro, S., Zucca, A., Petretto, G. L., Cinellu, M.A., Minghetti, G., Manassero, M., *J. Organmet. Chem.*, **2006**, 4135.

(28) Abel, E. W.; Orrell, K. G.; Osbourne, A. G.; Pain, H. M.; Sik, V.; Hursthouse, M. B.; Malik, K. M. A. *J. Chem. Soc. Dalt. Trans.: Inorg. Chem.* **1996**, *1996*, 253-254.

(29) Abel, E. W.; Orrell, K. G.; Osbourne, A. G.; Pain, H. M.; Sik, V.; Hursthouse, M. B.; Malik, K. M. A. *J. Chem. Soc. Dalt. Trans.: Inorg. Chem.* **1994**, *23*, 3441-3449.

(30) Rotondo, E.; Giordano, G.; Minniti, D. *J. Chem. Soc. Dalt. Trans.: Inorg. Chem.* **1996**, *2*, 253.

(31) Zucca, A.; Doppiu, A.; Cinellu, M. A.; Stoccoro, S.; Minghetti, G.; Manassero, M. *Organmet.* **2002**, *21*, 783-785.

(32) Zucca, A.; Cinellu, M. A.; Minghetti, G.; Stoccoro, S.; Manassero, M. *Eur. J. Inorg. Chem.* **2004**, *22*, 4844-4490.

(33) Cardenas, D. J.; Echavarren, A. M.; Carmen Ramirez de Arellano, M. *Organmet.* **1999**, *18*, 3337-3341.

(34) Cave, G. W. V.; Fanizzi, F. P.; Deeth, R. J.; Errington, W.; Rourke, J. P. *Organometallics* **2000**, *19*, 1355-1364.

(35) Cave, G. W. V.; Hallet, A. J.; Errington, W.; Rourke, J. P. *Angew. Chem. Int. Ed.* **1998**, *37*, 3270-3272.

(36) Zhao, S.-B.; Wang, R.-Y., ;; Wang, S. *J. Am. Chem. Soc.* **2007**, *129*, 3092-3093.

(37) Bergman, R. G. *Nature* **2007**, *446*, 391-393 and references therein.

(38) Bailey, J. A. H., M. G.; Marsh, R. E.; Miskowski, V. M.; Schaefer, W. P.; Gray, H. B. *Inorg. Chem.* **1995**, *34*, 4591-4599.

(39) Halcrow, M. A. *Coord. Chem. Rev.* **2005**, *249*, 2880-2908.

Chapter 2

A Luminescent Platinum(II) 2,6-*bis*(*N*-pyrazolyl)pyridine Complex[†]

Introduction.

Since Jameson and Goldsby's report on the regulation of redox potentials of ruthenium(II) complexes with tridentate *bis*(*N*-pyrazolyl)pyridyl ligands,[2] including bpp and bdmpp, there has been growing interest in using these ligands as easily synthesized substitutes for terpyridyl chelating groups, such as tpy.[3-6] Whereas luminescent complexes with tpy ligands were well known at the time this work was first reported,[7,8] there have been no reports of emissive transition metal complexes with *bis*(*N*-pyrazolyl)pyridyl ligands. In the case of ruthenium(II) complexes, this result is not surprising since bpp is regarded as both a poorer σ-donor and π-acceptor than tpy.[2] Consequently, complexes such as $Ru(bpp)_2^{2+}$ are expected to have low-lying, triplet ligand field states (^{3}LF) that facilitate rapid non-radiative decay, decreasing the probability of radiative emission. The situation will not necessarily improve for platinum(II) complexes. In fact, low-lying ligand field states have been suggested to account for low quantum yields and short emission lifetimes of some platinum(II) terpyridyl complexes,[6d,9] though only indirect evidence for these states is presently available. For these reasons, we were surprised to observe intense emission from solid samples of the hexafluorophosphate salt of $Pt(bpp)(Ph)^+$ at 77 K. Here we report the first examples of platinum(II) complexes with *bis*(*N*-pyrazolyl)pyridyl ligands and their luminescence properties.

[†] Most of the contents of Chapter 2 appeared in a manuscript in *Inorganic Chemistry*.[1]

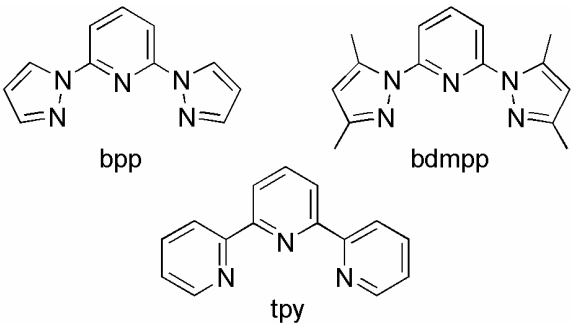

Figure 2.1. Terpyridine (tpy) and analogs, 2,6-*bis*(*N*-pyrazolyl)pyridine (bpp) and 2,6-*bis*(3,5-dimethyl-*N*-pyrazolyl)pyridine (bdmpp), of *mer*-coordinating tridentate ligands.

Experimental Section.

K_2PtCl_4 was purchased from Pressure Chemical, and COD (1,5-cyclooctadiene) was obtained from Aldrich. All other reagents were obtained from Acros. The ligands, 2,6-*bis*(*N*-pyrazolyl)pyridine (bpp)[10] and 2,6-bis(3,5-dimethyl-*N*-pyrazolyl)pyridine (bdmpp),[10] as well as Pt(COD)(Ph)Cl,[11] were prepared according to published procedures. ^{1}H NMR spectra were recorded at room temperature using a Bruker AC 250 MHz instrument. Deuterated solvents were purchased from Cambridge Isotope Laboratories. Mass spectra were obtained by electrospray ionization using either an Ionspec HiRes ESI-FTICRMS instrument or a Micromass Q-TOF-II instrument. Observed isotope patterns agreed well with predicted patterns based on natural isotopic abundancies. UV-visible absorption spectra were obtained using a HP8453 Diode Array Spectrometer. Elemental analyses were performed by Atlantic Microlab (Norcross, GA). Electrochemical measurements were recorded using a standard three-electrode cell and CV50w potentiostat from Bioanalytical Systems. Scans were recorded in distilled acetonitrile solution containing 0.1 M tetrabutylammonium hexafluorophosphate ($TBAPF_6$), which was recrystallized at least twice from methanol and dried under vacuum prior to use. All scans were

recorded using a Pt wire auxiliary electrode, a Ag/AgCl (3.0 M NaCl) reference electrode and a 0.79 mm^2 Au working electrode. Reported potentials are referenced vs. Ag/AgCl (3.0 M NaCl). Potentials for irreversible reduction couples are reported as the peak potential of the cathodic wave (E_{pc}). Reduction of these complexes resulted in a return oxidation wave at positive potentials characteristic of adsorption. Therefore, the working electrode was polished between scans with 0.05 μm alumina, rinsed with distilled water and dried using a Kimwipe. Steady-state emission data were collected using a SPEX Fluorolog-3 fluorimeter as previously described[12] and corrected for instrumental response. Emission samples for lifetime measurements were excited using 4-6 ns pulses from a Continuum Panther Optical Parametric Oscillator (500 nm, <0.3 mJ), pumped with the third harmonic (355 nm) of a Surelite II Nd:YAG laser. Emission transients were detected with a modified PMT connected to a Tektronix TD5580D oscilloscope, and data were modeled by a non-linear least squares fitting procedure using in-house software on a Microsoft Excel platform. Time-resolved emission spectra were collected using a similar setup, except the PMT/oscilloscope was replaced with an Andor DH520-25U ICCD (25 mm, 1024 x 256 pixels).

[Pt(bpp)Cl]Cl·H_2O. K_2PtCl_4 (0.50 g, 1.20 mmol) and bpp (0.30 g, 1.42 mmol) were refluxed in water (100 mL) for 4 days. The yellow-tan mixture was filtered, and the filtrate was roto-evaporated to dryness. The yellow solid was washed with ether and hexanes. Yield 0.484 g (1.01 mmol, 84%). Anal. Calcd. for $PtC_{11}H_9N_5Cl_2 \cdot H_2O$: C, 26.68; H, 2.24; N, 14.14. Found: C, 26.57; H, 2.23; N, 14.08. ^1H NMR (CD_3OD, δ): 7.04 (2 H, m), 8.05 (2 H, d, *J*=3 Hz), 8.13 (2 H, d, *J*=9 Hz), 8.65 (1 H, t, *J*=9 Hz), 9.11 (2 H, d, *J*=4 Hz). MS-ESI (acetonitrile) *m/z*: 441.014 ($Pt(bpp)Cl^+$ calc'd 441.019).

[Pt(bdmpp)Cl]Cl·H_2O. Prepared by the same procedure as for [Pt(bpp)Cl]Cl substituting the following materials: K_2PtCl_4 (0.250 g, 0.602 mmol), bdmpp (0.193 g, 0.722 mmol) and 50 mL of water. Yield 0.223 g (0.418 mmol, 69%). Anal. Calcd. for $PtC_{15}H_{17}N_5Cl_2·H_2O$: C, 32.68; H, 3.47; N, 12.70. Found: C, 32.43; H, 3.27; N, 12.65. ^{1}H NMR (CD_3OD, δ): 2.49 (6 H, s), 3.30 (6 H, s), 6.59 (2 H, s), 7.91 (2 H, d, *J*=9 Hz), 8.51 (1 H, dd, *J*=9, 9 Hz). MS-ESI (acetonitrile) *m/z*: 498.077 ($Pt(bdmpp)Cl^+$ calc'd 498.081).

[Pt(bpp)(Ph)](PF_6). A mixture of 0.246 g (0.592 mmol) Pt(COD)(Ph)Cl and 0.150 g (0.593 mmol) $AgPF_6$ in 10 mL of acetone was stirred at room temperature for 30 min in the dark. The mixture was filtered, and 0.125 g (0.592 mmol) bpp were added to the filtrate. The pale yellow solution was stirred for 1 day at room temperature and reduced to dryness by rotary evaporation to give a yellow-orange solid. The crude product was recrystallized from acetonitrile and diethyl ether. Yield 0.247 g (0.393 mmol, 66%). Anal. Calcd. for $PtC_{17}H_{14}N_5PF_6$: C, 32.49; H, 2.25; N, 11.15. Found: C, 32.58; H, 2.25; N, 11.27. ^{1}H NMR (CD_3CN, δ): 6.89 (2 H, dd, *J*=3, 3 Hz, with Pt satellites, $J_{H\text{-}Pt}$=16 Hz), 7.18 (3 H, m), 7.49 (2 H, d, *J*=7 Hz, with Pt satellites, $J_{H\text{-}Pt}$=33 Hz), 7.93 (4 H, m, *J*=9 Hz), 8.53 (1 H, dd, *J*=9, 9 Hz), 8.76 (2 H, d, *J*=3 Hz). MS-ESI (acetonitrile) *m/z*: 483 ($Pt(bpp)(Ph)^+$ calc'd 483).

[Pt(bdmpp)(Ph)](PF_6). Prepared by the same procedure as for [Pt(bpp)(Ph)](PF_6), substituting the following materials: 0.200 g (0.481 mmol) Pt(COD)(Ph)Cl, 0.122 g (0.483 mmol) $AgPF_6$, 10 mL of acetone, and 0.129 g (0.483 mmol) bdmpp. Yield 0.131 g (0.191 g, 40%). Anal. Calcd. for $PtC_{21}H_{22}N_5PF_6$: C, 36.85; H, 3.24; N, 10.23. Found: C, 36.85; H, 3.11; N, 9.91. ^{1}H NMR (CD_3CN, δ): 1.71 (6 H, s), 2.78 (6 H, s), 6.31 (2H, s, with Pt satellites, $J_{H\text{-}Pt}$=19 Hz), 6.96 (1 H, t, *J*=7 Hz), 7.11 (2 H, dd, *J*=7, 7 Hz), 7.55 (2 H, d, *J*=8 Hz, with Pt

satellites $J_{H\text{-}Pt}$=33 Hz), 7.78 (2 H, d, *J*=8 Hz), 8.35 (1 H, dd, *J*=9, 9 Hz). MS-ESI (acetonitrile) *m/z*: 539.155 (Pt(bdmpp)(Ph)$^+$ calc'd 539.153).

X-ray Crystallography. Crystals of [Pt(bpp)Cl]Cl·2H_2O were grown by slow evaporation of a methanol solution, and intensity data were collected using a Bruker SMART 1K CCD diffractometer. Crystals of [Pt(bpp)(Ph)](PF_6)·CH_3CN were grown by diffusion of ether into an acetonitrile solution, and intensity data were collected using a SMART6000 CCD diffractometer. For both crystals, graphite-monochromated Mo Kα radiation (λ = 0.71073 Å) was used. Data frames were processed using the SAINT program,[13] and reflection data were corrected for decay, Lorentz and polarization effects. Absorption and beam corrections were applied based on the multiscan technique using SADABS.[14] For the chloro complex, the structure was solved by a combination of direct methods using SHELXTL v5.03[15] and the difference Fourier technique. For the phenyl complex, the structure was solved by a combination of the Patterson method using SHELXTL v6.12[15] and the difference Fourier technique. In both cases, the models were refined by full-matrix least squares on F^2. Non-hydrogen atoms were refined with anisotropic parameters. Ligand based H atoms were located either directly or calculated based on geometric criteria. The isotropic factors for H atoms were defined as 1.2 times U_{eq} of the adjacent atom. The water H atoms for [Pt(bpp)Cl]Cl·2H_2O were held fixed where located with minor adjustment to the positions of H30 and H31. The U_{iso} was set at 0.05. For [Pt(bpp)(Ph)](PF_6)·CH_3CN, the PF_6^- counterion shows typical disorder. Crystallographic data are summarized in Tables 2.1 and 2.2.

Table 2.1. Crystallographic Data for [Pt(bpp)Cl]Cl·2H_2O and [Pt(bpp)(Ph)](PF_6)·CH_3CN.

	[Pt(bpp)Cl]Cl·2H_2O	[Pt(bpp)(Ph)](PF_6)·CH_3CN
formula	$[C_{11}H_9N_5ClPt]Cl·2H_2O$	$[C_{17}H_{14}N_5Pt]PF_6·CH_3CN$
fw, g/mol	513.25	669.45
space group	$P2_1/n$	$P\bar{1}$
a, Å	11.3218(5)	8.3620(3)
b, Å	6.7716(3)	10.7185(4)
c, Å	20.6501(6)	13.4273(5)
α, °	90	96.057(1)
β, °	105.883(2)	104.175(1)
γ, °	90	110.046(1)
V, Å^3	1522.73(11)	1072.16(7)
ρ_{calcd} (g cm^{-3})	2.239	2.074
μ, mm^{-1}	9.576	6.690
Z	4	2
T, K	150(2)	150(2)
reflns collected	15406	14810
ind reflns	3735	5330
R_{int}	0.0591	0.0245
GOF on F^2	1.034	1.040
$R1/wR2$ [$I > 2\sigma(I)$][a]	0.0310/0.0727	0.0218/0.0498
$R1/wR2$ (all data)[a]	0.0529/0.0825	0.0277/0.0521

[a] $R1 = \Sigma ||F_o| - |F_c|| / \Sigma |F_o|$; $wR2 = [\Sigma w(F_o^2 - F_c^2)^2 / \Sigma w(F_o^2)^2]^{1/2}$

Results and Discussion.

Synthesis and Characterization. The chloride salts of the two chloro complexes, $Pt(bpp)Cl^+$ and $Pt(bdmpp)Cl^+$, were prepared by refluxing the free *bis*(*N*-pyrazolyl)pyridine ligands with K_2PtCl_4. The hexafluorophosphate salts of phenyl derivatives, $Pt(bpp)(Ph)^+$ and $Pt(bdmpp)(Ph)^+$, were prepared by allowing $Pt(COD)(Ph)Cl$[11] to react with silver hexafluorophosphate. After removal of silver chloride by filtration, one equivalent of bpp or bdmpp was added to give $Pt(bpp)(Ph)^+$ or $Pt(bdmpp)(Ph)^+$, respectively. All four compounds gave satisfactory elemental analyses and mass spectra. Both chloro products were found to retain one equivalent of H_2O with tenacity reminiscent of $[Pt(tpy)Cl]Cl{\cdot}2H_2O$.[16] The ^1H NMR spectra exhibit the expected patterns of resonances. For each complex, characteristic doublet and triplet pyridyl proton resonances occur in the ranges of 7.2-8.2 and 8.4-8.7 ppm, respectively. In the case of the bpp complexes, resonances for the β-pyrazolyl protons occur between 6.3 and 7.0 ppm and show only weak splitting. For the phenyl derivatives, resonances for the phenyl protons occur from 6.9 ppm to 7.6 ppm. Distinct ^{195}Pt satellites are associated with the α-proton resonances ($J_{Pt\text{-}H}$=33 Hz). Surprisingly, ^{195}Pt satellites also are resolved for the β-pyrazolyl proton resonance in the spectrum of $[Pt(bdmpp)(Ph)](PF_6)$, resulting from four bond coupling ($J_{Pt\text{-}H}$=19 Hz).

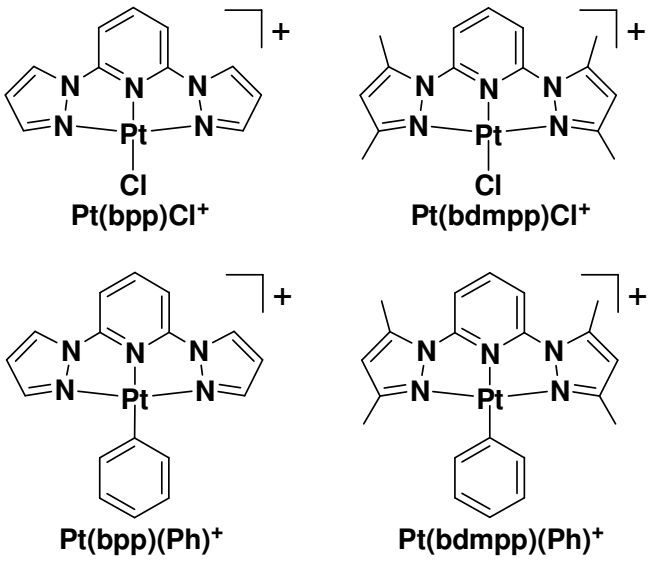

Figure 2.2. Line drawings of the four cationic platinum complexes.

Crystal Structures. The molecular structures of the cations $Pt(bpp)Cl^+$ and $Pt(bpp)(Ph)^+$ were confirmed by X-ray crystallographic studies of crystals of $[Pt(bpp)Cl]Cl{\cdot}2H_2O$ and $[Pt(bpp)(Ph)](PF_6){\cdot}CH_3CN$ at 150 K. ORTEP diagrams are shown in Figures 2.3 and 2.4, and data are summarized in Tables 2.1 and 2.2.

In both crystals, the bpp ligands adopt a tridentate coordination geometry, bonding to the Pt center through two pyrazolyl N atoms and the pyridine N atom to give a nearly planar Pt(bpp) unit. The fourth coordination site is occupied by the anionic ligand. Bond distances and angles of the cations are normal.[17] The central Pt-N1 distance is shorter than the peripheral Pt-N3 and Pt-N5 distances, as expected for the constrained bite angle of the bpp ligand.[5] The Pt-N1 distance is shorter for the chloro complex (1.950(4) Å) than for the phenyl derivative (1.999(3) Å), in keeping with the relative *trans* influence of the anionic ligands. The resulting N3-Pt-N5 angles (chloro, 161.3(2)°; phenyl, 158.7(1)°) lie outside the range observed for Ru(II) complexes with similar ligands (154.9-158.0°),[2a-c,4,5] but in the case of the chloro complex, the value is

Table 2.2. Selected Distances (Å) and Angles (°) for [Pt(bpp)Cl]Cl·2H_2O and [Pt(bpp)(Ph)](PF_6)·CH_3CN.

	[Pt(bpp)Cl]Cl·2H_2O	[Pt(bpp)(Ph)](PF_6)·CH_3CN
Pt-N1	1.950(4)	1.999(3)
Pt-N3	2.000(5)	2.012(3)
Pt-N5	1.991(5)	2.006(2)
Pt-L[a]	2.298(1)	2.007(3)
N1-C6	1.331(6)	1.334(4)
N1-C2	1.337(7)	1.334(4)
N2-C6	1.421(7)	1.407(4)
N4-C2	1.408(6)	1.402(4)
N2-N3	1.400(6)	1.393(4)
N4-N5	1.391(6)	1.390(4)
N1-Pt-N5	80.6(2)	79.39(10)
N1-Pt-N3	80.7(2)	79.34(10)
N5-Pt-N3	161.3(2)	158.73(11)
N1-Pt-L[a]	178.91(13)	176.38(10)
N5-Pt-L[a]	98.35(14)	101.26(12)
N3-Pt-L[a]	100.34(14)	99.97(11)
C6-N1-Pt	119.3(4)	118.7(2)
C2-N1-Pt	118.7(3)	118.6(2)
N3-N2-C6	118.1(4)	118.7(3)
N5-N4-C2	117.9(4)	119.1(2)
N2-N3-Pt	110.8(3)	111.82(18)
N4-N5-Pt	111.4(3)	111.68(19)

[a] L = chlorine (Cl1) for [Pt(bpp)Cl]Cl·2H_2O and carbon (C13) for [Pt(bpp)(Ph)](PF_6)·CH_3CN

comparable to those observed for $Pt(tpy)Cl^+$ salts ($CF_3SO_3^-$, 161.8(2)°;[8a] ClO_4^-, 163.5(7), 161.2(6)°).[8] Similarly, the N1-Pt-N3 and N1-Pt-N5 angles (79.3-80.7°) for $Pt(bpp)Cl^+$ and $Pt(bpp)(Ph)^+$ are less acute than those generally observed for Ru(II) complexes (77.3-79.6°),[2a-c,4,5] but smaller than observed for $Pt(tpy)Cl^+$ salts (79.8-82.6°),[8,8a,18] in agreement with the relative ligand bite angles.[17]

In crystals of $[Pt(bpp)Cl]Cl\cdot 2H_2O$, the approximately square planar $Pt(bpp)Cl^+$ cations stack in a head-to-tail fashion to give columns parallel to the *b* axis (Figure 1b). Consecutive complexes along the stack are related by an inversion center, resulting in spacings of approximately 3.33 Å between the coordination planes, defined by the Pt atom and the four coordinating atoms. The stacking arrangement results in a nearly linear chain of Pt atoms (Pt···Pt···Pt, 170.2°) with alternating short Pt···Pt distances (3.39, 3.41 Å) that are characteristic of platinum(II) linear-chain structures with intermolecular metal···metal interactions.[19] The salt crystallizes as a dihydrate, resulting in a hydrogen-bonding network linking the anion and water subunits. The hydrogen bonding scheme was inferred from short intermolecular contacts between the chloride anion (Cl2) and water O atoms, Cl2···O1 (3.204(5) Å) and Cl2···O2 (3.172(5), 3.203(5) Å), as well as between the two water O atoms, O1···O2 (2.982(7) Å). There also are short contacts between the bpp H atoms and the Cl atoms, C4···Cl1 (3.456(6) Å), C5···Cl2 (3.648(6) Å) and C10···Cl1 (3.548(7) Å), as well as between the bpp H atoms and the water groups, C8···O1 (3.423(8) Å), C9···O1 (3.432(8) Å) and C12···O2 (3.483(8) Å).

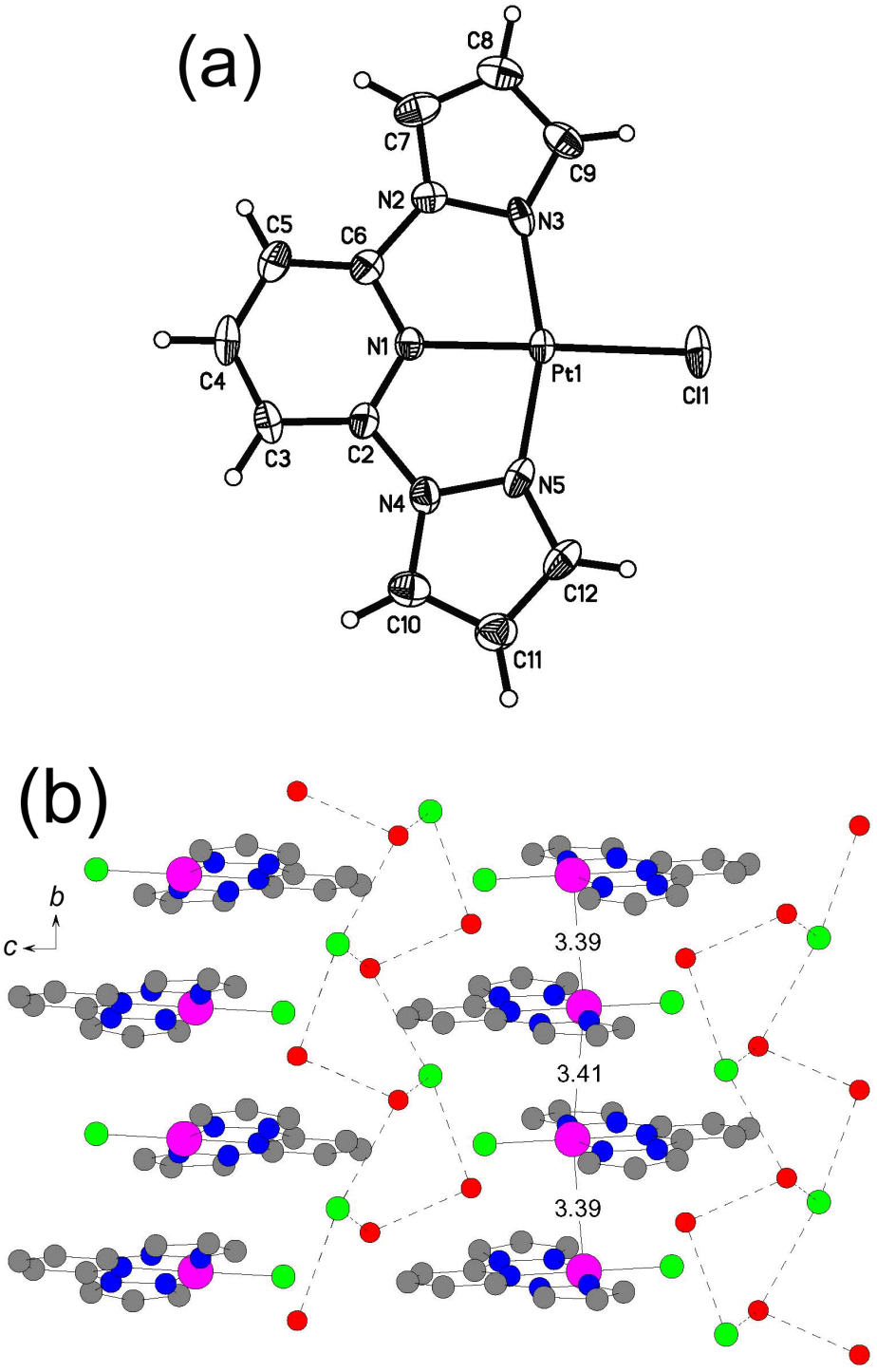

Figure 2.3. (a) ORTEP diagram of the cation in crystals of [Pt(bpp)Cl]Cl·2H_2O with 50% probability ellipsoids, and (b) diagram showing columnar packing parallel to *b* axis with Pt···Pt spacings of 3.39 and 3.41 Å. H-atoms omitted for clarity.

In crystals of $[Pt(bpp)(Ph)](PF_6)\cdot CH_3CN$, the $Pt(bpp)(Ph)^+$ cations also stack in a head-to-tail fashion, forming columns parallel to the *a* axis (Figure 2b). The coordination plane is slightly canted with respect to the *bc* plane, resulting in a 19.3(1)° dihedral angle. Consecutive complexes along the stack are related by an inversion center, resulting in alternating interplanar spacings of ~4.38 and ~4.58 Å. The resulting Pt···Pt separations of 4.48 and 4.71 Å are considerably longer than observed for crystals containing $Pt(bpp)Cl^+$. Nevertheless, it is noteworthy that the approximately planar phenyl group forms a 36.9(2)° dihedral angle with the coordination plane. This value lies outside the 55° to 90° range typically observed for platinum(II) phenyl complexes with bidentate or tridentate ligands.[20,21] Kaim *et. al.* have suggested that a dihedral angle of ~60° between the pyridyl and phenyl rings in $Pt(diimine)(Ph)_2$ complexes provides optimal overlap between the phenyl rings and the π-system of the diimine ligand.[21] The angle for $Pt(bpp)(Ph)^+$ is remarkably similar to that found for two $Pt(Ph)_2$ units bridged by 1,2,4,5-tetra(1-N7-azaindolyl)benzene (36.0°), in which intramolecular steric constraints presumably are responsible for the relatively small angle.[22] Similarly, it is conceivable the relatively acute angle found for $Pt(bpp)(Ph)^+$ is a consequence of the compressed columnar packing arrangement of the cations.

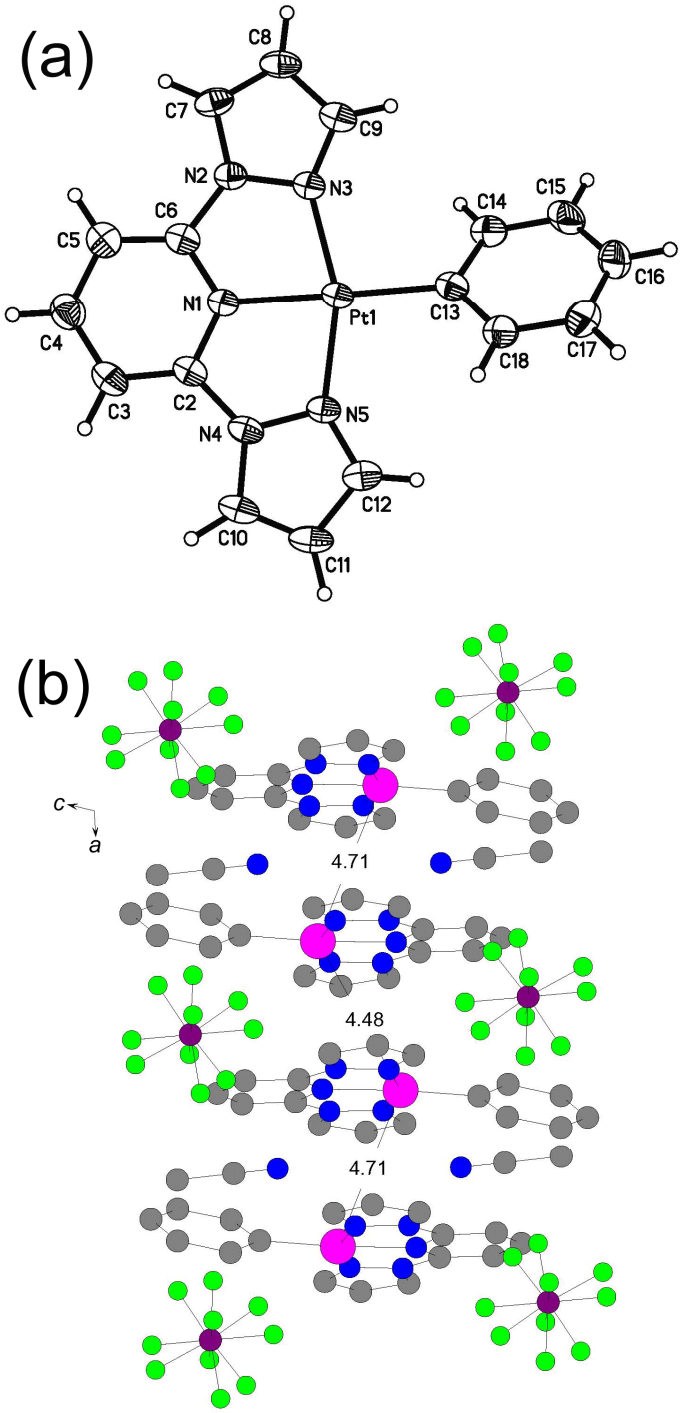

Figure 2.4. (a) ORTEP diagram of the cation in crystals of [Pt(bpp)(Ph)](PF_6)·CH_3CN with 50% probability ellipsoids, and (b) diagram showing columnar packing parallel to *a* axis with Pt···Pt spacings of 4.48 and 4.71 Å. H-atoms omitted for clarity.

Cyclic Voltammetry. To investigate the electronic properties of these complexes, their cyclic voltammograms were recorded in 0.1 M $TBAPF_6$ acetonitrile solution. None of the complexes was oxidized at <1.0 V vs. Ag/AgCl. However, all four compounds underwent a chemically irreversible process between -1.0 and -1.3 V (0.25 V/s). Even at 50 V/s, the reductions were completely irreversible. For the chloro complexes, a second irreversible process occurred near -1.45 V. The -1.0 to -1.3 V processes involve reduction of the *bis*(*N*-pyrazolyl)pyridine ligand and/or reduction of the metal center. Distinguishing between these two possibilities is presently difficult, in part because the observed processes are irreversible and the E_{pc} values do not necessarily represent thermodynamic potentials. In addition, both the unoccupied ligand π* and $d_x2_{-y}2$(Pt) levels are arguably accessible at these potentials. To illustrate this point, we can obtain crude estimates of the relative orbital energies from accumulated electrochemical data. The cyclic voltammogram of $Ru(bpp)_2^{2+}$ exhibits an irreversible ligand-centered reduction wave at -1.66 V vs. SSCE (0.1 M $TBAF_6/CH_3CN$).[2] $Ru(tpy)_2^{2+}$ is reversibly reduced at more positive potentials (-1.25 V vs. SSCE;[2] -1.26 V vs. Ag/AgCl (1.0 M KCl), 0.1 M $TBAPF_6$/DMF),[23] reflecting the relative energies of the π*(bpp) and π*(tpy) orbitals when bonded to Ru(II).[2] In the case of $Pt(tpy)Cl^+$ in DMF, ligand-centered reduction occurs at -0.74 V vs. Ag/AgCl (1.0 M KCl).[23] Hill and coworkers[23] have attributed the 0.52 V anodic shift of the $Pt(tpy)Cl^+$ reduction potential with respect to that of $Ru(tpy)_2^{2+}$ to stabilization of the π*(tpy) levels as a result of mixing with the $6p_z$(Pt) orbital.[23] Similar stabilization of the π*(bpp) level of $Pt(bpp)Cl^+$ with respect to $Ru(bpp)_2^{2+}$ would shift the thermodynamic reduction potential of the platinum complex to -1.14 V vs. SSCE, in the vicinity of the irreversible reductions observed for this series of platinum(II) *bis*(*N*-pyrazolyl)pyridyl complexes. On the other hand, $Pt(tpy)Cl^+$ undergoes a second chemically reversible reduction in

DMF at -1.30 V, generally attributed to addition of an electron to the $d_x2_{-y}2$(Pt) orbital.[23,24] From Hill and coworkers' 0.38 eV estimate for the energy gap between π*(tpy) and $d_x2_{-y}2$(Pt) levels[25] and assuming similar crystal field strengths, we obtain a crude estimate of -1.12 V vs. Ag/AgCl (1.0 M KCl) for the one-electron reduction of the $d_x2_{-y}2$(Pt) orbital. The reduction could be expected to occur at even more positive potentials for $Pt(bpp)Cl^+$ since bpp is weaker σ-donor than tpy.

Though the observed reductions are irreversible, it is noteworthy that within this series of platinum(II) *bis*(*N*-pyrazolyl)pyridyl complexes, the peak potentials follow expected trends based on inductive effects, which are expected to shift the energies of the $d_x2_{-y}2$(Pt) and π*(bpp) levels in the same direction. Reduction of the bdmpp complexes is slightly less favorable than their bpp counterparts. Similarly, reduction of the phenyl derivatives is ~0.2 V less favorable than the chloro complexes, as expected for the relative donor properties of the ancillary ligands. Overall, the reduction potentials of these complexes are cathodically shifted from those of related Pt(II) terpyridyl complexes,[8b-d,23,26] including $Pt(tpy)(Ph)^+$ (-0.91, -1.42 V vs. Ag/AgCl, 1.0 M $TBAPF_6/CH_3CN$),[27] in keeping with the established view that the bpp ligand is a weaker π-acceptor than tpy.

Absorption Spectroscopy. The yellow complexes dissolve to give pale yellow methanol solutions, and their UV-visible absorption spectra are reported in Table 2.3 and Figure 2.5. The UV region for each complex is dominated by strong absorptions from 230-330 nm. The spectra of the free ligands confirm that ligand-centered bands occur in this region, though other charge-transfer transitions also may contribute significant intensity. As observed for the four platinum(II) complexes, the spectrum of Ru(bpp)(1,3-dimethyl-β-diketonate)Cl^+ exhibits an intense absorption near 270 nm (~27,000 $M^{-1}cm^{-1}$),[6,28] suggesting this transition is centered on

the *bis*(*N*-pyrazolyl)pyridine ligand.[29] For comparison, coordination of 2,2'-bipyridine to an acidic metal center is known to result in intense and structured π-π* absorption in the vicinity of 290-310 nm that is very different than observed in the spectrum of the free ligand.[30] Related transitions in the spectra of all four platinum(II) complexes are expected to be essentially unperturbed by the electronic properties of the monodentate ligand. For the two bdmpp complexes, a band occurs near 330 nm (12,000-15,000 $M^{-1}cm^{-1}$) with a shoulder at ~317 nm. The relative insensitivity of this band to the donor properties of the monodentate ligand and to solvent (*e.g.*, $Pt(bdmpp)(Ph)^+$: CH_3OH, 330 nm; CH_2Cl_2; 333 nm) is suggestive of a bdmpp-centered π-π* transition. The corresponding transition in the bpp complex may occur at shorter wavelengths, possibly associated with the feature near 320 nm, coincident in the spectra of $Pt(bpp)Cl^+$ and $Pt(bpp)(Ph)^+$.

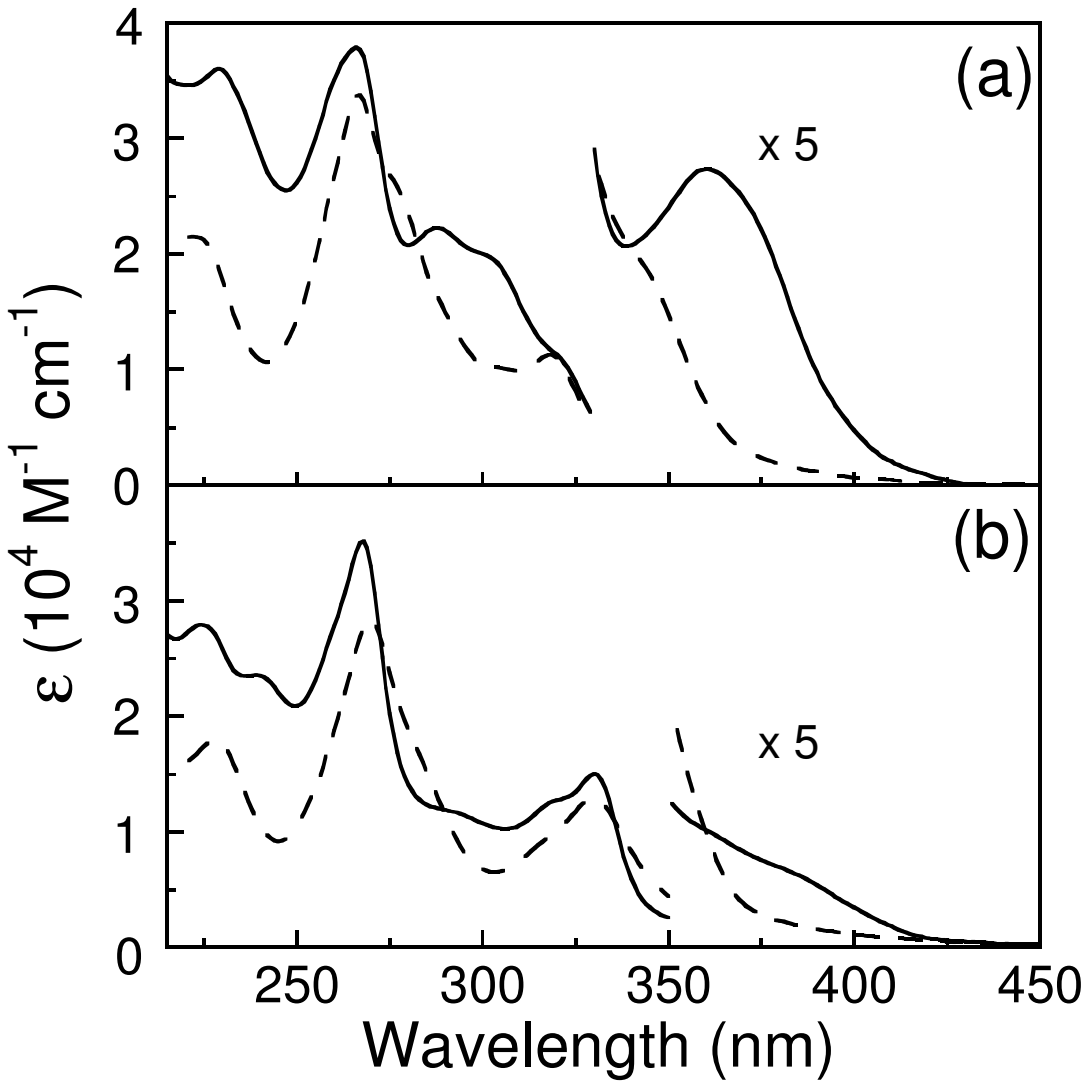

Figure 2.5. UV-visible absorption spectra of salts of (a) $Pt(bpp)(Cl)^+$ (-----), $Pt(bpp)(Ph)^+$ (——), (b) $Pt(bdmpp)(Cl)^+$ (-----), and $Pt(bdmpp)(Ph)^+$ (——) in methanol solution.

At longer wavelengths (λ>330 nm), the bpp complexes exhibit an additional absorption band, whereas the bdmpp complexes exhibit a tailing absorption profile. For both $Pt(bpp)(Ph)^+$ and $Pt(bdmpp)(Ph)^+$, the phenyl complexes absorb at longer wavelengths than the chloro adducts.

Table 2.3. UV-Visible Absorption[a] and Electrochemical Data[b] for [Pt(bpp)Cl]Cl, [Pt(bdmpp)Cl]Cl, [Pt(bpp)(Ph)](PF_6), and [Pt(bdmpp)(Ph)](PF_6).

Compound	Absorption λ_{max}, nm (ε, $cm^{-1}M^{-1}$) [a]	E_{pc}, V[b]
bpp	239 (27700), 245 (34000), 264 (12300), 270sh (11300), 301(18700)	–
bdmpp	247 (22700), 265sh (11000), 295(14400)	–
[Pt(bpp)Cl]Cl	222 (21500), 267 (33800), 278 (25200), 318(11300), 340sh (4100)	-1.07, -1.44
[Pt(bpp)(Ph)](PF_6)	229 (36000), 266 (37800), 288 (22300), 300sh (20000), 320sh (11300), 360 (5500)	-1.24
[Pt(bdmpp)Cl]Cl	228 (17900), 270 (28400), 316sh (9100), 330 (12900)	-1.12, -1.48
[Pt(bdmpp)(Ph)](PF_6)	224 (27900), 239 (23500), 268 (35100), 295sh (11400), 318sh (12500), 330 (14800)	-1.34

[a] in methanol solution; [b] cyclic voltammograms were recorded in 0.1 M $TBAPF_6$/acetonitrile at 0.25 V/s and referenced vs. Ag/AgCl (3.0 M NaCl).

Interpretation is complicated by the prospect that in addition to *bis*(*N*-pyrazolyl)pyridine-centered transitions, metal-to-ligand(*bis*(*N*-pyrazolyl)pyridine) charge transfer (MLCT), chloride or phenyl ligand-to-metal charge-transfer (LMCT), and chloride or phenyl ligand-to-ligand(*bis*(*N*-pyrazolyl)pyridine) charge transfer (LLCT) transitions can conceivably occur in this region.[31,32] Additionally, Klein, Záliš, van Slageren, Kaim and coworkers[33] have noted that orbital mixing in related platinum(II) complexes can result in excited states with significant admixtures of these states.

The absorption shift to longer wavelengths associated with substitution of the chloro ligand with more electron releasing phenyl groups is consistent with stabilization of MLCT, LMCT and LLCT states. In the case of $Pt(bpp)(Ph)^+$, a distinct, solvent-sensitive band maximizes at 360 nm (CH_3CN: 359 nm, 7000 $M^{-1}cm^{-1}$; CH_2Cl_2: 377 nm, 5800 $M^{-1}cm^{-1}$). Though a definitive assignment is not possible, the bandshape is suggestive of vibronic structure, resulting from *bis*(*N*-pyrazolyl)pyridyl involvement. The bathochromic shift with decreasing solvent polarity and the band intensity resemble the lowest spin-allowed metal-to-ligand(tpy) charge-transfer transition of $Pt(tpy)Cl^+$ (CH_3CN, 377, 2200 $M^{-1}cm^{-1}$, 390sh; CH_2Cl_2: 388sh, 405 nm).[8b,d] Thus, in keeping with the notion of a relatively low-lying unoccupied bpp π^* orbital, this band is tentatively assigned as having significant charge-transfer-to-ligand(bpp) character. The corresponding transition in the spectrum of $Pt(bpp)Cl^+$ must occur at wavelengths <345 nm, shifted at least 0.28 eV to the blue of that observed for $Pt(tpy)Cl^+$.[8b,d] For $Pt(bpp)(Ph)^+$ in alcohol solution, the transition is shifted by ~0.5 eV to the blue of that observed for $Pt(tpy)(Ph)^+$ (4:1 methanol:ethanol, λ_{max}=424 nm, 2000 $M^{-1}cm^{-1}$),[34] in accord with the view that the poorer σ-donor and π-acceptor properties of bpp will tend to destabilize MLCT states. Similar features are less pronounced and apparently weaker in the spectra of $Pt(bdmpp)(Ph)^+$. However, in CH_2Cl_2 solution, a distinct shoulder is evident near 380 nm (2000 $M^{-1}cm^{-1}$), suggesting a transition energy similar to that of the bpp complex. Evidently destabilization of the π^* level by the methyl groups of the bdmpp ligand is approximately offset by increased electron-donation to the metal center.

Emission Spectroscopy. At room temperature, emissions from solution and solid samples of each of the four complexes under UV irradiation are exceedingly weak. Even upon cooling to 77 K, salts of $Pt(bpp)Cl^+$, $Pt(bdmpp)(Ph)^+$ and $Pt(bdmpp)Cl^+$ only exhibit very weak

emissions that could not be reliably recorded. In contrast, the emission from solid [Pt(bpp)(Ph)](PF_6) is a remarkably intense pink color at 77 K, and this observation prompted further investigation.

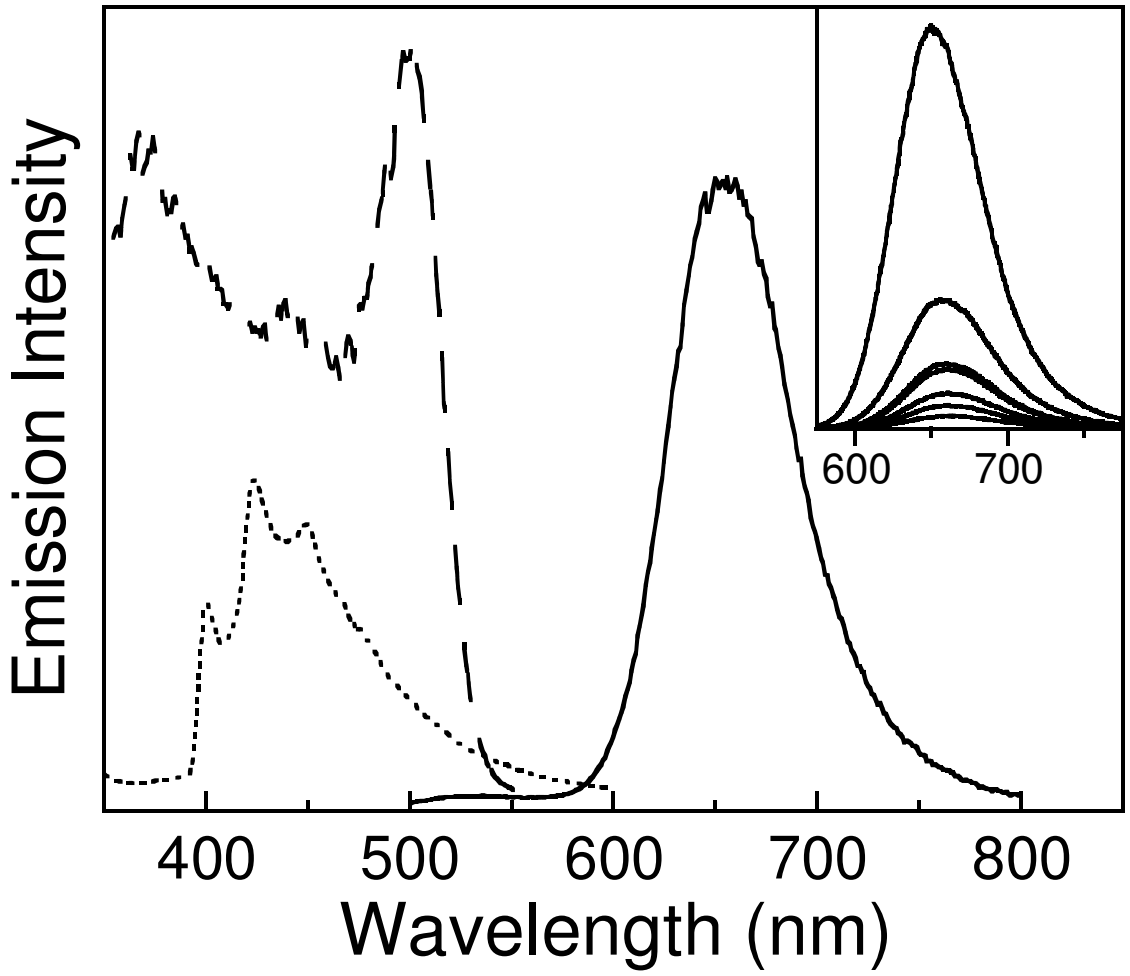

Figure 2.6. 77 K emission (——, λ_{ex}=410 nm) and excitation (— — —, λ_{em}=640 nm) spectra of solid [Pt(bpp)(Ph)](PF_6) and emission spectrum of a butyronitrile glassy solution (-----, λ_{ex}=330 nm). Inset shows time-resolved emission spectra recorded during 90 ns integration windows at 500 ns intervals from (0-4 μs), following a 500 nm excitation pulse.

The emission from 77 K solid samples of [Pt(bpp)(Ph)](PF_6) is centered at 655 nm (Figure 2.6). The maximum is independent of excitation wavelength, and the band is nearly symmetrical and relatively narrow as indicated by the full-width-at-half-maximum (FWHM) of ~1660 cm^{-1}. The excitation spectrum is not consistent with the solution absorption spectrum, showing significant emission intensity for excitation wavelengths as long as 520 nm. Notably, the lowest-energy band in the excitation spectrum occurs near 500 nm with an estimated FWHM of ~1200 cm^{-1}. Interestingly, the solid still appeared yellow at 77 K. When the sample was removed from the liquid nitrogen bath and allowed to warm slightly above 77 K, the emission intensity weakened considerably. Luminescence lifetime measurements show that the 77 K emission signal decay is not single-exponential. The data are adequately described with a biexponential function corresponding to emission lifetimes of approximately 120 and 1550 ns, consistent with a predominantly spin-forbidden process. Despite the complex decay kinetics, time-resolved emission spectra indicate the shape of the emission profile remains essentially constant during the decay, though the maximum undergoes a gradual shift from 650 nm to 660 nm during the first several hundred nanoseconds (Figure 2.6). The emission properties of a 10^{-4} M butyronitrile 77 K glassy solution of $Pt(bpp)(Ph)^+$ are strikingly different. The emission is exceedingly weak, but discernibly shifted to much shorter wavelengths (λ_{max}=401, 424, 450 nm; Figure 4) than that of the solid. The apparent vibronic structure with spacings of ~1350 cm^{-1} is suggestive of emission originating from a lowest ligand-centered π-π^* state.

The accumulated data are largely consistent with the presence of intermolecular interactions in low temperature solid samples of [Pt(bpp)(Ph)](PF_6) that perturb the emission properties of the complexes. The 77 K emission properties of solid [Pt(bpp)(Ph)](PF_6) bear a striking qualitative resemblance to those of dimers[35,36] and linear chain materials[8a,37,38] composed

of weakly interacting platinum(II) complexes. In these materials, the occupied $5d_z2$(Pt) orbitals of adjacent complexes interact to form an antibonding (dσ*) HOMO, as well as a lower-energy, bonding (dσ) molecular orbital. Similar interactions between unoccupied $6p_z$ levels of adjacent complexes yield pσ and pσ* molecular orbitals, and intense emission from these solids often originates from a lowest ^{3}(dσ*→pσ) state. In the case of platinum(II) terpyridyl complexes, the LUMO has mostly π*(tpy) character, and the resulting intense emission arises from a lowest ^{3}(dσ*→π*) state.[37] For both classes of these materials, the ~80 K emission profiles tend to be nearly symmetrical with FWHM of 1000-1600 cm^{-1}.[35,36,8a,37,38] At first glance, either of these excited states seems a tempting candidate for assignment of the emission from [Pt(bpp)(Ph)](PF_6).[39] The excitation band at 500 nm could be reasonably assigned as the corresponding spin-allowed absorption, which is consistent with typical Stokes shifts and apparent singlet-triplet splittings in chain materials.[40] However, a troubling inconsistency is the absence of unusually short intermolecular interactions in crystals of [Pt(bpp)(Ph)](PF_6) at 150 K. In fact, the shortest Pt···Pt interactions are considerably longer (4.48, 4.71 Å) than those of crystalline [Pt(bpp)Cl]Cl·$2H_2O$ (3.39, 3.41 Å), which is an exceedingly weak emitter. One possibility is that crystals of [Pt(bpp)(Ph)](PF_6) undergo a phase change below 150 K, resulting in an arrangement of cations having significantly shorter Pt···Pt distances. Indeed, phase changes in linear chain materials are well documented;[41] however in the present case there is no corroborating evidence to thoroughly support this suggestion. Variable temperature results for crystals of the [Pt(bpp)(Ph)](PF_6) complex were recorded from 150 to 85 K (Tables 2.4-2.6). The data suggest that the unit cell parameters do not vary and the crystal symmetry remains triclinic. Furthermore, the bonding parameters (distances, angles and torsions) do not vary appreciably. Therefore, there is no data supporting a phase change or rearrangement over the

temperature range studied. Unfortunately, we were not able to record data from 85 to 77 K. Furthermore, the lowering of temperatures below 85K results in an intense emission and a substantial decrease in non-radiative decay. This is observed when the solid sample is cooled in liquid nitrogen. Under UV radiation, the sample rapidly loses its bright pink intensity when removed and allowed to warm to room temperature.

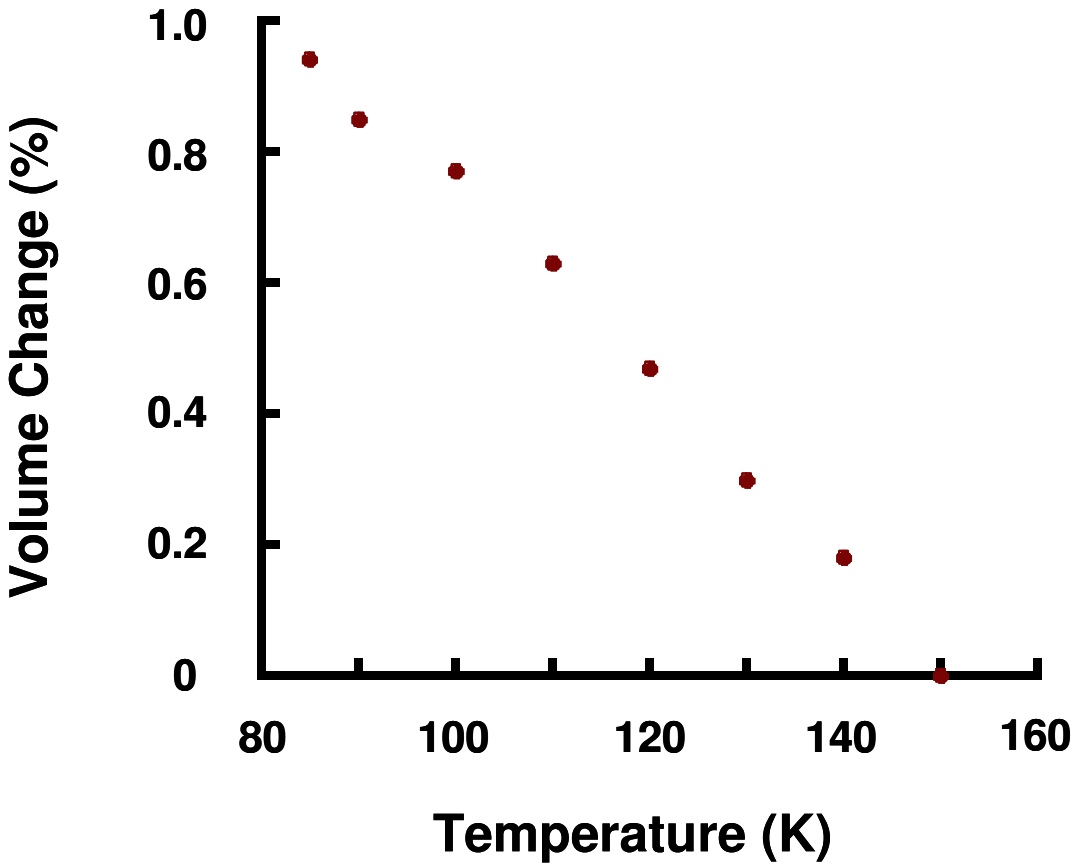

Figure 2.7. Percent volume change of the crystal lattice of the [Pt(bpp)(Ph)](PF_6) complex recorded from 150 to 85 K.

The intense emission from 77 K samples of solid [Pt(bpp)(Ph)](PF_6) contrasts sharply with the relatively broad and weak ^{3}LF emissions observed for many platinum(II)

complexes.[12,42,43] Low-lying LF excited states has been proposed to account for low quantum yields and short emission lifetimes of some platinum(II) terpyridyl complexes,[6d,9] and a similar explanation for weak emission from several of these platinum(II) *bis*(*N*-pyrazolyl)pyridyl complexes also may apply. In the case of [Pt(bpp)(Ph)](PF_6), assuming the emission originates from the lowest excited state, we can confidently conclude that the lowest LF states for this complex must be near or at higher energies than the emission onset ($\leq$16900 cm^{-1}).[44] The relative donor properties of the bpp and tpy ligands suggest that the lowest LF states of platinum(II) terpyridyl complexes are likely to lie at even higher energies than those of related bpp complexes.

Table 2.4. Crystallographic Data for [Pt(bpp)(Ph)](PF_6)·CH_3CN from 150-85 K.

Temperature	**85K**	**90K**	**100K**	**110K**	**120K**	**130K**	**140K**	**150K**	**150K**[a]
Crystal system	Triclinic	Triclinic	Triclinic	Triclinic	Triclinic	Triclinic	Triclinic	Triclinic	Triclinic
Space group	P-1	P-1	P-1	P-1	P-1	P-1	P-1	P-1	P-1
a, Å	8.2823(4)	8.2887(4)	8.3002(4)	8.3145(4)	8.3279(3)	8.3416(3)	8.3533(2)	8.3656(2)	8.3620(3)
b, Å	10.7626(5)	10.7603(5)	10.7479(5)	10.7390(5)	10.7338(4)	10.7319(4)	10.7244(3)	10.7210(3)	10.7185(4)
c, Å	13.3127(6)	13.3240(6)	13.3403(6)	13.3592(6)	13.3766(5)	13.3923(4)	13.4072(3)	13.4200(4)	13.4273(5)
α, deg	95.867(2)	95.864(2)	95.893(2	95.915(2)	95.931(2)	95.963(1)	95.996(1)	96.018(1)	96.057(1)
β, deg	102.906(2)	103.002(2)	103.185(2)	103.398(2)	103.608(2)	103.796(1)	103.956(1)	104.090(1)	104.175(1)
γ, deg	110.400(2)	110.395(2)	110.326(2)	110.273(2)	110.223(2)	110.176(1)	110.113(1)	110.043(1)	110.046(1)
Volume, $Å^3$	1062.89(9)	1063.88(9)	1064.78(9)	1066.29(9)	1067.94(7)	1069.84(6)	1071.14(5)	1073.03(5)	1072.16(7)
Z	2	2	2	2	2	2	2	2	2
Reflections collected	8530	8485	8556	8573	8633	8555	8655	8750	14810
Independent reflections	3506	3496	3507	3507	3525	3517	3525	3544	5330
R_{int}	0.0418	0.0448	0.0443	0.0427	0.0418	0.0457	0.0407	0.0424	0.0245
Goodness-of-fit on F^2	1.1090	1.1210	1.0880	1.0670	1.0910	1.0940	1.1130	1.1140	1.0400
Final R indices [I>2σ(I)]:									
$R1$[b]	0.0334	0.0355	0.0367	0.0365	0.0330	0.0387	0.0319	0.0330	0.0218
$wR2$[b]	0.0851	0.0940	0.0971	0.0959	0.0814	0.0966	0.0779	0.0793	0.0498
R indices (all data):									
$R1$[b]	0.0338	0.0359	0.0370	0.0368	0.0333	0.0390	0.0322	0.0332	0.0277
$wR2$[b]	0.0856	0.0945	0.0975	0.0962	0.0816	0.0970	0.0781	0.0795	0.0521

[a]original structure determination; note this was a different sample/crystal from a different crystallization effort.
[b]how the treatment of the PF6 disorder is resolved has a big effecron the final R-factor; 85K to 130K: PF_6 disorder not completely resolved; 300 parameters indicates no disorder model at all, i.e., All F atoms in at full occupancy.

Table 2.5. Selected Distances (Å) and Angles (˚) for [Pt(bpp)(Ph)](PF_6)·CH_3CN.

Temperature	**85K**	**90K**	**100K**	**110K**	**120K**	**130K**	**140K**	**150K**	**150K**[a]
Pt(1)-N(1)	2.011(4)	2.003(5)	2.006(5)	2.001(5)	2.008(4)	2.002(5)	2.010(4)	2.013(4)	1.999(3)
Pt(1)-N(5)	2.002(4)	2.008(4)	2.005(4)	2.003(5)	2.006(4)	2.012(5)	2.008(4)	2.008(4)	2.006(2)
Pt(1)-N(3)	2.017(4)	2.016(5)	2.024(5)	2.022(5)	2.021(4)	2.018(5)	2.015(4)	2.018(4)	2.012(3)
Pt(1)-C(13)	2.030(6)	2.020(6)	2.034(6)	2.027(6)	2.025(5)	2.026(6)	2.032(5)	2.029(5)	2.007(3)
N(1)-C(6)	1.333(7)	1.331(7)	1.335(8)	1.331(8)	1.323(7)	1.343(8)	1.326(6)	1.325(6)	1.334(4)
N(1)-C(2)	1.328(7)	1.339(8)	1.336(9)	1.338(9)	1.333(7)	1.333(8)	1.336(7)	1.336(7)	1.334(4)
N(2)-N(3)	1.399(6)	1.395(6)	1.388(7)	1.387(7)	1.390(6)	1.388(6)	1.397(5)	1.394(5)	1.393(4)
N(4)-N(5)	1.407(6)	1.398(7)	1.402(7)	1.402(7)	1.397(6)	1.403(7)	1.400(5)	1.395(6)	1.390(4)
N(1)-Pt(1)-N(5)	79.49(17)	79.37(19)	79.4(2)	79.5(2)	79.35(17)	79.41(19)	79.53(16)	79.49(16)	79.39(10)
N(1)-Pt(1)-N(3)	79.51(18)	79.44(19)	79.3(2)	79.3(2)	79.31(17)	79.3(2)	79.42(16)	79.29(16)	79.34(10)
N(5)-Pt(1)-N(3)	159.00(18)	158.8(2)	158.8(2)	158.8(2)	158.66(17)	158.7(2)	158.95(17)	158.78(17)	158.73(11)
N(1)-Pt(1)-C(13)	176.36(16)	176.51(18)	176.57(18)	176.54(18)	176.48(15)	176.31(18)	176.37(14)	176.30(14)	176.38(10)
N(5)-Pt(1)-C(13)	100.8(2)	100.9(2)	100.7(2)	100.8(2)	101.05(19)	101.0(2)	100.95(18)	101.03(18)	101.26(12)
N(3)-Pt(1)-C(13)	100.1(2)	100.3(2)	100.5(2)	100.4(2)	100.25(19)	100.2(2)	100.06(18)	100.16(18)	99.97(11)
C(6)-N(1)-Pt(1)	118.7(4)	119.0(4)	119.2(4)	119.6(4)	118.8(4)	119.0(4)	118.8(3)	118.8(3)	118.7(2)
C(2)-N(1)-Pt(1)	118.3(4)	118.7(4)	118.7(4)	118.7(4)	118.6(3)	118.7(4)	118.1(3)	117.9(3)	118.6(2)
N(2)-N(3)-Pt(1)	111.1(3)	111.2(3)	110.9(3)	111.1(3)	111.3(3)	111.4(3)	111.2(3)	111.2(3)	111.82(18)
N(4)-N(5)-Pt(1)	112.0(3)	111.9(3)	111.8(3)	111.9(3)	112.0(3)	111.7(3)	111.7(3)	111.8(3)	111.68(19)

[a]original structure determination; note this was a different sample/crystal from a different crystallization effort

Table 2.6. Least Squares Planes Deviation from Planarity (Å) and Dihedral Angles (˚) of [Pt(bpp)(Ph)](PF_6)·CH_3CN.

Least Squares Planes Deviation from Planarity (Å)	**85 K**	**90K**	**100K**	**110K**	**120K**	**130K**	**140K**	**150K**	**150K[a]**
Pt1 N1 N2 N3 N4 N5 **(1)**	0.0267	0.0248	0.0249	0.0236	0.0238	0.0230	0.0232	0.0237	0.0210
C13 C14 C15 C16 C17 C18 **(2)**	0.0108	0.0111	0.0099	0.0091	0.0112	0.0144	0.0123	0.0118	0.0130
N2 N3 C7 C8 C9 **(3)**	0.0010	0.0010	0.0009	0.0014	0.0006	0.0017	0.0023	0.0019	0.0023
N1 C2 C3 C4 C5 C6 **(4)**	0.0028	0.0055	0.0039	0.0041	0.0042	0.0021	0.0024	0.0025	0.0050
N4 N5 C10 C11 C12 **(5)**	0.0028	0.0020	0.0032	0.0035	0.0030	0.0011	0.0013	0.0014	0.0009
Dihedral Angles (˚)									
(1)-(2)	36.1(1)	36.0(1)	36.2(2)	36.4(2)	36.4(1)	36.6(2)	36.7(1)	36.9(1)	36.8(1)
(3)-(4)	5.5(3)	5.5(4)	5.7(4)	5.6(4)	5.5(3)	5.4(4)	5.1(3)	5.2(3)	4.7(2)
(4)-(5)	2.9(3)	3.1(4)	3.1(4)	2.9(4)	2.8(3)	2.7(4)	2.6(3)	2.5(3)	2.5(2)
(2)-(4)	36.3(2)	36.1(2)	36.4(2)	36.6(2)	36.7(2)	37.1(2)	37.1(2)	37.2(2)	37.1(1)

[a]original structure determination; note this was a different sample/crystal from a different crystallization effort.

References.

(1) Willison, S. A.; Jude, H.; Antonelli, R. M.; Rennekamp, J. M.; Eckert, N. A.; Krause Bauer, J. A.; Connick, W. B. *Inorg. Chem.* **2004**, *43*, 2548-2555.

(2) Jameson, D. J.; Blaho, J. K.; Kruger, K. T.; Goldsby, K. *Inorg. Chem.* **1989**, *28*, 4312-4314.

(3) See for example: (a) Bessel, C. A.; See, R. F.; Jameson, D. L.; Churchill, M. R.; Takeuchi, K. J. *J. Chem. Soc., Dalton Trans.* **1993**, *10*, 1563-1576; (b) Fung, W.-H.; Cheng, W.-C.; Yu, W.-Y.; Che, C.-M.; Mak, T. C. W. *Chem. Commun.* **1995**, 2007-2008; (c) Fung, W.-H.; Yu, W.-Y.; Che, C.-M. *J. Org. Chem.* **1998**, *63*, 7715-7726; (d) Begley, M. J.; Hubberstey, P.; Stroud, J. *J. Chem. Soc., Dalton Trans.* **1996**, 4295-4301; (e) Rülke, R. E.; Kaasjager, V. E.; Kliphuis, D.; Elsevier, C. J.; van Leeuwen, P. W. N. M.; Vrieze, K.; Goubitz, K. *Organometallics* **1996**, *15*, 668-677; (f) Holland, J. M.; Kilner, C. A.; Thornton-Pett, M.; Halcrow, M. A. *Polyhedron* **2001**, *20*, 2829-2840; (g) Chryssou, K.; Stergiopoulos, T.; Falaras, P. *Polyhedron* **2002**, *21*, 2773-2781; (h) Chryssou, K.; Catalano, V. J.; Kurtaran, R.; Falaras, P. *Inorg. Chim. Acta* **2002**, *328*, 204-209; (i) Calderazzo, F.; Englert, U.; Hu, C.; Marchetti, F.; Pampaloni, G.; Passarelli, V.; Romano, A.; Santi, R. *Inorg. Chim. Acta* **2003**, *344*, 197-206; (j) Beach, N. J.; Spivak, G. J. *Inorg. Chim. Acta* **2003**, *343*, 244-252; (k) Ayers, T.; Turk, R.; Lane, C.; Goins, J.; Jameson, D.; Slattery, S. J. *Inorg. Chim. Acta* **2004**, *357*, 202-206.

(4) Bessel, C. A.; See, R. F.; Jameson, D. L.; Churchill, M. R.; Takeuchi, K. J. *J. Chem. Soc., Dalton Trans.* **1991**, 2801-2805.

(5) Catalano, V. J.; Kurtaran, R.; Heck, R. A.; Ohman, A.; Hill, M. G. *Inorg. Chim. Acta* **1999**, *286*, 181-188.

(6) Slattery, S. J.; Bare, W. D.; Jameson, D. L.; Goldsby, K. A. *J. Chem. Soc., Dalton Trans.* **1999**, 1347-1352.

(7) See for example: (a) Creutz, C.; Chou, M.; Netzel, T. L.; Okumura, M.; Sutin, N. *J. Am. Chem. Soc.* **1980**, *102*, 1309-1319; (b) Juris, A.; Campagna, S.; Bidd, I.; Lehn, J. M.; Ziessel, R. *Inorg. Chem.* **1988**, *27*, 4007-4011; (c) Ayala, N. P.; Flynn, C. M., Jr.; Sacksteder, L.; Demas, J. N.; DeGraff, B. A. *J. Am. Chem. Soc.* **1990**, *112*, 3837-3844; (d) Aldridge, T. K.; Stacy, E. M.; McMillin, D. R. *Inorg. Chem.* **1994**, *33*, 722-727; (e) Crites Tears, D. K.; McMillin, D. R. *Coord. Chem. Rev.* **2001**, *211*, 195-205.

(8) Bailey, J. A. H., M. G.; Marsh, R. E.; Miskowski, V. M.; Schaefer, W. P.; Gray, H. B. *Inorg. Chem.* **1995**, *34*, 4591-4599.

(9) (a) Yip, H.-K.; Cheng, L.-K.; Cheung, K. K.; Che, C. M. *J. Chem. Soc. Dalton Trans.* **1993**, 2933-2938; (b) Crites Tears, D. K.; Cunningham, C. T.; McMillin, D. R. *Inorg. Chim. Acta* **1998**, *273*, 346-353; (c) Lai, S.-W.; Chan, M. C. W.; Cheung, K.-K.; Che, C.-M. *Inorg. Chem.* **1999**, *38*, 4262-4267; (d) Michalec, J. F.; Bejune, S. A.; McMillin, D. R. *Inorg. Chem.* **2000**, *39*, 2708-2709; (e) Michalec, J. F.; Bejune, S. A.; Cuttell, D. G.; Summerton, G. C.; Gertenbach, J. A.; Field, J. S.; Haines, R. J.; McMillin, D. R. *Inorg. Chem.* **2001**, *40*, 2193-2200; (f) Yang, Q.-Z.; Wu, L.-Z.; Wu, Z.-X.; Zhang, L.-P.; Tung, C.-H. *Inorg. Chem.* **2002**, *41*, 5653-5655.

(10) Goldsby, K. A. J., D. L. *J. Org. Chem* **1990**, *55*, 4992-4994.

(11) Eaborn, C. O., K. J.; Pidcock, A. *J. Chem. Soc., Dalton Trans.* **1978**, 357-368.

(12) Jude, H.; Krause Bauer, J. A.; Connick, W. B. *Inorg. Chem.* **2002**, *41*, 2275-2281.

(13) Bruker SMART (v5.051 for [Pt(bpp)Cl]Cl·2H_2O; v5.628 for [Pt(bpp)(Ph)](PF_6)·CH_3CN) and SAINT (v5.A06 for [Pt(bpp)Cl]Cl·2H_2O; v6.28A for [Pt(bpp)(Ph)](PF_6)·CH_3CN) programs were used for data collection and data processing, respectively. Bruker Analytical X-Ray Instruments, Inc., Madison WI.

(14) SADABS was used for the application of semi-empirical absorption and beam corrections for the CCD data. G. M. Sheldrick, University of Goettingen, Germany, 1996.

(15) SHELXTL v5.03 ([Pt(bpp)Cl]Cl·$2H_2O$) and SHELXTL v6.12 ([Pt(bpp)(Ph)](PF_6)·CH_3CN) were used for the structure solutions and generation of figures and tables. G. M. Sheldrick, University of Goettingen, Germany and Siemens Analytical X-ray Instruments, Inc., Madison, WI.

(16) Howe-Grant, M.; Lippard, S. J. *Inorg. Synth.* **1980**, *20*, 101-105.

(17) Bessel, C. A.; See, R. F.; Jameson, D. L.; Churchill, M. R.; Takeuchi, K. J. *J. Chem. Soc., Dalton Trans.* **1992**, 3223-3228.

(18) Wong, Y.-S.; Lippard, S. J. *Chem. Commun.* **1977**, 824-825.

(19) (a) Miller, J. S. *Extended Linear Chain Compounds*; Miller, J. S., Ed., Ed.; Plenum Press: New York, 1982; Vol. 1-3; (b) Connick, W. B.; Marsh, R. E.; Schaefer, W. P.; Gray, H. B. *Inorg. Chem.* **1997**, *36*, 913-922.

(20) (a) Bruno, G.; Lanza, S.; Nicolo, F. *Acta Crystallogr.* **1990**, *C46*, 765-767; (b) Deacon, G. B.; Hilderbrand, E. A.; Tiekink, E. R. T. *Z. Kristallogr.* **1993**, *205*, 340-342; (c) Ito, M.; Ebihara, M.; Kawamura, T. *Inorg. Chim. Acta* **1994**, *218*, 199-202; (d) Sato, M.; Mogi, E.; Kumakura, S. *Organometallics* **1995**, *14*, 3157-3159; (e) Ng, Y.-Y.; Che, C.-M.; Peng, S.-M. *New J. Chem.* **1996**, *20*, 781-789; (f) Morton, M. S.; Lachicotte, R. J.; Vicic, D. A.; Jones, W. D. *Organometallics* **1999**, *18*, 227-234; (g) Muller, C.; Iverson, C. N.; Lachicotte, R. J.; Jones, W. D. *J. Am. Chem. Soc.* **2001**, *123*, 9718-9719; (h) Johansson, M. H.; Malmström, T.; Wendt, O. F. *Inorg. Chim. Acta* **2001**, *316*, 149-152; (i) Zucca, A.; Doppiu, A.; Cinellu, M. A.; Stoccoro, S.; Minghetti, G.; Manassero, M. *Organometallics* **2002**, *21*, 783-785; (j) Harkins, S. B.; Peters, J. C. *Organometallics* **2002**, *21*, 1753-1755; (k) Romeo, R.; Scolaro, L. M.; Plutino, M. R.; Romeo, A.; Nicolo, F.; Del Zotto, A. *Eur. J. Inorg. Chem.* **2002**, 629-638.

(21) Klein, A.; McInnes, E. J. L.; Kaim, W. *J. Chem. Soc., Dalton Trans.* **2002**, 2371-2378.

(22) Song, D.; Sliwowski, K.; Pang, J.; Wang, S. *Organometallics* **2002**, *21*, 4978-4983.

(23) Hill, M. G., Bailey, J.A., Miskowski, V.M., Gray, H.B. *Inorg. Chem.* **1996**, *35*, 4585-4590.

(24) Liu, X.; McInnes, E. J. L.; Kilner, C. A.; Thornton-Pett, M.; Halcrow, M. A. *Polyhedron* **2001**, *20*, 2889-2900.

(25) The π^*(tpy)-d_{x2-y2}(Pt) energy gap for Pt(tpy)Cl^+ was estimated in ref. 20 from the difference of the first two reduction potentials (0.56 V), crudely corrected for electrostatic effects using the difference between the first two reduction potentials of $Ru(bpy)_3^{2+}$ (0.18 V).

(26) (a) Yam, V. W.-W.; Tang, R. P.-L.; Wong, K. M.-C.; Cheung, K.-K. *Organometallics* **2001**, *20*, 4476-4482; (b) Jude, H.; Krause Bauer, J. A.; Connick, W. B. *J. Am. Chem. Soc.* **2003**, *125*, 3446-3447; (c) Jude, H.; Carroll, G. T.; Connick, W. B. *Chemtracts - Inorg. Chem.* **2003**, *16*, 13-22.

(27) Jude, H.; Krause Bauer, J. A., Connick, W. B., *in preparation*.

(28) It is assumed the concentration of the solution reported in Figure 3 of ref. 5 was 5.5 x 10^{-5} M.

(29) A similar band assignment has been made for a Eu(III) and Tb(III) complexes with a related ligand, 2,6-*bis*(3-carboxy-1-pyrazolyl)pyridine (Remuiñán, M. J.; Román, H.; Alonso, M. T.; Rodríguez-Ubis, J. C. *J. Chem. Soc., Perkins Trans. 2* **1993**, 1099-1102).

(30) (a) Bray, R. G.; Ferguson, J.; Hawkins, C. J. *Aust. J. Chem.* **1969**, *22*, 2091-103; (b) Ohno, T.; Kato, S. *Bull. Chem. Soc. Jpn.* **1974**, *47*, 2953-2957.

(31) The possibility of Pt d→p can be excluded on energetic grounds since the lowest spin-allowed d→p transitions in platinum(II) complexes generally occur at wavelengths shorter than 250 nm (Mason, W. R.; Gray, H. B. *J. Am. Chem. Soc.* **1968**,

90, 5721-5729; Patterson, H. H.; Tewksbury, J. C.; Martin, M.; Krogh-Jesperson, M.-B.; LoMenzo, J. A.; Hooper, H. O.; Viswanath, A. K. *Inorg. Chem.* **1981**, *20*, 2297-2301; Roberts, D. A.; Mason, W. R.; Geoffroy, G. L. *Inorg. Chem.* **1981**, *20*, 789-796; Isci, H.; Mason, W. R. *Inorg. Chem.* **1984**, *23*, 1565-1569; Mason, W. R. *Inorg. Chem.* **1986**, *25*, 2925-2929.)

(32) Triplet components of these charge-transfer transitions and spin-allowed Pt-centered d-d transitions also are candidates, but likely to have relatively weak intensities (<1000 $M^{-1}cm^{-1}$).

(33) (a) Klein, A.; van Slageren, J.; Záliš, S. *Eur. J. Inorg. Chem.* **2003**, 1917-1928; (b) Klein, A.; van Slageren, J.; Záliš, S. *Inorg. Chem.* **2002**, *41*, 5216-5225; (c) Kaim, W.; Dogan, A.; Wanner, M.; Klein, A.; Tiritiris, I.; Schleid, T.; Stufkens, D. J.; Snoeck, T. L.; McInnes, E. J. L.; Fiedler, J.; Záliš, S. *Inorg. Chem.* **2002**, *41*, 4139-4148; (d) van Slageren, J.; Klein, A.; Záliš, S. *Coord. Chem. Rev.* **2002**, *230*, 193-211.

(34) Arena, G.; Calogero, G.; Campagna, S.; Scolaro, L. M.; Ricevuto, V.; Romeo, R. *Inorg. Chem.* **1998**, 2763-2769.

(35) Yip, H.-K.; Che, C. M.; Zhou, Z.-Y.; Mak, T. C. W. *J. Chem. Soc., Chem. Commun.* **1992**, 1369-1371.

(36) Bailey, J. A.; Miskowski, V. M.; Gray, H. B. *Inorg. Chem.* **1993**, *32*, 369-370.

(37) (a) Field, J. S.; Haines, R. J.; McMillin, D. R.; Summerton, G. C. *J. Chem. Soc., Dalton Trans.* **2002**, 1369-1376; (b) Field, J. S.; Gertenbach, J.-A.; Haines, R. J.; Ledwaba, L. P.; Mashapa, N. T.; McMillin, D. R.; Munro, O. Q.; Summerton, G. C. *J. Chem. Soc., Dalton Trans.* **2003**, 1176-1180; (c) Büchner, R.; Cunningham, C. T.; Field, J. S.; Haines, R. J.; McMillin, D. R.; Summerton, G. C. *J. Chem. Soc., Dalton Trans.* **1999**, 711-718; (d) Büchner, R.; Field, J. S.; Haines, R. J.; Cunningham, C. T.; McMillin, D. R. *Inorg. Chem.* **1997**, *36*, 3952-3956.

(38) Gliemann, G.; Yersin, H. *Struct. Bonding* **1985**, *62*, 87-153.

(39) The $d\sigma^* \rightarrow \pi^*$ assignment appears more likely since the enegies of the emissions from tetracyanoplatinate salts with predominant lowest $d\sigma^* \rightarrow p\sigma$ excited state character only approach that observed here for very short metal···metal spacings ~3.1 Å (ref. 37). The absence of a vibronic component characteristic of ligand excited-state distortion is consistent with the ~80 K emission spectra of Pt(II) tpy dimers and linear chain compounds, in which this feature is sometimes, but not always evident (refs. 35-36).

(40) Miskowski, V. M.; Houlding, V. H. *Inorg. Chem.* **1991**, *30*, 4446-4452.

(41) Yersin, H.; Gliemann, G.; Räde, H. S. *Chem. Phys. Lett.* **1978**, *54*, 111-116.

(42) Miskowski, V. M.; Houlding, V. H.; Che, C.-M.; Wang, Y. *Inorg. Chem.* **1993**, *32*, 2518-2524.

(43) (a) Yersin, H.; Otto, H.; Zink, J. H.; Gliemann, G. *J. Am. Chem. Soc.* **1980**, *102*, 951-955; (b) Miskowski, V. M.; Houlding, V. H. *Inorg. Chem.* **1989**, *28*, 1529-1533.

(44) The weak emission observed from glassy solutions suggests the lowest LF states could lie at significantly higher energies (>25000 cm^{-1}).

Chapter 3

A Platinum(II) Molecular Triangle with a Deep Intramolecular Cavity†

Introduction.

Considerable effort is currently directed toward the self-assembly of supramolecular macrocyclic architectures using platinum(II)-containing subunits because of the metal center's predictable square planar coordination geometry and kinetic stability. The prevailing strategy focuses on cyclic structures in which *trans*-coordination of linker groups is used to extend edge units and *cis*-coordination is used to create vertices.[2] Already this approach has generated a wide variety of macrocycles with varying cavity shapes and sizes (Scheme 3.1).[3] A limitation of this chemistry is that the resulting molecules tend to have annulus-like structures often characterized by low barriers to rotation of edge groups[4] and shallow cavities with limited surface area available for interaction with an encapsulated guest. Typically, chemical elaboration by substitution of non-bridging ligands is not practical due to the kinetic lability of the linker groups, and unless chiral ligands are employed,[5] the structures are achiral.

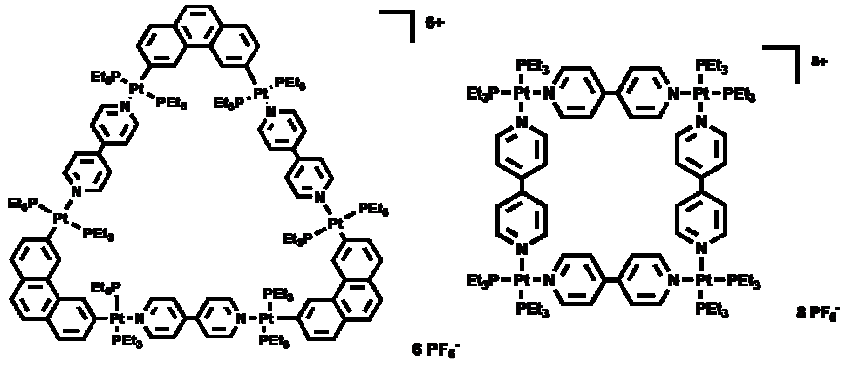

Scheme 3.1. Two examples of molecular polygons with platinum metal centers as edge and vertex components.[2,6]

† Most of the contents of Chapter 3 appeared in a manuscript in *Inorganic Chemistry.*[1]

The use of bridging ligands capable of chelating one or both metal centers can be expected to produce more rigid macrocycles. In this regard, conventional meridional tridentate chelates such as tpy and bpp would appear to be unlikely bridging groups because of their tendency to favor tridentate coordination. However, it may be anticipated that the relative geometric constraints of the five-membered pyrazolyl rings of bpp, as compared to six-membered pyridyl rings, will tend to destabilize tridentate coordination.[7] In support of this view, we have recently discovered that bpzph$^-$ favors bidentate coordination of platinum(II), allowing a second pyrazolyl group to bridge to another metal center. Here we report the one-pot synthesis of the resulting remarkably stable chiral molecular triangle, which has an unusually deep intramolecular cavity.

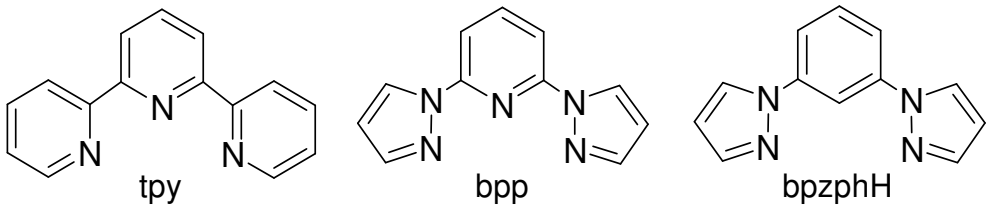

Experimental Section.

All reagents were purchased from Aldrich, Acros or Pressure Chemical and used as received. Deuterated solvents were purchased from Cambridge Isotope Laboratories. ^{1}H NMR spectra were recorded using either a Bruker AC 400 MHz or AMX-400 Bruker spectrometer, and chemical shifts were referenced to TMS. Mass spectra were obtained by electrospray ionization using an IonSpec HiResESI-FTICRMS instrument; the observed isotope patterns were in good agreement with those predicted based on natural abundances.

Preparation of bpzphH: Following a modification of the Kauffmann and Lexy method for the preparation of 1,3,5-tri(1-pyrazolyl)benzene,[8] excess pyrazole (5.11 g, 75 mmol) was dissolved in nitrobenzene (10 mL) under argon. CuI (2.54 g, 13 mmol), K_2CO_3 (8.29 g, 60 mmol) and 1,3-dibromobenzene (0.605 mL, 5 mmol) were added. The mixture was refluxed for 3 h. After cooling to room temperature, the mixture was filtered to give a yellow-green filtrate, which was reduced to dryness. The residue was dissolved in methylene chloride and hexanes were added to induce precipitation. The mixture was filtered, and the filtrate was reduced to dryness to yield a yellow-orange oil. Chromatography on silica (CH_2Cl_2: hexanes, 2:1) afforded an orange oil. Yield, 0.524 g (2.49 mmol, 49.8%). ^{1}H NMR (400 MHz, $CDCl_3$, δ): 6.49 (2H, m), 7.51 (1H, t), 7.62 (2H, d), 7.75 (2H, d), 8.01 (2H, d), 8.11 (1H, d). ^{1}H NMR (400 MHz, DMF-d_7, δ): 6.64 (2H, m), 7.67 (1H, t), 7.85-7.89 (4H, m), 8.49 (1H, d), 8.71 (2H, d).

Pt(bpzph)Cl: Following the method suggested in the report of Sotoyama et al.,[9] 0.050g bpzphH (0.238 mmol) and 0.1076g K_2PtCl_4 (0.259 mmol) were refluxed in 20 mL of acetic acid for 2 days. The mixture was cooled to room temperature and filtered. The brown precipitate was washed with methylene chloride, methanol, water and ether and then dried. Yield 0.0877g (84%). ^{1}H NMR (400 MHz, $CDCl_3$, δ): 6.64 (2H, m), 7.03 (2H, d), 7.26 (1H, m), 8.03 (4H, m). ^{1}H NMR (400 MHz, DMF-d_7, δ): 6.90 (2H, s), 7.41 (1H, t), 7.58 (2H, d), 8.03 (2H, s), 9.00 (2H, d). MS-ESI (*m*/*z*): 843.6, $[2M - Cl]^+$; 477.1, $[M(DMF) - Cl]^+$; 445.1, $[M(CH_3CN) - Cl]^+$; 404.0 $[M - Cl]^+$. Crystallographic data for Pt(bpzph)Cl: $C_{12}H_9N_4ClPt$, MW=439.77, T=173 K, λ=0.7750 Å, monoclinic, *C*2/*c*, *a*=10.4065(7), *b*=14.7195(9), *c*=7.8539(5) Å, *β*=99.944(2)°, *V*=1184.97(13) Å^3, *R*1=0.0208, *wR*2=0.0528 for data with $I>2\sigma(I)$. Deposit number: CCDC-656112.

[Pt(μ-bpzph)Cl]$_3$: bpzphH (0.033g, 0.157 mmol) and K_2PtCl_4 (0.066g, 0.159 mmol) were refluxed in 4.5 mL of acetic acid for 11 days. The mixture was cooled to room temperature and filtered. The brown precipitate was washed with methylene chloride and dried. Yield 0.063g (91%). ^{1}H NMR (400 MHz, $CDCl_3$, δ): 5.95 (1H, d), 6.48 (1H, s), 6.66 (2H, m), 7.88 (1H, d), 8.03 (1H, d), 8.13 (2H, m), 8.60 (1H, d). ^{1}H NMR (400 MHz, DMF-d_7, δ): 6.07 (1H, d), 6.71 (1H, s), 6.90 (1H, s), 7.04 (1H, d), 8.08 (1H, s), 8.21 (1H, s), 8.35 (1H, s), 8.46 (1H, s), 8.62 (1H, s). MS-ESI (*m*/*z*): 1324.1, $[M(CH_3CN) - Cl]^+$; 1283.1, $[M - Cl]^+$. Crystallographic data for [Pt(μ-bpzph)Cl]$_3$·DMF·0.5Et$_2$O, $C_{36}H_{27}N_{12}Cl_3Pt_3$·DMF·0.5Et$_2$O, MW=1429.47, T=150K, λ=1.54178 Å, triclinic, *P*-1, *a*=11.8105(4), *b*=14.1236(5), *c*=14.6980(5) Å, α=68.355(1), β=73.082(1), γ=82.618(2)°, *V*=2179.61(13) Å^3, *R*1=0.0311, *wR*2=0.0751 for data with $I>2\sigma(I)$. Deposit number: CCDC-656113.

Pt(bpzph)Br/[Pt(μ-bpzph)Br]$_3$ mixture: [Pt(μ-bpzph)Cl]$_3$ (0.030g ,0.069mmol) was dissolved in 5 mL of DMF and $TlPF_6$ (0.031g, 0.088mmol) was added and allowed to stir for 30 minutes. The mixture was filtered through celite and NaBr (0.009g, 0.069mmol) was added to the solution and allowed to stir for 24 hours. The solution was concentrated to dryness resulting a mixture of monomer and trimer products. Yield 0.033g (99%). ^{1}H NMR (400 MHz, $CDCl_3$, δ): 5.92 (1H, d), 6.45 (1H, m), 6.65-6.67 (3H, m), 7.04 (1H, t), 7.30 (2H, d), 7.87 (1H, m), 8.03 (1H, m), 8.12 (2H, m), 8.29 (1H, m), 8.68 (1H, m). ^{1}H NMR (400 MHz, DMF-d_7, δ): 6.05 (1H, d), 6.71 (1H, m), 6.90-6.93 (3H, m), 7.07 (1H, d), 7.43 (1H, t), 7.58 (2H, d), 8.10 (2H, m), 8.20 (1H, m), 8.26 (1H, m), 8.37 (1H, m), 8.58 (1H, m), 8.63 (1H, m), 9.01 (2H, m). MS-ESI (*m*/*z*): 403.9, $[M - Br]^+$; 614.1, $[M(bpzph)_2 - Br]^+$; 887.9, $[M_2 - Br]^+$; 1372.0 $[M_3 - Br]^+$; 1412.9,

$[M_3(CH_3CN) - Br]^+$; 1855.9, $[M_4 – Br]^+$. Crystallographic data for Pt(bpzph)Br: $C_{12}H_9N_4BrPt$, MW=484.23, T=193 K, λ=0.77490 Å, monoclinic, *C*2/*c*, *a*=10.4363(11), *b*=15.0036(11), *c*=7.8523(7) Å, *β*=100.482(2)°, *V*=1209.01(19) Å^3, *R*1=0.0198, *wR*2=0.0507 for data with $I>2\sigma(I)$.

Results and Discussion.

Synthesis and Characterization. The reaction of $K_2[PtCl_4]$ and bpzphH in refluxing acetic acid yielded a tan solid, which upon washing with methylene chloride was found to contain Pt(bpzph)Cl, $[Pt(\mu\text{-bpzph})Cl]_3$ or a mixture of these products in overall high yield (typically 50-90%) (Scheme 3.1). The identities of both products were confirmed by single-crystal X-ray diffraction studies (Figure 3.1). For the C_{2v}-symmetric monomer, the bpzph$^-$ ligand is tridentate with the Pt bonded at the 2-position of the phenyl group; the fourth coordination site of the metal is occupied by a chloride ligand. In the case of the C_3-symmetric trimer, each bpzph$^-$ ligand is bidentate with the metal bonded to a pyrazolyl group (pz) and to the phenyl group at the 6-position; the remaining pyrazolyl group (pz') is bonded to a different platinum center, resulting in a trans arrangement of the two N-donor pyrazolyl groups bonded to each Pt. The two products are readily distinguished by their ESI mass and ^{1}H NMR spectra (Figures 3.5-3.10). It is noteworthy that the highest sample peaks in the ESI mass spectra of $[Pt(\mu\text{-bpzph})Cl]_3$ are consistent with loss of one chloride, and there is no evidence of tetramers or higher-order aggregates (Figure 3.10).

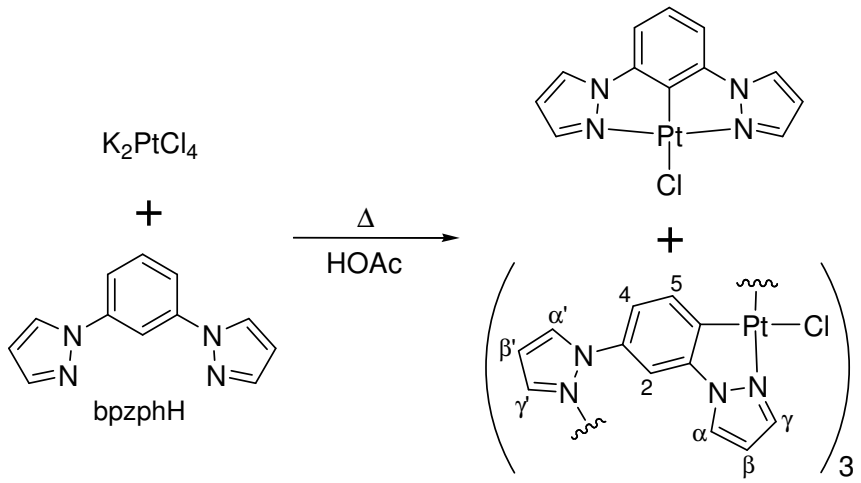

Scheme 3.2. Synthetic scheme for the Pt(bpzph)Cl and [Pt(μ-bpzph)Cl]$_3$.

Each complex can be selectively prepared by controlling the initial concentration of platinum starting material and the duration of the reaction. Although the concentration/time parameter space was not fully explored, a series of 18 reactions employing different initial platinum concentrations ([Pt], 8-220 mM) and reaction times (t, 2-14 days) were performed (Figure 3.1). The results showed that exclusively trimer is isolated for [Pt]≥50 mM and t≥9 days; shorter reaction times yielded monomer/trimer mixtures. However, for [Pt]<15 mM and t≤14 days, only the monomer was isolated.

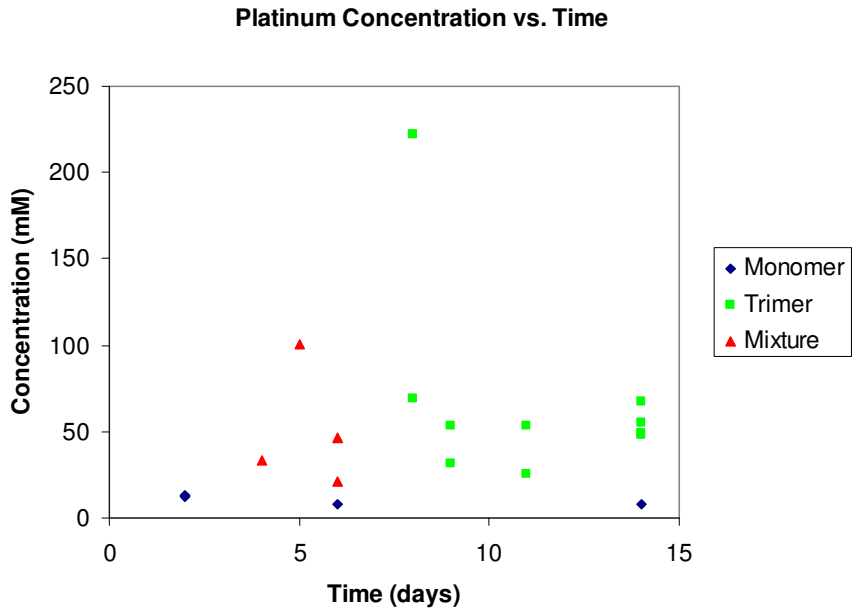

Figure 3.1. Platinum Concentration (mM) with respect to time (days) resulting in monomer, trimer, or a mixture of the two products.

Mass Spectrometry. ESI mass spectra were obtained by electrospray ionization using an IonSpec HiResESI-FTICRMS. For samples of [Pt(μ-bpzph)Cl]$_3$ and Pt(bpzph)Cl, a variety of solvent conditions were employed, including DMF, DMF/CH_3OH, CH_3OH, $CH_3OH/CHCl_3$, CH_3CN, and $CH_3CN/CHCl_3$; the observed isotope patterns were in good agreement with predicted patterns based on natural abundances. The spectra of DMF/CH_3OH solutions in the presence of a 50:50 acetonitrile:water solution and 0.1% formic acid buffer are shown in Figures 3.8 and 3.9.

X-ray crystallography. APEX2 v2.0-2, SMART v5.631 and SAINT v6.45A programs were used for data collection and data processing, respectively (Bruker Analytical X-ray Instruments, Inc., Madison, WI).[10] SADABS v2.10 was used for semi-empirical absorption and beam corrections.[10] SHELXTL v6.14 was used for the structure

solution and generation of figures and tables (G.M. Sheldrick, University of Göttingen, Germany and Bruker Analytical X-ray Instruments, Inc., Madison, WI).[11] Neutral-atom scattering factors were used as stored in this package. DIAMOND v3.1e and PLATON were used to generate the packing and void space diagrams, respectively.[12,13] The structures were solved by a combination of direct methods in SHELXTL and the difference Fourier technique and refined by full-matrix least squares on F^2 for reflections out to 0.75Å resolution for Pt(bpzph)Cl, 0.83 Å resolution for [Pt(μ-bpzph)Cl]$_3$·DMF·0.5Et$_2$O, and 0.80 Å for Pt(bpzph)Br. Non-hydrogen atoms were refined with anisotropic displacement parameters. Weights were assigned as $w^{-1}=[\sigma^2(F_o^2)+ (0.0324P)^2+3.625P]$ where $P=0.33333F_o^2+0.66667F_c^2$. The H-atom positions were calculated and treated with a riding model; isotropic displacement parameters were defined as $1.2*U_{eq}$ of the adjacent atom. Crystallographic refinement parameters are collected in Table 3.1.

Single crystals of Pt(bpzph)Cl were obtained as pale yellow plates from DMF-Et$_2$O or CH$_2$Cl$_2$-hexanes. For X-ray examination and data collection, a suitable crystal, approximate dimensions 0.15 x 0.07 x 0.02 mm, was mounted in a loop with paratone-N and transferred immediately to the goniostat bathed in a cold stream. Intensity data were collected at 173 K on a D8 goniostat equipped with a Bruker Platinum200 CCD detector at Beamline 11.3.1 at the Advanced Light Source (Lawrence Berkeley National Laboratory) using synchrotron radiation tuned to λ=0.77500 Å. The detector was set at a distance of 7.4 cm from the crystal. A series of 1-s data frames measured at 0.2^o increments of ω were collected to calculate a unit cell. For data collection, frames were measured for a duration of 1-s at 0.3^o intervals of ω with a maximum θ value of ~62^o.

The data frames were collected using the program APEX2 and processed using the program SAINT routine within APEX2.[11] The data were corrected for absorption, and beam corrections were applied based on the multi-scan technique as implemented in SADABS.

Single crystals of [Pt(μ-bpzph)Cl]$_3$·DMF·0.5Et_2O were obtained from diffusion of ether into a DMF/CH_2Cl_2 solution to produce colorless plates. Intensity data were collected at 150 K using a Bruker SMART6000 CCD diffractometer with graphite-monochromated Cu Kα radiation (λ=1.54178 Å). For X-ray examination and data collection, a suitable crystal, approximate dimensions 0.15 x 0.05 x 0.04 mm, was mounted in a Cryo-loop with paratone-N and immediately transferred to the goniostat bathed in a cold stream. The data were corrected for decay, Lorentz and polarization effects as well as absorption and beam corrections based on the multi-scan technique. One molecule of DMF and a half-molecule of Et_2O appear in the lattice. The oxygen atom, O1, of the Et_2O molecule appears on a special position, and the complete molecule is generated by symmetry. The methylene carbon, C37, of the ether solvent is disordered, occupancy set at 0.5. The DMF molecule shows disorder as indicated by the enlarged anisotropic displacement parameters. The anisotropic displacement parameters of O2 were set equivalent to the better behaved N13.

Single crystals of Pt(bpzph)Br were obtained as pale yellow needles from DMSO. For X-ray examination and data collection, a suitable crystal, approximate dimensions 0.11 x 0.02 x 0.01 mm, was mounted in a loop with paratone-N and transferred immediately to the goniostat bathed in a cold stream. Intensity data were collected at 193 K on a Kappa goniostat equipped with a Bruker Platinum200 CCD detector at Beamline

11.3.1 at the Advanced Light Source (Lawrence Berkeley National Laboratory) using synchrotron radiation tuned to λ=0.7749 Å. A series of 2-s data frames measured at 0.2° increments of ω were collected to calculate a unit cell. For data collection, frames were measured for a duration of 2-s at 0.3° intervals of ω with a maximum θ value of ~60°. The data frames were collected using the program APEX2 and processed using the program SAINT routine within APEX2.[11] The data were corrected for absorption, and beam corrections were applied based on the multi-scan technique as implemented in SADABS.

Product mixtures were readily purified by fractional crystallization from DMF. Upon diffusion of ether into a DMF solution, the trimer crystallizes as plates leaving a supernatant enriched in the monomer product. The supernatant was decanted from the trimer crystals and allowed to evaporate resulting in monomer crystals. The accumulated observations are consistent with initial formation of monomer, as expected for coordination of the pyrazolyl N-donor groups driving C-H activation.[14] Subsequent conversion of the monomer to trimer involves an unusual [1,3]-metallotropic shift accompanied by a [3,1]-proton shift. From studies of the cis and trans isomers of Pt(phpy)(py)Cl,[15] (phpyH=2-phenylpyridine) we infer that the resulting trans disposition of the halide and phenyl groups is thermodynamically more stable than the alternative cis arrangement. Crystallographic data and selected geometric parameters are summarized in Tables 3.1 and 3.2, respectively.

Table 3.1. Crystallographic Data[†] for Pt(bpzph)Cl, [Pt(μ-bpzph)Cl]$_3$·DMF·0.5Et$_2$O and Pt(bpzph)Br.

	Pt(bpzph)Cl	[Pt(μ-bpzph)Cl]$_3$·DMF·0.5Et$_2$O	Pt(bpzph)Br
formula	$C_{12}H_9N_4ClPt$	$C_{36}H_{27}N_{12}Cl_3Pt_3$·DMF·0.5Et$_2$O	$C_{12}H_9N_4BrPt$
fw, g/mol	439.77	1429.47	484.23
space group	C2/*c*	*P*-1	C2/*c*
A, Å	10.4065(7)	11.8105(4)	10.4363(11)
B, Å	14.7195(5)	14.1236(5)	15.0036(11)
C, Å	7.8539(5)	14.6980(5)	7.8523(7)
A, °	90	68.355(1)	90
B, °	99.944(2)	73.082(1)	100.482(2)
γ, °	90	82.618(2)	90
V, Å^3	1184.97(13)	2179.61(13)	1209.01(19)
ρ_{calcd} (g cm^{-3})	2.465	2.178	2.660
μ, mm^{-1}	14.944	19.759	18.439
Z	4	2	4
T, K	173	150	193
reflns collected	7272	18352	6575
ind reflns	1466	7489	1236
R_{int}	0.0567	0.0358	0.0514
GOF on F^2	1.024	1.089	1.052
$R1/wR2$ [$I > 2\sigma(I)$][a]	0.0208/0.0528	0.0311/0.0751	0.0198/0.0507
$R1/wR2$ (all data)[a]	0.0209/0.0528	0.0340/0.0767	0.0204/0.0512

[†] Deposit numbers: Pt(bpzph)Cl, CCDC-656112; [Pt(μ-bpzph)Cl]$_3$·DMF·0.5Et$_2$O, CCDC-656113.

The crystal structure of Pt(bpzph)Cl shows that the entire Pt(bpzph)Cl unit is planar with rms deviation from a best-fit plane of 0.0066 Å for 18 non-hydrogen atoms (Figure 3.1a).[16] Despite a short Pt-C bond distance (1.924(5) Å), the N-Pt-N bite angle (158.89(14)°) is significantly smaller than found for $Pt(bpp)Cl^+$ (161.3(2)°)[7] and eight $Pt(tpy)Cl^+$ salts (162.0(6)°),[17] which may in part account for the tendency of the monomer to convert to trimer. By contrast, the average Pt-C distance (1.990(5) Å) is somewhat longer for crystals of $[Pt(\mu\text{-bpzph})Cl]_3 \cdot DMF \cdot 0.5Et_2O$ with the average N(pz)-Pt-N(pz') angle (173(1)°) approaching the idealized 180° angle. The adjoining phenyl and pz' groups form a dihedral angle ranging from 41.4(3) to 47.9(3)°, and the N-N-Pt-Cl torsion angles involving pz' range from 101.3(4) to 110.6(4)°.

Table 3.2. Selected Bond Distances (Å) and Angles (°) for Pt(bpzph)Cl, [Pt(μ-bpzph)Cl]$_3$·DMF·0.5Et$_2$O and Pt(bpzph)Br.

Pt(bpzph)Cl		**[Pt(μ-bpzph)Cl]$_3$·DMF·0.5Et$_2$O**						**Pt(bpzph)Br**
Pt-C4	1.924(5)	Pt1-C9	1.999(5)	Pt2-C16	1.978(5)	Pt3-C28	1.994(5)	1.921(5)
Pt-N1	2.021(3)	Pt1-N1	1.991(5)	Pt2-N5	1.988(5)	Pt3-N9	1.992(5)	2.011(3)
Pt-X[a]	2.416(10)	Pt1-X1	2.3974(13)	Pt2-X2	2.4014(13)	Pt3-X3	2.4012(13)	2.525(5)
C4-C5	1.380(4)	C4-C9	1.403(8)	C17-C16	1.398(8)	C29-C28	1.386(8)	1.367(4)
N2-C5	1.411(4)	N2-C4	1.428(7)	N6-C17	1.421(7)	N10-C29	1.418(7)	1.409(4)
N2(A)-C5(A)	1.411(4)	C6-N12	1.419(7)	C13-N4	1.423(7)	C25-N8	1.430(7)	1.409(4)
N2-N1	1.378(3)	N2-N1	1.351(7)	N6-N5	1.346(6)	N10-N9	1.371(7)	1.380(4)
C4-Pt-N1	79.45(7)	C9-Pt1-N1	81.4(9)	C16-Pt2-N5	80.8(2)	C28-Pt3-N9	81.0(2)	79.63(9)
N1-Pt-N1(A)	158.89(14)	N1-Pt-N3	172.98(18)	N5-Pt2-N7	174.16(18)	N9-Pt3-N11	171.90(19)	159.26(17)
C4-Pt-X[a]	180.0	C9-Pt1-X1	172.42(16)	C16-Pt2-X2	173.94(16)	C28-Pt3-X3	172.90(16)	180.0
N1-Pt-X[a]	100.55(7)	N1-Pt1-X1	93.51(14)	N5-Pt2-X2	94.29(14)	N9-Pt3-X3	94.71(14)	100.37(9)
C5-C4-Pt	119.4(2)	C4-C9-Pt1	113.1(4)	C17-C16-Pt2	114.2(4)	C29-C28-Pt3	114.1(4)	119.4(2)
N1-N2-C5	116.1(2)	N1-N2-C4	116.0(4)	N5-N6-C17	115.4(4)	N9-N10-C29	115.6(4)	115.9(3)
N2-N1-Pt	113.55(18)	N2-N1-Pt1	114.7(3)	N6-N5-Pt2	115.4(3)	N10-N9-Pt3	114.3(4)	113.4(2)
N2(A)-N1(A)-Pt	113.55(18)	N4- N3-Pt1	126.7(3)	N8- N7-Pt2	125.7(3)	N12- N11-Pt3	127.0(3)	113.4(2)

[a] X = Cl, Br.

Table 3.3. Least Squares Planes Deviation from Planarity (Å) and Dihedral Angles (˚) for [Pt(μ-bpzph)Cl]$_3$·DMF·0.5Et$_2$O.

Least Squares Planes Deviation from Planarity (Å)		**Dihedral Angles (˚)**	
Pt1 N1 N2 C4 C9 **(1)**	0.0292	**(1)-(2)**	69.5(2)
N3 N4 C10 C11 C12 **(2)**	0.0090	**(2)-(3)**	47.9(3)
C13 C14 C15 C16 C17 C18 **(3)**	0.0098		
Pt2 N5 N6 C16 C17 **(4)**	0.0045	**(4)-(5)**	77.4(2)
N7 N8 C22 C23 C24 **(5)**	0.0014	**(5)-(6)**	47.9(3)
C25 C26 C27 C28 C29 C30 **(6)**	0.0137		
Pt3 N9 N10 C31 C32 C33 **(7)**	0.0138	**(7)-(8)**	73.6(3)
N11 N12 C34 C35 C36 **(8)**	0.0071	**(8)-(9)**	43.2(3)
C4 C5 C6 C7 C8 C9 **(9)**	0.0146		

When viewed perpendicular to the plane defined by the three Pt atoms, [Pt(μ-bpzph)Cl]$_3$ has a triangular shape with the pz' groups and Cl atoms at the vertices (Figure 3.2b). However, in contrast to conventional platinum(II) molecular polygons, the intramolecular cavity is unusually deep (~8 Å) with the metal coordination planes lining its walls. The intramolecular Pt···Pt distances range from 6.669(1) to 6.897(1) Å, and half of a diethyl ether molecule occupies ~65 Å^3 of the interior volume of the cavity (Figure 3.2c). Because of the trans-arrangement of the pyrazolyl groups, each complex is chiral, having a cyclodextrin-like structure. Thus, the chloride and pz groups are situated at one opening of the molecular cavity, and the phenyl-pz' groups lie at the other. However, each coordination plane forms a ~79° angle with the plane defined by the three Pt atoms, and consequently, the cavity is somewhat narrower at the phenyl-pz' end with estimated shortest inter-ligand phenyl H···H contacts ranging from 2.89-3.07 Å. Molecular models suggest that small bond rotations can slightly open the narrower end of the cavity, but the polygon is too sterically hindered to fully invert and thereby switch chirality. Enantiomeric pairs of complexes, related by an inversion center, come together at the more open end of their cavities to encapsulate a disordered diethyl ether molecule (Figure 3.2c). DMF molecules lie at either end of the trimer pairs near the narrower openings to the molecular cavities. Thus, when viewed along the [111] direction, the complexes give the appearance of forming channels containing solvate (Figure 3.2d).

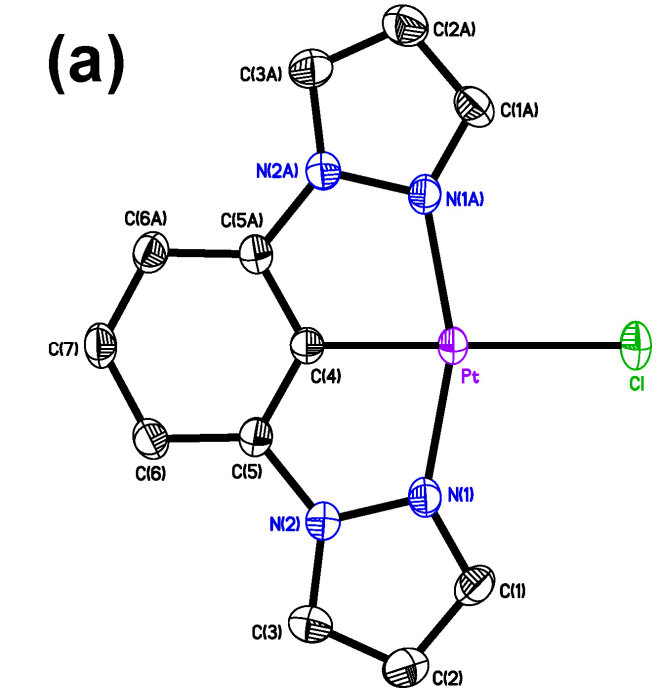
(a)
C(2A)
C(3A)
C(1A)
N(2A)
N(1A)
C(6A)
C(5A)
C(7)
C(4)
Pt
Cl
C(6)
C(5)
N(1)
N(2)
C(1)
C(3)
C(2)

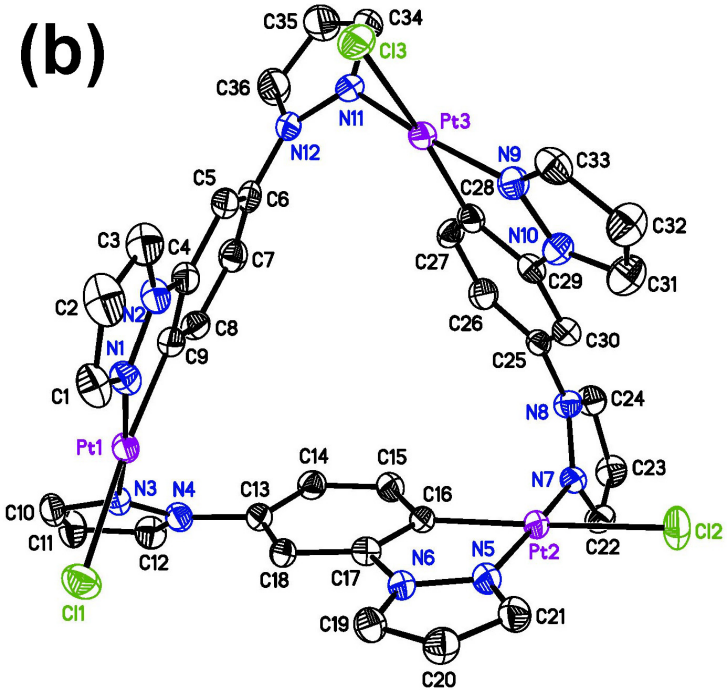
(b)
C35
C34
Cl3
C36
N11
Pt3
N12
N9
C33
C5
C28
C6
C32
C3
C4
N10
C7
C27
C29
C31
C2
N2
C26
C8
C30
N1
C9
C25
C1
N8
C24
Pt1
C14
C15
N7
C23
N3
N4
C13
C16
C10
Cl2
C11
C12
C18
C17
N6
N5
Pt2
C22
Cl1
C19
C21
C20

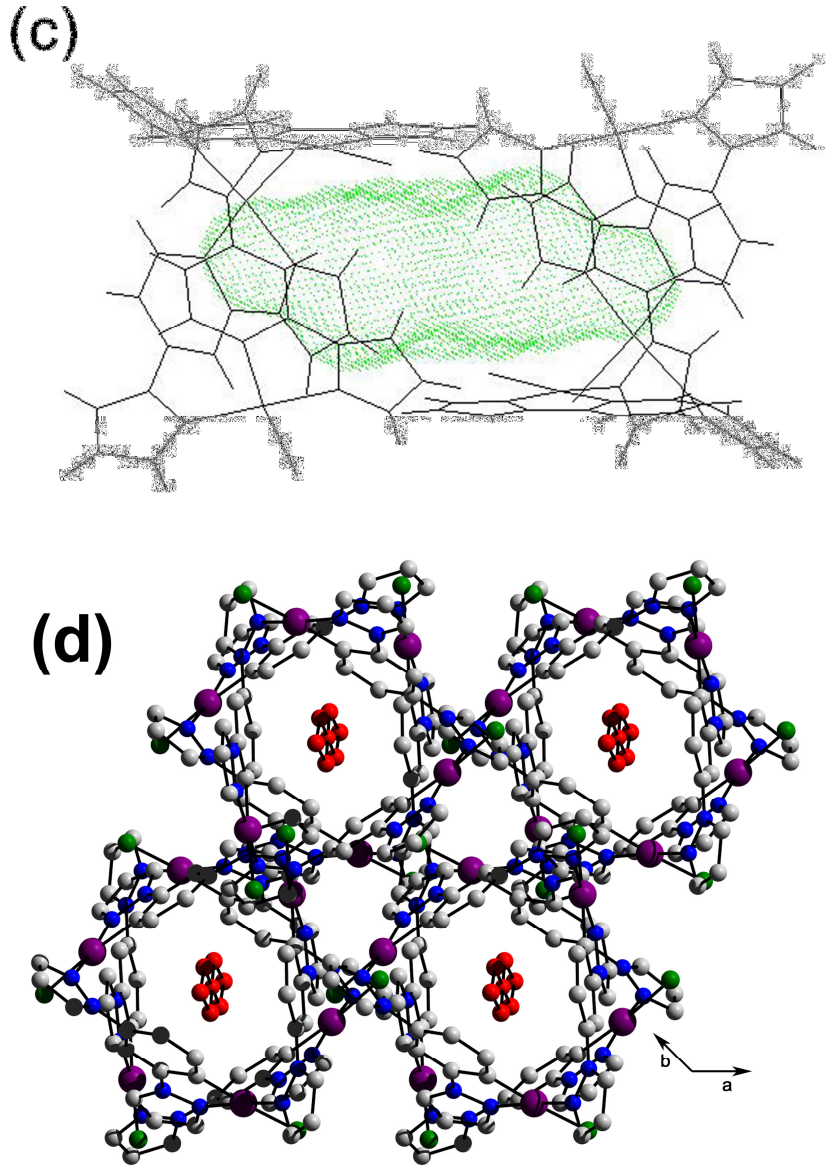

Figure 3.2. ORTEP diagrams of (a) Pt(bpzph)Cl and (b) the complex in crystals of [Pt(μ-bpzph)Cl]$_3$·DMF·0.5Et$_2$O. H atoms are omitted for clarity. (c) Void space occupied by the Et$_2$O molecule in the cavities of a pair of [Pt(μ-bpzph)Cl]$_3$ complexes. (d) Packing diagram of the molecular triangle viewed along the [111] direction. H-atoms and DMF molecules are omitted for clarity. Disordered Et$_2$O molecules in red.

The monomer and trimer are both stable in DMF solution, as determined by NMR spectroscopy. The ^{1}H NMR spectrum of Pt(bpzph)Cl exhibits four resonances with coincidental overlap of the pyrazolyl α proton and solvent resonances at 8.0 ppm.

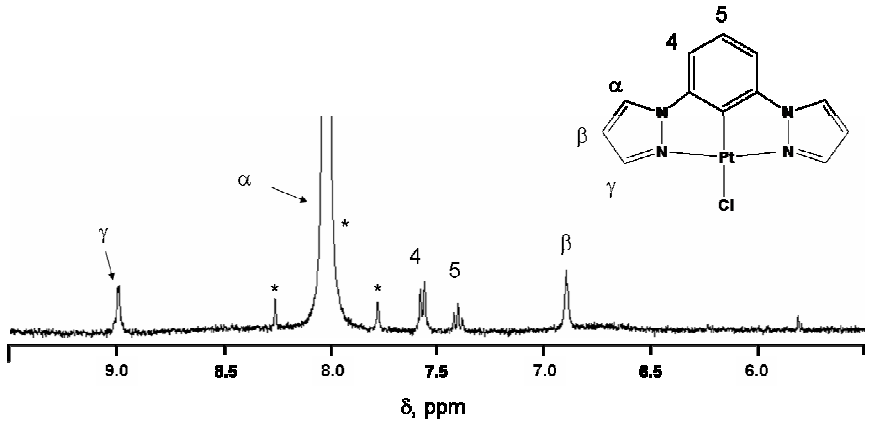

Figure 3.3. ^{1}H NMR of Pt(bpzph)Cl in DMF. (* marks resonances present in the solvent blank; resonance labeled α is buried under a solvent resonance.)

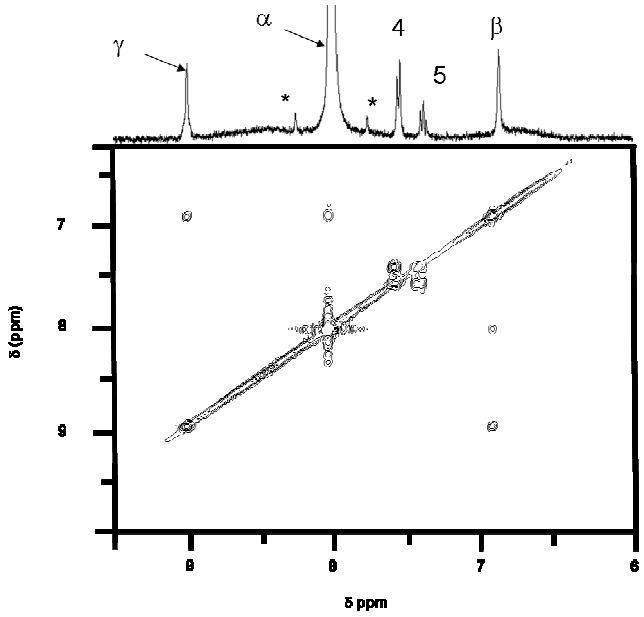

Figure 3.4. Two-dimensional COSY NMR spectrum of Pt(bpzph)Cl in DMF. (* marks resonances present in the solvent blank; resonance labeled α is presumed to be buried under a solvent resonance.)

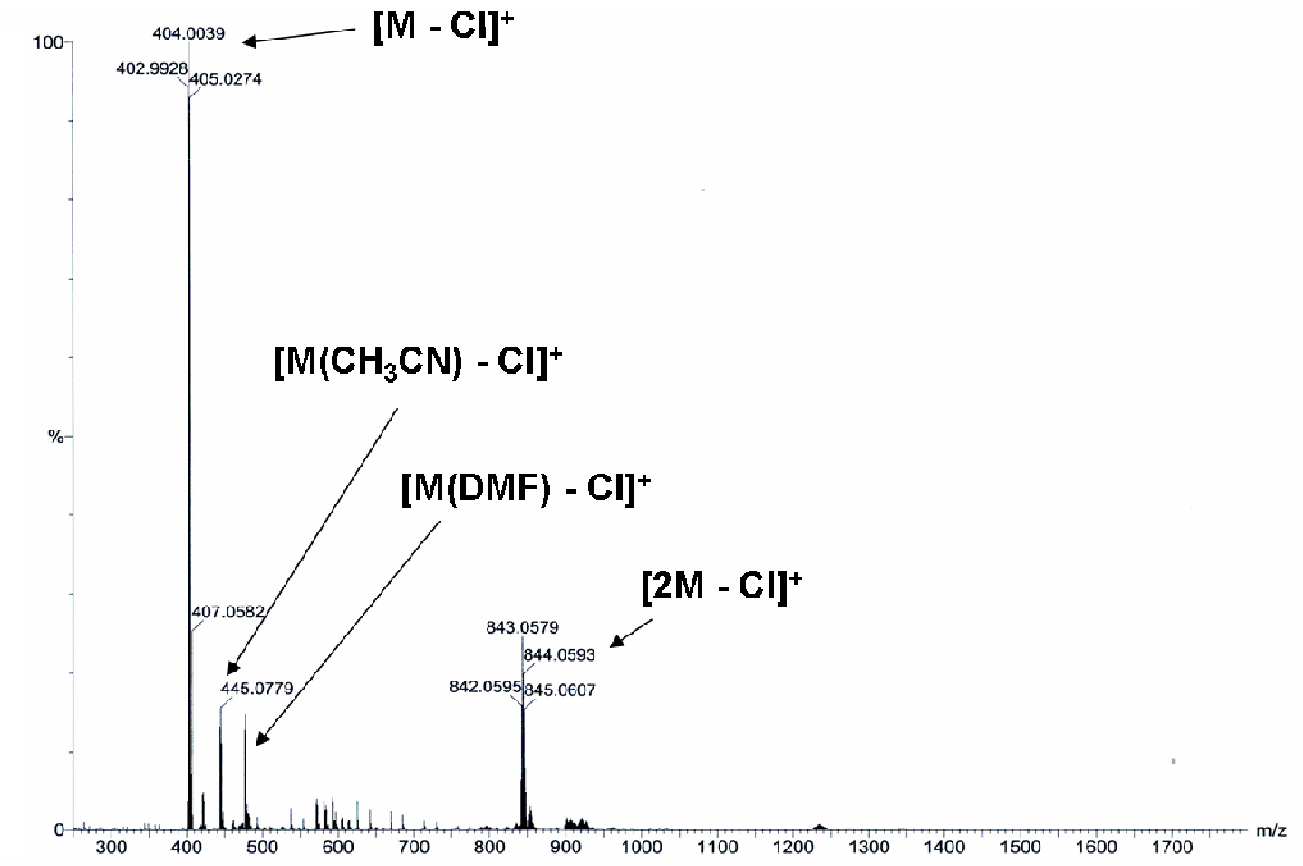

Figure 3.5. ESI mass spectrum of Pt(bpzph)Cl (**M**) in DMF/CH_3OH solution in the presence of a 50:50 acetonitrile:water solution and 0.1% formic acid buffer.

As expected from studies of 1-phenylpyrazole complexes,[15,18] the pyrazolyl resonances are shifted slightly downfield from those of the free ligand ($\Delta\delta$, 0.2-0.3 ppm), whereas the phenyl resonances are shifted slightly upfield ($\Delta\delta$, -0.2 ppm) (Figures 3.6-7).

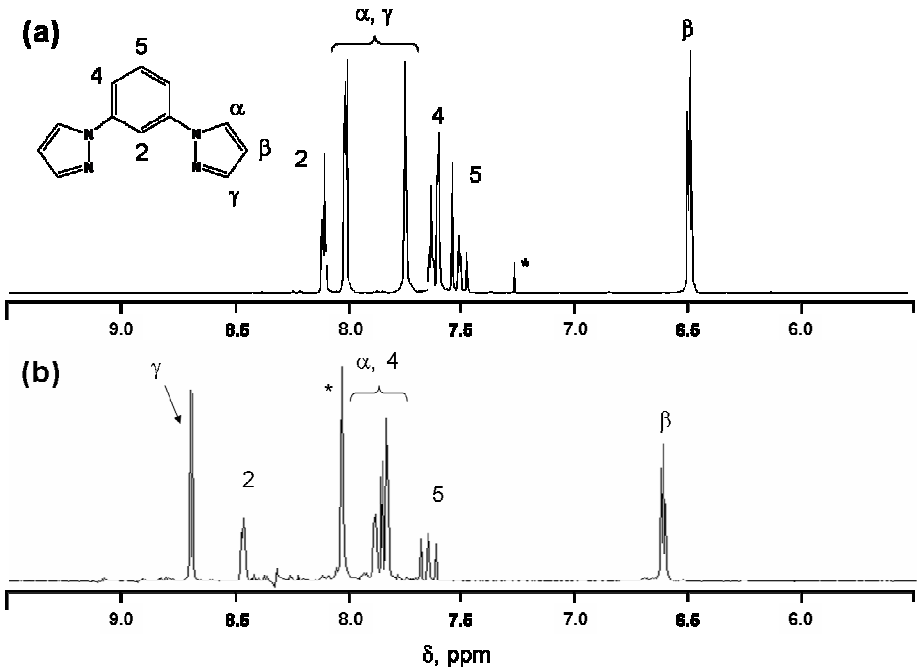

Figure 3.6. ^{1}H NMR spectra of bpzphH in (a) $CDCl_3$ and (b) DMF-d_7. (* marks resonances present in the solvent blank.)

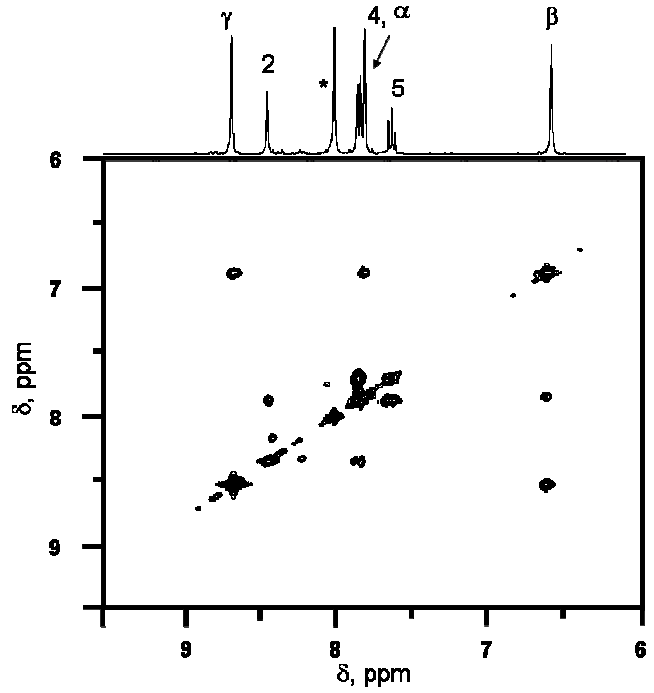

Figure 3.7. Two-dimensional COSY NMR spectrum of bpzphH in DMF-d_7. (* marks resonances present in the solvent blank.)

The spectrum of [Pt(μ-bpzph)Cl]$_3$ consists of nine sharp resonances, which were fully assigned using COSY and NOESY techniques (Figures 3.8-9). The α', γ', α, and γ proton pyrazolyl resonances fall between 8.55 and 8.05 ppm along with the 2-phenyl proton resonance of bpzph$^-$; the β and β' resonances occur slightly downfield from those of the free ligand. Interestingly, the resonances for the protons at the 4- and 5-positions on the phenyl group are strongly shifted upfield by 0.8 and 1.6 ppm, respectively, from those of the free ligand. These observations are consistent with strong transannular interactions between the ligand phenyl rings.[19] The large shift for the 4-phenyl proton is in agreement with the crystal structure, which suggests that the hydrogen atom is directed toward one face of the pz' 5-membered ring, resulting in shortest H(4-phenyl)···N(pz') contacts ranging from 2.64 to 2.77 Å. Strong inter-ring NOE signals between the α'-pyrazoyl and 4-phenyl protons, as well as between the 2-phenyl and α-pyrazoyl protons, confirm the connectivity observed in the solid state.

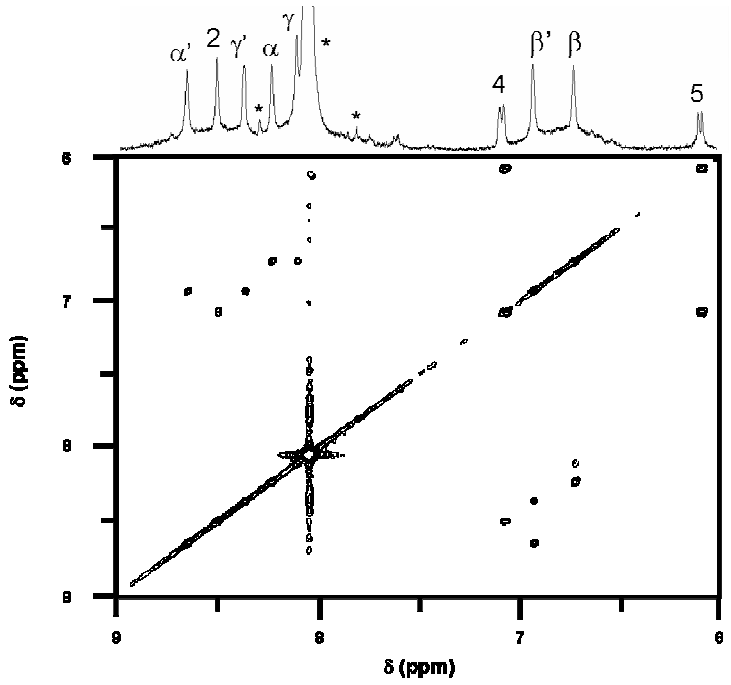

Figure 3.8. Two-dimensional COSY NMR spectrum of [Pt(μ-bpzph)Cl]$_3$ in DMF-d_7. (* marks resonances present in the solvent blank.)

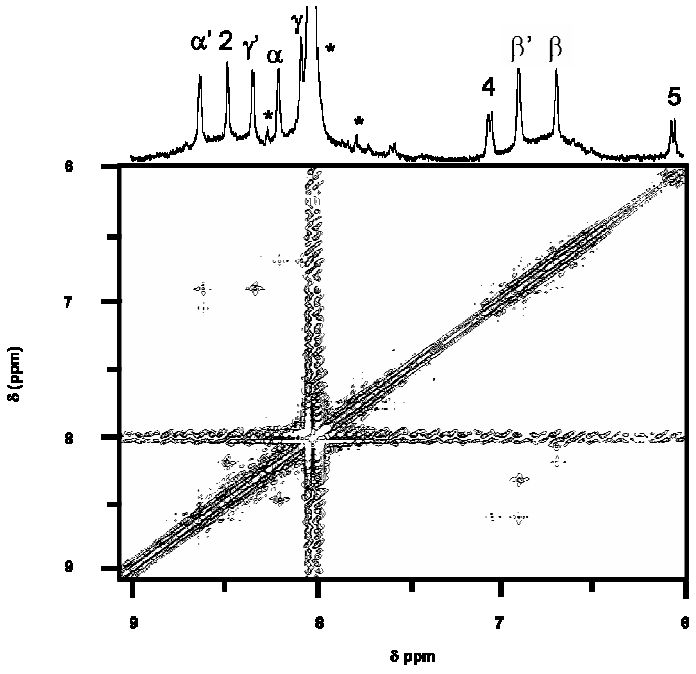

Figure 3.9. Two-dimensional NOESY NMR spectrum of [Pt(μ-bpzph)Cl]$_3$ in DMF-d_7. (* marks resonances present in the solvent blank.)

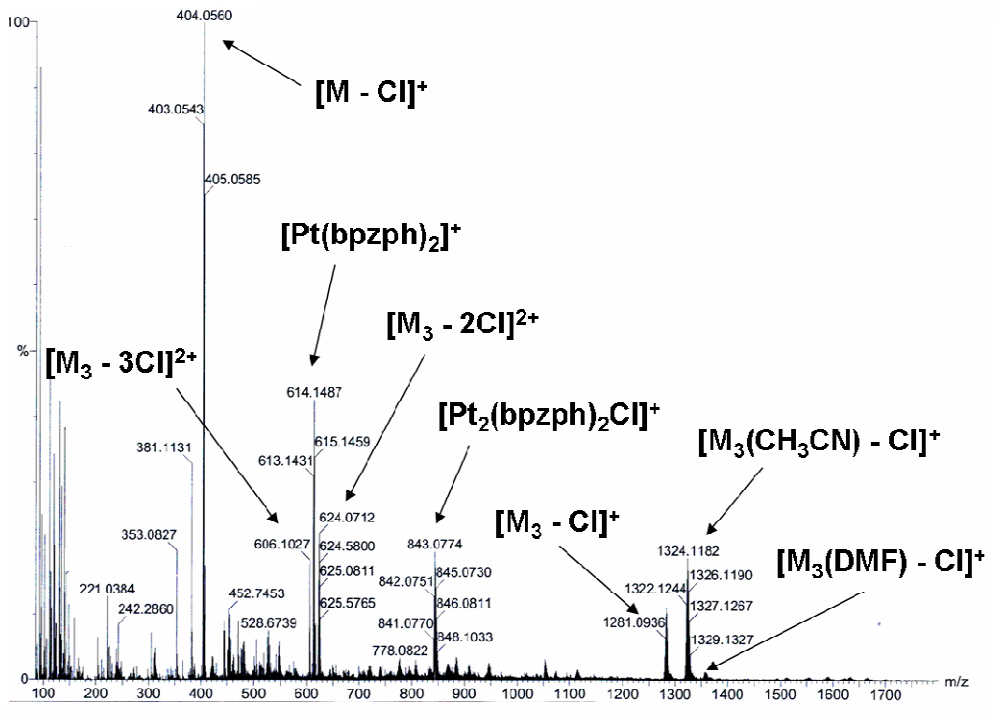

Figure 3.10. ESI mass spectrum of [Pt(μ-bpzph)Cl]$_3$ (**M$_3$**) in DMF/CH_3OH solution in the presence of a 50:50 acetonitrile:water solution and 0.1% formic acid buffer.

To investigate its thermal stability, [Pt(μ-bpzph)Cl]$_3$ was heated for 30 minute periods in DMF-d_7 at a series of progressively higher temperatures (100, 120, 135, 140, 150, 158°C), and the room-temperature spectrum was recorded between each period. The spectrum was unchanged after heating at 120°C. At higher temperatures, a small amount of black precipitate was detected, and resonances due to bpzphH were observed in the NMR spectrum. However, the decomposition was slow, as indicated by the persistence of trimer proton resonances throughout the experiment; and no resonances associated with the monomer or other complexes were detected. Similarly, heating mixtures of the Pt(bpzph)Cl and [Pt(μ-bpzph)Cl]$_3$ in DMF did not result in new products or a change in the ratio of monomer to trimer. Stirring the trimer with six equivalents of NaBr in DMF also did not result in any reaction. It seems likely that coordination of pz'

trans to pz in the trimer, rather than trans to the labilizing phenyl group, contributes to the observed stability. On the other hand, treatment of [Pt(μ-bpzph)Cl]$_3$ in DMF with three equivalents of $TlPF_6$, followed by addition of 3.5 equivalents of NaBr gave two new products, Pt(bpzph)Br and [Pt(μ-bpzph)Br]$_3$. The reaction solution was reduced to dryness to yield a brown solid. The ESI mass spectrum shows a peak at 1372.8, corresponding to $Pt_3(bpzph)_3Br_2^+$; no chloride-containing products were detected (Figure 3.11). The ^{1}H NMR spectrum of the brown solid dissolved in DMF-d_7 is consistent with clean conversion to monomer and trimer in a 1:1 ratio. As expected for halide substitution, the trimer resonances are shifted slightly downfield relative to the chloro adduct with the γ-pyrazolyl and 2-phenyl proton resonances being the most affected (Δδ, ~0.15 ppm).

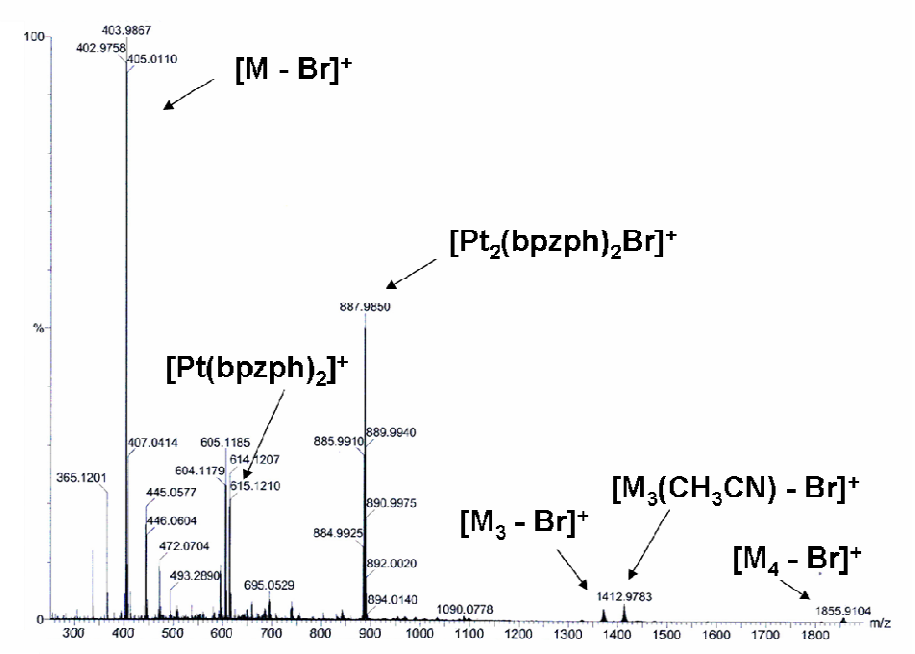

Figure 3.11. ESI mass spectrum of [Pt(μ-bpzph)Br]$_3$ (**M$_3$**) and Pt(bpzph)Br (**M**) formed in halide metathesis reaction of [Pt(μ-bpzph)Cl]$_3$.

Single crystals of Pt(bpzph)Br were obtained as pale yellow needles from a DMSO solution of the product, thereby confirming formation of this compound (Figure 3.11). The chloro and bromo adducts are isomorphous. The Pt-Br distance (2.525(5) Å) is slightly longer than observed for Pt-Cl (2.416(10) Å), as expected. The remaining distances and angles observed for Pt(bpzph)Br are similar to those observed for Pt(bpzph)Cl (Tables 3.2-3). .

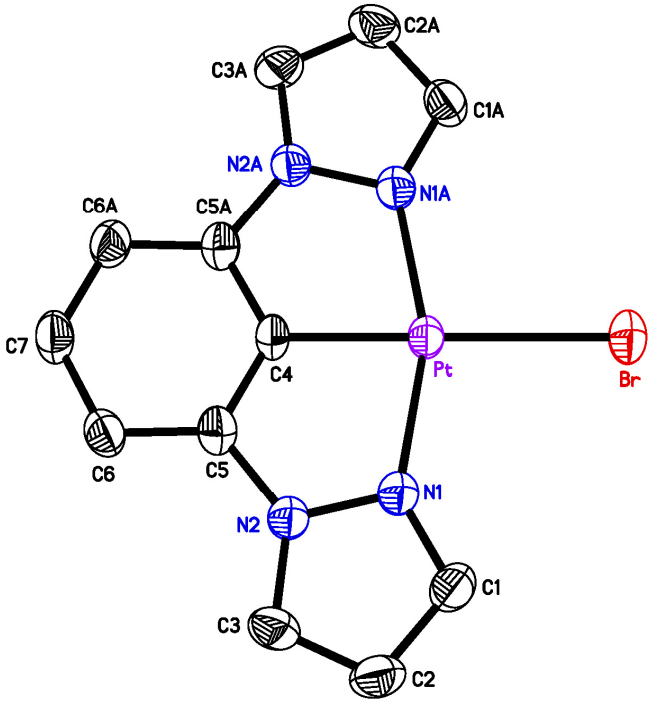

Figure 3.12. ORTEP diagram of Pt(bpzph)Br. H atoms omitted for clarity.

Conclusion.

The results presented here show that a conventional meridional tridentate chelate can support assembly of platinum(II) centers to give a comparatively rigid molecular polygon. The product in this case is a racemic mixture of enantiomers that exhibit

remarkable thermodynamic and kinetic stability. Moreover, the complex possesses an unusually deep molecular cavity. The chloride groups at one opening of the molecular cavity afford the opportunity to elaborate on the structure by ligand substitution in order to expand the cavity, introduce functionalities, or couple trimers to form larger molecular containers.

References.

(1) Willison, S. A.; Krause, J. A.; Connick, W. B. *Inorg. Chem.* **accepted**.

(2) a) P. J. Stang, B. Olenyuk, *Acc. Chem. Res.* **1997**, *30*, 502; b) S. Leininger, B. Olenyuk, P. J. Stang, *Chem. Rev.* **2000**, *100*, 853; c) R. S. Seidel, P. J. Stang, *Acc. Chem. Res.* **2002**, *35*, 972.

(3) For examples, see: (a) Schnebeck, R. D.; Freisinger, E.; Glahe, F.; Lippert, B. *J. Am. Chem. Soc.* **2000**, *122*, 1381-1390. (b) Sautter, A.; Schmid, D. G.; Jung, G.; Wurthner, F. *J. Am. Chem. Soc.* **2001**, *123*, 5424-5430. (c) Kryschenko, Y. K.; Seidel, S. R.; Arif, M.; Stang, P. J. *J. Am. Chem. Soc.* **2003**, *125*, 5193-5198. (d) Qin, Z.; Jennings, M. C.; Puddephatt, R. J. *Inorg. Chem.* **2003**, *42*, 1956-1965. (e) Chi, K.-W.; Addicott, C.; Arif, A. M.; Stang, P. J. *J. Am. Chem. Soc.* **2004**, *126*, 16569-16574. (f) Zhang, L.; Niu, Y. H.; Jen, A. K.-Y.; Lin, W. *Chem. Commun.* **2005**, 1002-1004.

(4) Tarkanyi, G.; Jude, H.; Palinkas, G.; Stang, P. J. *Organ. Let.* **2005**, *7*, 4971-4973.

(5) (a) Jiang, H.; Lin, W. *J. Am. Chem. Soc.* **2003**, *125*, 8084-8085. (b) Jiang, H.; Lin, W. *J. Org. Met. Chem.* **2005**, *690*, 5159-5169.

(6) For examples, see: a) R. D. Schnebeck, E. Freisinger, F. Glahe, B. Lippert, *J. Am. Chem. Soc.* **2000**, *122*, 1381; b) A. Sautter, D. G. Schmid, G. Jung, F. Wurthner, *J. Am. Chem. Soc.* **2001**, *123*, 5424; c) Y. K. Kryschenko, S. R. Seidel, M. Arif, P. J. Stang, *J. Am. Chem. Soc.* **2003**, *125*, 5193; d) Z. Qin, M. C. Jennings, R. J. Puddephatt, *Inorg. Chem.* **2003**, *42*, 1956; e) K.-W. Chi, C. Addicott, A. M. Arif, P. J. Stang, *J. Am. Chem. Soc.* **2004**, *126*, 16569; f) L. Zhang, Y. H. Niu, A. K.-Y. Jen, W. Lin, *Chem. Commun.* **2005**,1002.

(7) Willison, S. A.; Jude, H.; Antonelli, R. M.; Rennekamp, J. M.; Eckert, N. A.; Krause Bauer, J. A.; Connick, W. B. *Inorg. Chem.* **2004**, *43*, 2548-2555.

(8) Lexy, H.; Kauffman, T. *Chem. Ber.* **1980**, *113*, 2749-2754.

(9) Sotoyama, W.; Satoh, T.; Sawatari, N. (Fujitsu Limited) *U.S. Patent Appl.* 20060093854, 2006.

(10) APEX2 v2.0-2. SMART v5.631 and SAINT v6.45A data collection and data processing programs, respectively. Bruker Analytical X-ray Instruments, Inc., Madison, WI; SADABS v2.10 semi-empirical absorption and beam correction program. G.M. Sheldrick, University of Göttingen, Germany.

(11) SHELXTL v6.14 for structure solution, figures and tables, neutral-atom scattering factors as stored in this package. G.M. Sheldrick, University of Göttingen, Germany and Bruker Analytical X-ray Instruments, Inc., Madison, WI.

(12) *Diamond v3.1d*, Crystal Impact; Brandenburg, K.; Putz, H. 2007.

(13) Spek, A. L. *Acta Cryst.* **1990**, *A46*, c34.

(14) Doppiu, A.; Minghetti, G.; Cinellu, M. A.; Stoccoro, S.; Zucca, A.; Manassero, M. *Organometallics* **2001**, *20*, 1148-1152.

(15) Black, D. S. C.; Deacon, G. B.; Edwards, G. L. *Australian Journal of Chemistry* **1994**, *47*, 217-227.

(16) Pt(bpzph)Cl: C12H9N4ClPt, T=173 K, λ=0.7750 Å, monoclinic, C2/c, *a*=10.4065(7), *b*=14.7195(9), *c*=7.8549(5) Å, β=99.944(2)°, V=1184.97(13) Å^3, R1=0.0208, CCDC-656112. [Pt(μ-bpzph)Cl]$_3$, $C_{36}H_{27}N_{12}Cl_3Pt_3$.DMF·0.5$Et_2O$, T=150K, λ=1.54178 Å, triclinic, P-1, *a*=11.8105(4), *b*=14.1236(5), *c*=14.6980(5) Å, α=68.355(1), β=99.944(2), γ=82.618(2)°, V=1184.97(13) Å^3, R1=0.0311, CCDC-656113.

(17) (a) Wong, Y.-S.; Lippard, S. J. *Chem. Commun.* **1977**, 824-825. (b) Yip, H.-K.; Cheng, L.-K.; Cheung, K. K.; Che, C. M. *J. Chem. Soc. Dalton Trans.* **1993**, 2933-2938. (c) Bailey, J. A.; Hill, M. G.; Marsh, R. E.; Miskowski, V. M.; Schaefer, W. P.; Gray, H. B. *Inorg. Chem.* **1995**, *34*, 4591-4599. (d) Cini, R. D., A.; Giannettoni, R. *Inorg. Chim. Acta* **2001**, *315*, 73-80. (e) Tzeng, B.-C.; Lee, G.-H.; Peng, S.-M. *Inorg. Chem. Commun.* **2003**, *6*, 1341-1343. (f) Sengul, A. *Turk. J. Chem.* **2004**, *28*, 667-672.

(g) Angle, C. S.; DiPasquale, A. G.; Rheingold, A. L.; Doerrer, L. H. *Acta Cryst*. **2006**, *C62*, m340-m342. (h) Tastan, S.; Krause, J. A.; Connick, W. B., **2007** *to be submitted*.

(18) (a) Nonoyama, M.; Takayanagi, H. *Trans. Met. Chem.* **1976**, *1*, 10-13. (b) Chassot, L.; von Zelewsky, A. *Inorg. Chem.* **1987**, *26*, 2814-2818.

(19) Sheehan, M.; Cram, D. J. *J. Am. Chem. Soc.* **1969**, *91*, 3553-3558.

Chapter 4

The Influence of Ligand Methyl Group Substituents on the Formation of Monomeric and Macrocyclic Platinum(II) Compounds with *Bis*-2,6-Pyrazolyl-Phenyl Anionic Ligands

Introduction.

C-H activation reactions have been widely studied due to their importance in synthesis and catalysis.[1] Direct metal-aryl-carbon bond formation resulting in chelation of tridentate ligands has been successfully achieved with N-C-N or N-N-C pincer-type ligands. However the synthetic methodology for activating C-H bonds of aryl molecules is not always straightforward, resulting in unpredictable products with unusual metal-ligand coordination geometries.[2-6] Although the mechanism of C-H activation of chelating ligands is not yet fully understood, often the first step involves coordination of the ligand through one or more Lewis base donor group. Thus, to help facilitate the oxidative addition reaction, strong peripheral donor groups, such as N, P and S are frequently employed. In the cases of N-C-N, P-C-P, and S-C-S pincer ligands, the Lewis basic donor groups are believed to first chelate the metal, keeping the C-H bond and metal center in close proximity until the reaction occurs.[7]

Unusual metal-ligand coordination geometries can result from C-H activation of potential tridentate ligands with aryl groups. The activated ligands can chelate the metal center or bridge metals to form more elaborate architectures.[8] For example, as discussed in Chapter 3, two products were isolated from the reaction of *bis*-1,3-pyrazolyl-benzene (**1H**) with $PtCl_4^{2-}$ in acetic acid (Scheme 4.1).[9] For the C_{2v}-symmetric monomeric product, $\mathbf{1}^-$ is tridentate with the Pt bonded at the 2-position of the phenyl group; the

fourth coordination site of the metal is occupied by a chloride ligand. In the case of the C_3-symmetric trimer product, each **1**$^-$ ligand is bidentate with the metal bonded to a pyrazolyl group (pz) and to the phenyl group at the 6-position; the remaining pyrazolyl group (pz') is bonded to a different platinum center, resulting in a trans arrangement of the two N-donor pyrazolyl groups bonded to each Pt. The resulting molecular polygon is remarkably stable and has an unusually deep intramolecular cavity. Preliminary investigations have shown that concentrated reaction solutions and long reaction times give exclusively trimeric products, whereas more dilute solutions and shorter reaction times give only monomer products. Thus, careful control of the reaction conditions allows for selective activation of C-H bonds on the ligand.

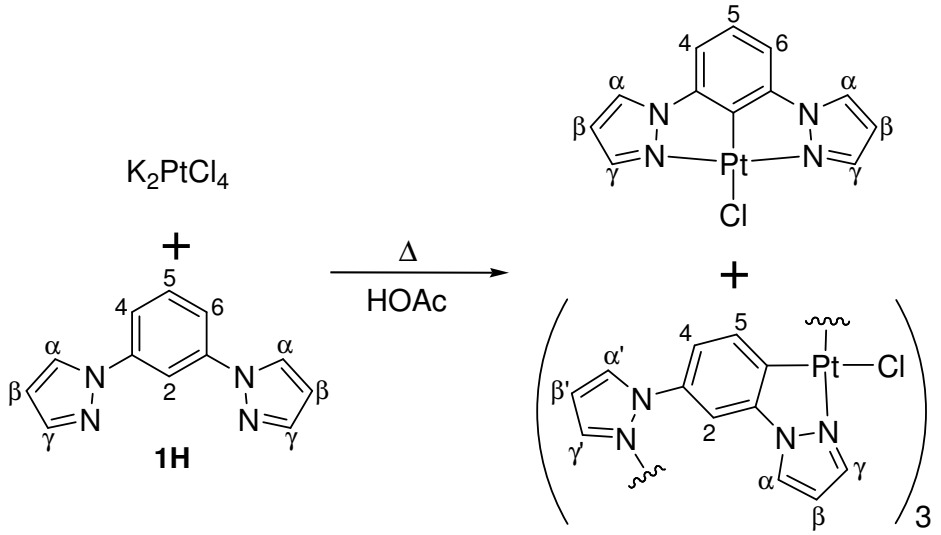

Scheme 4.1. Synthetic scheme for the Pt(**1**)Cl and [Pt(μ-**1**)Cl]$_3$.

A possible alternative strategy for controlling selectivity is to block specific sites by introducing one or more methyl substitutents on the center phenyl ring. For example, substitution of **1H** with methyl groups at the 4- and 6-positions to give **3H** (Figure 4.1) is expected to prevent formation of the trimer product. Conversely, substitution at the 2-

position to give **7H** is expected to prevent formation of the monomer product. It is less obvious how substituents at the 5-position of the phenyl or at the α-, β- and γ-positions of the pyrazolyl groups will influence product formation; modifications at these sites are of interest because they may provide a means of elaborating on the architecture of the metallocycle. In order to investigate the influence of methyl substitution of **1H** on the synthesis of platinum(II) complexes, we have examined the reactivity of the series of protonated ligands (**LH**) shown in Figure 4.1. At the outset of this work, **2H** and **3H** were expected to favor monomer products, whereas **7H** and **8H** were expected to favor macrocyclic products. The influence of the substituted pyrazolyl ligands in **4H**-**6H** was not certain. In the case of **9**, we hypothesized that it might be possible to form a trimer with a +3 charge. In this chapter, we report the products formed in the reactions of **LH** with platinum(II). The isolated products include the expected monomers and trimers, as well as surprising new dimeric products.

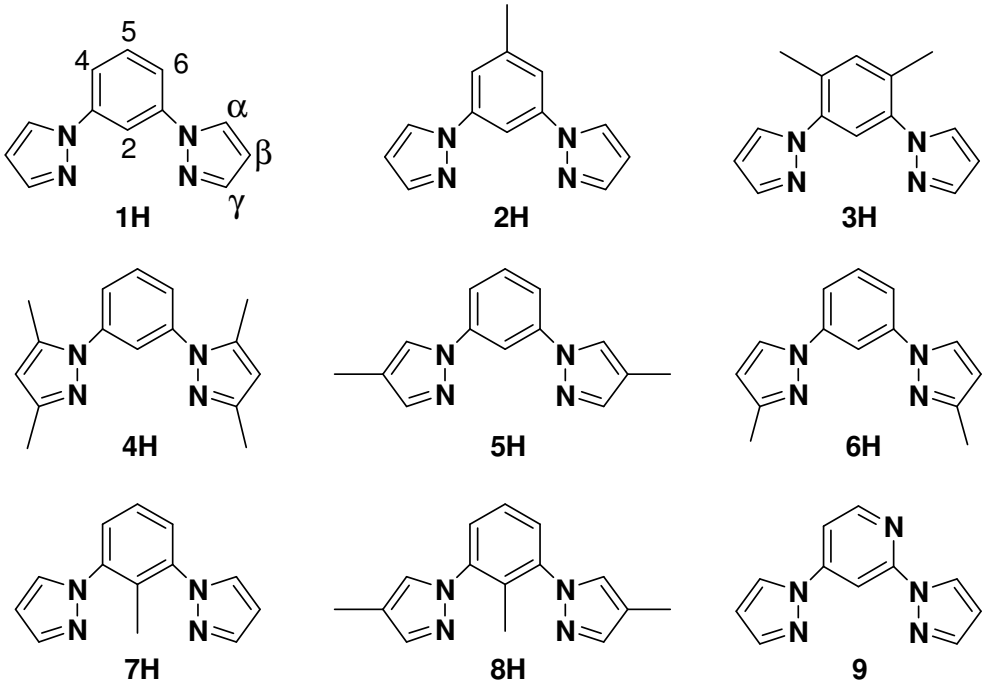

Figure 4.1. Nine ligand precursors. **1H** was previously reported in Chapter 3.

Experimental Section.

K_2PtCl_4 was purchased from Pressure Chemical. All other reagents were obtained from Acros, Alfa Aesar, or Aldrich. Pt(**1**)Cl and [Pt(μ-**1**)Cl]$_3$ were prepared as described in Chapter 3. ^{1}H NMR spectra were recorded at room temperature using a Bruker AC 400 MHz instrument. Deuterated solvents were purchased from Cambridge Isotope Laboratories. Mass spectra were obtained by electrospray ionization using either an Ionspec HiRes ESI-FTICRMS instrument or a Micromass Q-TOF-II instrument. Observed isotope patterns agreed well with predicted patterns based on natural isotopic abundances. Samples were dissolved in CH_3OH, $CH_3OH/CHCl_3$, $CH_3CN/CHCl_3$ or isopropyl alcohol (IPA) and, unless otherwise noted, subsequently mixed with an ESI buffer solution consisting of 0.1% formic acid in 50:50 acetonitrile:water. Representative spectra are shown in Figures 4.5, 4.8, 4.17, 4.23, 4.29, 4.32 and 4.41.

1,3-bis(*N*-pyrazolyl)toluene (2H). The product was prepared following a modification of the procedure for mono-substituted *N*-phenyl-pyrazoles described by Cristau and Taillefer.[10,11] Two 50 ml Schlenk flasks with stir bars, were heated in an oven overnight. Pyrazole (0.545 g, 8 mmol), 5 mol% Cu_2O (0.286 g, 0.2 mmol), two equivalents of Cs_2CO_3 (2.61 g, 8 mmol) and 20 mol% (1S,2S)-[N,N'-bis-((2'-pyridine)-methylene)]-1,2-diaminocyclohexane (Chxn-Py-Al)[10] 0.234 g, 0.2 mmol) were added to the first flask, which was subsequently charged with argon. In the second flask, 3,5-dibromotoluene (1.00 g, 4 mmol) in 3 ml of CH_3CN was bubble degassed for 25-30 minutes. The solution was cannula transferred under argon to the first flask, and the resulting mixture was refluxed for 2 days. After cooling to room temperature, the mixture was filtered affording an orange filtrate, which was concentrated to dryness. The

solid was dissolved in methylene chloride, and hexanes were added to induce precipitation. The mixture was filtered through a glass frit and the filtrate was rotary evaporated to give an orange oil. The product was purified by column chromatography on silica (CH_2Cl_2: hexane, 2:1). The desired product was obtained as an orange oil from the first of three bands to elute from the column. Yield, 0.272 g (1.21 mmol, 30.3%). ^{1}H NMR (400 MHz, $CDCl_3$, δ): 2.48 (3H, s, CH_3), 6.47 (2H, m, CH), 7.46 (2H, d, CH), 7.73 (2H, d, CH), 7.85 (1H, s, CH), 7.98 (2H, d, CH).

1,3-bis(*N*-pyrazolyl)-*m*-xylene (3H). The product was purified as an orange oil following a modification of the procedure for **2H** by substituting 4,6-diiodo-*m*-xylene (0.200 g, 0.6 mmol) for 3,5-dibromotoluene and salicylaldoxime,(salox) 0.015 g, 0.1 mmol) for Chxn-Py-Al. Yield, 0.085 g (0.356 mmol, 63.8%). ^{1}H NMR (400 MHz, $CDCl_3$, δ): 2.27 (6H, s, CH_3), 6.43 (2H, m, CH), 7.27 (1H, s, CH), 7.34 (1H, s, CH), 7.61 (2H, d, CH), 7.72 (2H, d, CH).

1,3-bis(3,5-dimethyl-*N*-pyrazolyl)benzene (4H). The product was purified as an orange oil following a modification of the procedure for **2H** by substituting 1,3-diiodobenzene (1.98 g, 6 mmol) for 3,5-dibromotoluene, 3,5-dimethyl pyrazole (0.390 g, 4 mmol) for pyrazole and 2.4 ml of DMF for CH_3CN. The reaction mixture was refluxed for 4 days. Yield, 0.849 g (3.19 mmol, 55.3%). ^{1}H NMR (400 MHz, $CDCl_3$, δ): 2.29 (3H, s, CH_3), 2.34 (3H, s, CH_3), 6.00 (2H, m, CH), 7.42 (2H, d, CH), 7.52-7.55 (2H, m, CH).

1,3-bis(4-methyl-*N*-pyrazolyl)benzene (5H). The product was purified as an orange oil following a modification of the procedure for **2H** by substituting 1,3-diiodobenzene (1.53 g, 4.3 mmol) for 3,5-dibromotoluene, 4-methylpyrazole (0.328 g, 4

mmol) for pyrazole and salox (0.110 g, 0.8 mmol) for Chxn-Py-Al. Yield, 0.444 g (1.86 mmol, 38.9%). ^{1}H NMR (400 MHz, $CDCl_3$, δ): 2.16 (6H, s, CH_3), 7.40-7.55 (5H, m, CH), 7.78 (2H, s, CH), 7.99 (1H, s, CH).

1,3-bis(3-methyl-N-pyrazolyl)benzene (6H). The product was purified as an orange oil following a modification of the procedure for **2H** by substituting 1,3-diiodobenzene (1.53 g, 4.3 mmol) for 3,5-dibromotoluene, 3-methylpyrazole (0.328 g, 4 mmol) for pyrazole and salox (0.110 g, 0.8 mmol) for Chxn-Py-Al. The ^{1}H NMR spectrum of the crude mixture exhibited a complex pattern of resonances in the aliphatic and aromatic regions. As previously noted, the reaction of iodobenzenes with 3-methylpyrazole results in a mixture of the α- and γ-methyl isomers.[10] Each isomer can be distinguished based on ^{1}H NMR chemical shifts as described in previous studies of substituted pyrazoles.[10,12,13] The product was purified by column chromatography on silica, eluting with CH_2Cl_2:hexanes solution. The CH_2Cl_2:hexanes ratio was gradually increased from 2:1 to 9:1, and the first major band to elute from the column was found to contain the product. The chromatography was repeated until the product was pure. The product was inferred to be methylated at the γ-position because the chemical shift for the pyrazolyl resonance at 7.89 ppm is similar to the value obtained for γ methyl-substituted *N*-phenylpyrazole (*i.e.*, 3-methyl-1-phenyl-1*H*-pyrazole). By contrast, the γ proton resonance for 5-methyl-1-phenyl-1*H*-pyrazole occurs at 7.58 ppm in $CDCl_3$..[10] Yield, 0.1095 g (0.460 mmol, 15.2 %). ^{1}H NMR (400 MHz, $CDCl_3$,δ): 2.39 (6H, s, CH_3), 6.26 (2H, m, CH), 7.45 (1H, t, CH), 7.53 (2H, d, CH), 7.89 (2H, d, CH), 7.99 (1H, s, CH).

2,6-bis(*N*-pyrazolyl)toluene (7H). The compound was prepared by a modification of the method of Kauffmann and Lexy[14] for the preparation of 1,3,5-tri(1-

pyrazolyl)benzene. Using dry glassware as in the preparation of **2H**, excess pyrazole (3.00 g, 44 mmol) was dissolved in nitrobenzene (15 ml) under argon. CuI (1.72 g, 8.8 mmol), K_2CO_3 (4.88 g, 35 mmol) and 2,6-dibromotoluene (0.457 mL, 2.9 mmol) were added, and the mixture was stir under refluxing conditions for 6 days. After cooling to room temperature, the mixture was filtered affording a yellow-green filtrate, which was reduced to dryness. The solid was dissolved in methylene chloride, and hexanes were added to induce precipitation. The mixture was filtered via suction filtration through a glass frit, and the filtrate was rotary evaporated to produce a yellow-orange oil. The filtrate was purified on silica (CH_2Cl_2: hexanes, 2:1) giving three bands. The first of three bands was found to contain a monosubstituted product. The desired product was obtained as a tan solid from the second band. Yield, 0.191 g (0.9 mmol, 29.0%). ^{1}H NMR (400 MHz, $CDCl_3$, δ): 2.03 (3H, s, CH_3), 6.49 (2H, m, CH), 7.39-7.42 (3H, m, CH), 7.66 (2H, d, CH), 7.76 (2H, d, CH).

2,6-bis(4-methyl-*N*-pyrazolyl)toluene (8H). The product was crystallized as a tan solid from CH_2Cl_2:hexanes after following a modification of the procedure for **2H** by substituting 2,6-dibromotoluene (0.321 g, 1.3 mmol) for 3,5-dibromotoluene and 4 ml of DMF for CH_3CN. Yield, 0.143 g (0.568 mmol, 71%). ^{1}H NMR (400 MHz, $CDCl_3$, δ): 2.06 (3H, s, CH_3), 2.18 (6H, s, CH_3), 7.34-7.41 (5H, m, CH), 7.55 (2H, d, CH).

2,4-bis(*N*-pyrazolyl)pyridine (9). The product was crystallized as a yellow crystalline solid from CH_2Cl_2:hexanes after following a modification for **2H** by substituting 2,4-dibromopyridine (0.473 g, 2.0 mmol) for 3,5-dibromotoluene and 3 ml of DMF for CH_3CN. Yield, 0.256 g (1.2 mmol, 57%). ^{1}H NMR (400 MHz, $CDCl_3$, δ): 6.48 (1H, s, CH), 6.53 (1H, s, CH), 7.66 (1H, d, CH), 7.71-7.78 (2H, m, CH), 8.14 (1H, s,

CH), 8.22 (1H, s, CH), 8.42 (1H, s, CH), 8.59 (1H, s, CH). (400 MHz, DMF, δ): 6.64 (1H, m, CH), 6.72 (1H, m, CH), 7.91-7.92 (2H, m, CH), 7.95 (1H, s, CH), 8.51 (1H, s, CH), 8.57 (1H, d, CH), 8.71 (1H, s, CH), 8.91 (1H, s, CH).

Pt(2)Cl. 2H (0.2289g, 1.02 mmol) was dissolved in 5 ml of acetic acid. K_2PtCl_4 (0.4236g, 1.02 mmol) was added, and the mixture was refluxed for 4 days. The mixture was cooled to room temperature and filtered. The brown precipitate was washed with methylene chloride and allowed to dry. Yield 0.4405g (95.1%). ^{1}H NMR (400 MHz, $CDCl_3$, δ): 2.41 (3H, s, CH_3), 6.65 (2H, m, CH_3), 6.89 (2H, s, CH), 8.01-8.13 (4H, m, CH). ^{1}H NMR (400 MHz, DMSO-d_6, δ): 1.91 (3H, s, CH_3), 6.84 (2H, s, CH_3), 7.39 (2H, s, CH), 7.92 (2H, s, CH), 8.90 (2H, s, CH). MS-ESI ($CH_3OH/CHCl_3$/ESI buffer) *m/z*: 418.0685, [Pt(**2**)]$^+$; 868.4185, [Pt(**2**)(**2H**)^2]$^+$.

Pt(3)Cl. 3H (0.0350g, 0.147 mmol) was dissolved in 5 ml of acetic acid. K_2PtCl_4 (0.061g, 0.147 mmol) was added, and the mixture was refluxed for 7 days. The mixture was cooled to room temperature and filtered. The brown precipitate was washed with methylene chloride and allowed to dry. Yield 0.0491g (71.5%). ^{1}H NMR (400 MHz, $CDCl_3$, δ): 2.61 (6H, s, CH_3), 6.63 (2H, m, CH), 6.78 (1H, s, CH), 8.02 (2H, d, CH), 8.16 (2H, d, CH). ^{1}H NMR (400 MHz, DMF-d_7, δ): 1.98 (6H, s, CH_3), 6.88 (2H, m, CH), 7.04 (1H, s, CH), 8.03 (2H, d, CH), 8.72 (2H, d, CH). MS-ESI ($CHCl_3/CH_3CN$/ESI buffer) *m/z*: 432.0818, [Pt(**3**)]$^+$; 473.1059, [Pt(**3**)(CH_3CN)]$^+$; 882.3994, [2(Pt(**3**)Cl) - Cl]$^+$.

Pt(4)Cl. 4H (0.1178g, 0.442 mmol) was dissolved in 11 ml of acetic acid. K_2PtCl_4 (0.1800g, 0.434 mmol) was added, and the mixture was refluxed for 3 days. The mixture was cooled to room temperature and filtered. The brown precipitate was washed

with methylene chloride, hexanes and ether and allowed to dry. Yield 0.1691g (78.6%). ^{1}H NMR (400 MHz, $CDCl_3$, δ): 2.72 (3H, s, CH_3), 2.79 (3H, m, CH_3), 6.04 (2H, s, CH), 7.02 (2H, d, CH), 7.16 (1H, t, CH). MS-ESI ($CH_3CN/CHCl_3$) *m/z*: 460.1039, $[Pt(\mathbf{4})]^+$; 501.1330, $[Pt(\mathbf{4})(CH_3CN)]^+$; 955.1686, $[2[Pt(\mathbf{4})Cl] - Cl]^+$.

Pt(5)Cl. 5H (0.0507g, 0.210 mmol) was dissolved in 20 ml of acetic acid. K_2PtCl_4 (0.0880g, 0.212 mmol) was added and the mixture was refluxed for 2 days. The mixture was cooled to room temperature and filtered. The tan precipitate was washed with CH_2Cl_2 and ether and allowed to dry. Yield 0.0496g (50.5%). ^{1}H NMR (400 MHz, $CDCl_3$, δ): 2.20 (6H, s, CH_3), 6.92 (2H, d, CH), 7.22 (1H, t, CH), 7.80-7.85 (4H, m, CH). MS-ESI ($CHCl_3/CH_3OH$) *m/z*: 432.0646, $[Pt(\mathbf{5})]^+$; 473.1094, $[Pt(\mathbf{5})(CH_3CN)]^+$; 899.0898, $[2(Pt(\mathbf{5})Cl) - Cl]^+$; 977.1475, $[2(Pt(\mathbf{5})) - 2Cl + DMSO]^+$.

Pt(6)Cl. 6H (0.1288g, 0.540 mmol) was dissolved in 5 ml of acetic acid. K_2PtCl_4 (0.2631g, 0.634 mmol) was added, and the mixture was refluxed for 5 days. The mixture was cooled to room temperature and filtered. The brown precipitate was washed with methylene chloride, hexanes and ether and allowed to dry. Yield 0.2400g (94.9%). ^{1}H NMR (400 MHz, $CDCl_3$, δ): 2.82 (3H, s, CH_3), 6.88 (2H, d, CH), 7.21 (1H, t, CH), 7.86 (2H, d, CH). MS-ESI (ESI) *m/z*: 432.0740, $[Pt(\mathbf{6})]^+$; 819.1038, $[Pt_2(\mathbf{6})(DMSO)_2Cl]^+$; 899.1384, $[2(Pt(\mathbf{6})Cl) - Cl]^+$.

[Pt(μ-5)Cl]$_3$. 5H (0.0507g, 0.213 mmol) was dissolved in 5 ml of acetic acid. K_2PtCl_4 (0.0882g, 0.212 mmol) was added, and the mixture was refluxed for 14 days. The tan solid was filtered, washed with CH_2Cl_2 and ether. Yield 0.0928g (93.4%). ^{1}H NMR (400 MHz, $CDCl_3$, δ): 2.20 (3H, s, CH_3), 2.25 (3H, s, CH_3), 5.99 (1H, d, CH), 6.58 (1H, d, CH), 7.52 (1H, s, CH), 7.75 (1H, s, CH), 7.90-7.92 (2H, m, CH), 8.35 (1H, s,

CH). MS-ESI (CH_3OH/ESI buffer) *m/z*: 432.0630, $[Pt(\mathbf{5})]^+$; 473.0812, $[Pt(\mathbf{5})(CH_3CN)]^+$; 899.0898, $[[Pt(\mathbf{5})Cl]_2 - Cl]^+$; 1367.1212, $[[Pt(\mathbf{5})Cl]_3 - Cl]^+$; 1408.1421, $[[Pt(\mathbf{5})Cl(CH_3CN)]_3 - Cl]^+$.

$[Pt_2(\mu\text{-}7H)(\mu\text{-}7)Cl_3]$. 7H (0.100g, 0.445 mmol) was dissolved in 5 ml of acetic acid. $Pt(MeCN)_2Cl_2$ (0.1548g, 0.445 mmol) was added, and the mixture was refluxed for 5 days. The mixture was filtered, and the pale yellow solid was washed with CH_2Cl_2 and ether. Yield 0.1915g (94.9%). ^{1}H NMR (400 MHz, DMF-d_7, δ): 2.41 (3H, s, CH_3), 2.55 (3H, s, CH_3), 6.50 (1H, d, CH), 6.74 (1H, m, CH), 6.76 (1H, m, CH), 6.85 (1H, m, CH), 6.99 (1H, m, CH), 7.25-7.29 (1H, m,CH), 7.51 (1H, d, CH), 7.97 (1H, d, CH), 8.02 (1H, d, CH), 8.13 (1H, d, CH), 8.31 (1H, d, CH), 8.34 (1H, d, CH), 8.45 (1H, d, CH), 8.70 (1H, d, CH), 8.75 (1H, d, CH), 8.77 (1H, d, CH). MS-ESI (IPA/ESI buffer) *m/z*: 417.0717, $[Pt(\mathbf{7})]^+$; 647.0020, $[Pt(\mathbf{7}) + Pt]^+$; 871.1127, $[[Pt(\mathbf{7})Cl]_2 - Cl]^+$; 908.0891, $[[Pt(\mathbf{7})Cl]_2 + H]^+$; 1325.1559, $[[Pt(\mathbf{7})Cl]_3 - Cl]^+$.

Reaction of 8H with K_2PtCl_4. 8H (0.0635g, 0.252 mmol) was dissolved in 4.6 ml of acetic acid. K_2PtCl_4 (0.1012g, 0.244 mmol) was added, and the mixture was refluxed for 14 days. The mixture was filtered, and the pale yellow solid was washed with CH_2Cl_2 and ether. The product was recrystallized from DMF/ether, filtered and dried to give a pale yellow solid. Yield 0.1160g (98.6%). ^{1}H NMR (400 MHz, $CDCl_3$, δ): 2.11-2.16 (12H, m, CH_3), 2.29 (3H, s, CH_3), 2.38 (3H, s, CH_3), 6.50 (1H, d, CH), 7.11 (1H, d, CH), 7.20-7.36 (2H, m, CH), 7.46 (1H, s, CH), 7.65 (1H, d, CH), 7.71 (1H, d, CH), 7.83 (1H, d, CH), 7.89 (1H, d, CH), 8.15 (2H, d, CH), 8.84 (1H, d, CH). MS-ESI (CH_3OH/ESI buffer) *m/z*: 432.0630, $[Pt(\mathbf{8})]^+$; 473.0812, $[Pt(\mathbf{8})(CH_3CN)]^+$; 899.0898, $[[Pt(\mathbf{8})Cl]_2 - Cl]^+$; 1367.1212, $[[Pt(\mathbf{8})Cl]_3 - Cl]^+$; 1408.1421, $[[Pt(\mathbf{8})Cl]_3(CH_3CN) - Cl]^+$.

Pt(9)Cl_2. K_2PtCl_4 (0.101g, 0.243 mmol) was dissolved in 5 ml of H_2O. Slightly less than one equivalent of **9** (0.0492g, 0.233 mmol) was added, and the mixture was refluxed for 1 day. The yellow solid was filtered, washed with H_2O and allowed to dry. Yield 0.095g (86.6%). ^{1}H NMR (400 MHz, DMF-d_7, δ): 6.84 (1H, d, CH), 7.18 (1H, d, CH), 8.09 (1H, s, CH), 8.25 (1H, d, CH), 8.32 (1H, d, CH), 8.93-8.96 (2H, m, CH), 9.24 (1H, d, CH), 9.57 (1H, d, CH). MS-ESI ($CHCl_3$/CH_3OH/ESI buffer) *m/z*: 441.0205, [Pt(**9**) - Cl]$^+$; 487.0783, [Pt(**9**) - Cl + COOH]$^+$; 509.0491, [Pt(**9**) - Cl + COONa]$^+$; 882.0542, [(Pt(**9**)$Cl)_2$]$^+$; 950.0705, [[Pt(**9**)]$_2$ - 2Cl + COONa]$^+$; 1427.1008, [[Pt(**9**)$Cl]_3$ - Cl + COOH]$^+$.

Reaction of Pt(9)Cl_2 with $TlPF_6$. $TlPF_6$ (0.033g, 0.094 mmol) was added to Pt(**9**)Cl_2 (0.051g, 0.107 mmol) dissolved in 15 ml of DMF. The mixture was stirred for 30-45 minutes. The cloudy yellow solution was filtered through Celite, and the filtrate was stirred for an additional 24 hours. The resulting yellow solution was concentrated to dryness to give an orange solid. Yield 0.058g (92.4%). ^{1}H NMR (400 MHz, DMF-d_7, δ): 6.84 (1H, d, CH), 7.18 (1H, d, CH), 8.09 (1H, s, CH), 8.25 (1H, d, CH), 8.32 (1H, d, CH), 8.99-9.00 (2H, m, CH), 9.24 (1H, d, CH), 9.63 (1H, d, CH). MS-ESI (CH_3CN) *m/z*: 515.9518, [Pt(**9**) - Cl +DMF]$^+$; 993.9526, [Pt(**9**) - Cl + DMF]$^+$; 1432.9272, [[Pt(**9**)$Cl]_3$]$^{3+}$.

X-ray Crystallography. APEX2 (v2.0-2 or v2.1-4) , SMART v5.631 and SAINT (v6.45A, v7.23A or v7.34A) programs were used for data collection and data processing, respectively.[15] SADABS (v2.10 or v2004/1) was used for semi-empirical absorption and beam corrections.[15] SHELXTL v6.14 was used for the structure solution and generation of figures and tables[16] Neutral-atom scattering factors were used as stored in this package. DIAMOND v3.1e was used to generate packing diagrams.[17,18]

Individual crystal details and acquisition parameters are collected in Table 4.1. Single crystals of each complex were mounted in a loop with paratone-N and transferred immediately to the goniostat bathed in a cold stream. Absorption and beam corrections were applied based on the multiscan technique as implemented in SADABS. The structures were solved by a combination of direct methods in SHELXTL and the difference Fourier technique and refined by full-matrix least squares on F^2. Non-hydrogen atoms were refined with anisotropic displacement parameters. Weights were assigned as $w^{-1}=[\sigma^2(F_o^2)+(aP)^2+bP]$ where $P=0.33333F_o^2+0.66667F_c^2$ and a,b are refined quantities. H-atom positions were either located directly from the difference map or calculated based on geometric criteria and treated with a riding model in subsequent refinements. All H-atom isotropic displacement parameters were defined as $a*U_{eq}$ of the adjacent atom (a=1.5 for methyl and 1.2 for all others).

Table 4.1. Single-Crystal Diffraction Data Collection Parameters.

Parameter	Pt(2)Cl[(a)]	Pt(**3**)Cl[(b)]	Pt(**4**)Cl[(b)] Orthorhombic Form	Pt(**4**)Cl[(a)] Monoclinic Form	Pt(**5**)Cl[(c)]	$Pt_2(\mu$-**6'**$)Cl_2((CH_3)_2SO)_2 \cdot (CH_3)_2SO$ [(c)]	$Pt_2(\mu$-**7**$)(\mu$-**7H**$)Cl_3$[(c)]$\cdot H_2O$	Pt_2(**8'**$)Cl_2((CH_3)_2SO)_2$[(c)]	$[Pt(\mu$-**1'**$)Cl_2]_3$[(a)]	Pt(**9**$)Cl_2$[(a)]
Crystal Information										
Crystallization solvent(s)	CH_3CN -Et_2O	DMSO	CH_3CN-Et_2O	CH_3CN -Et_2O	DMF-CH_2Cl_2	HOAc-CH_2Cl_2-hexane (workup-DMSO-DMF-Et_2O)	DMF-Et_2O-CH_2Cl_2	DMSO	DMF / *rac*-2-chlorobutane	DMF/ Et_2O
Color and morphology	Very pale yellow rods	Pale amber blades	Very pale yellow blades	Pale yellow blocks	Colorless blocks	Very pale yellow needles	Pale yellow plates	Very pale yellow rods	Very pale yellow plates	Pale yellow blocks
Size (mm)	0.14 x 0.05 x 0.04	0.45 x 0.05 x 0.01	0.19 x 0.05 x 0.01	0.11 x 0.10 x 0.06	0.09 x 0.05 x 0.03	0.19 x 0.02 x 0.02	0.05 x 0.04 x 0.02	0.14 x 0.04 x 0.04	0.10 x 0.09 x 0.03	0.04 x 0.03 x 0.02
T, K	173	150	150	193	150	150	150	150	195	195
λ, Å	0.77580	1.54178	1.54178	0.77580	0.77490	0.77490	0.77490	0.77490	0.77490	0.77490
Unit Cell Calculation										
data frame duration, s[(d)]	1	5	12	1	1	1	1	1	1	4
Intensity Data Collection										
data frame duration, s[(d)]	1	5	12	1	1	1	1	1	1	4
resolution, Å	0.80	0.80	0.80	0.85	0.75	0.75	0.75	0.80	0.80	0.80

(a) Data were collected ($2\theta_{max}$=58-60°) with a Bruker Platinum200 CCD detector at Beamline 11.3.1 at the Advanced Light Source (Lawrence Berkeley National Laboratory) using synchrotron radiation.
(b) Data were collected ($2\theta_{max}$~135°) with a standard Bruker SMART6000 CCD diffractometer using graphite-monochromated Cu Kα radiation
(c) Data were collected ($2\theta_{max}$ ~60°) with a Bruker APEXII CCD detector at Beamline 11.3.1 at the Advanced Light Source (Lawrence Berkeley National Laboratory) using synchrotron radiation
(d) All data were collected with narrow frame widths (0.2-0.3° increments of ω) and processed accordingly.

Results and Discussion.

Ligand Precursors. The eight ligand precursors (**LH**) and **9** shown in Figure 4.1 were prepared by modification of the procedures reported by Cristau,Taillefer,[10] Lexy and Kauffmann[14] for the preparation of substituted *N*-phenyl-pyrazoles (Scheme 4.2). In most cases, two equivalents of the appropriate pyrazole were allowed to react with a 1,3-dibromobenzene or 1,3-diiodobenzene derivative in the presence of two equivalents of Cs_2CO_3, and catalytic amounts of Cu_2O and a chelating Schiff-base ligand (Scheme 4.2 (a)). In the case of **7H**, standard CuI coupling conditions were used (Scheme 4.2 (b)).[14] The resulting compounds incorporate methyl substituents at the 4- and 6-positions (**3H**), 5-position (**2H**) or 2-position (**7H**, **8H**) of the benzene ring. Additionally, derivatives with methyl substituents at the α-, β- or γ-positions of the pyrazole groups were prepared (**4H**, **5H**, **6H**).

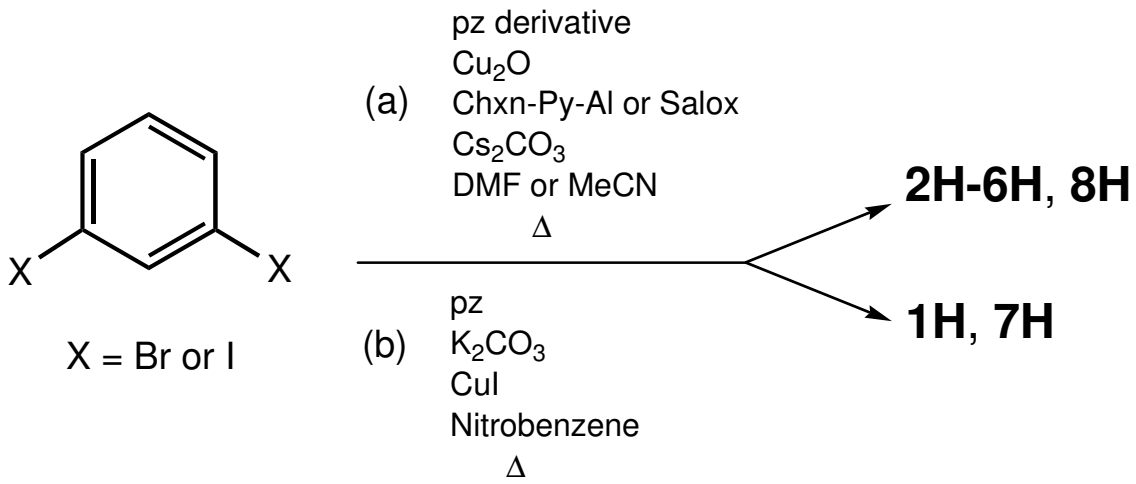

Scheme 4.2. Synthetic scheme for ligand precursors: (a) **2H-6H**, and **8H**, (b) **1H** and **7H**.

Monomer Products. Adapting the procedure for the preparation of Pt(**1**)Cl, each of the ligand precursors (**LH** = **2H**-**6H**,) was refluxed with one equivalent of $K_2[PtCl_4]$ in acetic acid for relatively short time periods (2-5 days) (Scheme 4.3). The resulting off-white precipitate was washed with methylene chloride to give the Pt(**L**)Cl product in high yield (50-95%). In the case of **5H**, the concentration of the ligand precursor was ≤15.0 mM in order to avoid formation of a trimeric product (*vide infra*). Interestingly, even at concentrations >100 mM, reactions involving **4H** and **6H** resulted in exclusively monomer products.

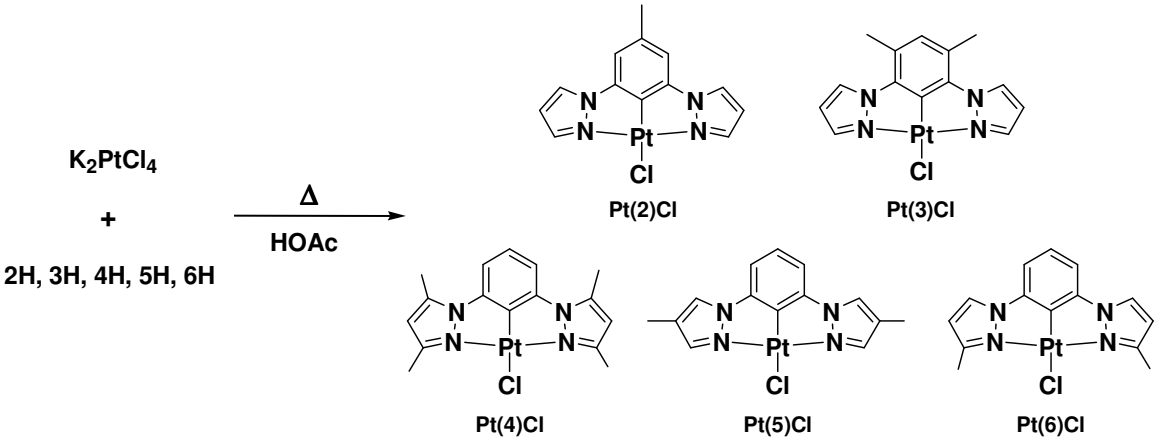

Scheme 4.3. Synthetic scheme for the five monomeric platinum products.

Each monomeric compound was readily characterized by ^{1}H NMR spectroscopy in $CDCl_3$. The patterns of resonances are consistent with those expected for C_{2v} symmetric products. Aromatic resonances corresponding to the protons on the phenyl ring are observed between 6.8 and 7.2 ppm, and the β-pyrazolyl resonances occur in the 6.0-6.6 ppm range. Splittings for the pyrazolyl resonances are poorly resolved. Distinguishing between the α- and γ-pyrazolyl resonances in the aromatic region is not always straightforward because of their close proximity in each spectrum. When a

methyl substituent is placed at the γ-position of the pyrazolyl (Figure 4.16), the α-proton resonance for the complex is observed at 7.9 ppm. When the methyl substituent is placed in the β-position, as in Pt(**5**)Cl (Figure 4.13), both α- and γ-pyrazolyl proton resonances appear near 7.8-7.9 ppm. In some cases (*e.g.*, Pt(**5**)Cl), ^{195}Pt satellites on the γ-proton resonance confirm that the α-proton resonance is shifted furthest downfield. For ligands with no methyl substituents on the pyrazolyl groups, a comparison can be made between the spectra of the free ligand and the corresponding complex to reach a tentative assignment. Thus, as previously noted for Pt(**1**)Cl, the γ-proton resonance of Pt(**2**)Cl is shifted downfield from that of the free ligand as expected for the close proximity to the platinum metal center (Figure 4.3). Based on these trends, it appears that the α-proton resonances occur near 7.9 ppm, whereas the γ-resonances lie within the 7.8-8.3 ppm range. The β-proton resonances occur in the 6.0-6.7 ppm range and tend to shift upfield with increasing methylation of the pyrazolyl groups.

Mass spectra were recorded for the monomer compounds Pt(**L**)Cl (**L=2**-**6**) dissolved in $CHCl_3/CH_3OH$/ESI, $CHCl_3/CH_3CN$/ESI, $CH_3CN/CHCl_3$, $CHCl_3/CH_3OH$ or ESI buffer solution (Figures 4.5, 4.8 and 4.17). A peak associated with Pt(**L**)$^+$ is identifiable in each spectrum. The spectra also show higher mass peaks, which are attributed to charged species generated during the ESI process. For example, each spectrum shows a mass peak consistent with the solvent-substituted adduct Pt(**L**)(solvent)$^+$. Most spectra also show a peak consistent with formation of a dimer $Pt_2(\mathbf{L})_2Cl^+$. The lone exception is Pt(**2**)Cl in $CHCl_3/CH_3OH$/ESI buffer solution, which shows a mass peak at 868 and an isotope profile consistent with only one platinum being present. The mass and isotope profiles are consistent with Pt(**2**)(**2H**)$_2^+$, however it is

interesting that no peaks consistent with $\mathbf{2H_2}^+$ or Pt(**2**)(**2H**)$^+$ are observed. Pt(**5**)Cl and Pt(**6**)Cl give rise to peaks at 977 and 819, respectively. In the case of Pt(**5**)Cl, workup of the sample included DMSO solvent, which was later removed by evaporation; the resulting solid was dissolved in a $CHCl_3/CH_3OH$ solution and recorded to give the mass spectrum (Figure 4.14). The isotope profile centered at 977 is consistent with $Pt_2(\mathbf{5})_2(DMSO)Cl^+$. The crystal structure of Pt(**5**)Cl was obtained from a different sample, which was not introduced to DMSO. In the case of Pt(**6**)Cl, workup of the sample also included DMSO solvent; the resulting solid was dissolved in ESI buffer solution and recorded to give the mass spectrum (Figure 4.17). The isotope profile centered at 819 is consistent with $Pt_2(\mathbf{6})(DMSO)_2Cl^+$, whose formation is favored in DMSO solution (*vide infra*). No peaks were observed at higher mass values that could be attributed to trimers or higher-order aggregates.

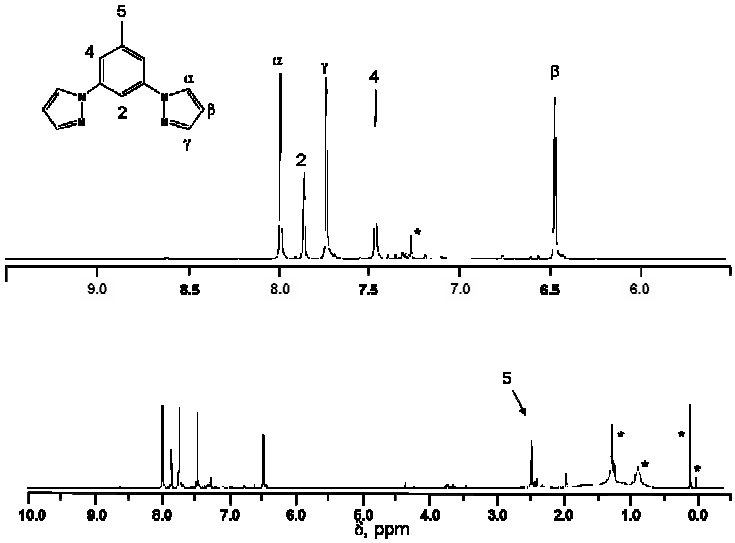

Figure 4.2. ^{1}H NMR spectrum of **2H** in $CDCl_3$. (* marks characteristic solvent and impurity resonances; grease, 0.1 ppm, hexanes, 0.88 and 1.26 ppm.)

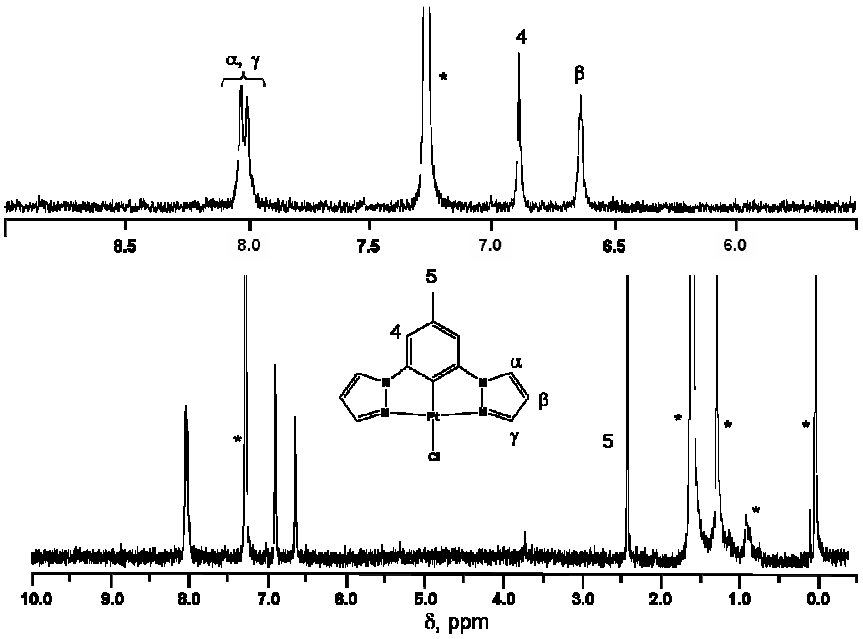

Figure 4.3. ^{1}H NMR spectrum of Pt(**2**)Cl in $CDCl_3$. (* marks characteristic solvent and impurity resonances; hexanes, 0.88 and 1.26 ppm, water, 1.56 ppm.)

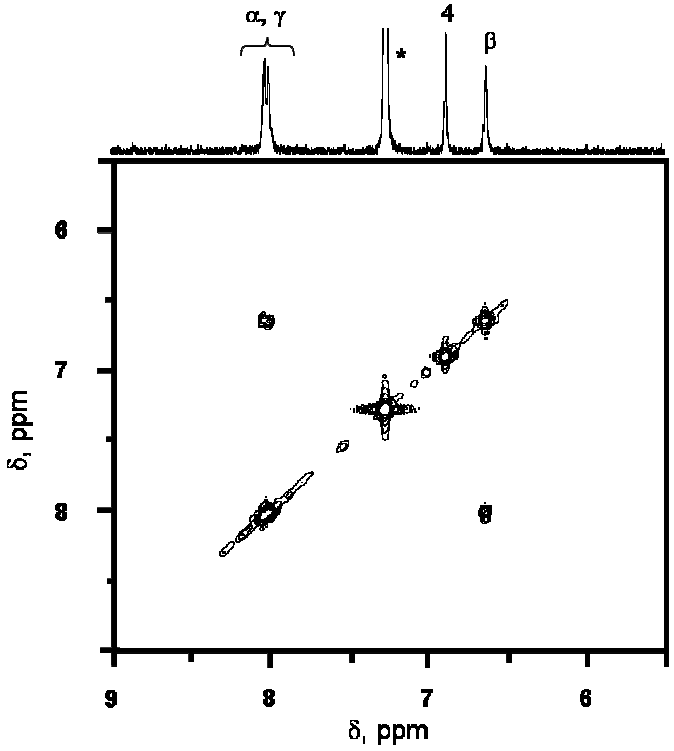

Figure 4.4. Two-dimensional COSY NMR spectrum of Pt(**2**)Cl in $CDCl_3$. (* marks characteristic solvent resonance.)

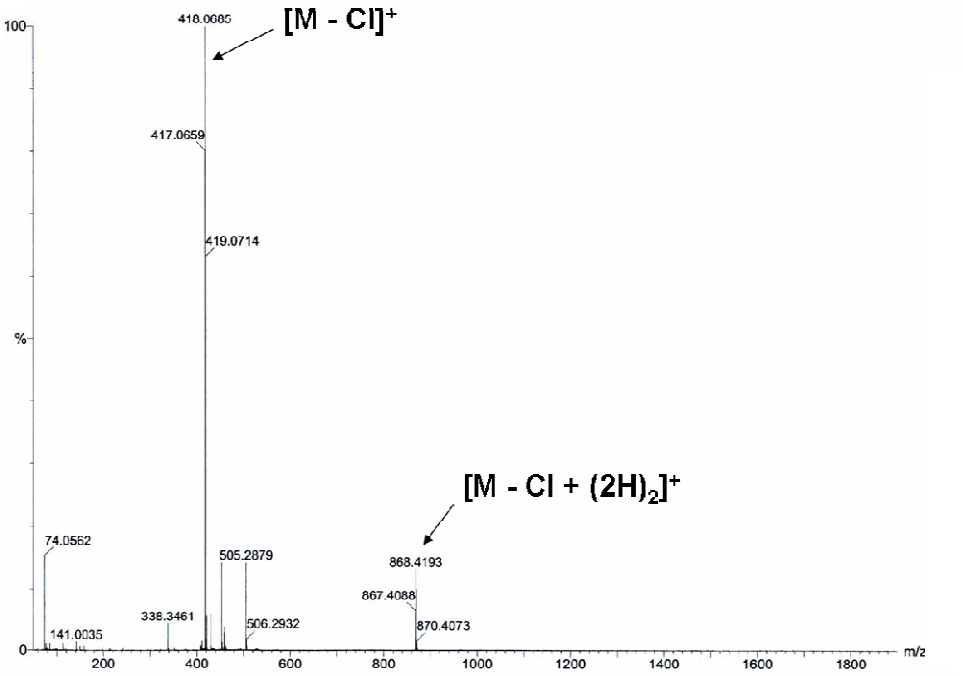

Figure 4.5. ESI mass spectrum of Pt(**2**)Cl (M) in $CHCl_3/CH_3OH$/ESI buffer solution.

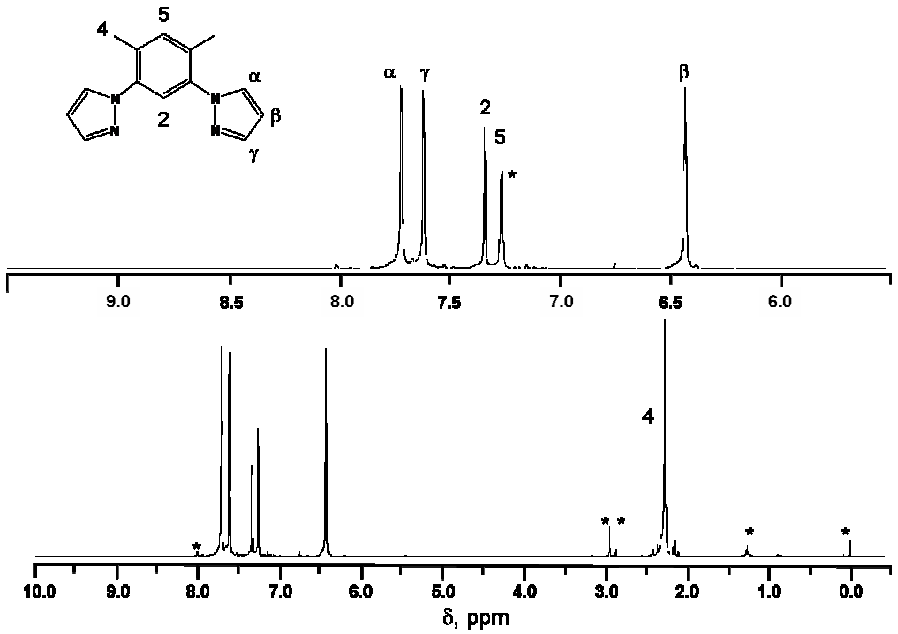

Figure 4.6. ^{1}H NMR spectrum of **3H** in $CDCl_3$. (* marks characteristic solvent and impurity resonances; hexanes, 0.88 and 1.26 ppm, water, 1.56 ppm, DMF, 2.88, 2.96 and 8.02 ppm.)

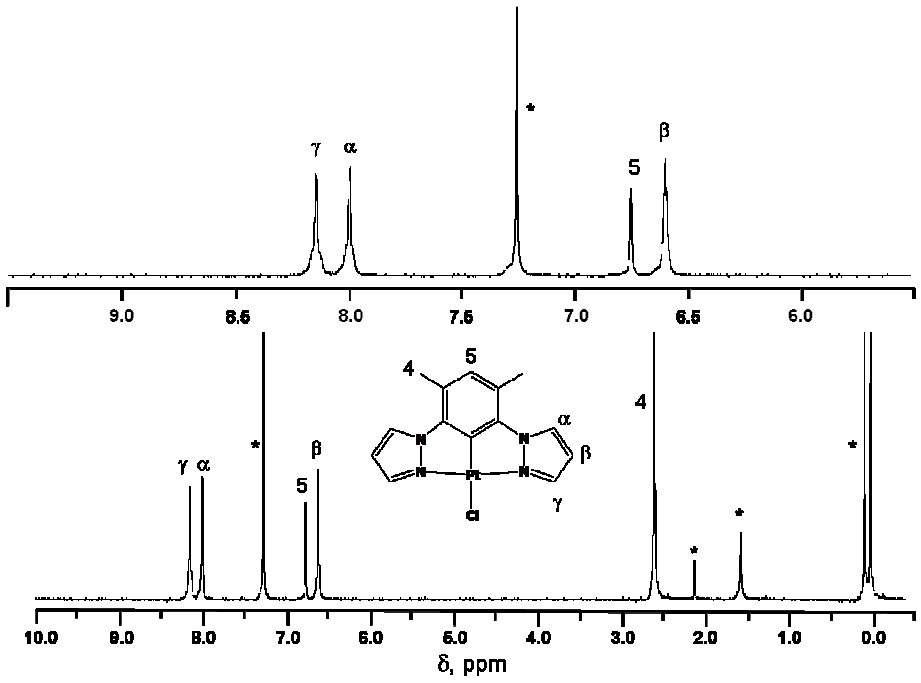

Figure 4.7. ^{1}H NMR spectrum of Pt(**3**)Cl in $CDCl_3$. (* marks characteristic solvent and impurity resonances; water, 1.56 and acetone, 2.18 ppm.)

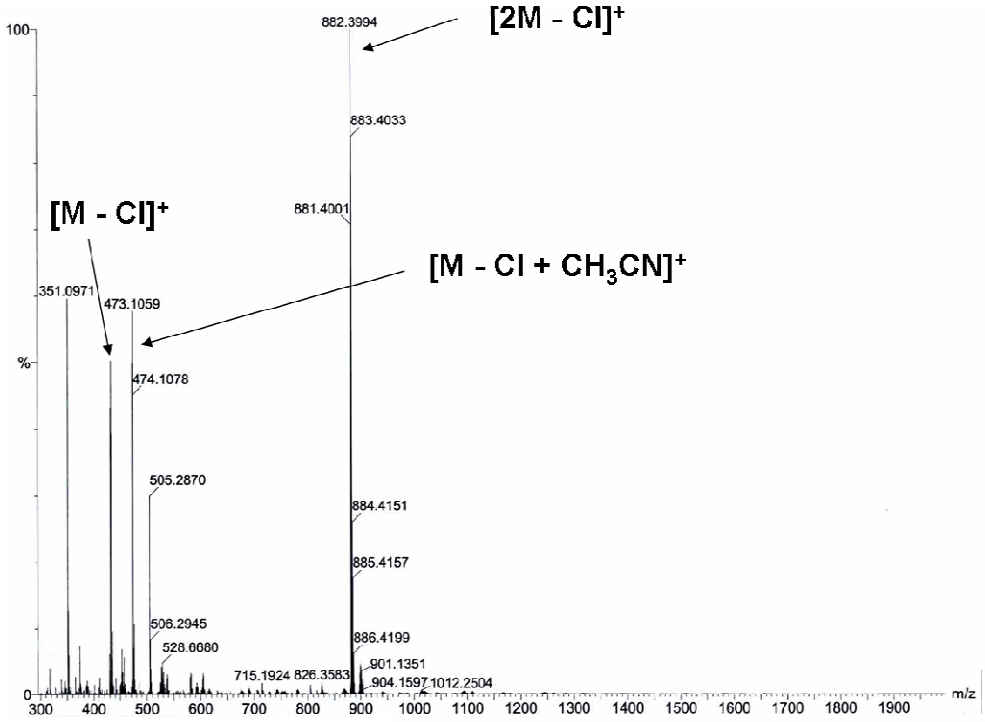

Figure 4.8. ESI mass spectrum of Pt(**3**)Cl (M) in $CH_3CN/CHCl_3$/ESI buffer solution.

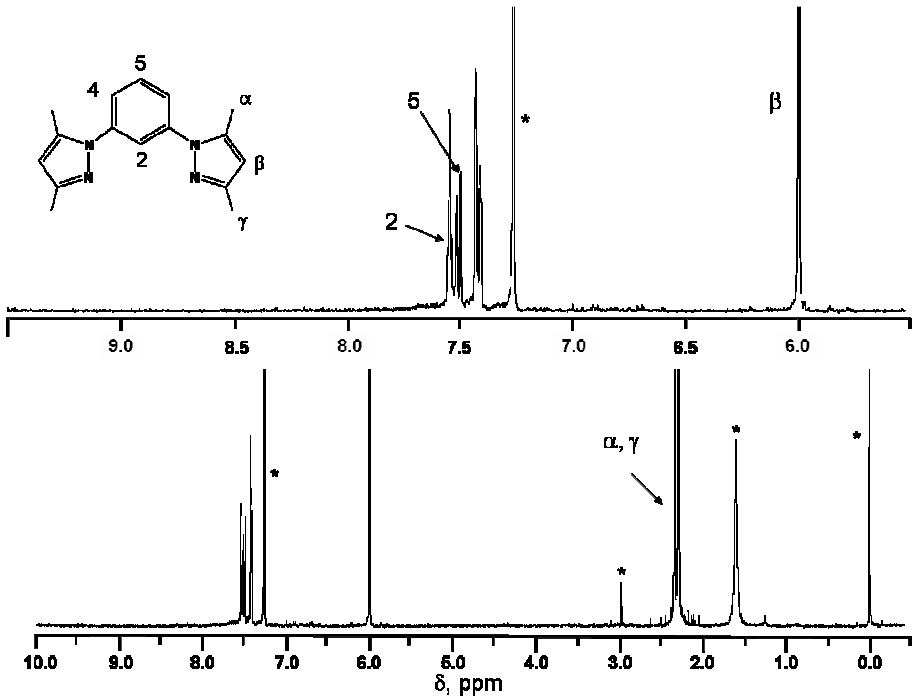

Figure 4.9. ^{1}H NMR spectrum of **4H** in $CDCl_3$. (* marks characteristic solvent and impurity resonances; water, 1.56.)

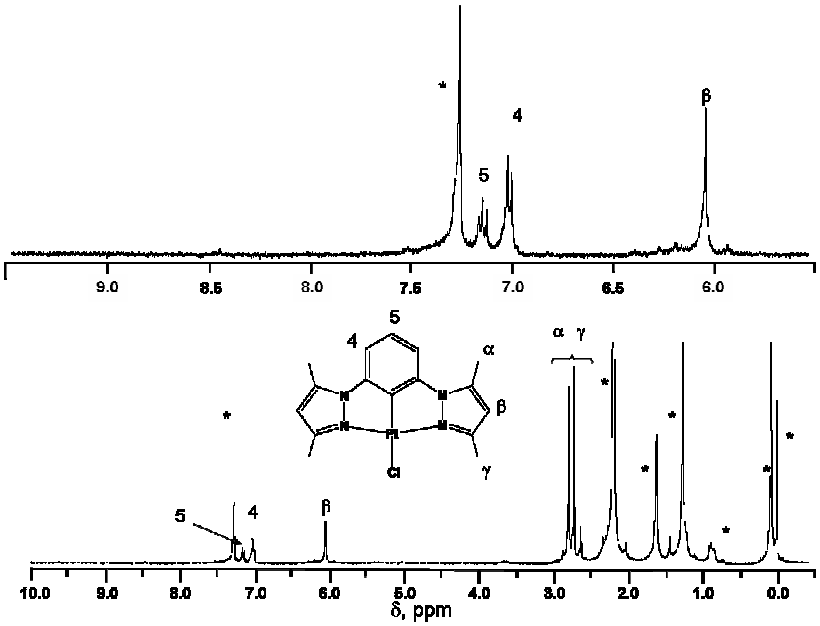

Figure 4.10. ^{1}H NMR spectrum of Pt(**4**)Cl in $CDCl_3$. (* marks characteristic solvent and impurity resonances; grease, 0.07, hexanes, 0.88 and 1.26 ppm, water, 1.56 ppm, acetone, 2.18 ppm.)

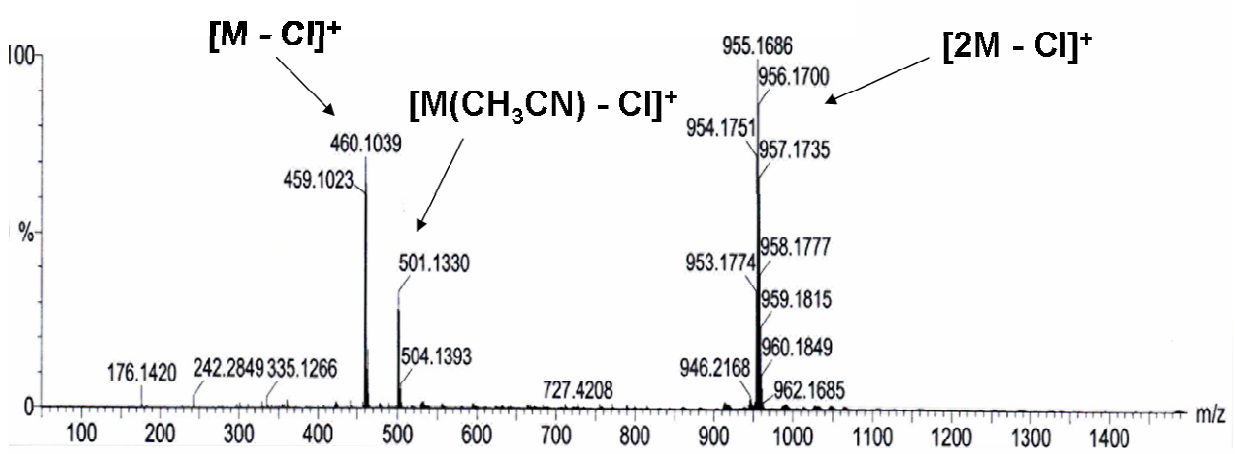

Figure 4.11. ESI mass spectrum of Pt(**4**)Cl (M) in $CHCl_3/CH_3CN$ solution.

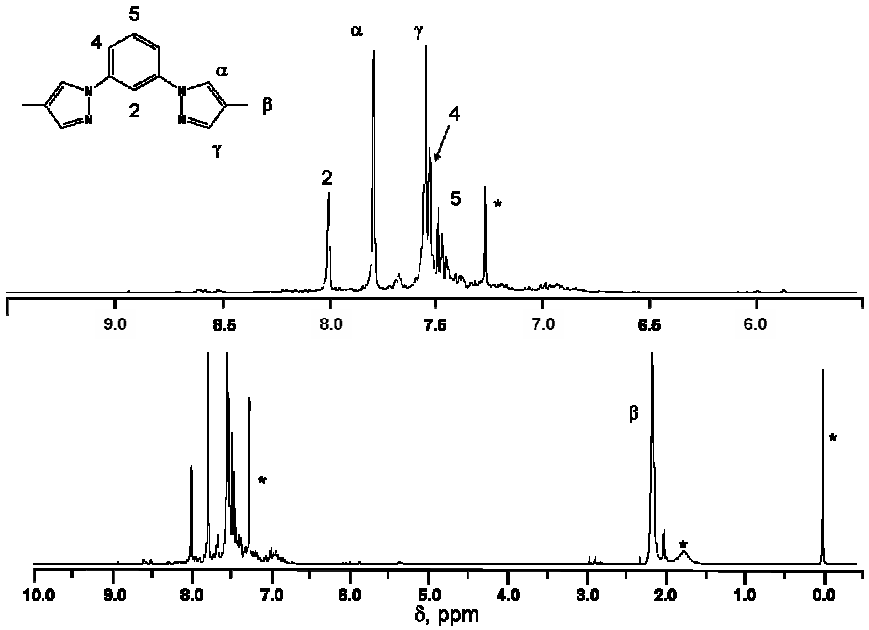

Figure 4.12. ^{1}H NMR spectrum of **5H** in $CDCl_3$. (* marks characteristic solvent and impurity resonances; water, 1.56 ppm.)

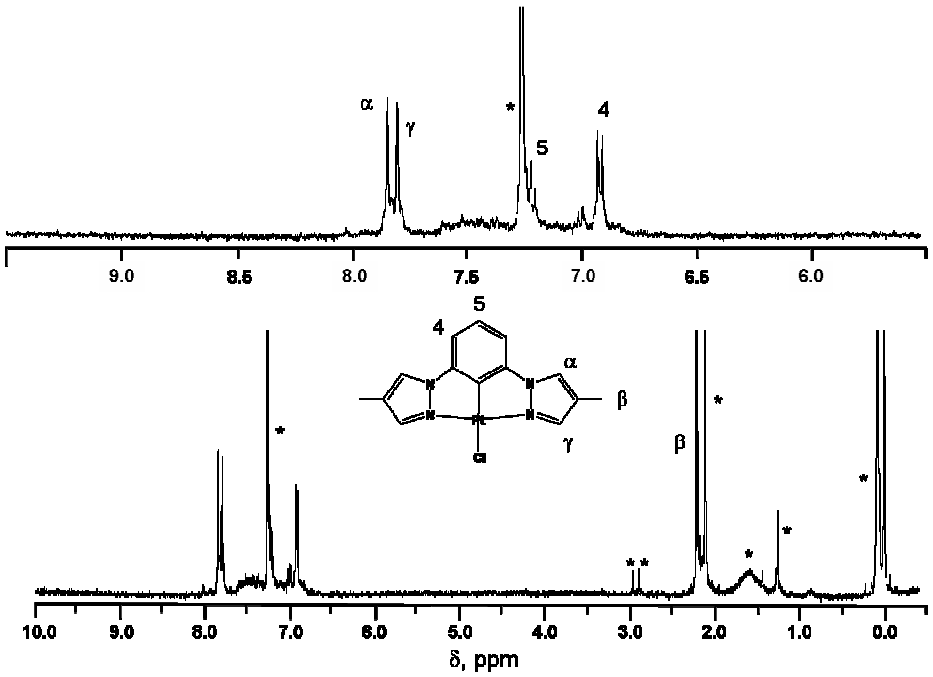

Figure 4.13. ^{1}H NMR spectrum of Pt(**5**)Cl in $CDCl_3$. (* marks characteristic solvent and impurity resonances; hexanes, 0.88 and 1.26 ppm, water, 1.56 ppm, DMF, 2.88 and 2.96 ppm.)

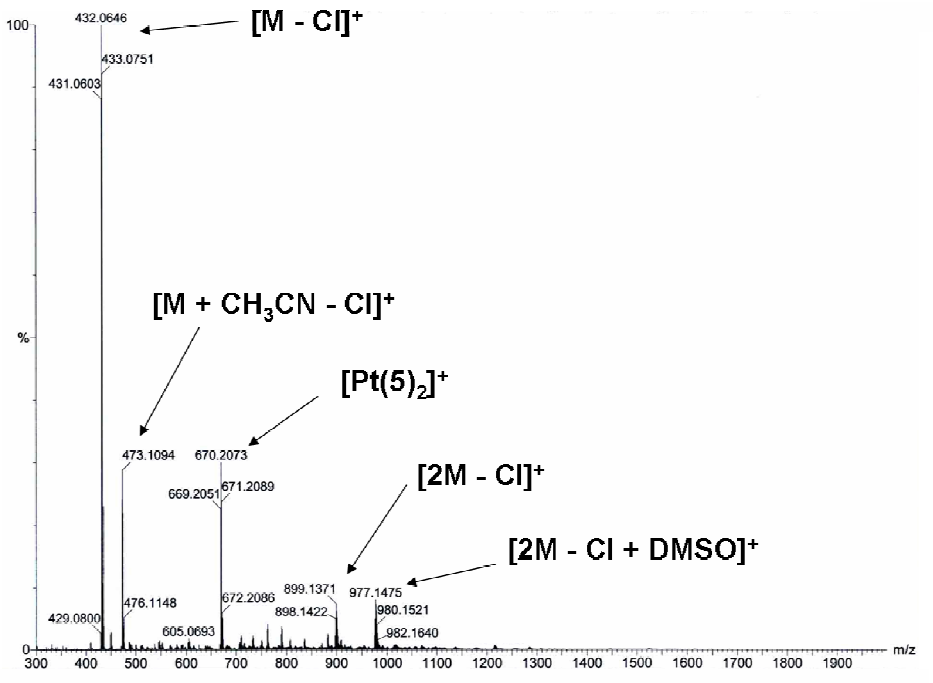

Figure 4.14. ESI mass spectrum of Pt(**5**)Cl, (M) in $CHCl_3/CH_3OH$ solution.

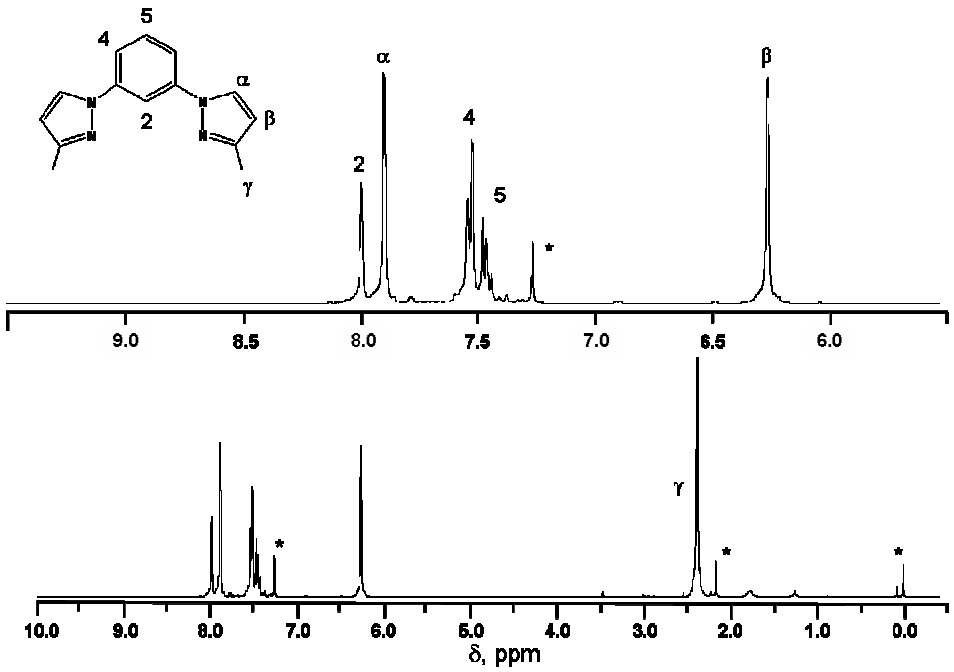

Figure 4.15. ^{1}H NMR spectrum of **6H** in $CDCl_3$. (* marks characteristic solvent and impurity resonances; acetone, 2.18 ppm.)

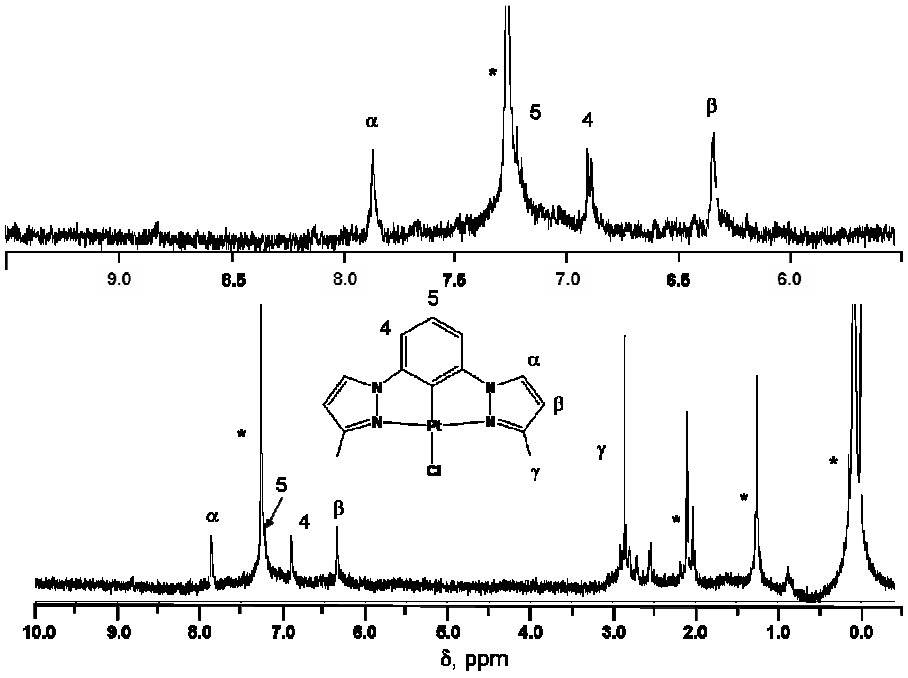

Figure 4.16. ^{1}H NMR spectrum of Pt(**6**)Cl in $CDCl_3$. (* marks characteristic solvent and impurity resonances; hexanes, 0.88 and 1.26 ppm, acetone, 2.18 ppm.)

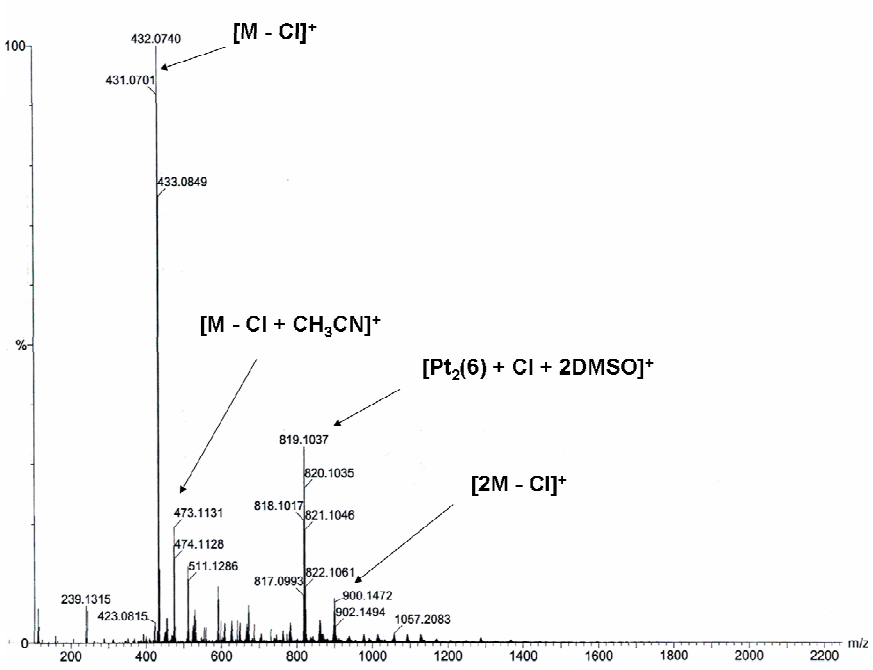

Figure 4.17. ESI mass spectrum of Pt(**6**)Cl (**M**) in ESI buffer solution.

The identities of Pt(**2**)Cl, Pt(**3**)Cl, Pt(**4**)Cl, and Pt(**5**)Cl were confirmed by single-crystal X-ray diffraction studies. ORTEP diagrams are shown in Figure 4.18, and the data are summarized in Tables 4.2 and 4.3. In each case, **L** adopts a tridentate coordination geometry around the platinum metal center, bonding through the central carbon of the phenyl ring with the two pyrazolyl N atoms in a trans arrangement. The fourth coordination site is occupied by a chloride ligand. The metrical parameters describing the coordination geometries are very similar to those of Pt(**1**)Cl.[9] Notably, the Pt-C distance (1.90-1.93 Å) is short. The Pt-C and Pt-N(pyrazolyl) bonds are slightly longer for Pt(**4**)Cl than for the other compounds, suggesting that methyl groups in the α- and γ-positions tend to weaken bonding to the metal. As expected, the smaller 5-membered pyrazolyl rings result in a more acute N-Pt-N bond angle for Pt(**L**)Cl (**L=1**-**6**, 158.89(14)-160.03(11) Å) than found for pyridine analogs (161.1(2) Å).[6]

Table 4.2. Crystallographic Data for Pt(**2**)Cl, Pt(**3**)Cl, Pt(**4**)Cl and Pt(**5**)Cl.

	Pt(**2**)Cl	Pt(**3**)Cl	Pt(**4**)Cl Orthorhombic Form	Pt(**4**)Cl Monoclinic Form	Pt(**5**)Cl
Formula	$C_{13}H_{11}N_4ClPt$	$C_{14}H_{13}N_4ClPt$	$C_{16}H_{17}N_4ClPt$	$C_{16}H_{17}N_4ClPt$	$C_{14}H_{13}N_4ClPt$
fw, g/mol	453.80	467.82	495.88	495.88	467.82
Crystal System	Monoclinic	Monoclinic	Orthorhombic	Monoclinic	Monoclinic
Space Group	*C*2/*c*	$P2_1/c$	*Pbca*	$P2_1/n$	$P2_1/n$
a, Å	25.015(2)	7.6983(2)	17.8821(6)	10.454(3)	7.2446(8)
b, Å	14.4698(11)	10.1755(2)	9.0829(3)	14.687(4)	14.4215(10)
c, Å	11.0195(8)	17.5563(4)	18.9415(7)	11.494(3)	13.6113(5)
α, °	90	90	90	90	90
β, °	95.510(2)	97.055(1)	90	115.926(4)	98.131(4)
γ, °	90	90	90	90	90
V, Å^3	3970.1(5)	1364.84(5)	3076.50(18)	1587.3(8)	1407.79(19)
ρ_{calcd} (g cm^{-3})	2.278	2.277	2.141	2.075	2.207
μ, mm^{-1}	13.421	20.984	18.666	11.201	12.583
Z	12	4	8	4	4
T, K	173(2)	150(2)	150(2)	193(2)	150(2)
reflns collected	29293	11093	23810	18541	16981
ind reflns	3968	2442	2759	3974	3476
R_{int}	0.0713	0.0438	0.0489	0.0612	0.0591
GOF on F^2	1.050	1.107	1.035	1.072	1.047
*R*1/*wR*2 [$I > 2\sigma(I)$][a]	0.0267/0.0686	0.0209/0.0518	0.0240/0.0581	0.0255/0.0665	0.0293/0.0787
*R*1/*wR*2 (all data)[a]	0.0275/0.0692	0.0218/0.0524	0.0298/0.0609	0.0276/0.0679	0.0324/0.0804
Weighting scheme (a/b)[a]	0.0432/4.1200	0.0285/1.1342	0.0345/4.5904	0.0298/1.1092	0.0430/0.0

[a] $w^{-1}=[\sigma^2(F_o^2)+(aP)^2+bP]$ where $P=0.33333F_o^2+0.66667F_c^2$ and a,b are refined quantities.

Table 4.3. Selected Bond Distances(Å) and Angles(˚) for Pt(**2**)Cl, Pt(**3**)Cl, Pt(**4**)Cl (orthorhombic and triclinic forms), and Pt(**5**)Cl.

	Pt(**2**)Cl (Mol A)[a]	Pt(**2**)Cl (Mol B)[b]	Pt(**3**)Cl	Pt(**4**)Cl Orthorhombic Form	Pt(**4**)Cl Monoclinic Form	Pt(**5**)Cl
Pt-C4	1.901(4)	1.900(5)	1.916(3)	1.931(4)	1.931(3)	1.905(4)
Pt-N1	2.010(3)	2.012(3)	2.005(3)	2.046(3)	2.044(3)	2.010(4)
Pt-N3	2.005(3)	2.012(3)	2.011(3)	2.031(4)	2.053(3)	2.011(4)
Pt-Cl	2.3821(10)	2.3977(14)	2.4088(8)	2.4113(11)	2.4093(11)	2.4091(11)
C4-C5	1.382(5)	1.374(5)	1.379(5)	1.393(6)	1.402(4)	1.389(6)
C4-C9	1.385(5)	1.374(5)	1.391(5)	1.374(6)	1.383(4)	1.378(6)
N2-C5	1.434(5)	1.430(5)	1.439(4)	1.422(5)	1.422(4)	1.420(6)
N4-C9	1.434(5)	1.430(5)	1.436(4)	1.420(5)	1.431(4)	1.430(5)
N1-N2	1.383(5)	1.377(5)	1.370)4_	1.395(4)	1.403(4)	1.385(5)
N4-N3	1.368(5)	1.377(5)	1.376(4)	1.392(5)	1.412(4)	1.388(5)
N1-Pt-N3	159.61(15)	159.07(19)	160.03(11)	159.23(13)	159.96(10)	159.91(15)
N3-Pt-C4	79.89(15)	79.54(9)	80.24(12)	79.47(15)	79.90(11)	79.43(17)
N1-Pt-C4	79.74(16)	79.54(9)	79.80(12)	79.77(15)	80.11(12)	80.48(17)
N1-Pt-Cl	100.40(11)	100.46(9)	98.84(8)	100.94(9)	99.65(8)	98.86(11)
N3-Pt-Cl	99.98(10)	100.46(9)	101.13(8)	99.83(9)	100.36(8)	101.23(12)
N4-N3-Pt	113.7(2)	113.7(2)	113.9(2)	113.6(2)	112.42(18)	113.8(3)
N2-N1-Pt	113.7(2)	113.7(2)	114.46(19)	112.7(2)	112.86(19)	113.3(3)
C5-N2-N1	115.7(3)	115.6(3)	115.2(3)	116.5(3)	116.1(2)	115.6(4)
C4-C5-N2	110.1(4)	110.4(4)	111.0(3)	111.4(3)	111.8(3)	111.5(4)
C9-N4-N3	116.2(3)	115.6(3)	115/7(3)	115.2(3)	115.8(2)	115.5(4)
C4-C9-N4	109.8(3)	110.4(4)	111.0(3)	112.3(3)	111.8(3)	110.2(4)

[a]Pt(**2**)Cl crystallizes with 2 independent molecules in the lattice.
[b]The atom designators in column 1 refer to labeling in Molecule A.

(a)

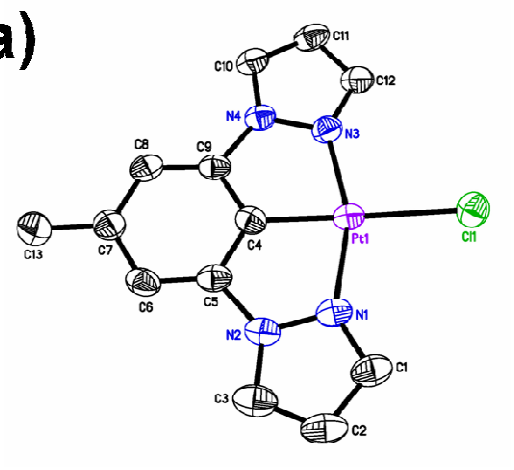

Molecule A

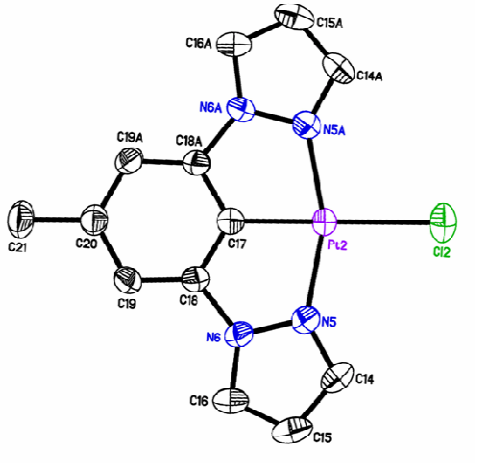

Molecule B

(b)

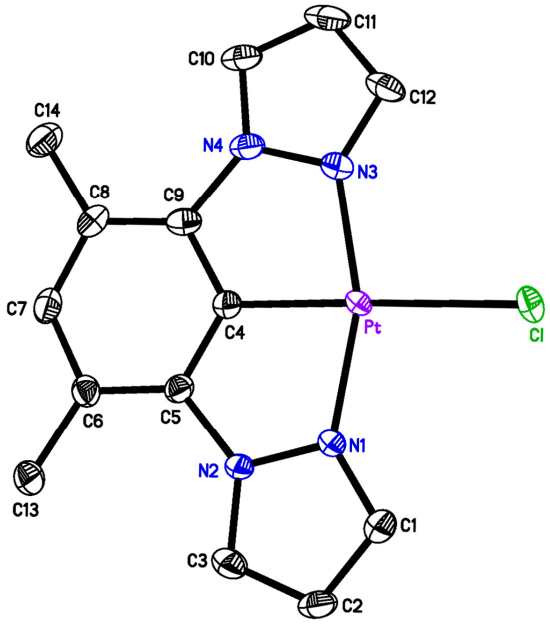

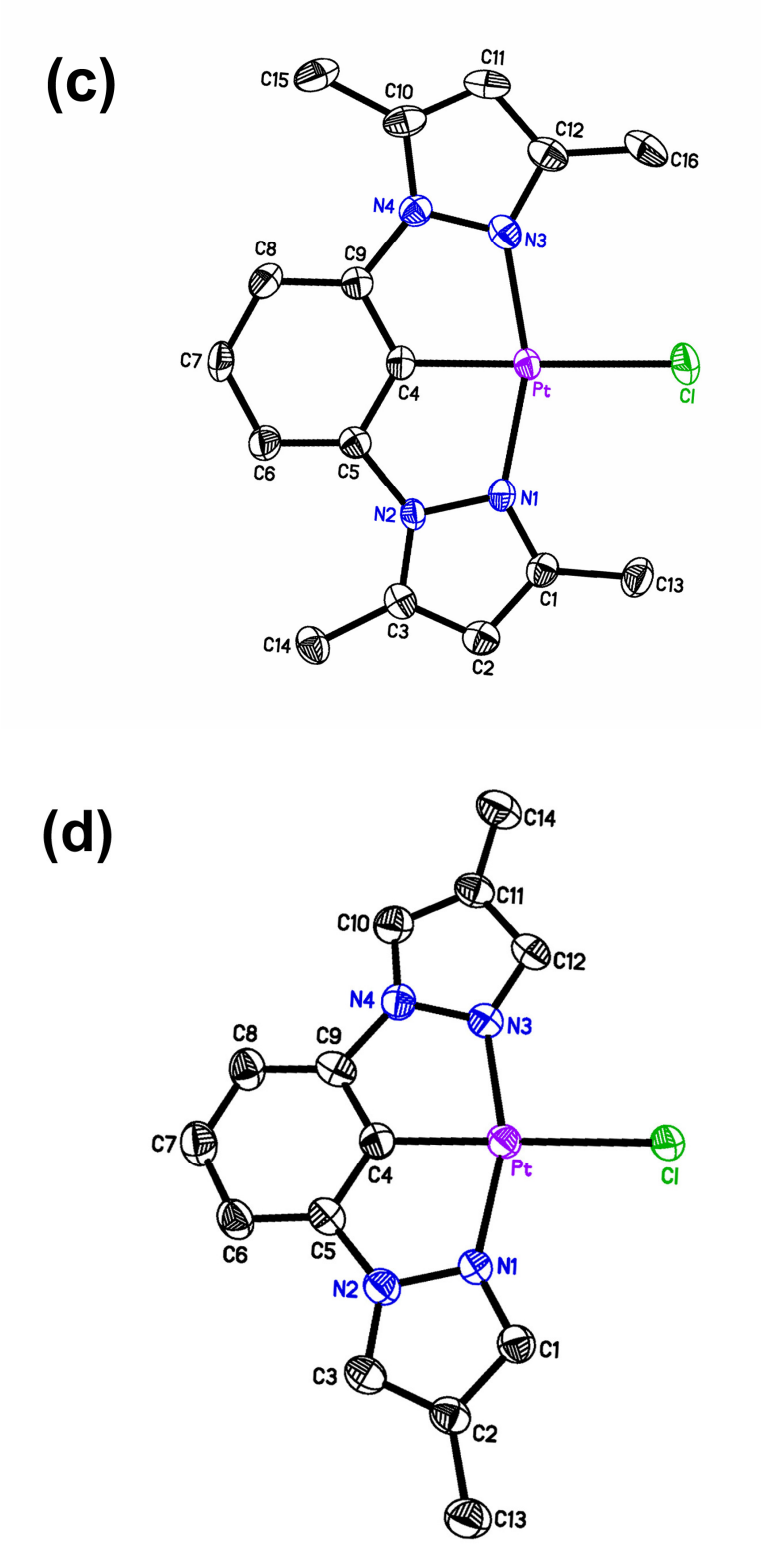

Figure 4.18. ORTEP diagrams of (a) Pt(**2**)Cl (both independent molecules are shown), (b) Pt(**3**)Cl, (c) Pt(**4**)Cl (orthorhombic) and (d) Pt(**5**)Cl. H atoms are omitted for clarity.

Trimer Product. To investigate the possibility of preparing a macrocycles with **5**$^-$, comparatively concentrated solutions (>42 mM) of **5H** was refluxed with one equivalent of $K_2[PtCl_4]$ for relatively long time periods (14 days). The resulting off-white solids were washed with methylene chloride and diethyl ether to give the [Pt(μ-**5**)Cl]$_3$ in >90% yield (Scheme 4.4).

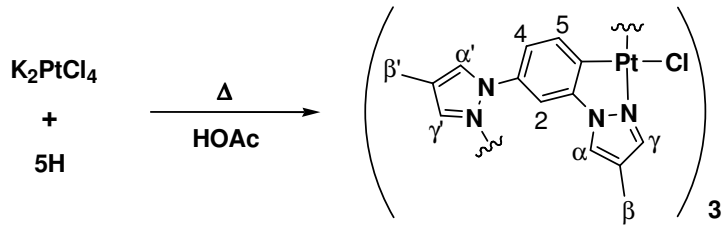

Scheme 4.4. Synthesis of [Pt(μ-**5**)Cl]$_3$.

[Pt(μ-**5**)Cl]$_3$ was fully characterized by ^{1}H NMR spectroscopy using NOESY and COSY techniques (Figures 4.19-4.22). No resonances associated with the monomer Pt(**5**)Cl product were observed. The ^{1}H NMR spectrum bears a striking resemblance to that of [Pt(μ-**1**)Cl]$_3$.[9] Notably, two doublets corresponding to protons at the 4- and 5-positions of the phenyl ring occur at 6.6 ppm and 5.9 ppm, respectively. These resonances are shifted upfield by 0.88 and 1.46 ppm, respectively, from those of the free ligand, as expected for strong transannular interactions between the ligand phenyl rings; the corresponding changes in chemical shifts ($\Delta\delta$) for **1H** and [Pt(μ-**1**)Cl]$_3$ are 0.94 and 1.55 ppm, respectively. Of the remaining resonances, the 2-phenyl proton resonance is shifted furthest downfield, occurring at 8.4 ppm. The methyl resonances appear at 2.1 ppm and 2.2 ppm. The remaining α-, α'- γ- and γ'- resonances occur in the 7.6-7.9 ppm region. A strong NOE signal between the 2-phenyl and α-pyrazoyl protons is consistent

with the connectivity observed for [Pt(μ-**1**)Cl]$_3$ in the solid state (Figure 4.22). Unfortunately, no NOE signal was observed between the 4-H phenyl and γ'-pyrazolyl protons or for any other resonances. However, as noted in Table 4.3, the chemical shifts for [Pt(μ-**5**)Cl]$_3$ are remarkably similar to those observed for [Pt(μ-**1**)Cl]$_3$. The 4- and 5-phenyl proton resonances are within 0.08 ppm of those of [Pt(μ-**1**)Cl]$_3$. For reasons that are not entirely understood, the resonance assigned to the 2-phenyl proton is shifted upfield by 0.25 ppm relative to that of [Pt(μ-**1**)Cl]$_3$; this may indicate that the 2-phenyl proton of [Pt(μ-**5**)Cl]$_3$ is slightly further from the deshielding Pt and Cl atoms, which would be expected if the end of the cavity displaying the pz groups is slightly more open because of methylation of the pyrazoyl groups at the β-position. Table 4.3 also shows that the pyrazolyl resonances are shifted slightly upfield for [Pt(μ-**5**)Cl]$_3$ as a consequence of the electron releasing properties of the methyl substituent at the β-pyrazolyl position.

Table 4.4. ^{1}H NMR chemical shifts (δ) for [Pt(μ-**1**)Cl]$_3$ and [Pt(μ-**5**)Cl]$_3$ in $CDCl_3$.

Position	[Pt(μ-**1**)Cl]$_3$	[Pt(μ-**5**)Cl]$_3$
Phenyl		
2-H	8.60	8.35
4-H	6.66	6.58
5-H	5.95	5.99
Pyrazolyl		
α, α'	8.03, 7.88	7.75, 7.52
β, β'	—	2.25, 2.20
γ, γ'	8.13-8.15	7.90-7.92

The mass spectrum of [Pt(μ-**5**)Cl]$_3$ was recorded in CH_3OH/ESI buffer solution (Figure 4.23). The spectrum exhibits mass peaks consistent with the presence of $\mathbf{M_3}$ in the sample, where **M** has the mass of Pt(**5**)Cl. For example, mass peaks corresponding to $[\mathbf{M_3} - Cl]^+$, $[\mathbf{M_3} - Cl + CH_3CN]^+$ and $[\mathbf{M_3} - 2Cl]^{2+}$ appear in the spectrum (Figures 4.23). Overall, the mass spectrum is strikingly similar to that observed for [Pt(μ-**1**)Cl]$_3$. No peaks were observed at higher mass values that could be attributed to higher order aggregates.

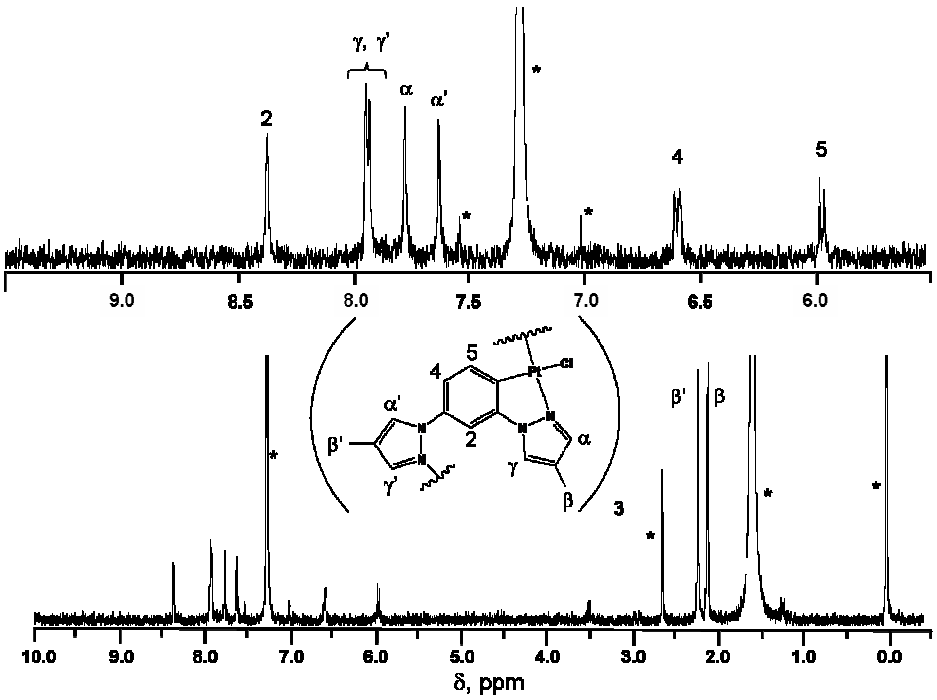

Figure 4.19. ^{1}H NMR of [Pt(μ-**5**)Cl]$_3$ in $CDCl_3$. (* marks characteristic solvent and impurity resonances; water, 1.56 ppm.)

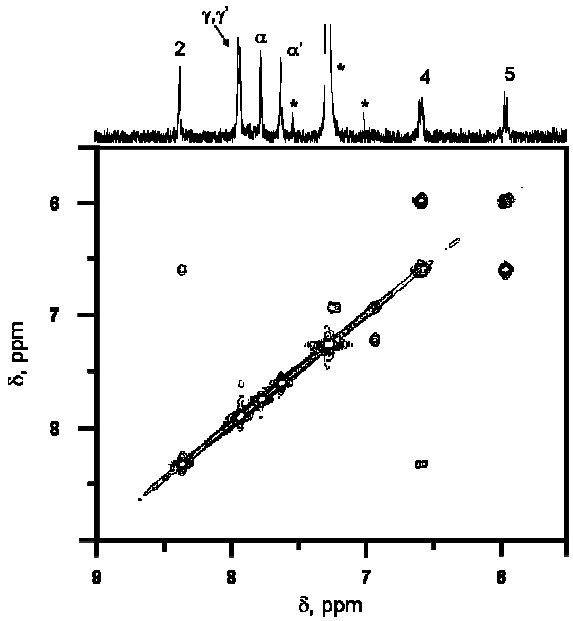

Figure 4.20. Two-dimensional COSY NMR spectrum of [Pt(μ-**5**)Cl]$_3$ in $CDCl_3$. (* marks characteristic solvent resonances.)

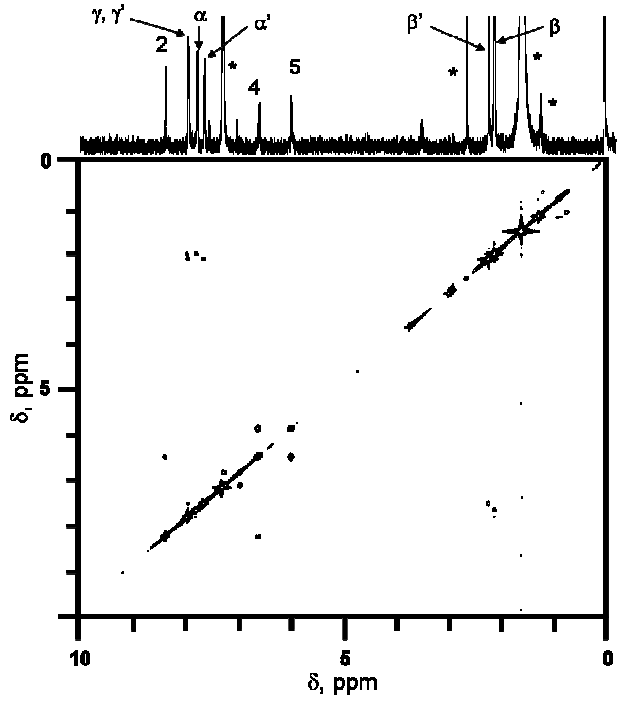

Figure 4.21. Two-dimensional COSY NMR spectrum of [Pt(μ-**5**)Cl]$_3$ in $CDCl_3$.

(* marks characteristic solvent and impurity resonances; water, 1.56 ppm.)

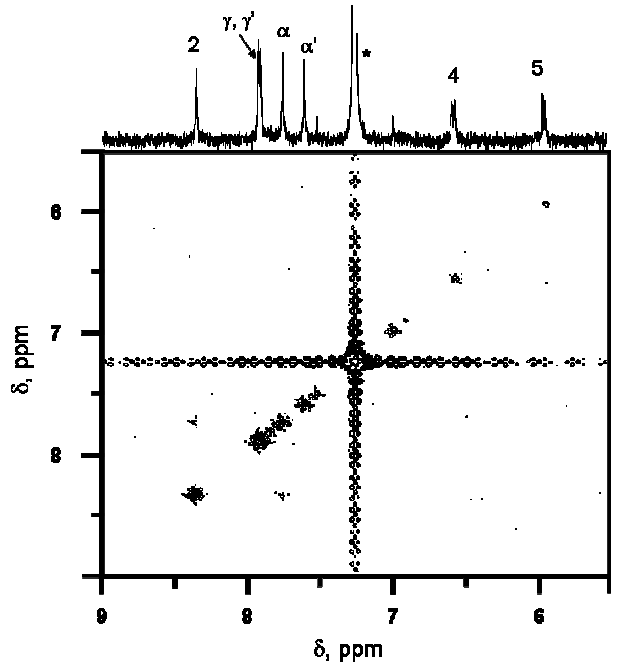

Figure 4.22. Two-dimensional NOESY NMR spectrum of [Pt(μ-**5**)Cl]$_3$ in $CDCl_3$.

(* marks characteristic solvent resonance.)

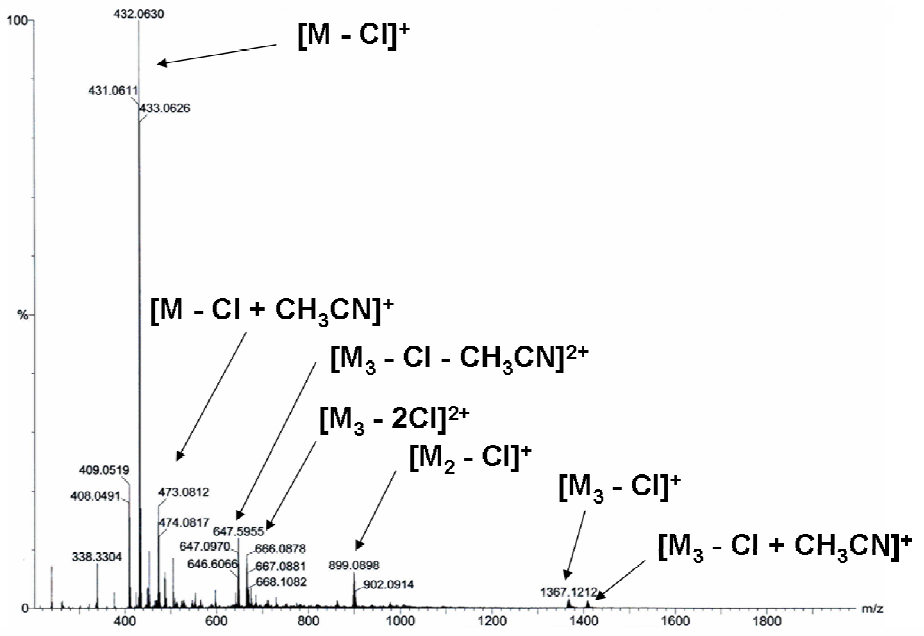

Figure 4.23. ESI mass spectrum of [Pt(μ-**5**)Cl]$_3$ (**M$_3$**) in CH_3OH/ESI buffer solution.

Dimers. During attempts to prepare a trimer macrocycle with **7**$^-$, an unexpected dimeric product was isolated. The ligand precursor, **7H**, was refluxed with one equivalent of $Pt(CH_3CN)_2Cl_2$ in acetic acid for 5 days (Scheme 4.5). The resulting yellow precipitate was washed with methylene chloride and recrystallized from DMF/ether to give Pt_2(μ-**7H**)(μ-**7**)Cl_3 in high yield (93-98%).

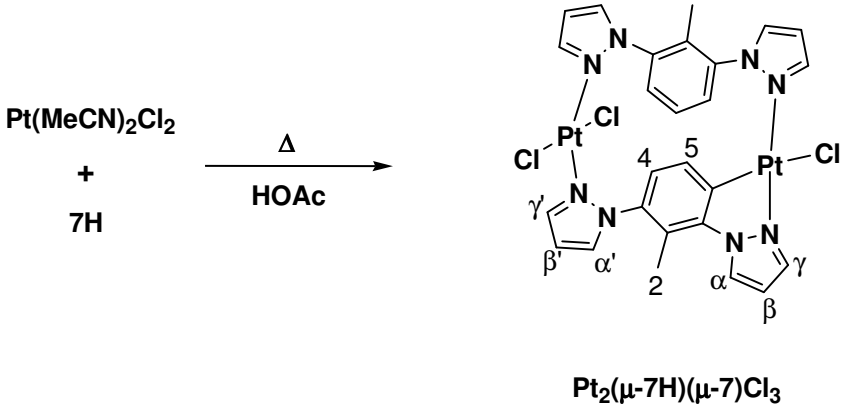

Scheme 4.5. Synthesis of Pt_2(μ-**7H**)(μ-**7**)Cl_3.

Pale yellow crystals of $Pt_2(\mu\text{-}\mathbf{7H})(\mu\text{-}\mathbf{7})Cl_3 \cdot H_2O$ were obtained by evaporation of DMF (workup included CH_2Cl_2-DMF-Et_2O), and their composition was confirmed by single-crystal X-ray diffraction studies. An ORTEP diagram is shown in Figure 4.24, and the data are summarized in Tables 4.4 and 4.5. The protonated ligand (**7H**) bridges the metal centers in a symmetrical fashion, bonding to each platinum through a pyrazolyl group. The $\mathbf{7}^-$ ligand is bonded bidentate to Pt1 through a N(pz) atom and the C atom at the 6-position of the phenyl group. The remaining pyrazoyl group (pz') is bonded to Pt2 and positioned trans to the pyrazoyl group of **7H**. The fourth coordination site of Pt1 and the two remaining coordination sites on Pt2 are occupied by chloride ligands. Thus, the coordination geometry around the Pt1 is similar to that observed for the $[Pt(\mu\text{-}\mathbf{1})Cl]_3$ trimer. The coordination geometry for the Pt2 also bears similarities to that of the trimer in that the pyrazolyl groups are trans to each other. The metals are essentially non-interacting with an intramolecular Pt···Pt separation of 6.56(6) Å. However, there are short C···C inter-ligand contacts involving C8 of $\mathbf{7}^-$ and the phenyl group of **7H** (C8···C18, 3.44(7); C8···C19, 3.37(7) Å). This geometry places H8 near the face of the pyrazolyl ring resulting in short H···N inter-ligand contacts (C8···N7, 3.398(7); H8···N7, 2.80; C8···N8, 3.181(7); H8···N8, 2.70 Å)

The ^{1}H NMR spectrum of the crystals of $Pt_2(\mu\text{-}\mathbf{7H})(\mu\text{-}\mathbf{7})Cl_3$ matches that obtained for the bulk reaction product, confirming that the dimer is the major product (Figure 4.26). The ^{1}H NMR spectrum of $Pt_2(\mu\text{-}\mathbf{7H})(\mu\text{-}\mathbf{7})Cl_3$ exhibits 15 identifiable resonances in the aromatic region and two resonances in the aliphatic region (Figures 4.26-4.28); the COSY NMR spectrum is consistent with a sixteenth aromatic resonance overlapping with

the DMF solvent resonance at 8.03 ppm. Four resonances of equal intensity occur in the 6.7-7.0 ppm range, where β-pyrazolyl resonances typically occur. Each of these resonances is coupled to a set of two other aromatic resonances in the 8.0-8.6 ppm range, which are assigned as the α- and γ-pyrazolyl resonances. Thus, we can assign twelve resonances of equal intensity to four chemically inequivalent pyrazolyl groups. For the remaining resonances, the COSY spectrum shows coupling between resonances at 7.5 and 6.5 ppm, as well as between resonances at 8.7 and 7.3 ppm. The doublet appearing at 6.5 ppm is tentatively assigned to the proton at the 5-position of the phenyl ring of **7**$^-$. Support for this comes from the crystal structure which shows short inter-ligand contacts involving the C-H group at this position. A possible alternative assignment is to the proton at the adjacent 4-position since the chemical shift is similar to that observed for $[Pt(\mu\text{-}\mathbf{1})Cl]_3$ (6.66 ppm) and $[Pt(\mu\text{-}\mathbf{5})Cl]_3$ (6.58 ppm); however, this assignment is less easily reconciled with the other features of the spectra. The COSY spectrum shows coupling of this resonance to a doublet at 7.5 ppm, which is assigned to the proton at the 4-position of the phenyl group of **7**$^-$ (Figure 4.28). The latter resonance is only shifted slightly from that of the free ligand. By contrast, the corresponding resonance in the spectra of $[Pt(\mu\text{-}\mathbf{1})Cl]_3$ and $[Pt(\mu\text{-}\mathbf{5})Cl]_3$ is strongly shifted upfield, as a result of strong transannular interactions. However, the crystal structure of the dimer shows that the H atom at the 4-position (*i.e.*, H7) has short contacts to Pt2 (2.97(1) Å) and Cl2 (3.08(1) Å) resulting in an environment reminiscent of that found for the H atom at the 2-position in the structure of $[Pt(\mu\text{-}\mathbf{1})Cl]_3$ (average distances: H···Pt, 2.92(9); H···Cl, 2.93(6) Å). For the trimer, the corresponding resonance is shifted strongly upfield to 8.60 ppm. Therefore, it appears that the modest chemical shift in the case of the dimer reflects an

approximate balancing of the deshielding effects of the nearby Pt and Cl atoms and the shielding effects of the transannular interactions. Three remaining resonances are attributable to the phenyl protons of **7H**. The resonance at 8.8 ppm is assigned to the proton at the 4'-position on the phenyl ring, since the crystal structure shows the H20···Pt1 distance to be 2.99(1) Å (C20···Pt1, 3.338(5) Å). The overlapping resonances at 7.3 ppm are attributed to protons at the 5'- and 6'-positions of the phenyl ring. The spectrum of the bulk reaction product also shows several minor resonances that are attributed to an unidentified side product.

The mass spectrum of $Pt_2(\mu\text{-}\mathbf{7H})(\mu\text{-}\mathbf{7})Cl_3$ was recorded in an IPA/ESI buffer solution (Figure 4.29). The spectrum exhibits major mass peaks at 871 and 909 that have isotopte profiles consistent with the presence of a $Pt_2(\mathbf{7})_2Cl^+$ and $Pt_2(\mathbf{7})(\mathbf{7H})Cl_2$, respectively. The spectrum also shows a mass peak at 1325 consistent with the presence of $Pt_3(\mathbf{7})_3Cl_2^+$, suggesting that a trimer product is conceivably the impurity observed in the ^{1}H NMR spectrum. The mass spectrum also shows very small signals assignable to tetramers and pentamers.

The reaction of $Pt_2(\mu\text{-}\mathbf{7H})(\mu\text{-}\mathbf{7})Cl_3$ was carried out for a shorter time period than used in the preparation of $Pt(\mu\text{-}\mathbf{5})Cl_3$, which could account for our success in isolating a dimer product. The structure is rather intriguing since it may be an intermediate in the formation of trimer. The dimer contains the characteristic $Pt(\eta^2\text{-L})$ unit of the trimer. One ligand shows C-H activation, whereas the second has not yet been activated. It is conceivable that C-H activation on the second ligand occurs after forming the observed bridged structure. The fact that the dimer forms in less time than it typically takes to produce exlucisvely trimer products with **1H** (>7 days) suggests that species such as

$Pt_2(\mu\text{-}\mathbf{7H})(\mu\text{-}\mathbf{7})Cl_3$ are present in typical reactions. It is conceivable that, if the reaction involving **7H** were allowed to run for longer time periods (~ 14 days), C-H activation of the phenyl ring of **7H** could occur forming a Pt-C bond. The dimer product would then convert to the desired trimeric product with the same coordination geometry around each metal center, as observed in $[Pt(\mu\text{-}\mathbf{1})Cl]_3$.

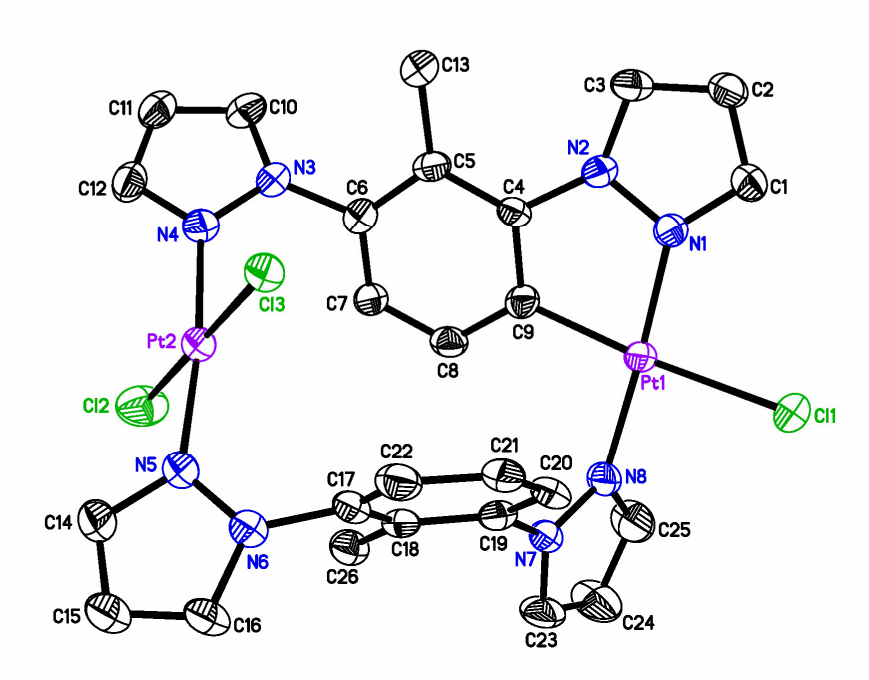

Figure 4.24. ORTEP diagram of $Pt_2(\mu\text{-}\mathbf{7H})(\mu\text{-}\mathbf{7})Cl_3$. H atoms omitted for clarity.

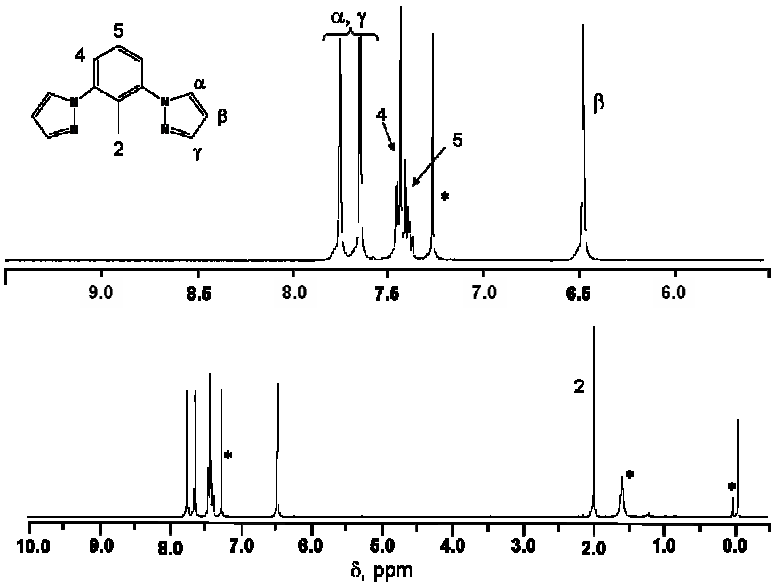

Figure 4.25. ^{1}H NMR spectrum of **7H** in $CDCl_3$. (* marks characteristic solvent and impurity resonances; grease, 0.07 ppm, water, 1.56 ppm.)

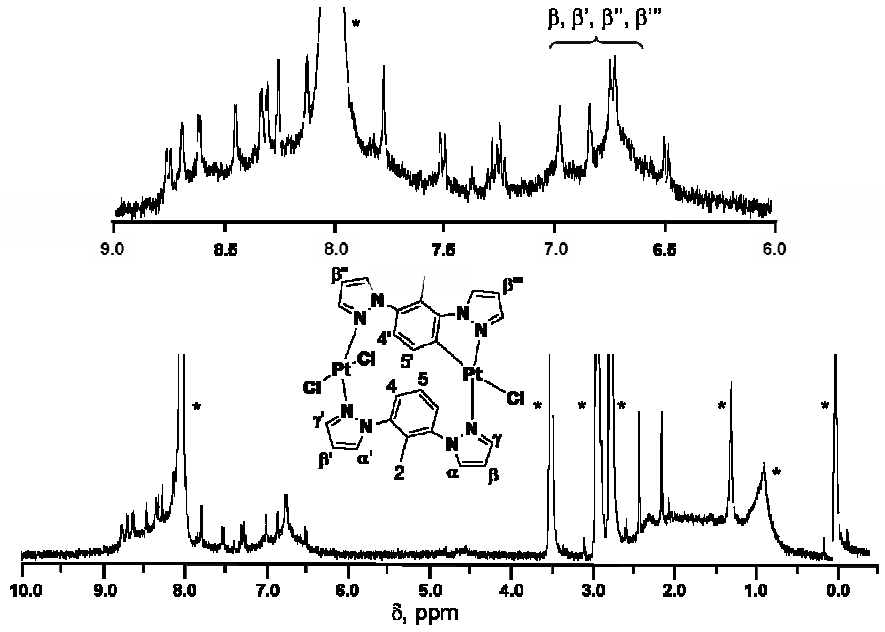

Figure 4.26. ^{1}H NMR spectrum of crystals of $Pt_2(\mu$-**7H**$)(\mu$-**7**$)Cl_3$ in DMF-d_7. (* marks characteristic solvent and impurity resonances; hexanes, 0.88 and 1.26 ppm, water, 3.50 ppm.)

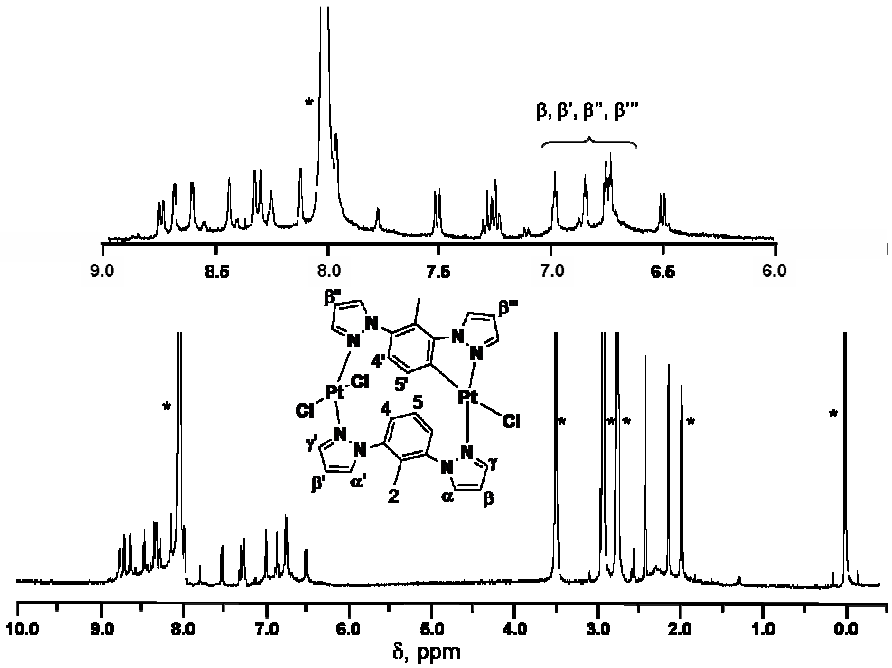

Figure 4.27. ^{1}H NMR spectrum of $Pt_2(\mu$-**7H**$)(\mu$-**7**$)Cl_3$ in DMF-d_7. (* marks characteristic solvent and impurity resonances; acetone, 2.00 ppm, water, 3.50 ppm.)

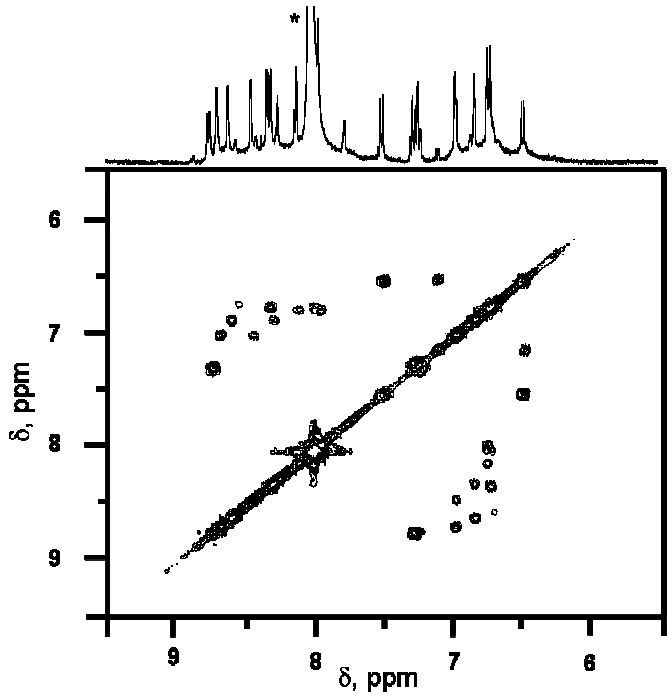

Figure 4.28. Two-dimensional COSY NMR spectrum of $Pt_2(\mu$-**7H**$)(\mu$-**7**$)Cl_3$ in DMF-d_7. (* marks characteristic solvent resonance.)

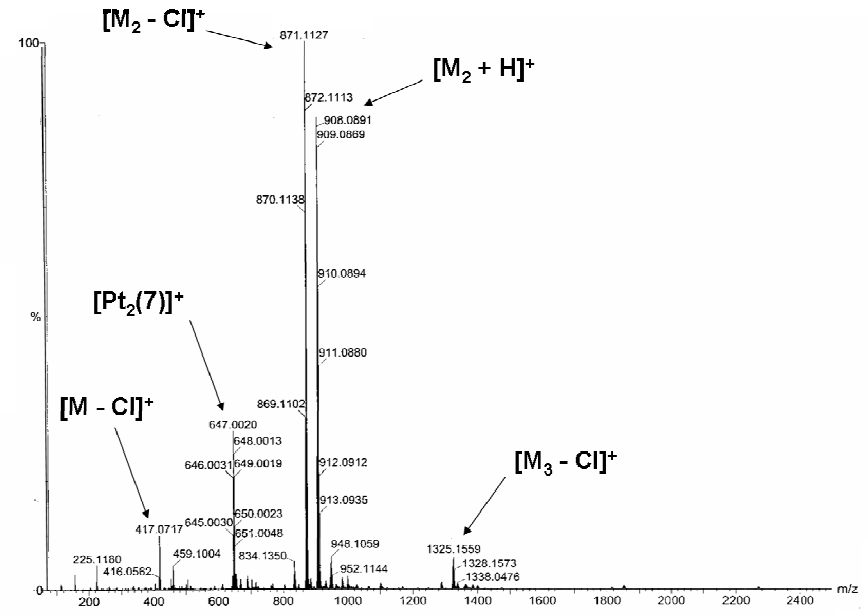

Figure 4.29. ESI mass spectrum of $Pt_2(\mu\text{-}\mathbf{7H})(\mu\text{-}\mathbf{7})_2Cl_3$ (M=Pt(**7**)Cl) in Isopropyl alcohol/ESI buffer solution.

The ^{1}H NMR spectrum of the product of the reaction of **8H** with $K_2[PtCl_4]$ shows at least 11 resonances in the aromatic region and six resonances in the aliphatic region attributable to methyl protons (Figure 4.31). The spectrum has nearly twice as many resonances as expected for a C_3-symmetric trimer product, and therefore we conclude that it does not have the same structure as observed for $[Pt(\mu\text{-}\mathbf{1})Cl]_3$. It is likely that a methyl group at the 2-position of the phenyl ring destabilizes the trimer structure since, as discussed above, the structure of $[Pt(\mu\text{-}\mathbf{1})Cl]_3$ shows that the H atom at this position has short intramolecular contacts to nearby Pt and Cl atoms. The product has not yet been fully characterized by NMR spectroscopy, and its identity is not certain. However, it is noteworthy that, in $CDCl_3$, two doublets occurs at 6.5 and 8.9 ppm, respectively; the spectrum of $Pt_2(\mu\text{-}\mathbf{7H})(\mu\text{-}\mathbf{7})Cl_3$ in DMF-d_7 shows two phenyl proton resonances at 6.5

and 8.8 ppm. However, because the spectra were recorded in different solvents, more detailed comparisons are not meaningful. The mass spectrum of the product was recorded in CH_3OH/ESI buffer solution (Figure 4.32). The spectrum exhibits major mass peaks consistent with the presence of $Pt_2(\mathbf{8})_2Cl^+$ and $Pt_2(\mathbf{8})_2Cl(CH_3CN)^+$. As also noted for $Pt_2(\mu\text{-}\mathbf{7H})(\mu\text{-}\mathbf{7})Cl_3$, there is a mass peak consistent with formation of a trimeric species, namely $Pt_3(\mathbf{8})_3Cl_2^+$.

Despite repeated efforts to prepare trimers from **4H** and **6H**, only monomeric products were isolated. Reactions involving **2H** at relatively high concentrations and for long reaction times were not investigated. Evidently methyl groups at the γ-position on the pyrazolyl groups tend to destabilize the trimer macrocycle. The crystal structure of $[Pt(\mu\text{-}\mathbf{1})Cl]_3$ shows that the distance from the γ-H pyrazolyl proton to the chlorine atom is 3.0 Å. Merely inserting a methyl group into the structure would result in a ~2 Å C···Cl contact in the hypothetical $[Pt(\mu\text{-}\mathbf{6})Cl]_3$ complex. Similarly, a space filling model suggests that there will be significant steric congestion if a methyl subsituent were added at the γ-position.

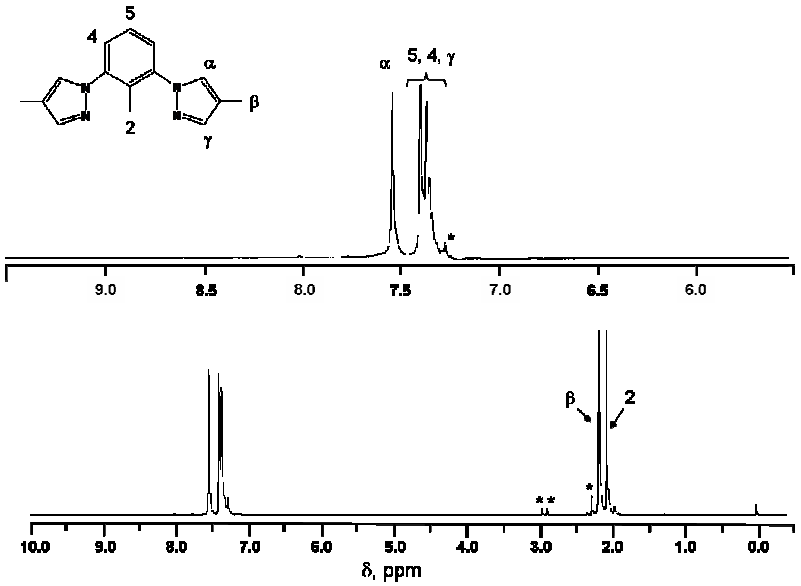

Figure 4.30. ^{1}H NMR spectrum of **8H** in $CDCl_3$. (* marks characteristic solvent and impurity resonances; acetone, 2,18 ppm, DMF, 2.88 and 2.96 ppm.)

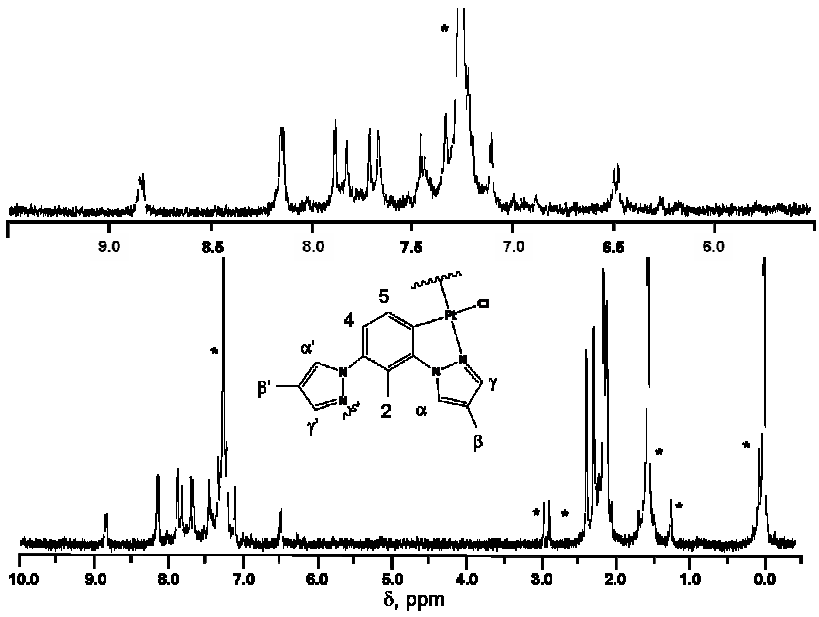

Figure 4.31. ^{1}H NMR spectrum of the product of the reaction of K_2PtCl_4 with **8H** in $CDCl_3$. (* marks characteristic solvent and impurity resonances; hexanes, 1.26 ppm, water, 1.56 ppm, DMF, 2.88 and 2.96 ppm.)

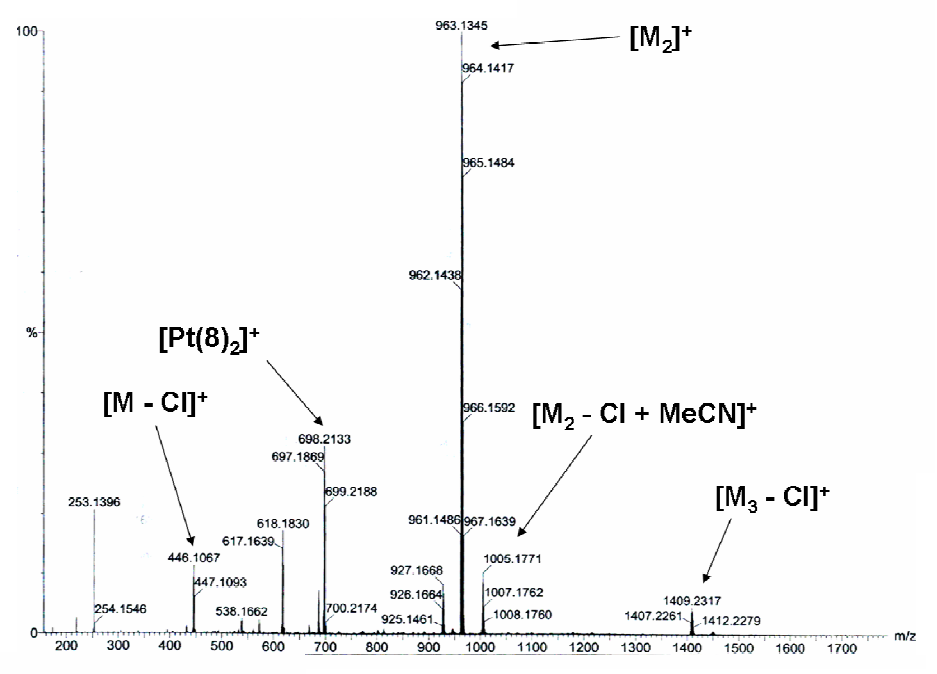

Figure 4.32. ESI mass spectrum of the product of the reaction of K_2PtCl_4 with **8H** in MeOH/ESI buffer solution (**M**=Pt(**8**)Cl).

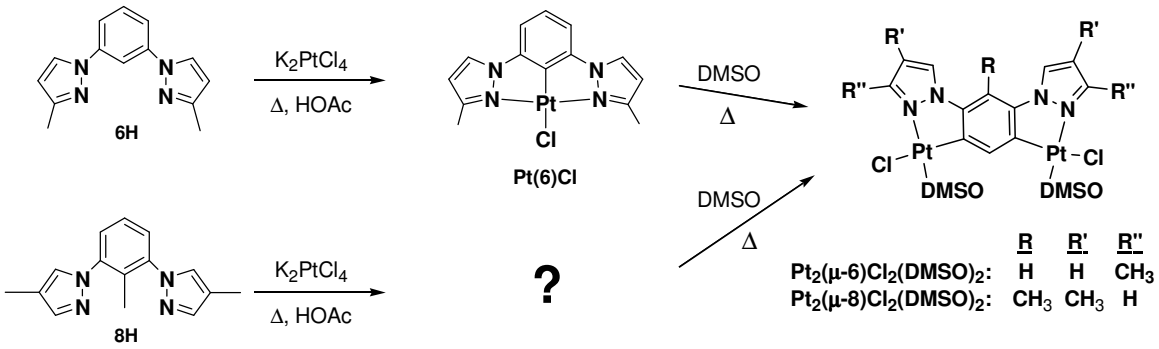

Scheme 4.6. Schematic representation of reactions in DMSO leading to dimeric products.

In the course of characterizing the Pt(**6**)Cl monomer, a second surprising dimer product was discovered (Scheme 4.6). A solid sample of Pt(**6**)Cl was dissolved in DMSO solvent in an effort to grow crystals. The solution was gradually allowed to

evaporate by placing a vial on top of an oven. Crystals formed inside the vial while the DMSO solvent was evaporated to dryness; the pale yellow needles were selected from the black residue. Single-crystal X-ray diffraction studies showed the crystals to contain Pt_2(**6'**)$Cl_2((CH_3)_2SO)_2$ (Figure 4.33), where **6'$^{2-}$** is the doubly deprotonated form of **6H**. The approximate C_2-symmetric product shows a second cyclometallation has occurred on the phenyl ring, resulting in the coordination of two platinum metal centers to one ligand. The **6'$^{2-}$** ligand bridges two approximately square planar platinum centers, bonding to each through the central phenyl ring and a N atom from the pyrazolyl moiety. For each platinum center, the DMSO molecule is trans to the pyrazolyl group, and the remaining coordination site is occupied by a chloride ligand. Due to steric repulsions between H4 and the sulfur atoms, the coordination geometries are slightly non-planar, and the S atoms are displaced slightly above (S1, 0.53 Å) and below (S2, 0.58 Å) a best-fit planed defined by the two Pt centers and the directly bonded C and N atoms (root mean square deviation of fitted atoms = 0.0623 Å). The 5-membered pyrazoyl rings are slightly twisted in opposite directions with respect to the 6-membered phenyl ring, resulting in dihedral angles of 5.9(2)° for the pyrazoyl bonded to Pt1 and 6.7(2)° for that bonded to Pt2.

A similar dimer product was obtained when the solid from the reaction of K_2PtCl_4 with **8H** was dissolved in DMSO and heated by placing a vial on top of an oven (Scheme 4.6). Single-crystal X-ray diffraction studies showed the crystals to contain Pt_2(μ-**8'**)$Cl_2(DMSO)_2$·DMSO (Figure 4.34). The **8'$^{2-}$** ligand bridges two platinum centers, bonding to each through the central phenyl ring and a N atom from the pyrazolyl moiety. Each DMSO ligand is trans to the pyrazolyl moiety as seen for Pt_2(**6'**)$Cl_2((CH_3)_2SO)_2$ with the four site on the platinum metal center occupied by a chloride. The S atoms are

displaced slightly above (S1, 0.37 Å) and below (S2, 0.30 Å) a best-fit planed defined by the two Pt centers and the directly bonded C and N atoms (root mean square deviation of fitted atoms = 0.0990 Å). In addition, the pyrazoyl groups are twisted slightly out of the plane of the phenyl group due to steric interactions with the methyl proton at the 2-position of the phenyl ring; the groups are twisted in the same direction, resulting in dihedral angles of 13.8(3)° for the pyrazoyl bonded to Pt1 and 9.8(3)° for that bonded to Pt2. Interestingly, the Pt-N distances (Pt1-N1, 2.011(6); Pt2-N3, 1.998(6) Å) are significantly shorter than found for Pt_2(**6'**)$Cl_2((CH_3)_2SO)_2$ (Pt1-N1, 2.067(3); Pt2-N3, 2.056(3) Å); in the latter case, there are likely greater steric interactions between the methyl substituent at the γ-position of the pyrazoyl ring and the chloride ligand, as suggested by the comparatively larger N1-Pt-Cl1 and N3-Pt2-Cl2 angles of 95.61(9) and 95.61(9)° (vs. 90.50(19) and 91.3(2)° for Pt_2(**8'**)$Cl_2((CH_3)_2SO)_2$). For both dimers, the Pt-C distances are nearly 0.1 Å shorter than found for the previously discussed monomer complexes and [Pt(μ-**1**)Cl]$_3$.

These initial studies suggest that dissolution in DMSO favors formation of dimeric products in which C-H activation has occurred at two sites on the ligand phenyl ring (Scheme 4.6). The molecular architecture is similar to those observed for other Pt(N-C-N)- and Pt(N-N-N)-containing dimers with DMSO ligands.[3,20] It is known that the bonding of one platinum to an aromatic ring will activate the ring toward further electrophilic substitution. It seems that a relatively soft polarizable donor ligand such as DMSO enhances this effect.

Table 4.5. Crystallographic Data for $Pt_2(\mu\text{-}\mathbf{7})(\mu\text{-}\mathbf{7H})Cl_3\cdot H_2O$, $Pt_2(\mu\text{-}\mathbf{6'})(Cl)_2(DMSO)_2\cdot DMSO$ and $Pt_2(\mu\text{-}\mathbf{8'})(Cl)_2(DMSO)_2$.

	$Pt_2(\mu\text{-}\mathbf{7})(\mu\text{-}\mathbf{7H})Cl_3\cdot H_2O$	$Pt_2(\mu\text{-}\mathbf{6'})(Cl)_2(DMSO)_2\cdot DMSO$	$Pt_2(\mu\text{-}\mathbf{8'})(Cl)_2(DMSO)_2$
formula	$C_{26}H_{23}N_8Cl_3Pt_2\cdot H_2O$	$C_{18}H_{24}N_4O_2S_2Cl_2Pt_2\cdot (CH_3)_2SO$	$C_{19}H_{26}N_4O_2S_2Cl_2Pt_2$
fw, g/mol	962.07	931.74	867.64
Crystal System	Monoclinic	Triclinic	Monclinic
Space Group	$P2_1/n$	P-1	$P2_1/n$
a, Å	8.5076(10)	7.4999(6)	12.6594(10)
b, Å	13.5037(15)	13.5049(12)	7.2756(6)
c, Å	24.794(3)	13.6857(12)	26.159(3)
α, °	90	78.527(2)	90
β, °	95.002(2)	75.983(3)	94.681(2)
γ, °	90	78.707(2)	90
V, Å^3	2837.6(6)	1302.03(19)	2401.3(4)
ρ_{calcd} (g cm^{-3})	2.252	2.377	2.400
μ, mm^{-1}	12.608	13.904	14.956
Z	4	2	4
T, K	150(2)	150(2)	150(2)
reflns collected	35603	18779	24741
ind reflns	7039	6337	4876
R_{int}	0.0731	0.0458	0.1011
GOF on F^2	1.020	1.056	1.052
$R1/wR2$ $[I > 2\sigma(I)]$[a]	0.0314/0.0768	0.0269/0.0731	0.0571/0.1456
$R1/wR2$ (all data)[a]	0.0381/0.0803	0.0292/0.0745	0.0597/0.1484
Weighting scheme (a/b)[a]	0.02631/2.2216	0.0356/0.2191	0.1109/0.0

[a] $w^{-1}=[\sigma^2(F_o^2)+(aP)^2+bP]$ where $P=0.33333F_o^2+0.66667F_c^2$ and a,b are refined quantities.

Table 4.6. Selected Bond Distances(Å) and Angles(°) for $Pt_2(\mu\text{-}\mathbf{7})(\mu\text{-}\mathbf{7H})Cl_3\cdot H_2O$, $Pt_2(\mu\text{-}\mathbf{6'})(Cl)_2(DMSO)_2\cdot DMSO$ and $Pt_2(\mu\text{-}\mathbf{8'})Cl_2(DMSO)_2$.

$Pt_2(\mu\text{-}\mathbf{7})(\mu\text{-}\mathbf{7H})Cl_3\cdot H_2O$				$Pt_2(\mu\text{-}\mathbf{6'})(Cl)_2(DMSO)_2\cdot DMSO$				$Pt_2(\mu\text{-}\mathbf{8'})Cl_2(DMSO)_2$			
Pt1-C9	1.973(5)	Pt2-Cl2	2.3059(14)	Pt1-C5	2.008(4)	Pt2-C9	2.006(3)	Pt1-C5	2.021(7)	Pt2-C9	2.015(8)
Pt1-N1	1.965(4)	Pt2-N4	2.007(4)	Pt1-N1	2.067(3)	Pt2-N3	2.056(3)	Pt1-N1	2.011(6)	Pt2-N3	1.998(6)
Pt1-N8	2.010(4)	Pt2-N5	1.999(4)	Pt1-S1	2.2040(10)	Pt2-S2	2.2023(10)	Pt1-S1	2.2067(18)	Pt2-S2	2.205(2)
Pt1-Cl1	2.3858(15)	Pt2-Cl3	2.2989(12)	Pt1-Cl1	2.3999(10)	Pt2-Cl2	2.4074(9)	Pt1-Cl1	2.3997(19)	Pt2-Cl2	2.396(2)
C4-C9	1.412(6)	C6-C7	1.380(6)	C4-C5	1.403(5)	C4-C9	1.397(5)	C4-C5	1.398(9)	C4-C9	1.396(10)
N2-C4	1.436(6)	N3-C6	1.426(6)	N2-C6	1.418(4)	N4-C8	1.417(5)	N2-C6	1.422(9)	N4-C8	1.431(9)
N7-C19	1.440(6)	N6-C17	1.435(6)	C6-C5	1.394(5)	C9-C8	1.389(5)	C6-C5	1.402(10)	C9-C8	1.404(11)
N1-N2	1.366(5)	N4-N3	1.359(6)	N2-N1	1.361(4)	N3-N4	1.371(4)	N2-N1	1.366(9)	N3-N4	1.369(9)
N1-Pt1-N8	176.91(17)	N4-Pt2-N5	173.72(16)	N1-Pt1-S1	168.48(9)	N3-Pt2-S2	167.18(10)	N1-Pt1-S1	175.34(19)	N3-Pt2-S2	177.7(2)
N8-Pt1-C9	96.98(18)	N5-Pt2-Cl2	88.51(13)	N1-Pt1-C5	80.68(13)	N3-Pt2-C9	80.80(14)	N1-Pt1-C5	79.7(3)	N3-Pt2-C9	79.7(3)
N1-Pt1-C9	80.02(18)	N5-Pt2-Cl3	92.43(12)	N1-Pt-Cl1	95.61(9)	N3-Pt2-Cl2	95.61(9)	N1-Pt-Cl1	90.50(19)	N3-Pt2-Cl2	91.3(2)
N1-Pt1-Cl1	94.73(12)	N4-Pt2-Cl2	88.37(12)	C5-Pt1-S1	93.62(11)	C9-Pt2-S2	94.07(11)	C5-Pt1-S1	95.82(19)	C9-Pt2-S2	99.8(2)
N8-Pt1-Cl1	88.29(13)	N4-Pt2-Cl3	90.76(12)	Cl1-Pt-S1	91.79(4)	Cl2-Pt2-S2	92.05(4)	Cl1-Pt-S1	94.05(7)	Cl2-Pt2-S2	89.34(8)
N7-N8-Pt1	127.3(3)	N5-N6-Pt2	129.0(3)	C6-C5-Pt1	113.9(3)	C8-C9-Pt2	114.0(3)	C6-C5-Pt1	114.5(5)	C8-C9-Pt2	114.6(6)
N2-N1-Pt1	117.2(3)	N3-N4-Pt2	127.5(3)	N2-N1-Pt1	112.6(2)	N4-N3-Pt2	112.8(2)	N2-N1-Pt1	116.1(5)	N4-N3-Pt2	116.5(5)
C4-N2-N1	113.6(4)	C6-N3-N4	120.2(4)	C6-N2-N1	116.7(3)	C8-N4-N3	116.2(3)	C6-N2-N1	115.0(6)	C8-N4-N3	113.9(6)
C19-N7-N8	122.1(4)	C17-N6-N5	124.7(4)	C4-C5-Pt1	129.7(3)	C4-C9-Pt2	128.9(3)	C4-C5-Pt1	128.5(5)	C4-C9-Pt2	127.6(6)

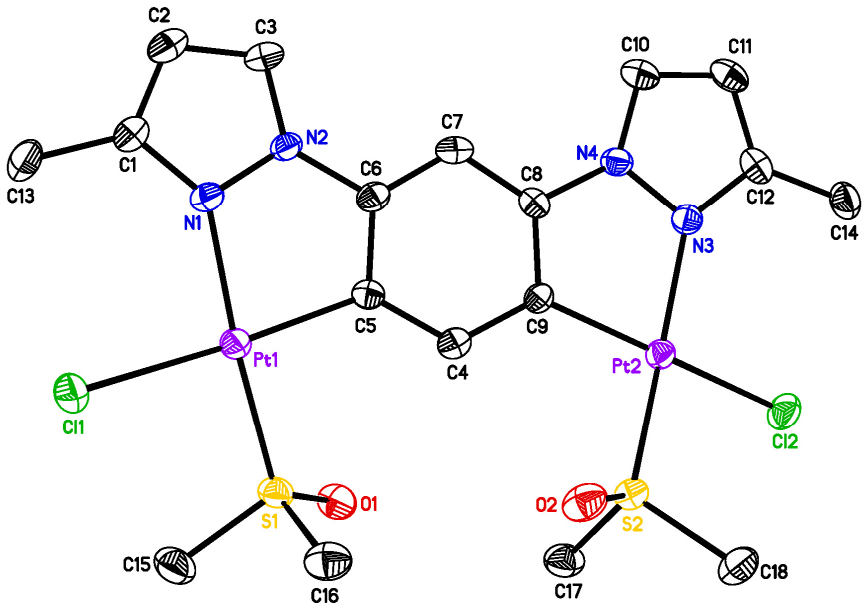

Figure 4.33. ORTEP diagram of dicyclometalated product $Pt_2(\mu\text{-}\mathbf{6'})(Cl)_2(DMSO)_2$. H atoms omitted for clarity.

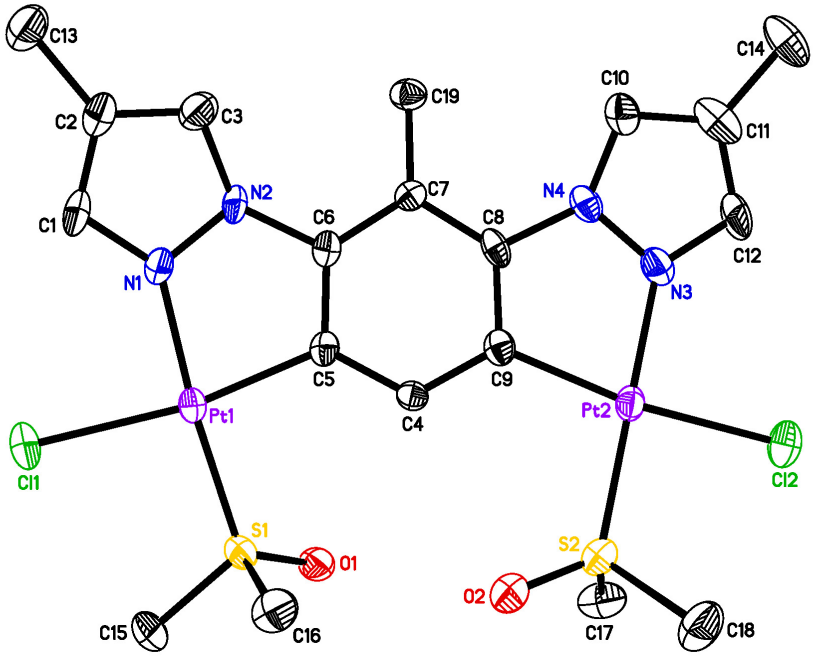

Figure 4.34. ORTEP diagram of dicyclometalated product $Pt_2(\mu\text{-}\mathbf{8'})(Cl)_2(DMSO)_2$. H atoms omitted for clarity.

Platinum(IV) Trimer. In an effort to develop strategies for separating enantiomers of $[Pt(\mu\text{-}\mathbf{1})Cl]_3$, we attempted to grow crystals of the trimer by vapor diffusion of racemic 2-chlorobutane into a DMF solution of $[Pt(\mu\text{-}\mathbf{1})Cl]_3$. Single-crystal X-ray diffraction studies of the resulting pale yellow crystals revealed the surprising result that the complex had been oxidized to give a platinum(IV) triangle, $[Pt(\mu\text{-}\mathbf{1'})Cl_2]_3$ where $\mathbf{1'^{2-}}$ is the doubly deprotonated form of **1H** (Figure 4.35). Crystallographic data are given in Tables 4.6 and 4.7. The conversion from $[Pt(\mu\text{-}\mathbf{1})Cl]_3$ to $[Pt(\mu\text{-}\mathbf{1'})Cl_2]_3$ is a net 6-electron oxidation that results from C-H activation of each $\mathbf{1}^-$ bridging ligand. Each bridging $\mathbf{1'^{2-}}$ ligand is bonded bidentate to two different platinum centers. As found for the parent platinum(II) trimer, the ligand bonds to one Pt center through the N atom of one pyrazolyl ring (pz) and the C atom at the 6-position of the phenyl group. In addition, each ligand is bonded to a metal through the N atom of the other pyrazoyl group (pz') and the C atom at the 2-position of the phenyl group. The remaining two coordination sites on each 6-coordinate platinum center are occupied by Cl atoms. Thus, **1H** has been activated at the 2- and 6-positions of the phenyl ring, whereas **6H** and **8H** were activated at the 4- and 6- positions in $Pt_2(\mu\text{-}\mathbf{L'})(Cl)_2(DMSO)_2$ ($\mathbf{L'}=\mathbf{6'^{2-}}, \mathbf{8'^{2-}}$).

The conversion from $[Pt(\mu\text{-}\mathbf{1})Cl]_3$ to $[Pt(\mu\text{-}\mathbf{1'})Cl_2]_3$ requires relatively little intramolecular rearrangement. The dihedral angles between the adjoining phenyl and pz' groups are significantly smaller (5.4(3) to 11.3(3)°) than found for the platinum(II) trimer (41.4(3) to 47.9(3)°), reflecting a flattening of these groups. By contrast, the remaining pyrazolyl group is significantly bent (rather than twisted) out of the plane of the phenyl ring resulting in dihedral angles ranging from 27.1(2) to 30.7(2)°. The ligand distortion results in slightly shorter intramolecular Pt···Pt distances (5.9451(4) to 5.9769(5) Å) than found for $[Pt(\mu\text{-}\mathbf{1'})Cl]_3$ (6.669(1) to 6.897(1) Å). In addition, there is a significant contraction in the opening of the trimer cavity

at the face where the pz groups are situated, as indicated by shorter interligand H(α)···H(γ) contacts (2.53-2.57 Å) than found for the platinum(II) complex (7.24-8.41 Å). By contrast, there is a slight enlargement of the opening at the other end of cavity, as reflected in larger interligand H(4)···H(5) contacts (4.29-4.38 Å) than observed for [Pt(μ-**1**)Cl]$_3$ (2.89-3.07 Å). Thus, the 6-electron oxidation effectively closes one end of the cavity and opens the other, suggesting the possibility of redox triggered pumping of reagents through channels of stacked trimers.

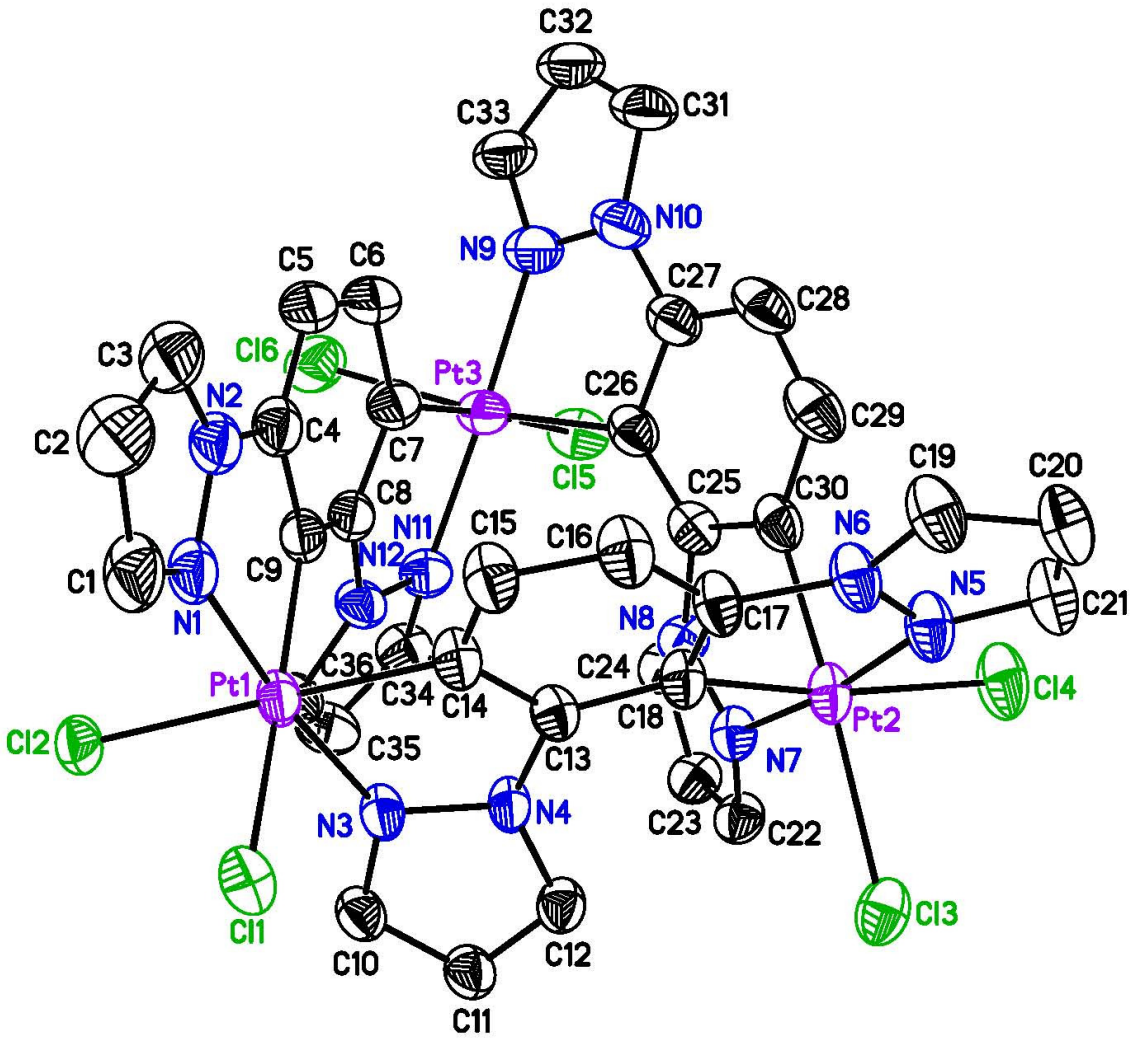

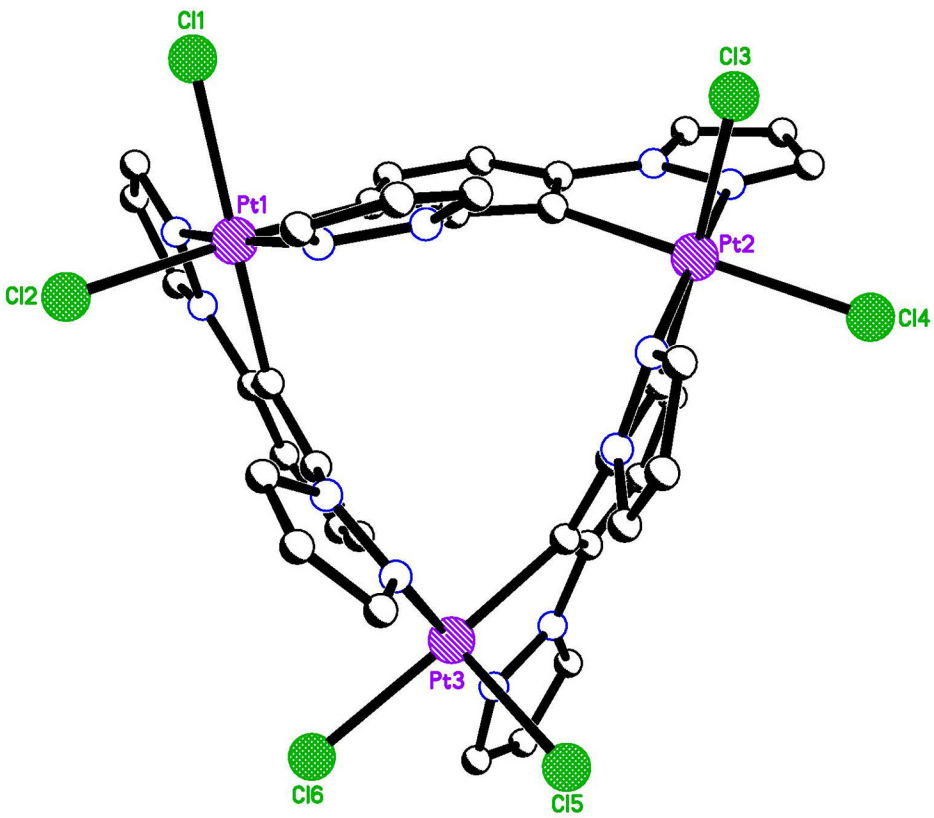

Figure 4.35. ORTEP diagram of platinum(IV) trimer, [Pt(μ-**1'**)$(Cl)_2]_3$ (top) and partially-labeled ball-n-stick drawing showing the triangular shape. H atoms omitted for clarity.

Table 4.7. Crystallographic Data for Pt(**9**)Cl_2 and [Pt(μ-**1'**)Cl_2]$_3$.

	Pt(**9**)Cl_2	[Pt(μ-**1'**)Cl_2]$_3$
Formula	$C_{11}H_9N_5Cl_2Pt$	$C_{36}H_{24}N_{12}Cl_6Pt_3$•$C_3H_7NO$·1/2$H_2O$
fw, g/mol	477.22	1504.75
Crystal System	Triclinic	Monoclinic
Space Group	*P*-1	$P2_1/n$
a, Å	8.7363(12)	14.4257(12)
b, Å	9.3218(13)	15.8148(13)
c, Å	9.3723(13)	20.4718(17)
α, °	69.127(3)	90
β, °	66.799(2)	98.766(2)
γ, °	83.456(2)	90
V, Å^3	655.19(16)	4615.9(7)
ρ_{calcd} (g cm^{-3})	2.419	2.165
μ, mm^{-1}	13.775	11.740
Z	2	4
T, K	195(2)	193(2)
reflns collected	8524	59555
ind reflns	2670	9400
R_{int}	0.0363	0.0565
GOF on F^2	1.050	1.060
*R*1/w*R*2 [I > 2σ(I)][a]	0.0285/0.0693	0.0268/0.0757
*R*1/w*R*2 (all data)[a]	0.0345/0.0713	0.0287/0.0767
Weighting scheme (a/b)[a]	0.0435/0.0	0.0418/7.4047

[a] $w^{-1}=[\sigma^2(F_o^2)+(aP)^2+bP]$ where $P=0.33333F_o^2+0.66667F_c^2$ and a,b are refined quantities.

Table 4.8. Selected Bond Distances(Å) and Angles(˚) for Pt(**9**)Cl_2 and [Pt(μ-**1'**)Cl_2]$_3$.

Pt(**9**)Cl_2		[Pt(μ-**1'**)Cl_2]$_3$					
Pt-N3	2.021(4)	Pt1-C9	2.055(5)	Pt2-C18	2.061(4)	Pt3-C26	2.065(5)
Pt-N1	1.978(5)	Pt1-C14	2.010(4)	Pt2-C30	2.028(13)	Pt3-C7	2.025(5)
Pt-Cl1	2.2876(16)	Pt1-N1	1.988(4)	Pt2-N5	1.999(4)	Pt3-N9	1.992(4)
Pt-Cl2	2.2874(15)	Pt1-N3	2.010(4)	Pt2-N7	2.002(4)	Pt3-N11	2.005(4)
N3-C4	1.351(7)	Pt1-Cl1	2.3973(13)	Pt2-Cl3	2.4356(13)	Pt3-Cl5	2.4165(12)
N4-C6	1.401(7)	Pt1-Cl2	2.4242(11)	Pt2-Cl4	2.3816(12)	Pt3-Cl6	2.3792(14)
N2-C4	1.403(7)	N2-C4	1.422(7)	N6-C17	1.416(6)	N10-C27	1.402(7)
N3-Pt-N1	79.83(18)	N4-C13	1.426(6)	N8-C25	1.418(6)	N12-C8	1.438(6)
N3-Pt-Cl1	95.44(14)	N2-N1	1.360(6)	N6-N5	1.348(5)	N10-N9	1.364(7)
N1-Pt-Cl2	93.77(14)	C9-Pt1-N1	80.80(18)	C18-Pt2-N5	80.17(16)	C26-Pt3-N9	80.09(19)
Cl1-Pt-Cl2	90.98(6)	C14-Pt1-N3	80.55(16)	C30-Pt2-N7	80.66(17)	C7-Pt3-N11	80.19(17)
N1-Pt-Cl1	175.04(13)	C14-Pt1-N1	91.46(17)	C30-Pt2-N5	92.30(18)	C7-Pt3-N9	93.86(18)
N3-Pt-Cl2	173.57(13)	N1-Pt1-N3	172.01(15)	N5-Pt2-N7	172.96(17)	N9-Pt3-N11	174.04(17)
C4-N3-Pt	114.9(4)	C9-Pt1-Cl1	170.99(13)	C18-Pt2-Cl4	170.66(13)	C26-Pt3-Cl6	170.31(13)
N1-N2-C4	116.3(4)	C14-Pt1-Cl2	175.78(13)	C30-Pt2-Cl3	176.02(13)	C7-Pt3-Cl5	176.03(13)
N2-N1-Pt	114.6(3)	N1-N2-C4	115.8(4)	N5-N6-C17	116.5(4)	N9-N10-C27	116.6(4)
C8-N3-Pt	128.2(4)	N3-N4-C14	116.1(3)	N7-N8-C25	116.1(4)	N11-N12-C8	116.3(4)

Reaction with an Analogous Pyridine Ligand. Ligand **9** was synthesized in order to investigate the possibility of forming a platinum metallocycle without C-H activation (Scheme 4.1). The resulting luminescent cationic trimer is expected to be useful for anionic substrate recognition. The monomer precursor, Pt(**9**)Cl_2, was prepared by refluxing K_2PtCl_4 and **9** in aqueous solution. The resulting precipitate was washed with water and to give a yellow solid in high yield (95%).

The ^{1}H NMR spectrum of Pt(**9**)Cl_2 exhibited the expected number of resonances and was fully assigned using COSY and NOESY techniques (Figures 4.38-4.40). As found for the free ligand and as expected for bonding of the pz group to the platinum(II) center, the pz proton resonances are shifted slightly downfield from those of pz'. Thus, the α-, β- and γ-pyrazolyl resonances occur at 7.2, 8.4 and 9.6 ppm, whereas those for pz' occur at 6.8, 8.1, and 8.9 ppm, respectively. The resonances for the 3- and 5-pyridine protons at 8.3 and 9.3 ppm, respectively, are shifted downfield from those of the previously discussed complexes with phenyl-containing ligands, as expected for replacement of a C atom with a N atom in the six-membered aromatic ring. The mass spectrum was recorded in $CHCl_3$/CH_3OH/ESI buffer solution. The most intense mass peak corresponds to Pt(**9**)(Cl)(COO)$(Na)^+$. Interestingly, there are higher mass peaks consistent formation of dimers and trimers (Figure 4.41).

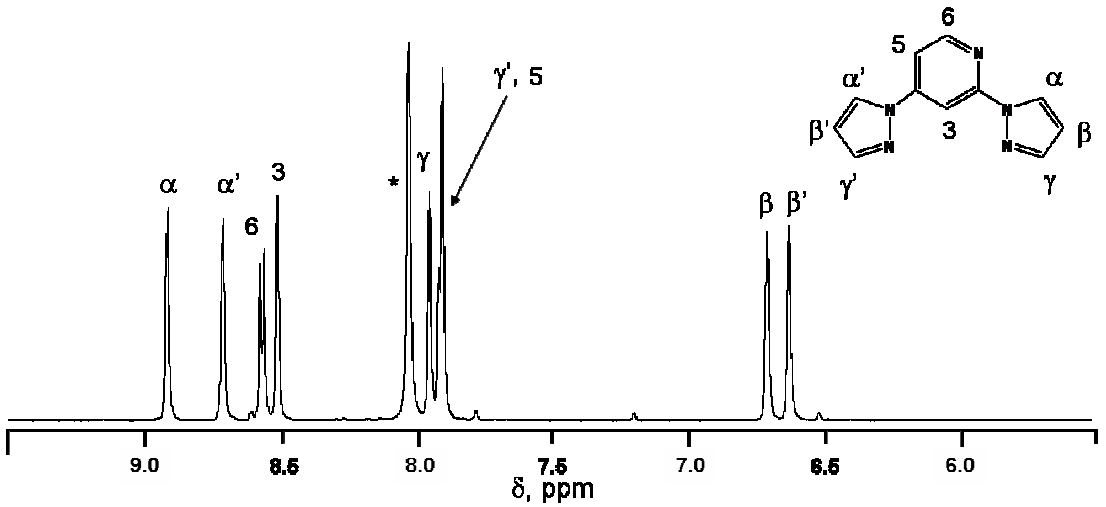

Figure 4.36. ^{1}H NMR spectrum of **9** in DMF-d_7. (* marks characteristic solvent resonance.)

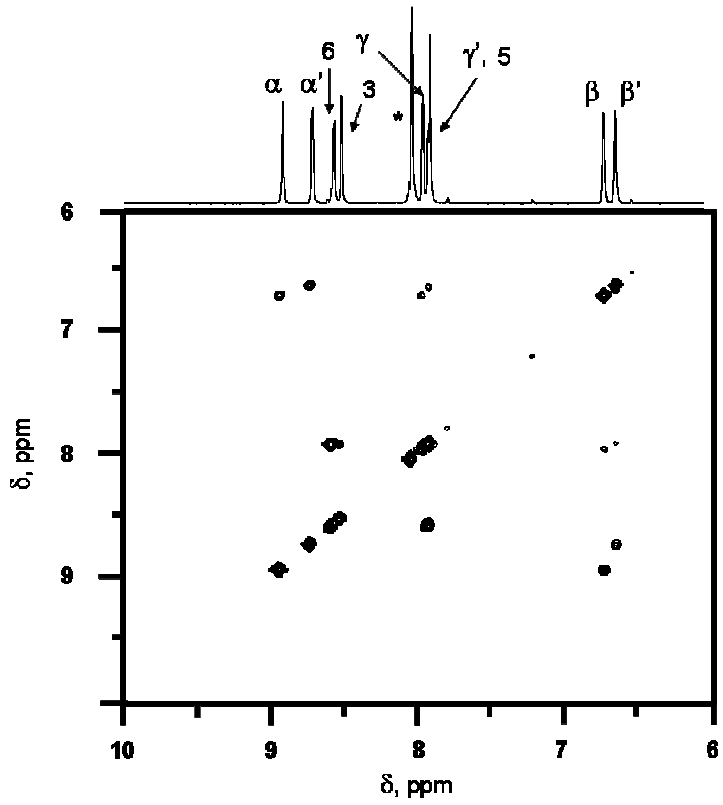

Figure 4.37. Two-dimensional COSY NMR spectrum of **9** in DMF-d_7. (* marks characteristic solvent resonance.)

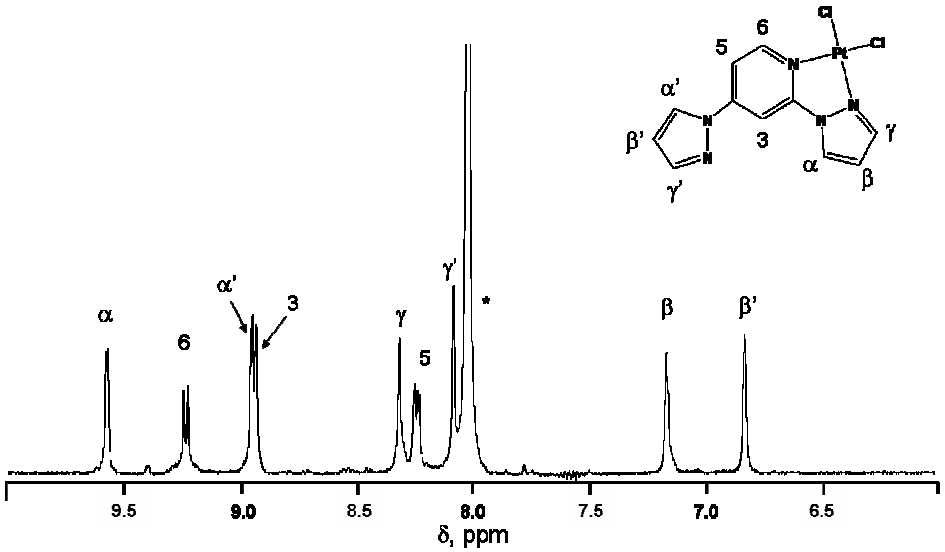

Figure 4.38. ^{1}H NMR spectrum of Pt(**9**)Cl_2 complex in DMF-d_7. (* marks characteristic solvent resonance.)

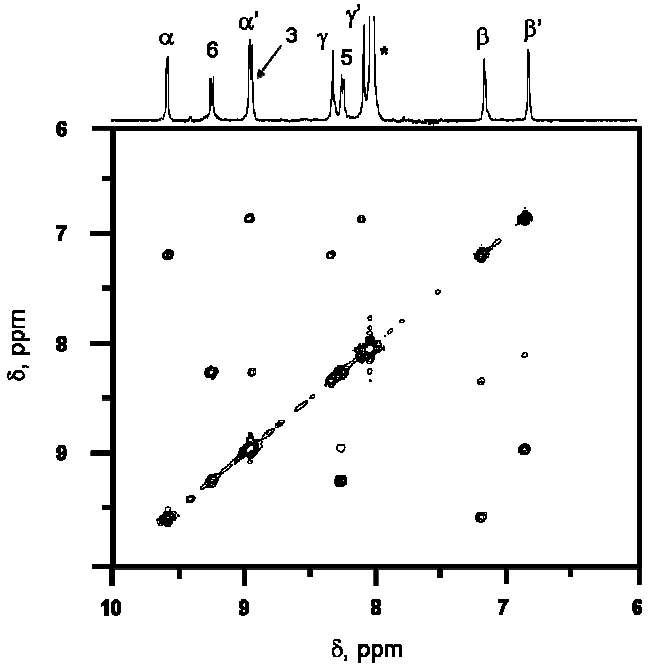

Figure 4.39. Two-dimensional COSY NMR spectrum of Pt(**9**)Cl_2 complex in DMF-d_7. (* marks characteristic solvent resonance.)

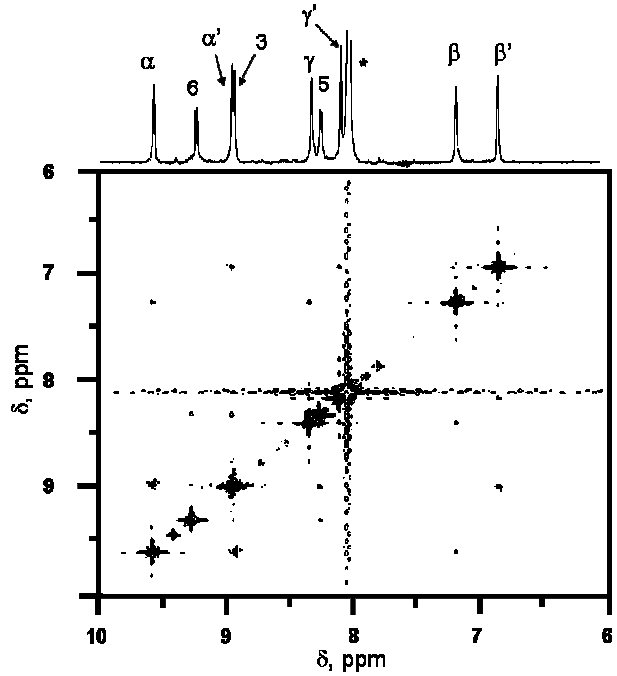

Figure 4.40. Two-dimensional NOESY NMR spectrum of Pt(**9**)Cl_2 complex in DMF-d_7. (* marks characteristic solvent resonance.)

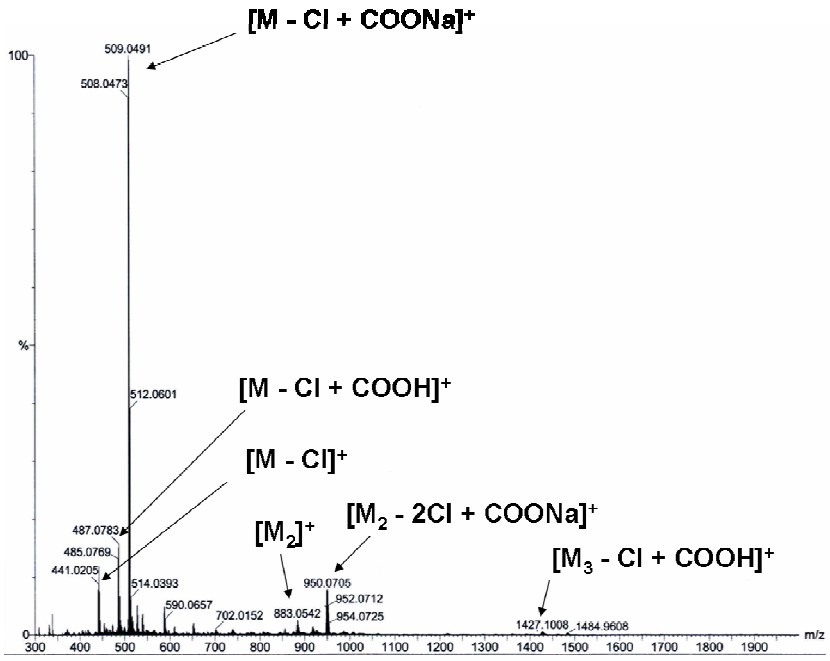

Figure 4.41. ESI mass spectrum of Pt(**9**)Cl_2 in $CHCl_3$/CH_3OH/ESI buffer solution.

The identity of Pt(**9**)Cl_2 was confirmed by X-ray crystallography. Single crystals of Pt(**9**)Cl_2 were grown by diffusion of diethylether into a DMF solution. Crystallographic data are reported in Tables 4.6 and 4.7. The ligand is bonded bidentate to the platinum metal center through the N atoms of the central pyridine ring and a pyrazolyl group (pz). Two chlorides ligands occupy the remaining two coordination sites (Figure 4.42). The bond lengths and angles for **9** are similar to those found for 2,6-*N*-pyrazolyl-pyridine (bpp) in $Pt(bpp)Cl^+$.[21] The Pt-N(pz) bond length (1.978(5) Å) is comparable to that found for $Pt(bpp)Cl^+$ (2.000(5), 1.991(5) Å), whereas the Pt-N(pyridine) bond length is significantly longer (2.021(4) Å vs. 1.950(4) Å). The resulting N(py)-Pt-N(pz) bond angle (79.83(18)°) is very similar to that reported for $Pt(bpp)Cl^+$ (80.6(2), 80.7(2)°).

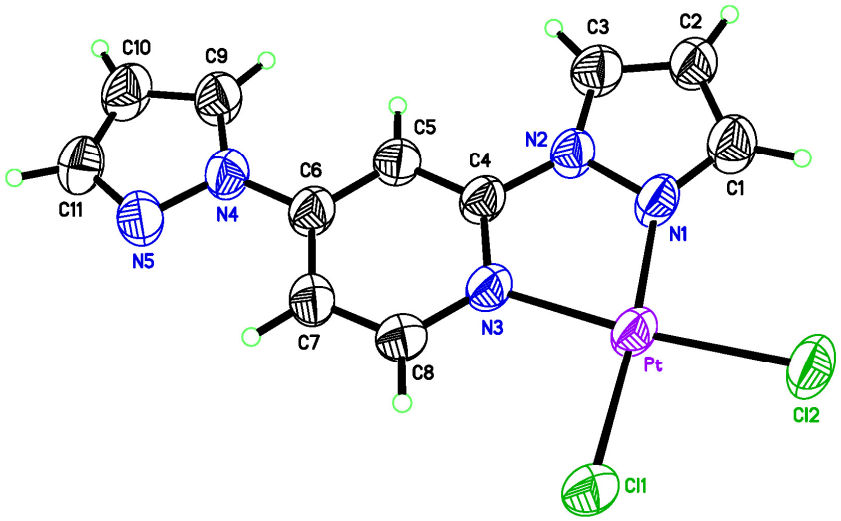

Figure 4.42. ORTEP diagram of Pt(**9**)Cl_2.

Reaction of Pt(9)Cl_2 with $TlPF_6$. In an attempt to prepare a metallocycle with **9** as a bridging ligand, we investigated a strategy for removing of one chloride ligand from Pt(**9**)Cl_2 by stirring the complex with thallium(I) hexafluorophosphate in DMF. The resulting precipitate was removed by filtration, and the filtrate was concentrated to dryness to give an orange solid (50-95%). The ^{1}H NMR and mass spectra are shown in Figures 4.43-4.44. The resonances in the ^{1}H NMR spectrum are essentially unshifted from those of Pt(**9**)Cl_2, and the resonances were assigned by analogy to that spectrum. It appears that no reaction has occurred or that only one (or both) chloride ligands have been substituted; water is the most likely ligand. It is noteworthy that the protons at the 5- and 6-positions of the pyridyl group are essentially unshifted from their positions in the monomer spectrum. By contrast, the corresponding resonances in the spectra of [Pt(μ-**1**)Cl]$_3$ and [Pt(μ-**5**)Cl]$_3$ were shifted strongly upfield. The mass spectrum also provides little evidence of trimer formation. The largest mass peak corresponds to Pt(**9**)(Cl)$(DMF)^+$. There are additional peaks that are consistent with dimer and trimer, however these products are equally likely to have formed in the ESI process.

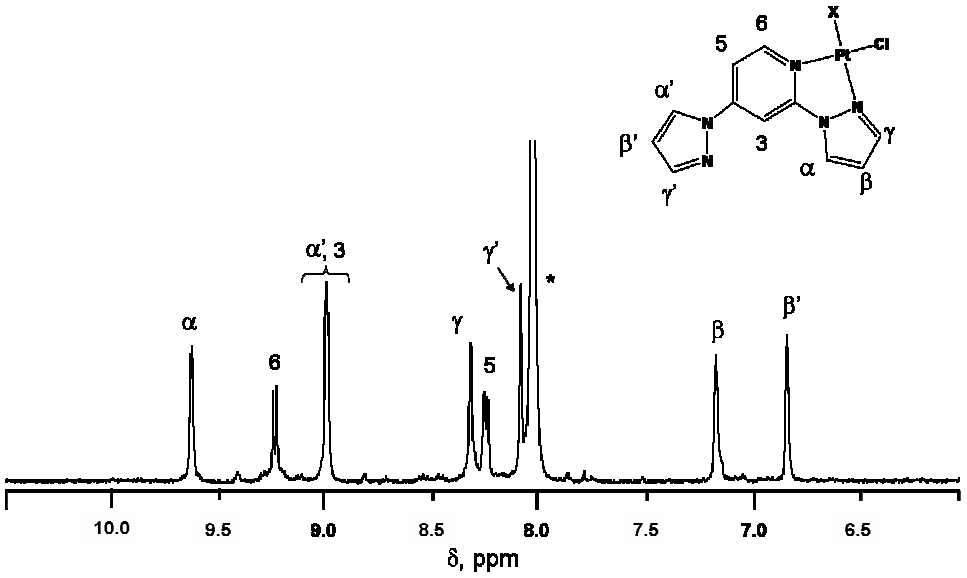

Figure 4.43. ^{1}H NMR spectrum of the product from the reaction of $[Pt(\mathbf{9})Cl]_2$ with $TlPF_6$ in DMF-d_7. (* marks characteristic solvent resonance.)

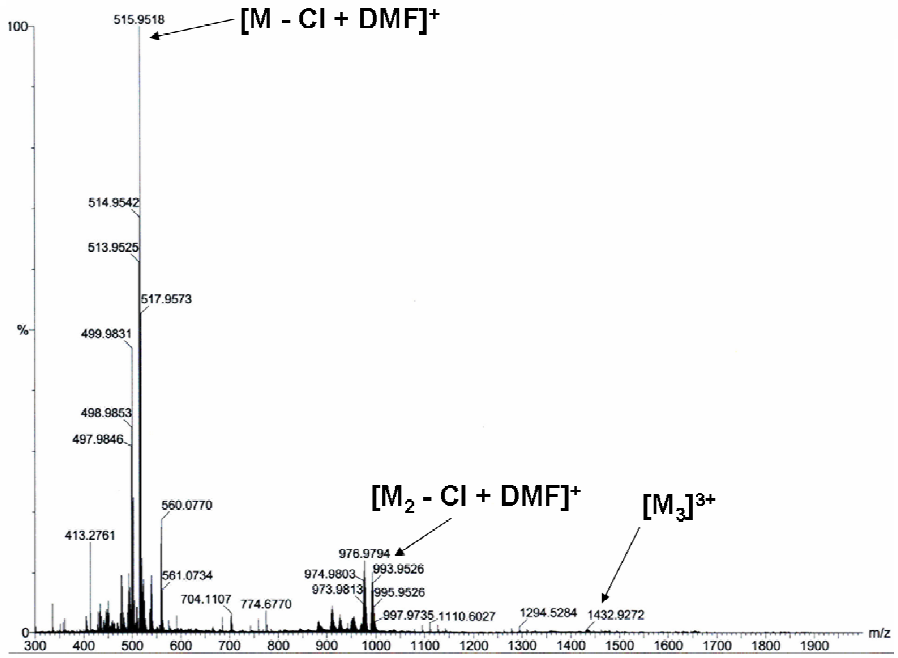

Figure 4.44. ESI mass spectrum of the product from the reaction of $Pt(\mathbf{9})Cl_2$ with $TlPF_6$ in CH_3CN solution.

Conclusions and Future Directions.

In this chapter, we have described how reactant concentration and reaction time influence cyclometallation products in the reaction of $K_2[PtCl_4]$ with *bis*-1,3-pyrazolyl-benzene ligand precursors in acetic acid. Our results are consistent with studies of **1H** reported in Chapter 3. For example, refluxing relatively low concentration acetic acid solution of **5H** (≤ 15 mM) with one equivalent of and $K_2[PtCl_4]$ for relatively short reaction times (2-5 days) gives exclusively monomer product. By contrast, higher reagent concentrations (≥42 mM) and longer reaction times (14 days) resulted in trimer formation, $[Pt(\mu\text{-}\mathbf{5})Cl]_3$. The precise role of the acetic acid solvent in these reactions remains uncertain. We also have determined the effectiveness of using methyl substituents as a means of blocking C-H activation sites on the central phenyl group of the ligand precursors. In all cases, methyl groups were found to prevent metal substitution at a given site. For example, methyl substituents prevented trimer formation in the case of **3H**. Similarly, a methyl substituent prevented formation of the C_{2v}-symmetric monomer in the case of **7H**. The reactions involving ligand precursors with methyl substituents in the γ-position on the pyrazolyl, **4H** and **6H**, yielded exclusively monomer products, suggesting that methyl groups at the γ-position disfavor trimer formation. These results are consistent with the previously reported crystal structure of $[Pt(\mu\text{-}\mathbf{1})Cl]_3$ (Chapter 3), which suggests that a methyl group at this position will result in unfavorable steric crowding. Interestingly, only monomer was isolated from the reaction of K_2PtCl_4 with **2H** for 4 days. It is unclear if the presence of a methyl substituent at the 5-position on the phenyl ring inhibits trimer formation; future experiments should address

this question by exploring longer reaction times and higher concentrations (*e.g.*, 14 days, >100 mM).

In the course of these investigations, we discovered two new dimeric architectures. In $Pt_2(\mu\text{-}\mathbf{7H})(\mu\text{-}\mathbf{7})_2Cl_3$, one 7H group has already undergone C-H activation, whereas the other has not. This dimer is likely present in refluxing acetic acid solutions of K_2PtCl_4 and *bis*-1,3-pyrazolyl-benzenes and may be an intermediate in the reaction to give trimer. A trimer containing $\mathbf{7}^-$ has not yet been isolated, and it is possible that the methyl substituent at the 2-position of **7H** destabilizes the trimer, thus allowing for isolation of the dimer. Future research should focus on testing this hypothesis by exploring longer reaction times with **7H**, as well as characterizing the product(s) of reactions with **8H** (***e.g.***, ^{1}H NMR spectrum in DMF-d_7).

Heating Pt(**6**)Cl, as well as heating the product of the reaction of K_2PtCl_4 with **8H** in DMSO, gave the unexpected dimer products $Pt_2(\mu\text{-}\mathbf{L'})(Cl)_2(DMSO)_2$ (**L' = 6'**, **8'**). In these products, **6H** and **8H** have undergone C-H activation at two sites on the central phenyl ring. In principle, it should be possible to monitor this reaction by ^{1}H NMR spectroscopy, and this experiment should be performed in future studies using Pt(**1**)Cl and Pt(**6**)Cl. Isolation and full characterization of the product will determine the product's stability in other solvents besides DMSO. It is conceivable that $Pt_2(\mu\text{-}\mathbf{L'})(Cl)_2(DMSO)_2$ is the thermodynamic product in DMSO solution, The possibility that the DMSO ligand activates the coordinated phenyl group toward electrophilic substitution offers a well-defined strategy for promoting C-H activation at specific sites on aryl groups. As a starting point for testing this hypothesis, the reaction should be repeated using Pt(**1**)Cl, $[Pt(\mu\text{-}\mathbf{1})Cl]_3$ and $Pt_2(\mu\text{-}\mathbf{7H})(\mu\text{-}\mathbf{7})Cl_3$.

In the case of **9**, a monomer product, Pt(**9**)Cl_2, was isolated in which the ligand is bidentate, rather than tridentate. We attempted to remove one of the chloride ligands by reaction with a thallium(I) salt. However, the ^{1}H NMR spectrum showed no evidence of a metallocycle, and it is unclear if a chloride ligand was even displaced. As with the original Pt(**9**)Cl_2 monomer, the mass spectrum showed trimer fragments, which were likely formed during the ESI process. Future studies should address the possibility of allowing the monomer to react longer with the thallium salt. In addition, silver(I) salts should be investigated as a means of removing a chloride ligand. A trimer based on **9** is especially interesting since the 3+ charged complex is anticipated to be luminescent. It may be possible to exploit this property for anion recognition.

References.

(1) Albrecht, M.; van Koten, G. *Angew. Chem. Int. Ed.* **2001**, *40*, 3750.

(2) Zucca, A.; Doppiu, A.; Cinellu, M. A.; Stoccoro, S.; Minghetti, G.; Manassero, M. *Organometallics* **2002**, *21*, 783-785.

(3) Stoccoro, S.; Zucca, A.; Petretto, G. L.; Cinellu, M. A.; Minghetti, G.; Manassero, M. *J. Organmet. Chem.* **2006**, *691*, 4135-4146.

(4) Cave, G. W. V.; Hallet, A. J.; Errington, W.; Rourke, J. P. *Angew. Chem. Int. Ed.* **1998**, *37*, 3270.

(5) Soro, B.; Stoccoro, S.; Minghetti, G.; Zucca, A.; Cinellu, M. A.; Manassero, M.; Gladiali, S. *Inorg. Chim. Acta* **2006**, *359*, 1879-1888.

(6) Cardenas, D. J.; Echavarren, A. M.; Arellano, M. C. R. *Organometallics* **1999**, *18*, 3337-3341.

(7) Fossey, J. S.; Richards, C. J. *Organometallics* **2002**, *21*, 5259-5264.

(8) Zhao, S.-B.; Wang, R.-Y.; Wang, S. *J. Am. Chem. Soc.* **2007**, *129*, 3092-3093.

(9) Willison, S. A.; Krause, J. A.; Connick, W. B. *Inorg. Chem.* accepted.

(10) Cristau, H.-J.; Cellier, P. P.; Spindler, J.-F.; Taillefer, M. *Eur. J. Org. Chem.* **2004**, 695-709.

(11) Cristau, H.-J.; Cellier, P. P.; Spindler, J.-F.; Taillefer, M. *Chem. Eur. J.* **2004**, *10*, 5607-5622.

(12) Grimmett, M. R.; Hartshorn, S. R.; Schofield, K.; Weston, J. B. *J. Chem. Soc. Perkin Trans 2* **1972**, 1654-1660.

(13) Tensmeyer, L. G.; Ainsworth, C. *J. Org. Chem.* **1966**, *31*, 1878-1883.

(14) Lexy, H.; Kauffman, T. *Chem. Ber.* **1980**, *113*, 2749-2754.

(15) APEX2 (v2.0-2. or 2.1-4), SMART v5.631 and SAINT (v6.45A, v7.23A or 7.34A) data collection and data processing programs, respectively. Bruker Analytical X-ray Instruments, Inc., Madison, WI; SADABS (v2.10 or v2004/1) semi-empirical absorption and beam correction program. G.M. Sheldrick, University of Göttingen, Germany.

(16) SHELXTL v6.14 for structure solution, figures and tables, neutral-atom scattering factors as stored in this package. G.M. Sheldrick, University of Göttingen, Germany and Bruker Analytical X-ray Instruments, Inc., Madison, WI.

(17) A. L. Spek, PLATON. Acta Cryst. **1990**, A46, C34.

(18) K. Brandenburg, Diamond v3.1d, Crystal Impact. **2007**.

(19) Cave, G. W. V.; Fanizzi, F. P.; Deeth, R. J.; Errington, W.; Rourke, J. P. *Organometallics* **2000**, *19*, 1355-1364.

(20) Doppiu, A.; Minghetti, G.; Cinellu, M. A.; Stoccoro, S.; Zucca, A. *Organometallics* **2001**, *20*, 1148-1152.

(21) Willison, S. A.; Jude, H.; Antonelli, R. M.; Rennekamp, J. M.; Eckert, N. A.; Krause Bauer, J. A.; Connick, W. B. *Inorg. Chem.* **2004**, *43*, 2548-2555.

Chapter 5

Platinum Complexes as Colorimetric Indicators for Allergenic Dithiocarbamate Compounds in Latex

Introduction.

Processing of natural rubber involves a series of steps aimed at improving the properties of the final product. These measures result in increased tensile strength and elasticity, decreased solubility, increased thermal stability, and reduced tackiness. One of these protocols is the vulcanization process, in which the material is heated with a cross-linking agent (*e.g.*, sulfur) in order to create a three dimensional network of polyisoprene chains. The resulting product is less tacky than natural rubber, recovers its shape after deformation, has improved resistance to abrasion, and is resistant to hardening or softening with changes in temperature. Within the last 100 years, it has become commonplace to use accelerators in the vulcanization process. These additives increase the rate of vulcanization and decrease the amount of cross-linking reagent needed, thereby improving the tensile properties of the latex for commercial products.[1]

Some of the first accelerators used to shorten the vulcanization process were magnesium, calcium and lead oxides. Today, mostly organic accelerators are used to provide an even quicker process at lower temperatures. Often there is a synergistic effect on the vulcanization process when an accelerator is used in used in conjunction with another accelerator or other additive, such as zinc oxide. Common organic accelerators fall into four main categories: benzothiazoles, thiurams, carba chemicals and amines. The most commonly used accelerators are dithiocarbamate compounds,which are a

subset of the carba chemicals. They tend to provide the fastest curing for latex compounding (Figure 5.1).

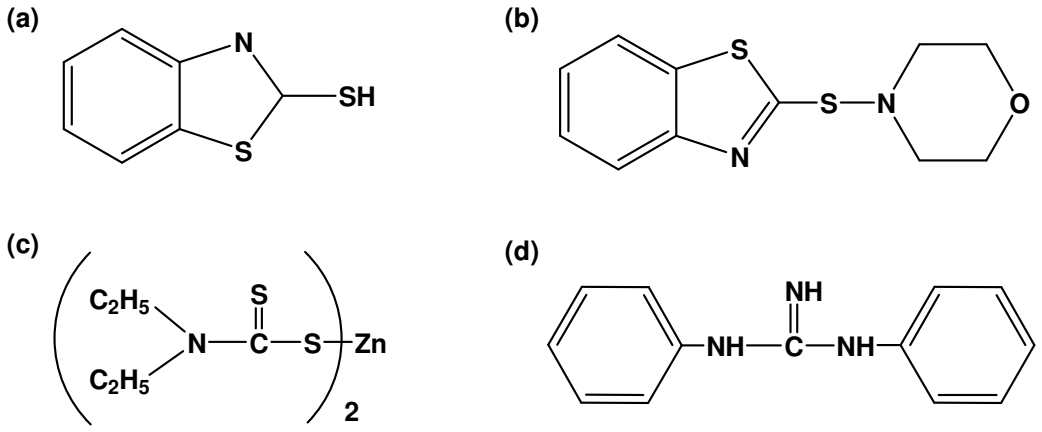

Figure 5.1. Line drawings of commonly used accelerators (a) 2-Mercaptobenzothiazole (MBT), (b) 2-Morpholinothiobenzothiazole (MBS), (c) Zinc diethyldithiocarbamate (ZDEC) and (d) Diphenylguanidine (DPG).

There are more than twenty commercially available dithiocarbamate accelerators.[1] A potential drawback to dithiocarbamate accelerators is that they are known to cause contact dermatitis.[2] Manufacturers of latex medical devices are required to adhere to FDA regulations (FDA 21 CFR section 177.2600: applicable to rubber articles intended for repeated use),[3] which require that accelerators not exceed 1.5% by weight of the rubber product and that only approved substances should be used due to some evidence suggesting that some accelerators are carcinogenic.[4] In addition to their presence in latex products, dithiocarbamates are used in pesticides, which have a maximum level of 7 ppm in fruits and vegetables.[4] Certain analytical methods have been successfully used to qualitatively and quantitatively detect the presence of dithiocarbamates. However, these methods have some drawbacks.[5] For example, when analyzed using HPLC methods, it

has been shown that metal exchange reactions occur between these accelerators and nickel from the stainless steel components of the chromatographic system, thereby interfering with detection and quantification. Furthermore, the presence of multiple accelerators complicates the analysis, making it more expensive and time consuming.

In the course of our investigations of platinum(II) complexes with *bis*-2,6-dipyrazolyl-phenyl ligands, we have discovered that selected complexes react with dithiocarbamate accelerators that are commonly used in latex processing. Here we report four complexes that give a colored response when applied to latex gloves. Similar colors are encountered when the complexes are applied directly to dithiocarbamate compounds which are used as accelerators. These results suggest that the platinum complexes could be utilized as a quick colorimetric screening test for the presence of residual allergenic dithiocarbamate accelerators in latex products.

Experimental Section.

The platinum compounds were synthesized and characterized as described in Chapters 3 and 4. *N*-cyclohexyl-2-benzothiazole sulfenamide (CBS), *N*-*tert*-butyl-2-benzothiazole sulfenamide (TBBS), *N*-oxydiethylene-2-benzothiazole sulfenamide (MBS) and *N*, *N*-dicyclohexyl-2-benzothiazole sulfenamide (DCBS) accelerators were obtained from Shepherd Chemical, and liquid latex samples were obtained from Cementex. Several latex samples were obtained from Ms. Allison Ryan at Hygenic Corporation. Latex glove samples were obtained from manufacturers listed in Table 5.3. Initial investigations were carried out using Pt(**1**)Cl/[Pt(μ-**1**)Cl]$_3$ mixtures (Scheme 5.1) on the latex surfaces (Figures 5.3 and 5.6), however, it was later discovered that the

monomer product (not the trimer product) was responsible for the observed color change. Even though four monomer compounds gave a response, Pt(**3**)Cl was used thereafter because of the better color contrast.

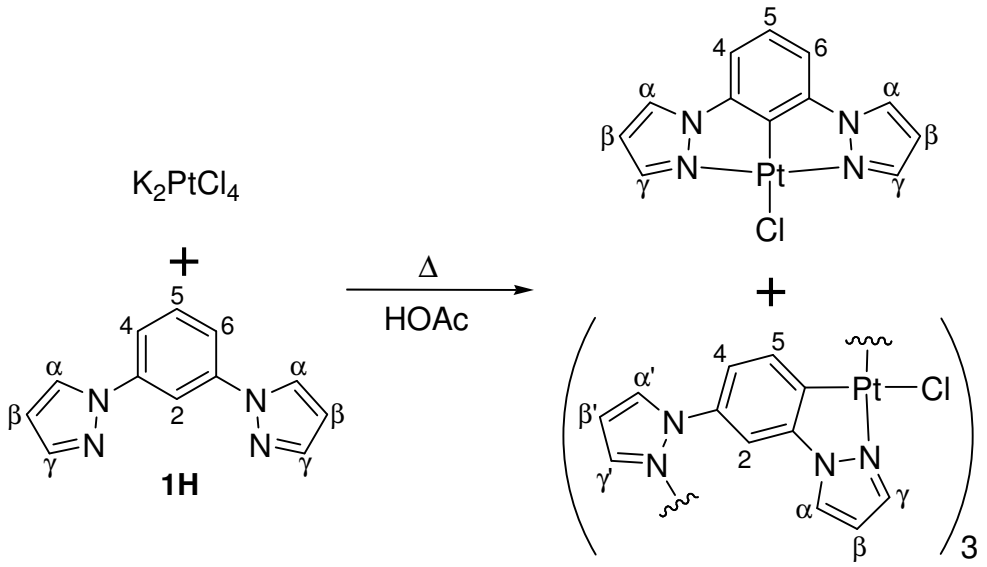

Scheme 5.1. Reaction scheme showing the synthesis of a Pt(**1**)Cl/[Pt(μ-**1**)Cl]$_3$ mixture.

Colorimetric measurements of the response of a platinum complex to latex or a specific accelerator were carried out as follows. The platinum complex was dissolved in methylene chloride, unless otherwise noted. The solution was applied directly to the substrate surface (*e.g.*, latex medical examination glove) using a glass pipette. The solution was allowed to evaporate, which usually occurred within 5-10 seconds. The color change was immediately visible upon evaporation (Figure 5.2). Unless otherwise specified, commercial latex substrates were not treated prior to testing. Preparation of the accelerator substrates was accomplished by allowing a concentrated methylene chloride solution of the accelerator to evaporate on a conventional microscope slide, leaving

behind a thick residue of the solid accelerator. Color changes were discernible for platinum concentrations as low as 10 ppm.

Inductively coupled plasma-mass spectrometry (ICP-MS) was performed in collaboration with Doug Richardson in Professor Joe Caruso's laboratory at the University of Cincinnati to investigate the amount of platinum that could be recovered from the latex surface. A 3:1 Pt(**1**)Cl/[Pt(μ-**1**)Cl]$_3$ mixture (1.2 mg) was dissolved in methylene chloride (0.5 ml) and deposited to the surface of a latex glove. The solution was allowed to evaporate. The resulting red-stained area was washed with water and allowed to air dry. The surface was washed with 30 mL of methylene chloride to remove the stain. The collected washings were concentrated to dryness by rotary evaporation. The same procedure was repeated except using an acetonitrile solution of the platinum complexes (1.11mg in 0.5 ml of CH_3CN). A dry sample of the monomer/trimer mixture (1.14 mg) was used as a standard. To each of the three samples, 0.5 mL of HNO_3 was added and placed in a CEM Discover microwave digestion system to allow for digestion of the samples at 150 ˚C for 4 minutes at 250 psi. A platinum standard from Professor Joe Caruso's laboratory was used to calibrate the instrument, starting with the first dilution at 10 ppm. Further dilutions were made using the platinum standard at concentrations of 5, 1, 0.5 and 0.1 ppm and these four dilutions were recorded for each sample using an Agilent 7500 series ICP-MS instrument. Water was used as a blank. Each dilution was collected five times, averaged (with relative standard deviations reported as 2 times the error) and plotted giving a linear calibration curve. Each of the three samples (CH_2Cl_2, CH_3CN and solid) was analyzed the same as in each dilution and the amount of platinum in each sample was estimated from the calibration curve. The

amount of measured platinum was divided by the calculated original amount of platinum applied to the latex surface, giving the amount of recovered platinum as a percentage of applied platinum.

Results and Discussion.

The compounds shown in Figure 5.4 were synthesized and characterized as described in Chapters 3 and 4. As noted previously, each compound forms an off-white or beige solid that dissolves in organic solvents (*e.g.*, CH_3OH, CH_2Cl_2, $CHCl_3$, DMF) to give a colorless solution. The solutions remain colorless when applied to a latex surface, such as a latex glove, bulb for disposable pipettes or an eraser. However, for solutions of four of the monomeric compounds (see Figure 5.5), evaporation on a latex surface results in a deep red or violet stain on the latex surface (Figure 5.2). Pt(**1**)Cl and Pt(**2**)Cl produce a red stain on latex, Pt(**5**)Cl gives a red/orange stain (Figure 5.5), whereas Pt(**3**)Cl produces a violet stain. Interestingly, the trimeric complex [Pt(μ-**1**)Cl]$_3$ did not give a stain under similar conditions. In the course of our investigations, Pt(**3**)Cl was subjected to the majority of experiments because it gave the most intense color change of all platinum compounds tested. Evaporation of Pt(**3**)Cl dissolved in a range of organic solvents (Table 5.1) consistently produces a violet stain on latex. It is important to note that the stain is reproduced irrespective of the solvent used to apply the compound. These results indicate that the solvent is not directly involved in the formation of the colored stain. Low boiling point solvents were found to be especially useful because they allow for rapid testing of latex materials. It is noteworthy that the stain does not wash off when rinsed with water. However, application of an organic solvent (*e.g.*, $CHCl_3$,

CH_2Cl_2, CH_3CN, acetone) to the latex causes the stain to disappear. Thus, the compound appears to act as a magic marker with the latex substrate.

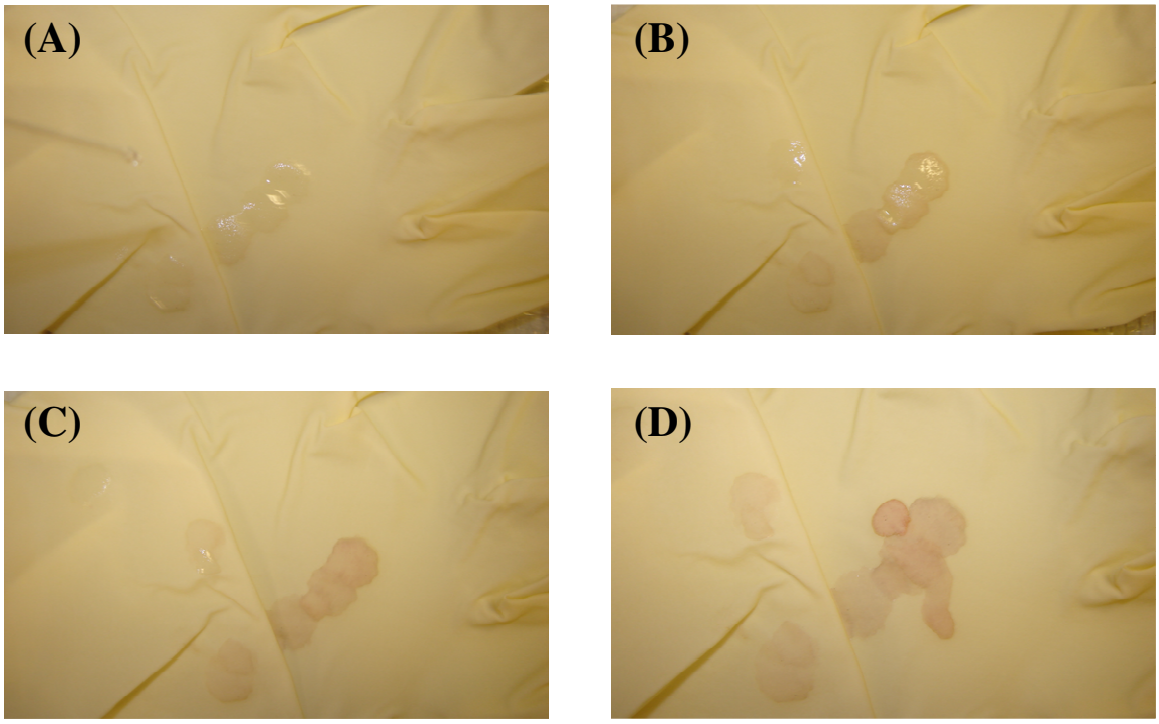

Figure 5.2. Four digital images showing formation of the stain. (A) methylene chloride solution of Pt(**3**)Cl immediately after deposition on a latex glove, (B) ~5 seconds later; solvent has begun to evaporate; (C) ~ 8 seconds after initial deposition; most of the solvent has evaporated and the stain has appeared; (D) ~ 15 seconds after initial deposition; sample is dry and stain has reached maximum color intensity.

The mechanistic details of the colorimetric response are not known. However, preliminary results suggest that a chemical reaction is occurring. For example, a solution of Pt(**3**)Cl in $CDCl_3$ was applied to the accelerator surface where upon evaporation gave a purple stain. Deuterated chlorform was reapplied to the latex surface resulting in the

removal of the purple stain. The $CDCl_3$ washings were collected, and the ^1H NMR spectrum recorded. Four of the resonances are approximate matches for the spectrum of Pt(**3**)Cl, but the agreement is not exact; the fifth resonance of Pt(**3**)Cl has significantly shifted and is presumed to overlap with the solvent resonance (Figure 5.3). The results suggest that substitution of the chloride ligand has occurred. On the other hand, the resonances assigned to the accelerator match those of the free accelerator in solution; it is noteworthy that a large excess of accelerator was used in this experiment, and resonances of unreacted accelerator could obscure those of products. The color observed after solvent evaporation is reminiscent of those observed for platinum(II) complexes with sulfur donor ligands (*e.g.*, thiolates, dithiocarbamates),[6] linear chain materials composed of square planar platinum(II) complexes with short Pt...Pt spacings (<3.5 Å),[7-9] and mixed oxidation state platinum systems (i.e., so-called platinum blues, reds, etc.)[10-12] At this stage, it is uncertain which of these types of compounds (if any) is the origin of the observed color.

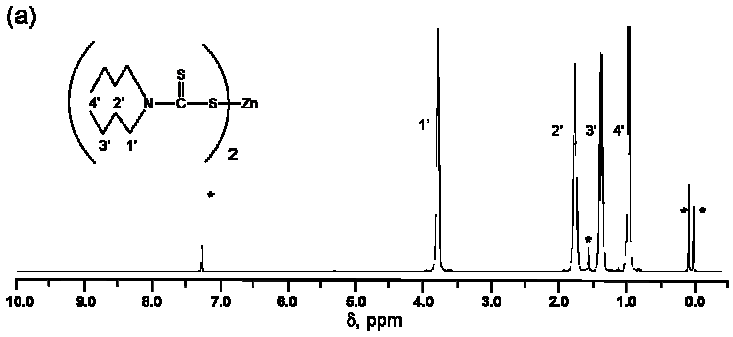

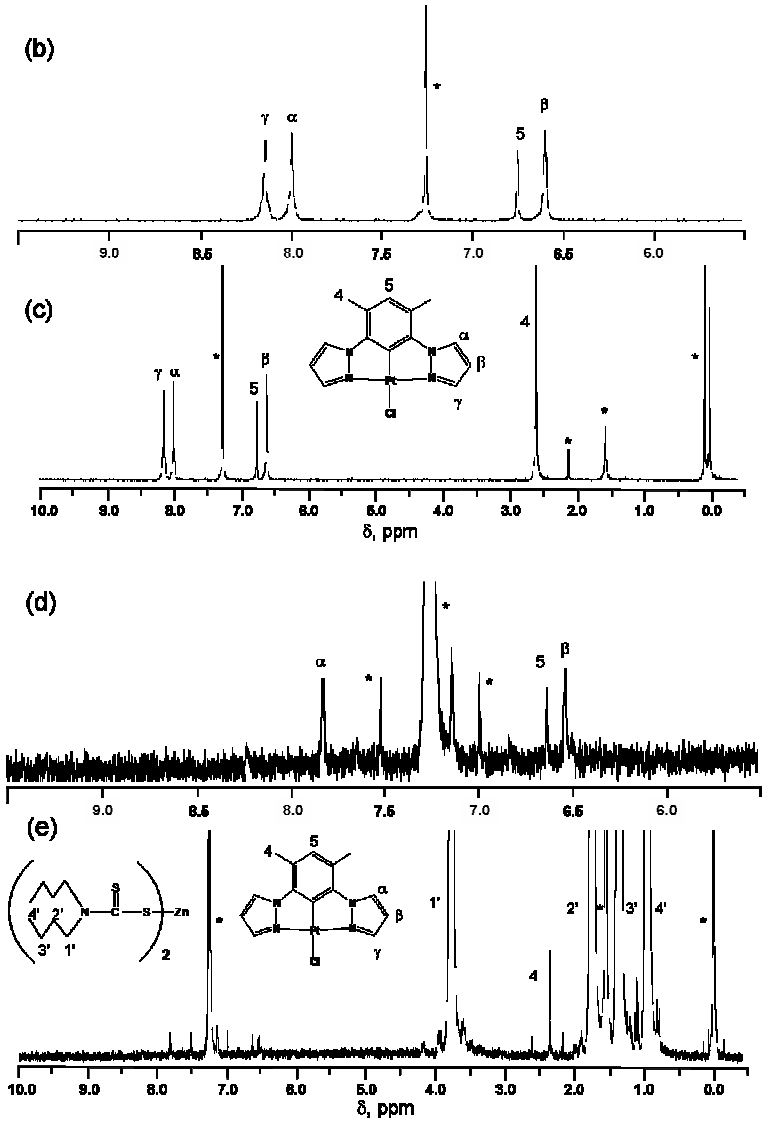

Figure 5.3. ^{1}H NMR spectra of $CDCl_3$ solutions of (a) the accelerator, (b) and (c) Pt(**3**)Cl, and (d) and (e) residue resulting from deposition of Pt(**3**)Cl on a solid sample of the accelerator. (* marks characteristic solvent resonances and assignable impurities.)

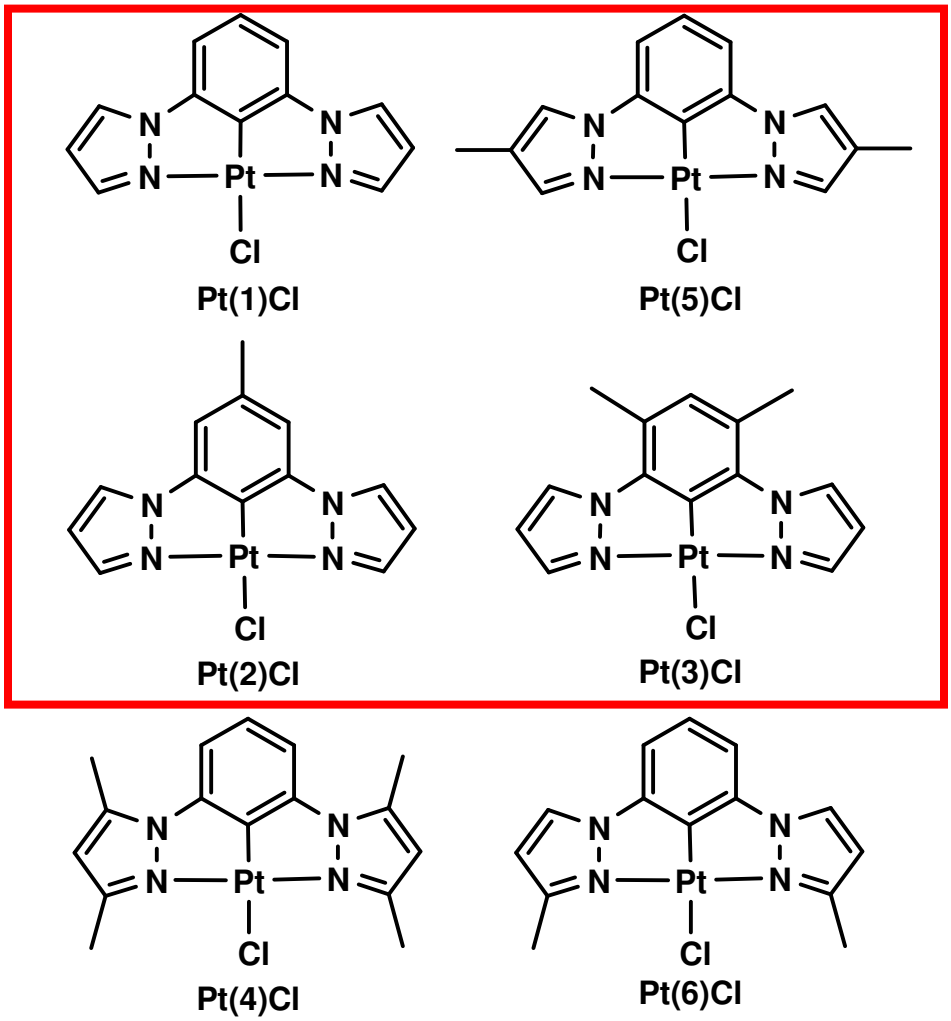

Figure 5.4. Line drawings of platinum compounds with *bis*-pyrazolylphenyl type ligands. Compounds exhibiting a response to dithiocarbamate compounds are contained within the red box. The bottom two compounds (Pt(**4**)Cl and Pt(**6**)Cl) do no exhibit a color change when applied to dithiocarbamate compounds or latex gloves.

The presence of platinum in the residue deposited on the latex glove was confirmed using ICP-MS. For a 3:1 Pt(**1**)Cl/[Pt(μ-**1**)Cl]$_3$ mixture deposited and washed with methylene chloride, 73.2 (18)% of the platinum was recovered. For a sample

deposited and washed with acetonitrile solution, 53.9 (14)% of the platinum was recovered. In both cases, the washings removed the color of the stain. Since the platinum deposited on the latex was a product mixture, if the monomer complex remained bonded to the latex surface, one would expect only 50% recovery of platinum in both experiments. These findings are consistent with the notion that at least some of the platinum-containing unit responsible for the color change can be washed off the surface. However, the incomplete recovery suggests that some of the platinum complex reacted irreversibly with the surface.

The response to commercial latex medical exam gloves and pipette bulbs is remarkably specific. For example, no stain was observed when methylene chloride solutions of Pt(**1**)Cl were evaporated on a variety of substrates, including glass, paper, stainless steel, wood, cotton, and disposable plastic lids and bags (Table 5.3). In each case, colorless solutions of the compounds, evaporated to give a beige solid (color of dry solid of platinum compounds). Application of a methylene chloride solution of Pt(**1**)Cl to raw latex did not produce an intensely colored stain (Figure 5.6). Raw latex has not been vulcanized and does not contain any additives/accelerators; therefore, these observations suggest that a processing additive plays a role in the observed chemistry. In support of this suggestion, it is noteworthy that that, after having soaked in water for 3 days, a latex sample gave only a faint red stain upon evaporation of a methylene chloride solution of Pt(**1**)Cl. It seems plausible that the soaking process removed or deactivated some of the reagent responsible for observed stain. Interestingly, low-protein latex samples also gave only a faint red stain (Table 5.3). Preparation of low-protein latex can involve different accelerators than employed for conventional latex processing, as well as an additional

enzyme washing step. Other anomalies, such as the lack of response from a latex condom, may also be related to the use of different additives.

In order to identify possible additives that might be responsible for the color change, a methylene chloride solution of Pt(**1**)Cl was applied to different substrates. In the case of cornstarch (used for moisture absorption in powder latex gloves), no color change was observed. Nor was a response observed when methylene chloride solutions were applied to solid samples of other latex additives, such as elemental sulfur, zinc oxide and a calcium salt ($Ca(NO_3)_2$).

To investigate the role of accelerators in the observed response, solutions of the metal compounds were allowed to evaporate on solid samples of eight accelerators pictured in Figure 5.8. As in the case of the latex substrates, no color change was observed when the solutions were applied to solid samples of the accelerators. In addition, no color change was observed when the compounds were added to solutions of the accelerators. Of the investigated accelerators, deposition of the platinum complexes on solid samples of the two dithiocarbamate compounds (sodium diethyldithiocarbamate and zinc dibutyldithiocarbamate) resulted in a very distinct orange-red to red to dark purple color (Figure 5.5). For example, application of Pt(**3**)Cl to either dithiocarbamate accelerator produced a dark purple stain on the slide (Figure 5.8). By contrast, application to most thiazole accelerators (MBS, CBS, DCBS and MBT, Figure 5.8, Table 5.2) produced what seems to be a faint yellow/orange stain, which might be a reaction. The platinum compounds in solution are yellowish/brown in color and the tested thiazole accelerators are yellowish/brown in color when dried on a glass slide, thus, it is difficult to establish whether a reaction has occurred between the thiazole accelerators and the

platinum compounds or if it is a combination of the colors from both that give a faint yellow/orange stain. In the case of Pt(**3**)Cl, the color and intensity observed on the solid samples of either dithiocarbamate accelerator is the same as that observed on the latex samples. As noted for the latex samples, each tested solvent with Pt(**3**)Cl gave a similar response (Table 5.1), suggesting that the color is not connected to specific interactions involving the solvent.

Depending on the platinum compound tested, the color of the stain on the solid dithiocarbamate substrate varied from orange-red to red to dark purple (Figure 5.5). As noted for manufactured latex samples, Pt(**4**)Cl and Pt(**6**)Cl, when applied to dithiocarbamates and allowed to dry, the resulting complexes gave the same color as the dry solid. The accumulated data suggest that treatment of solid samples of accelerators results in color changes that are qualitatively similar to those observed on a latex substrate. These observations support the tentative hypothesis that residual accelerators in latex are responsible for the observed staining behavior.

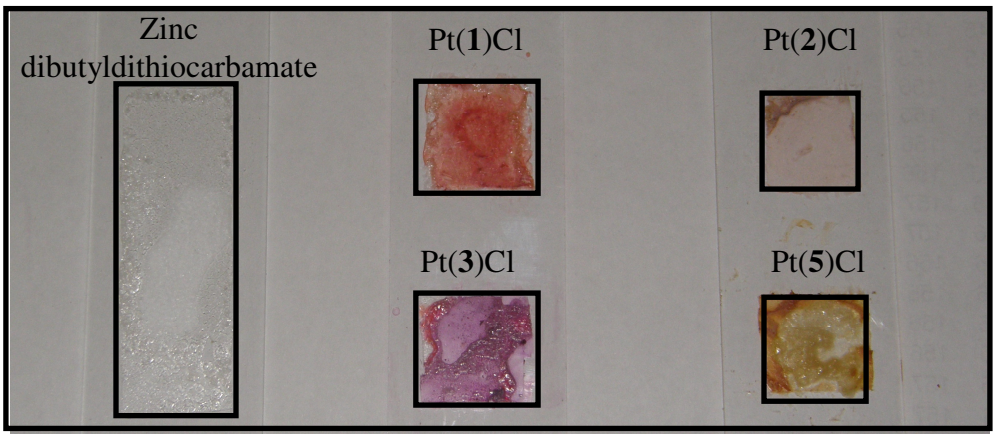

Figure 5.5. Digital images showing the solid residue of the zinc dibutyldithiocarbamate on a glass microscope slide (left). The two glass slides on the right show samples of zinc dibutyldithiocarbamate after exposure to four platinum complexes. Black boxes indicate the approximate region where the accelerator was applied.

Figure 5.6. Vial containing Pt(**1**)Cl (left). Latex glove from Kimberly-Clark after evaporation of methylene chloride solution of Pt(**1**)Cl (right).

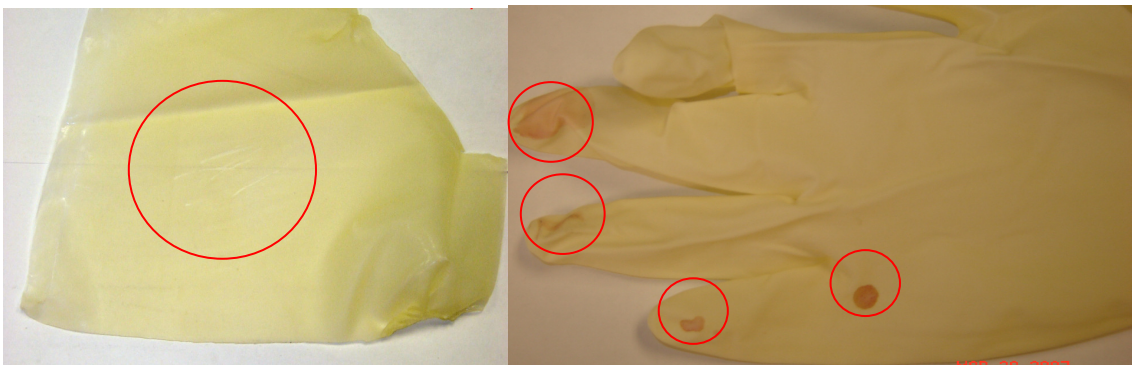

Figure 5.7. Left: circle marks where a solution of Pt(**1**)Cl was allowed to evaporate on the surface of a sample of raw latex (no additives/accelerators) provided by The Hygenic Corporation. Right: red circles indicates where Pt(**1**)Cl was allowed to evaporate on the surface of a latex glove from Kimberly-Clark, resulting in red color change.

Table 5.1. Color of the Stain Resulting from Evaporation of Pt(**3**)Cl in Various Solvents on a Solid Film of Zinc Dibutyldithiocarbamate Accelerator.

Compound	Solvent	Response
Pt(3)Cl	**Isopropyl Alcohol**	**Purple**
Pt(3)Cl	**Methanol**	**Purple**
Pt(3)Cl	**Ethanol**	**Purple**
Pt(3)Cl	**Acetone**	**Purple**
Pt(3)Cl	**Acetonitrile**	**Purple**
Pt(3)Cl	**Toluene**	**Purple**
Pt(3)Cl	**Methylene Chloride**	**Purple**
Pt(3)Cl	**Chloroform**	**Purple**
Pt(3)Cl	**Acetic Acid**	**Purple**
Pt(3)Cl	**DMF**	**Purple**

A variety of other platinum complexes were applied to solid samples of accelerators on microscope slides to test for a colorimetric response (Table 5.2). None of these model compounds exhibited a response (Table 5.2), suggesting that the observed reactivity is related to the chemical properties of platinum(II) bis-pyrazolylphenyl unit. Interestingly, Pt(**4**)Cl and Pt(**6**)Cl, which have methyl substituents at the γ-position of the pyrazolyl groups, also did not produce a colored stain on latex or accelerator samples. These observations are suggestive of a steric influence on the reaction (Figure 5.3).

Figure 5.8. Digital images of slides coated with accelerator (top) and after a methlene chloride solution of Pt(**3**)Cl was allowed to evaporate (bottom). Accelerators listed from left to right: Sodium Diethyldithiocarbamate, Zinc Dibutyldithiocarbamate, DPG, MBT, CBS, DCBS, TBBS and MBS.

Table 5.2. Observed Colors upon Evaporation of Solutions of Platinum Compounds on Various Accelerators.

Accelerators	Platinum Compound	Response
Tetraethylthiuram Disulfide	**Pt(3)Cl**	**None**
Diphenylguanidine (DPG)	**Pt(3)Cl**	**None**
***N-tert*-butyl-2-benzothiazole sulfenamide (TBBS)**	**Pt(3)Cl**	**None**
***N*-oxydiethylene-2-benzothiazole sulfenamide (MBS)**	**Pt(3)Cl**	**Orange/yellow**
***N*-cyclohexyl-2-benzothiazole sulfenamide (CBS)**	**Pt(3)Cl**	**Orange/yellow**
***N*, *N*-dicyclohexyl-2-benzothiazole sulfenamide (DCBS)**	**Pt(3)Cl**	**Orange/yellow**
2-Mercaptobenzothiazole (MBT)	**Pt(3)Cl**	**Orange/yellow**
Sodium Diethyldithiocarbamate	**Pt(3)Cl**	**Purple**
Zinc Dibutyldithiocarbamate	**Pt(3)Cl**	**Purple**
Zinc Dibutyldithiocarbamate	**Pt(5)Cl**	**Red/Orange**
Zinc Dibutyldithiocarbamate	**Pt(bpzph)Cl**	**Red**
Zinc Dibutyldithiocarbamate	**Pt(2)Cl**	**Red**
Model Compounds		
Zinc Dibutyldithiocarbamate	**Pt(4)Cl**	**None**
Zinc Dibutyldithiocarbamate	**Pt(6)Cl**	**None**
Zinc Dibutyldithiocarbamate	**Pt(1,4-cyclooctadiene)Cl_2**	**None**
Zinc Dibutyldithiocarbamate	**[Pt(bpp)Cl]Cl**	**None**
Zinc Dibutyldithiocarbamate	**[Pt(bpp)Cl][PF_6]**	**None**
Zinc Dibutyldithiocarbamate	**Pt(ph-py)Cl_2[PF_6]**	**None**
Zinc Dibutyldithiocarbamate	**[Pt(tpy)Cl]Cl**	**None**

Table 5.3. Observed color of the residue upon evaporation of Pt(**1**)Cl or Pt(**3**)Cl on Various Surfaces.

Vinyl Preferred LF/PF (Quantum)	Negative
Vinyl glove (Quantum) with aqueous $Ca(NO_3)_2$ evaporated on surface	Negative
$Ca(NO_3)_2$ (Fisher) solid on slide	Negative
Elemental Sulfur S_8 (Fisher)	Negative
Zinc Oxide	Negative
Cornstarch	Negative
Cotton	Negative
Glass	Negative
Latex Condom (Trojan)	Negative
Plastic/Sandwich Bag (Kroger)	Negative
Starbucks Cup/Lid (Starbucks)	Negative
Paper	Negative
Parafilm (Pechiney Plastic Packaging)	Negative
raw Natural Rubber Latex (Hygenic)	Negative
synthetic polyisoprene latex (Hygenic)	Negative
low protein Natural Rubber Latex (Hygenic)	Negative
guayle latex (Hygenic)	Negative
"Tru-touch" Vinyl Powdered Glove (Maxxim)	Negative
LF/PF Nitrile Glove (Quantum, Kimberly-Clark)	Negative
Synthetic LF/PF (PVC) (Quantum)	Negative
Cementex raw liquid latex	Negative
Textured PF Ultra-low Protein(<50μg/g) (Quantum)	Faint Positive
Green, powder-free synthetic glove (Ansell)	Positive
NRL PF Glove (chlorinated) (Ansell)	Positive
Compounded Natural Rubber Latex (Hygenic)	Positive
Nitrile powdered blue glove (Hygenic-supplied)	Positive
Nitrile PF blue glove (washed/chlorinated) (Hygenic-supplied)	Positive
Latex Pipet Bulb (Fisherbrand)	Positive
PF latex glove (Kimberly Clark, ADENNA, Quantum)	Positive
White Eraser from mechanical pencil (BIC)	Positive

Doctor's Choice PF Nitrile Glove (Quantum)	Positive
Softskin w/ Aloe vera PF Nitrile Glove (Quantum)	Positive
Softskin w/ Aloe vera PF Latex Ultra-low Protein Glove (<50µg/g) (Quantum)	Positive
Powdered Latex Exam Glove (Quantum, Formula One)	Positive
PF Latex Glove soaked in H_2O (3 days)	Faint Positive
PF Latex Glove soaked in CH_2Cl_2 (30 min)	Positive
Non-sterile Latex dusted with Absorbance Powder Glove (Formula One)	Positive
Evolution One PF Latex Glove (polymer coated non-sterile) (Microflex)	Positive

PF = Powder Free, LF = Latex Free, P = Powder, NRL = Natural Rubber Latex

Conclusion.

We have discovered that evaporation of solutions of each of four monomeric platinum(II) complexes with *bis*-2,6-dipyrazolyl-phenyl ligands on processed latex produces a red or violet colored stain. Thus, solutions of these compounds appear to act as a magic ink that only writes in the presence of a latex surface. The four platinum compounds can be used in a wide variety of solvent systems. The accumulated data are suggestive of a reversible chemical reaction on the surface of the latex. Interestingly, similar color changes were observed when solutions of the complexes were applied to solid samples of two common dithiocarbamate accelerators. These observations support the hypothesis that the observed reactivity on latex is a consequence of residual accelerators. Overall, these results suggest that these compounds can be used as colorimetric indicators for rapid detection of dithiocarbamate compounds, which are known to cause contact dermatitis in latex products.

It is suggested that future research focus on characterization of the product formed in the reaction of the platinum compound and dithiocarbamate accelerators. It may be possible to synthesize compounds in a one-to-one reaction of the dithiocarbamate with a given platinum complex. Our initial success in using ^{1}H NMR spectroscopy to characterize the reaction with dithiocarmbamates, suggest that this reaction should be repeated using stoichiometric amounts of dithiocarbamate. The resulting products may serve as models for the species formed on the latex surface. Furthermore, it would be desirable to obtain samples of latex that have been processed with dithiocarbamate accelerators and those that have been processed with other accelerators. Treating these samples with the platinum compounds would test the hypothesis that the dithiocarbamates are involved in the observed color change. It also may be possible to detect residual additives in latex samples using mass spectrometry to determine which correlate additives may be responsible for the observed reactivity; solid latex samples may be heated to release volatiles, or the additives may be extracted using ethylbenzene, cyclohexane or diethylene glycol prior to injection into the instrument. Lastly, it would be valuable to characterize the stains using diffuse reflectance spectroscopy in order to compare their spectra to those of target model complexes, as well as known thiolate complexes, platinum(II) linear chain materials and mixed-valent platinum compounds.

References.

(1) *The Vanderbilt Latex Handbook*; 3rd ed.; R.T. Vanderbilt Company, Inc.: Norwalk, CT, 1987.

(2) DermNetNZ; http:// www.dermnetnz.org/dermatitis/rubber-antioxidant-allergy.html, 2002.

(3) FDA; http:// www.accessdata.fda.gov/scripts/cdrh/cfdocs/cfcfr/-CFRSearch.cfm?FR=177.2600, 2007.

(4) Tinkler, J.; Gott, D.; Bootman, J. *Food and Chemical Toxicology* **1998**, *36*, 849-866.

(5) Depree, G. J.; Bledsoe, T. A.; Siegel, P. D. *J. Chromatographic Science* **2004**, *42*, 80-84.

(6) Bevilacqua, J. M.; Eisenberg, R. *Inorg. Chem.* **1994**, *33*, 2913-2923.

(7) Miller, J. S. *Extended Linear Chain Compounds*; Plenum Press: New York, N.Y., 1982; Vol. 2.

(8) Connick, W. B.; Marsh, R. E.; Schaefer, W. P.; Gray, H. B. *Inorg. Chem.* **1997**, *36*, 913-922.

(9) Houlding, V. H.; Miskowski, V. M. *Coord. Chem. Rev.* **1991**, *111*, 145-152.

(10) Gerisch, M.; Bruhn, C.; Steinborn, D. *Polyhedron* **1999**, *18*, 1953.

(11) Arrizabalaga, P.; Castan, P.; Laurent, J. P. *J. Am. Chem. Soc.* **1984**, *106*, 4814-4814.

(12) Weiser-Wallfahrer, M. *Zeitschrift fuer Naturforschung, B: Chemical Sciences* **1990**, *45*.

Chapter 6

Synthesis and Characterization of a Platinum(II) Complex with terpyridyl and *bis*-(pyrazolyl)phenyl Ligands: A Potential Two-Electron Reagent

Introduction.

Investigations of cooperative electron-transfer reactions are expected to provide insight into mutli-electron transfer processes that are important in multi-redox catalysis. In 2003, Jude *et al*. reported $Pt(pip_2NCN)(tpy)^+$ (Figure 1.3) to be the first example of an outer-sphere two-electron platinum reagent. The complex is composed of two potentially meridional coordinating ligands bonded to a platinum center. In the d^8-electron platinum(II) case, the terpyridyl ligand (tpy) is tridentate whereas the pip_2NCN^- ligand is monodentate, bonded through the central phenyl ring. In the d^6-electron platinum(IV) case, both ligands are believed to be tridentate.

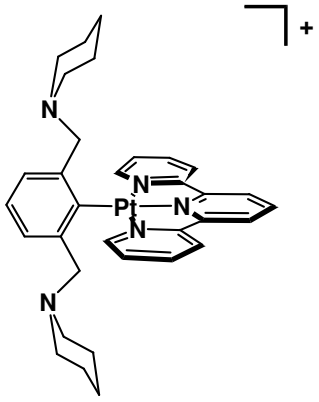

The cyclic voltammogram of $Pt(pip_2NCN)(tpy)^+$ (Figure 1.3) in 0.1 M $TBAPF_6$ in acetonitrile at 0.01 V/s shows a nearly a two-electron wave at 0.40 V vs. Ag/AgCl.[1,2] The separation between the anodic and cathodic peaks (ΔE_p) is 43 mV, which is well below the one-electron limit (59 mV) and near the two-electron limit (30 mV) for a

Nernstian process. The interconversion between the platinum(II) and platinum(IV) oxidation states by outer-sphere electron transfer is proposed to involve formation/cleavage of the axial Pt-N(piperidyl) bonds as shown in Figure 6.1.

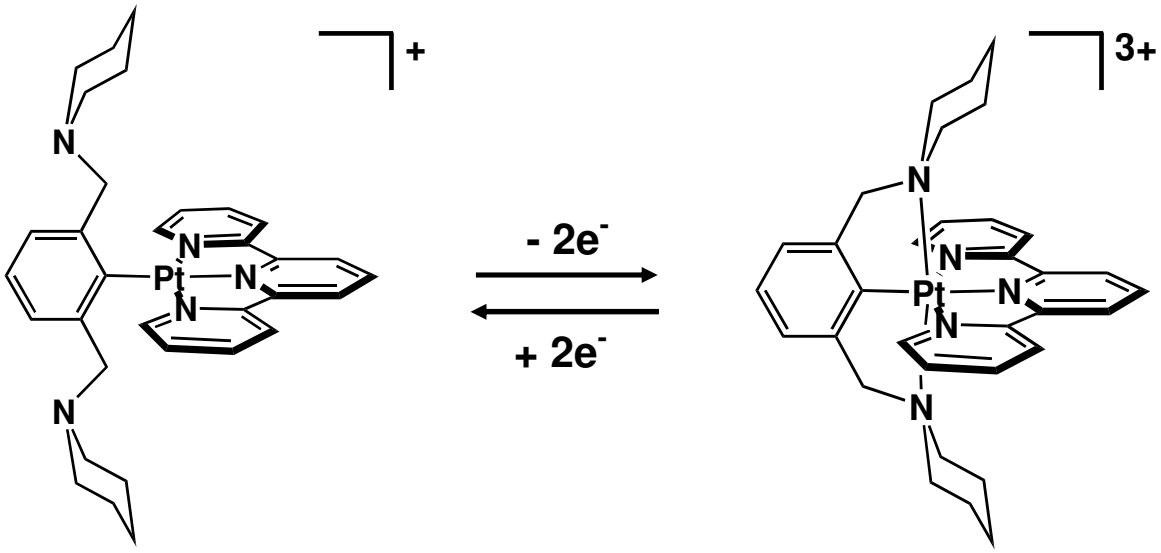

Figure 6.1. Representation of the reversible electron-transfer reaction of a two-electron platinum reagent with pip_2NCN^- and tpy ligands.

There is considerable interest in determining the factors that influence the mechanism, thermodynamics and kinetics of electron transfer in this system. However, one of the complications with $Pt(pip_2NCN)(tpy)^+$ is that it tends to be unstable in coordinating solvents resulting in dissociation of the terpyridyl ligand. In addition, efforts to prepare derivatives of this complex have met with difficulties. For example, attempts to prepare the analog with 2,6-*bis*(dimethylaminomethyl)phenyl anion (Me_4NCN^-) were thwarted by the tendency of the NCN^- ligand to displace the terpyridine ligand.[3] On the other hand, the diphenylamine analog, $Pt(Ph_4NCN)(tpy)^+$, is stable, but

does not exhibit similar two-electron chemistry. Presumably the steric demands of the phenyl groups interfere with coordination of the amine groups to the platinum(IV) center.[3]

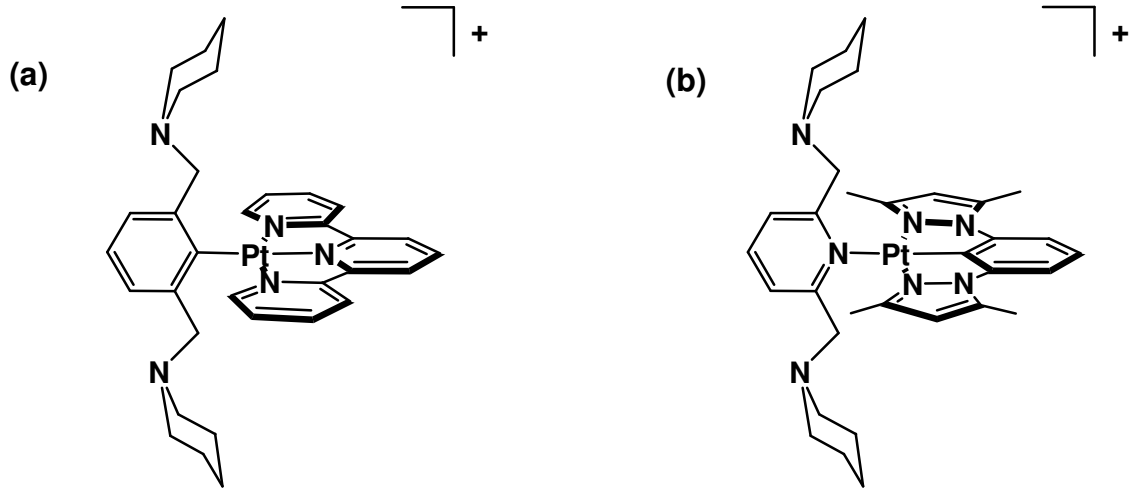

Figure 6.2. Line drawings of (a) Pt(pip_2NCN)(tpy)$^+$ and (b) Pt(**4**)(pip_2NNN)$^+$.

An intriguing alternative to pip_2NCN^- involves replacement of the middle phenyl group with a pyridyl group to give 2,6-*bis*(piperidylmethyl)pyridine (pip_2NNN). Unfortunately, initial attempts to use this ligand in place of either pip_2NCN^- or tpy were unsuccessful.[4] In the case of the Pt(pip_2NCN)(pip_2NNN)$^+$ target, ^{1}H NMR spectra are consistent with product mixtures. These results led to the hypothesis that the piperidyl groups compete for coordination sites. Therefore, new NCN^- ligands with more weakly donating side groups are expected to yield more stable products with the pip_2NNN ligand. To investigate this possibility, we have undertaken the preparation of Pt(**4**)(pip_2NNN)$^+$ (Figure 6.2 (b)), where **4H** is 1,3-*bis*(3,5-dimethylpyrazolyl)benzene, which was reported in Chapter 4. Herein we describe the synthesis and preliminary characterization of this potential two-electron reagent.

Experimental Section.

K_2PtCl_4 was purchased from Pressure Chemical Company. All other reagents were obtained from Acros, Alfa Aesar, or Aldrich. Pt(**4**)Cl was prepared as described in Chapter 4. ^1H NMR spectra were recorded at room temperature using a Bruker AC 400 MHz instrument. Deuterated solvents were purchased from Cambridge Isotope Laboratories. Mass spectra were obtained by electrospray ionization using an Ionspec HiRes ESI-FTICRMS instrument. The sample was dissolved in an ESI buffer solution, consisting of 50/50 water/acetonitrile and 0.1% formic acid. The observed isotope patterns agreed well with predicted patterns based on natural isotopic abundances.

Cyclic voltammetry measurements were carried out using a standard three-electrode cell and a 100 B/W electrochemical workstation from Bioanalytical Systems. Scans were recorded in dimethylformamide (DMF) solution containing 0.1 M tetrabutylammonium hexafluorophosphate, which was recrystallized at least twice from methanol and dried under vacuum prior to use. High-purity DMF for cyclic voltammetry was obtained from Burdick and Jackson. All scans were recorded using a Pt wire auxiliary electrode, a Ag/AgCl (3.0 M NaCl) reference electrode and a 0.79 mm^2 Pt working electrode. Reported potentials are referenced vs. Ag/AgCl (3.0 M NaCl). The working electrode was polished between scans with 0.05 μm alumina, rinsed with distilled water and dried using a Kimwipe.

X-ray Crystallography. Single crystals of $[pip_2NNNH_2](PF_6)_2 \cdot H_2O$ were obtained from $CHCl_3$-pentane. For X-ray examination and data collection, a suitable crystal, approximate dimensions 0.07 x 0.05 x 0.03 mm, was mounted in a loop with paratone-N and transferred immediately to the goniostat bathed in a cold stream.

Intensity data were collected at 150 K using a Bruker Platinum200 CCD detector at Beamline 11.3.1 at the Advanced Light Source (Lawrence Berkeley National Laboratory) with synchrotron radiation tuned to λ=0.77490 Å. A series of 2-s data frames measured at 0.2° increments of ω and φ were collected to calculate a unit cell. For data collection, frames were measured for a duration of 2-s at 0.3° intervals of ω with a maximum θ value of ~60°. The data frames were collected using the program APEX2 and processed using the program SAINT routine within APEX2.[5] Absorption and beam corrections were applied based on the multi-scan technique as implemented in SADABS. The structure was solved by a combination of direct methods in SHELXTL and the difference Fourier technique and refined by full-matrix least squares on F^2. Non-hydrogen atoms were refined with anisotropic displacement parameters. The N-H and O-H H-atom positions were located directly from the difference map. The N-H H-atoms positions were allowed to refine while the O-H H-atoms were held fixed at the located position. The remaining H-atoms were calculated and treated with a riding model. Isotropic displacement parameters were defined as a times U_{eq} of the adjacent atom (a=1.5 for O-H and 1.2 for all others). Crystallographic refinement parameters are collected in Table 6.1.

pip$_2$NNN. The pip$_2$NNN ligand was prepared by Seher Tastan in Professor Connick's laboratory at the University of Cincinnati. Piperidine (11.3 mL, 0.11 mol) was added to 20 mL of benzene under argon. After cannula transfer of a benzene solution of 2,6-bis(chloromethyl)pyridine (2.0 g, 0.0114 mol), the mixture was stirred for 2 h at room temperature. The white suspension was filtered, and the yellow filtrate was reduced in volume to give a yellow oil that was used in subsequent steps. Yield: 2.8 g,

90%. ^{1}H NMR ($CDCl_3$) δ (ppm): 1.46 (4H, m, CH_2), 1.60 (4H, m, CH_2), 2.44 (4H, m, CH_2), 3.62 (4H, s, pyridyl-CH_2), 7.28 (2H, d, CH), 7.60 (1H, t, CH).

[Pt(4)(pip$_2$NNN)](PF$_6$). Pt(**4**)Cl (0.025 g, 0.050 mmol) was dissolved in 5 ml of DMF. Excess $TlPF_6$ (0.0492 g, 0.070 mmol) was added, and the mixture was stirred at room temperature for 30 minutes. The resulting TlCl precipitate was removed by filtration through Celite. After addition of pip$_2$NNN (0.0146g, 0.053 mmol), the yellow solution was stirred for 12 hours The resulting yellow solution was concentrated to dryness by rotary evaporation, and the yellow solid was washed with Et_2O and hexanes and allowed to dry. Yield 0.022 g (49.8%). ^{1}H NMR (400 MHz, $CDCl_3$, δ): 1.32-1.79 (CH_2, m, 12H), 2.45-2.80 (CH_2, m, 8H), 3.82 (CH_2, m, 2H), 4.18 (CH_2, m, 2H), 6.14 (CH, s, 1H), 6.17 (CH, s, 1H), 7.05 (CH, m, 2H), 7.18 (CH, m, 1H), 7.80 (CH_2, d, 2H), 8.01 (CH, t, 1H). MS-ESI (*m*/*z*): 733.33027, [Pt(**4**)(pip$_2$NNN)]$^+$.

Results and Discussion.

Synthesis and Characterization. Synthetic efforts focused on complexes with **4**$^-$, because the methyl substituents on the pyrazole moiety are expected to prevent complications due to trimer formation (see Chapter 4). In addition, the steric demands of the methyl groups are anticipated to favor Pt···N(pyrazoyl) interactions,wich may be useful for Pt(II/IV) interconversion. Pt(**4**)Cl was synthesized and characterized as reported in Chapter 4. The pip$_2$NNN ligand was isolated by Seher Tastan from the reaction of 2,6-bis(chloromethyl)pyridine with excess piperidine. In the course of handling the [Pt(**4**)(pip$_2$NNN)](PF_6) product, crystals of pip$_2$NNNH_2(PF_6)$_2$·H_2O formed from diffusion of pentane into a chloroform solution. An ORTEP diagram of the

molecule is shown in Figure 6.3. Metrical data are consistent with that reported for $[pip_2NNNH_2](BF_4)_2 \cdot 0.5H_2O$.[6] Each protonated piperidyl group adopts a chair conformation with the benzylic group in the equatorial position and the proton in the axial position of the N atom. The N-H protons are directed toward the same O atom of the water molecule resulting in short NH···O contacts N2-H1···O1 = 2.991(3)Å, H2···O1 = 2.06(3)Å, 172(3)°; N3-H2···O1 = 2.991(3)Å, H1···O1 = 2.20(3)Å, 168(3)°).. The oxygen atom of the water lies near the plane defined by the pyridyl group in the pocket formed by the piperdyl groups, the O···N(pyridyl) distance is 3.153(3) Å. Thus, the molecule adopts a geometry reminiscent of that found for the chloride salt of $Pd(pip_2NNN)Cl^+$, in which the three N donor groups bond to the Pd center.[7] In the latter case, the Pd atom is in the axial position of one piperidyl group and the equatorial position of the other.

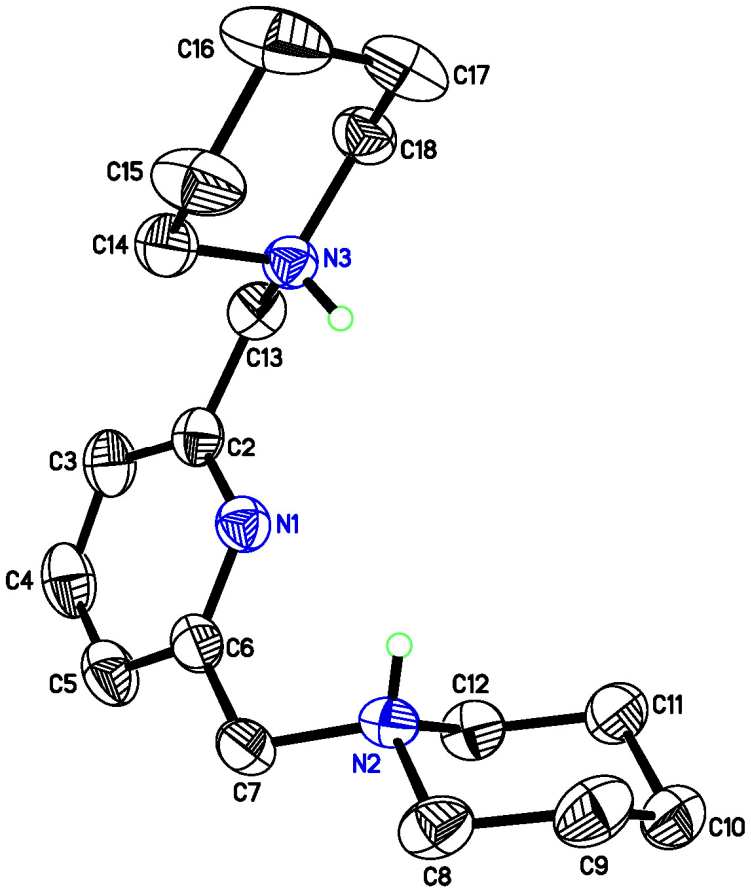

Figure 6.3. ORTEP diagram of $pip_2NNNH_2^{2+}$.

Table 6.1. Crystallographic Data for $[pip_2NNNH_2](PF_6)_2 \bullet H_2O$.

	$[pip_2NNNH_2](PF_6)_2 \bullet H_2O$
formula	$[C_{17}H_{29}N_3](PF_6)_2 \bullet H_2O$
fw, g/mol	583.39
space group	*C*2/*c*
a, Å	34.595(3)
b, Å	8.71259(8)
c, Å	17.9705(16)
α, °	90
β, °	118.9
γ, °	90
V, Å^3	4740.7(8)
ρ_{calcd} (g cm^{-3})	1.635
μ, mm^{-1}	0.367
Z	8
T, K	150(2)
reflns collected	29837
ind reflns	4788
R_{int}	0.0527
GOF on F^2	1.071
$R1/wR2$ [$I > 2\sigma(I)$][a]	0.0544/0.1435
$R1/wR2$ (all data)[a]	0.0660/0.1525

[Pt(**4**)(pip$_2$NNN)](PF$_6$) was prepared from the reaction of Pt(**4**)Cl with pip$_2$NNN. Pt(**4**)Cl was stirred with 1.4 equivalents of TlPF$_6$ in DMF for 30 min in order to remove the chloride ligand. After filtration, the pale yellow filtrate was stirred with approximately one equivalent of pip$_2$NNN for 12 hours. The solution was rotoevaporated to dryness to give a platinum-containing product. The resulting material was completely soluble in DMF, but only partially soluble in other organic solvents, such as chloroform, methylene chloride and acetonitrile.

The product was characterized by ^{1}H NMR spectroscopy and mass spectrometry. The ESI mass spectrum (Figure 6.4) is consistent with the proposed composition of the product, Pt(**4**)(pip$_2$NNN)$^+$ (Figure 6.2(b)). The parent ion peak and isotope profile (733.33) match those expected for Pt(**4**)(pip$_2$NNN)$^+$. All other mass peaks were appreciably less intense than the parent peak. Isotope profiles of the peaks at 274 and 501 are consistent with free pip$_2$NNN$^+$ and [Pt(**4**) + CH$_3$CN]$^+$, respectively.

The ^{1}H NMR spectrum in CDCl$_3$ shows characteristically broadened resonances (Figure 6.5), which may be a result of the fact that the sample was not completely dissolved. Alternatively, there may be some fluxionality. However, even the TMS resonance is broadened, which would be consistent with a heterogeneous sample or the presence of a paramagnetic impurity. These observations led to attempts to purify the complex by dissolution in methylene chloride followed by the addition of hexanes. The resulting mixture was filtered, and the yellow solid was dried under vacuum. No change was observed in the NMR spectrum, and the resonances remained broad.

The ^{1}H NMR spectrum of the recrystallized product (Figure 6.5) in CDCl$_3$ shows an apparent triplet at 8.07 ppm and a doublet 7.79 ppm, which are tentatively assigned to

pyridyl proton resonances of the pip_2NNN ligand. These resonances are shifted ~0.15 ppm upfield from those of the Pt(pip_2NNN)Cl complex.[6] Two resonances appear at 6.14 and 6.17 ppm in the β-pyrazole region of the spectrum. This result is unexpected for the structure shown in Figure 6.2(b), since the β-pyrazole protons are expected to be equivalent by symmetry. Resonances characteristic of the phenyl protons of $\mathbf{4}^-$ occur between 7.0-7.2 ppm, however no well-defined splittings are discernible. Two sets of resonances at 3.8 and 4.2 ppm also are consistent with inequivalent methylene proton resonances of the pip_2NNN ligand. Of these, the upfield resonance at 3.8 ppm appears to overlap with a piperidyl resonance. The presence of two methylene resonances also is in contradiction to the pattern expected for the structure shown in Figure 6.2(b). The remaining piperidyl resonances occur in the 1.2-1.8 ppm and 2.5-2.8 ppm ranges. Overall, the pattern of resonances observed in in the ^{1}H NMR spectrum is not consistent with the structure shown in Figure 6.2 (b). The accumulated data are most consistent with both ligands (pip_2NNN and **4**) being coordinated in a bidentate fashion to the platinum metal center as depicted in Figure 6.6.

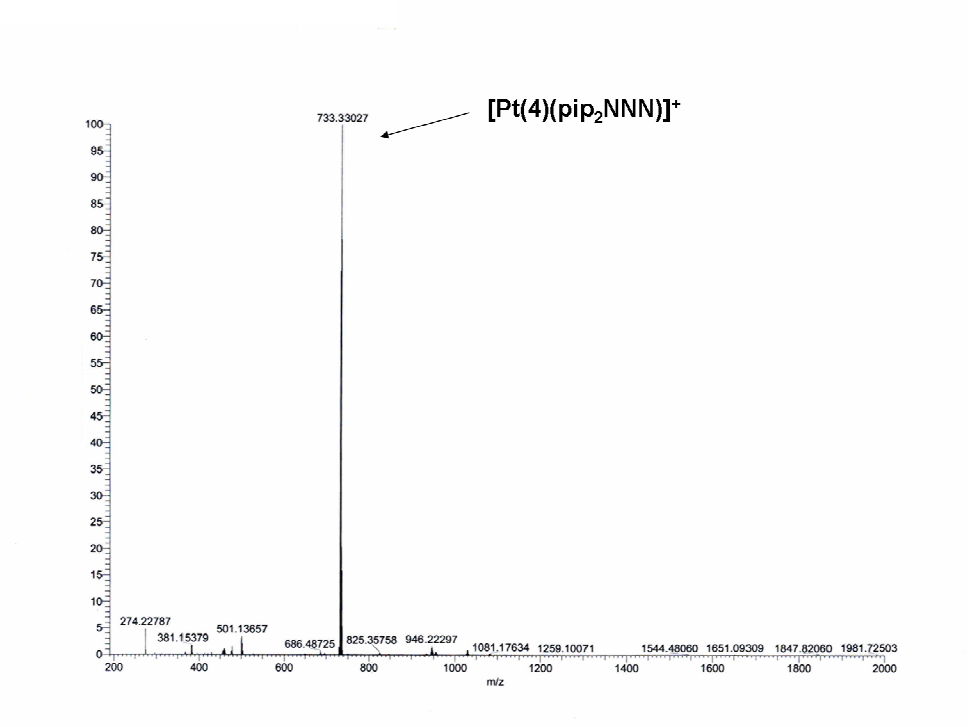

Figure 6.4. ESI mass spectrum of the proposed [Pt(**4**)(pip$_2$NNN)][PF$_6$] product in ESI buffer solution containing a 50/50 water/acetonitrile and 0.1% formic acid.

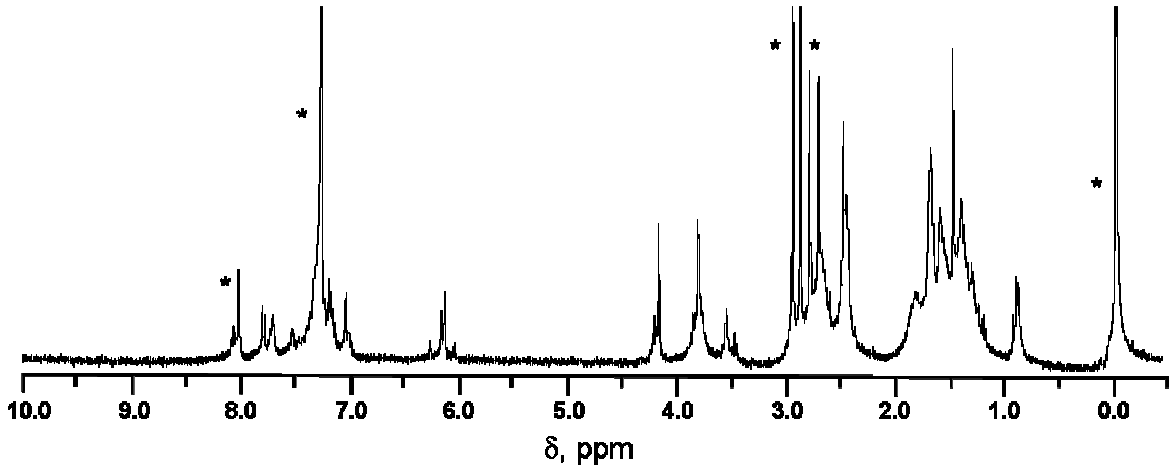

Figure 6.5. ^{1}H NMR spectrum of the proposed [Pt(**4**)(pip$_2$NNN)][PF$_6$] product in CDCl$_3$ solvent. (* marks characteristic solvent and TMS resonances; resonances at 8.0, 2.8 and 2.9 ppm are attributed to residual DMF solvent.)

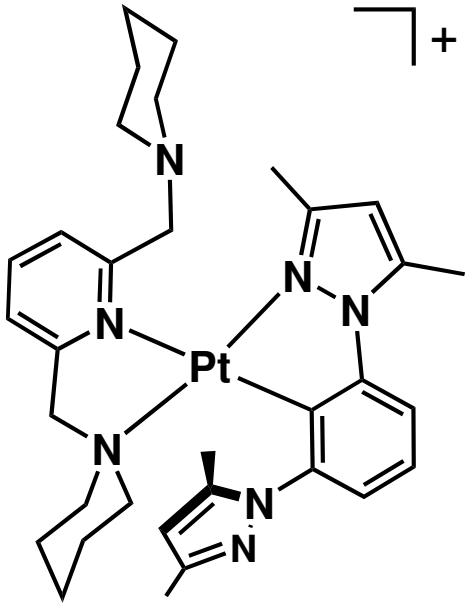

Figure 6.6. Proposed coordination geometry of Pt(**4**)(pip_2NNN)$^+$ showing bidentate chelation of both ligands to the metal center.

In an attempt to further purify the product, nitric acid was added dropwise to a solution of the complex in DMF solvent with the objective of protonating the piperdyl arms of the pip_2NNN ligand. The color of the solution changed from yellow to green. The solution was concentrated to dryness and the ^1H NMR spectrum of the residue was recorded. The ^1H NMR spectrum shows aromatic resonances consistent with coordination of **4**$^-$ to the metal center (Figure 6.7). However, there is no evidence of piperidyl resonances, suggesting that the ligand was displaced in the reaction. The mass spectrum is in qualitative agreement, showing isotope peak profiles consistent with pip_2NNNH^+ (274) and Pt(**4**)$^+$ (461) (Figure 6.8). The isotope peak profile at 501 matches that expected for Pt(**4**)(CH_3CN)$^+$.

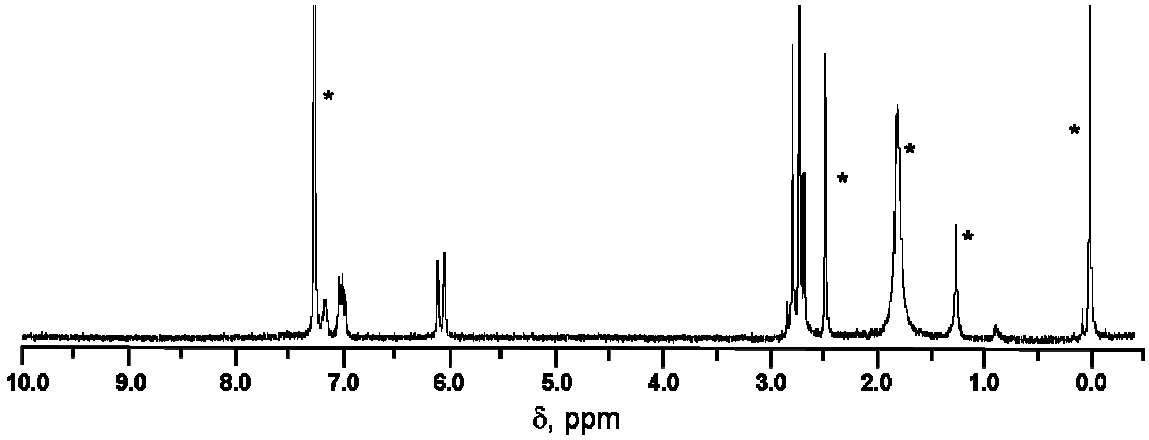

Figure 6.7. ^{1}H NMR spectrum of the proposed [Pt(**4**)(pip$_2$NNN)][PF$_6$] product after the addition of HNO_3; the sample was dissolved in $CDCl_3$ solvent. (* marks characteristic solvent and TMS resonances; resonances at 1.23, 1.56 and 2.50 ppm are attributed to hexane, H_2O and acetone respectively.)

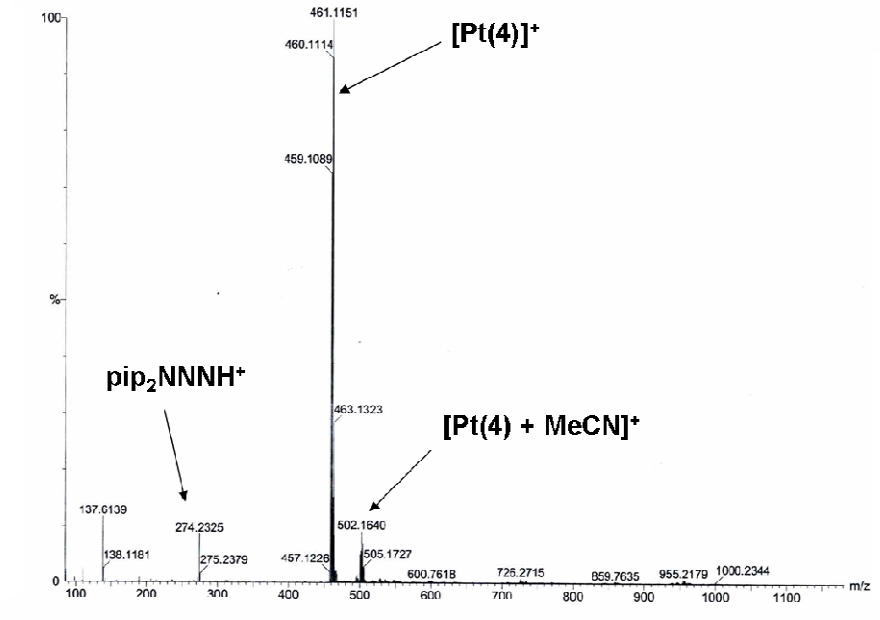

Figure 6.8. ESI mass spectrum of the proposed [Pt(**4**)(pip$_2$NNN)][PF$_6$] product after the addition of HNO_3; the sample was recorded in ESI buffer solution containing 50:50 acetonitrile/water and 0.1% formic acid.

Cyclic Voltammetry. Cyclic voltammograms of the proposed Pt(**4**)(pip$_2$NNN)$^+$ product were recorded in DMF with 0.1 M TBAPF$_6$ supporting electrolyte. Figure 6.6 shows a typical cyclic voltammogram. The compound is oxidized near 0.65 V. The anodic peak is not well-resolved, and therefore we are only able to determine that ΔE_p is greater than 60 mV. The scan rate was varied from 50 to 250 mV/s in an effort to resolve the anodic peak, however, the peak in the anodic wave remained unresolved. The oxidation process is quasi-reversible, as suggested by the return reduction wave at 0.6 V. At present, the stoichiometry of the process is not known.

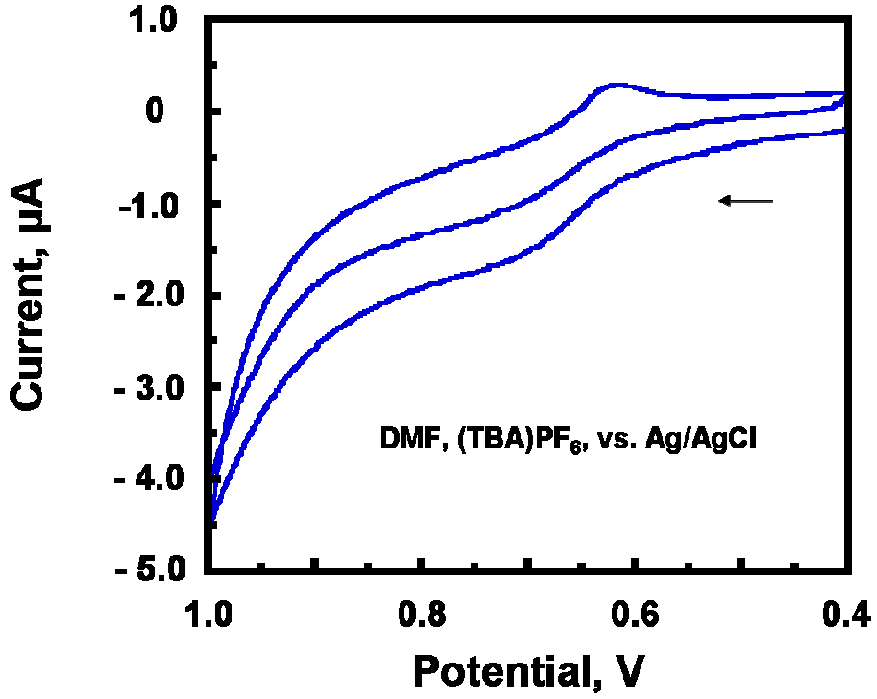

Figure 6.9. Cyclic voltammagram of Pt(**4**)(pip$_2$NNN)$^+$ in DMF solution with 0.1 M TBAPF$_6$ at 50 mV/s.

Conclusion.

As a first step towards designing two-electron reagents with deprotonated 1,3-*bis* (3,5-dimethylpyrazolyl)benzene ligands, we have prepared a new platinum(II) complex which is tentatively identified as Pt(**4**)(pip_2NNN)$^+$. ^{1}H NMR data suggest that the complex does not adopt the target structure shown in Figure 6.2(b). Instead, both ligands appear to adopt a bidentate coordination geometry as shown in Figure 6.3. Cyclic voltammetry measurements suggest that the complex undergoes a quasi-reversible oxidation near 0.65 V.

Because of these promising results, there is interest in further characterizing this system. It may prove easier to purify and characterize products with analogous ligands discussed in Chapter 4, notably the unmethylated derivative of **4**$^-$ (i.e., **1**$^-$). Future studies should first focus on interpreting the NMR spectra of these compounds and expanding these studies to include two-dimensional techniques and low-temperature experiments. The broadness of the resonances is likely due to impurities or heterogeneity. Since the complex reported here is only slightly soluble in most solvents ($CHCl_3$, CH_3CN), further recrystallization of the product should be attempted using a DMF/ether workup. It also may be possible to further purify the material by washing or extracting with solvents such as $CHCl_3$ or CH_3CN. IR spectroscopy may give additional insight into the coordination geometry. Ideally, it will be possible to grow crystals of these complexes suitable for single crystal X-ray diffraction studies. It also may be possible to obtain complexes with the reagents with a tridentate NNN ligand by using a modified ligand in which the piperidyl groups are replaced with more strongly donating and less sterically demanding amines (*e.g.*, $N(CH_3)_2$). Once the target compounds are better characterized, it will be

desirable to revisit the cyclic voltammetry experiments to better assess the electron-transfer reactivity.

References.

(1) Thompson, B. J., Ed. *In Energy, Simulation-Training, Ocean Engineering and Instrumentation: Research Papers of the Link Foundation Fellows.*; University of Rochester Press: Rochester, N.Y., **2003**; Vol. 3, pp 37-52.

(2) Jude, H. In *Synthesis and Characterization of Two-Electron Platinum Reagents; www. ohiolink.edu/etd/view.cgi?acc%5Fnum=ucin1077152*; University of Cincinnati, Ph.D. Dissertation: Cincinnati, OH, 2004, p 384.

(3) Jude, H.; Ellis, J.; Krause, J. A.; Connick, W. B. *unpublished data.*

(4) Tastan, S.; Krause, J. A.; Connick, W. B. *manuscript in preparation*.

(5) SHELXTL v6.14 for structure solution, figures and tables, neutral-atom scattering factors as stored in this package. G.M. Sheldrick, University of Göttingen, Germany and Bruker Analytical X-ray Instruments, Inc., Madison, WI.

(6) Tastan, S.; Krause, J. A.; Connick, W. B. *unpublished data.*

(7) Tastan, S.; Krause, J. A.; Connick, W. B. *Inorg. Chim. Acta* **2006**, *359*, 1889-1898.